Inactivation of *Clostridium perfringens* Spores in Anaerobically Digested Biosolids During BioElectro^{TM} Disinfection Process

Elham Safaei Takhtehfouladi

A thesis

in

The Department

of

Building, Civil and Environmental Engineering

Presented in Partial Fulfillment of the Requirements

For the Degree of Doctor of Philosophy (Civil Engineering)

Concordia University

Montréal, Québec, Canada

January 2012

©Elham Safaei Takhtehfouladi, 2012

Concordia University

School of Graduate Studies

This is to certify that the thesis prepared

By: **Ms. Elham Safaei Takhtehfouladi**

Entitled: **Inactivation of *Clostridium perfringens* Spore in Anaerobically Digested Biosolids During BioElectro$^{\text{TM}}$ Disinfection Process**

and submitted in partial fulfillment of the requirements for the degree of

Doctor of Philosophy (Civil Engineering)

complies with the regulations of this University and meets the accepted standards with respect to originality and quality.

Signed by the final examining committee:

Dr. Rabin Raut ——————————— Chair

Dr. Suresh D. Pillai ——————————— External Examiner

Dr. Fariborz Haghighat ——————————— Examiner

Dr. Catherine Mulligan ——————————— Examiner

Dr. William Zegres ——————————— Examiner

Dr. Maria Elektorowicz ——————————— Supervisor

Dr. Robert S. Reimers ——————————— Co–supervisor

Approved ———————————————————
          Chair of Department or Graduate Program Director

——— 2012 ———   ———————————————

Dr. Robin A.L. Drew, Dean

Faculty of Engineering and Computer Science

Abstract

Inactivation of *Clostridium perfringens* spores in anaerobically digested biosolids during BioElectro^TM process

Elham Safaei Takhtehfouladi, PhD

Concordia University, 2012

Treatment of municipal liquid wastes generates immense quantities of sludges that demands environmentally safe disposal or reuse. The past 40 years have seen the emergence of an increasing desire worldwide to attenuate the disposal of biosolids to landfills and to promote the options of the agricultural application of this by–product as soil conditioner and fertilizer. Consequently, post–treatment steps are commonly required as a means to adapt biosolids to the requirements of environmental legislations. Conventional methods are not generally effective enough; hence, novel and emerging methods are continually being sought.

This study was initiated to develop an eco–efficient process that produces a pathogen–free biosolids product which can be used beneficially for land application to meet or better stringent public health and environmental concerns. To achieve this goal BioElectro^TM, an enhanced 2D electric field process, was developed. The biosolids treatment experiments were performed at the average initial temperature, pH and ORP of 18°C, 8.17 and -57.3 mV, respectively. *Clostridium perfringens* spores in anaerobically digested biosolids were used as the bioindicator to assess the eficiency of BioElectro^TM process. It was evident that electrical field intensity between 2.5–2.8 (V/cm) was capable of reducing the number of viable *C. perfringens* spores below ceiling levels (>3 LRs).

Furthermore, the mechanism of disinfection during BioElectro^TM process was evaluated. Statistically significant effects of electric field intensity (E) and applied enhancement agents were ascertained at each time interval using multiple linear regression (MLR). Moreover, the shape of inactivation curves resulting from the BioElectro^TM treatment showed a triphasic pattern, starting with a short linear

part at low treatment times, followed by a shoulder or a lag period and finally a first–order inactivation kinetics. This was explained by effects of multiple stressors and mechanism of disinfection during the BioElectro$^{\text{TM}}$ treatment.

Ultrastructural analyses using transmission electron microscope were performed to investigate physiological changes in the fitness of treated spores. It was observed that electric field can be considered as an inducing factor in activating and consequent germination of dormant spore, and that can be responsible for shoulder formation in survival curves.

Also, an empirical model was developed by non–linear programming approach to quantify disinfection kinetics of BioElectro$^{\text{TM}}$ disinfection process. The proposed model was able to predict the spore inactivation very accurately.

Acknowledgments

I take pleasure to express my appreciation to my supervisor, Professor Maria Elektorowicz, for the continuous confidence, scientific advice and, especially, for the great independence she gave to me. Her support and patience made this work possible.

Very special thanks to Professor Robert S. Reimers, my co–supervisor, for his inspiration and very helpful discussions. I will never forget his encouragements.

My appreciations go to Professors Fariborz Haghighat, Catherine Mulligan, Suresh D. Pillai, Theodore Stathopoulos and William Zerges, members of my advisory committee, for their valuable advice.

My enormous debt of gratitude to my family in my beloved motherland, IRAN, to whom I dedicate this work. I would have never achieved anything without their unconditional love and support.

Finally, it was a great opportunity to conduct my studies at Concordia University. I have had such a valuable time and experience that I always remember.

Contents

List of Figures

List of Tables

Acronyms & abbreviations

Chapter 1

Introduction

The development of appropriate policies for the treatment and disposal of sewage sludge (biosolids) is a major issue worldwide [1, 2]. For instance, the generated amount of biosolids in Canada is more than 860,000 dry tons per year which is expected double by 2012 [2]. Approximately 60 percent of biosolids is used for land application based on the belief that biosolids should be considered a resource rather than a waste [3, 4]. However, biosolids applied to the land must meet quality standards for pathogens and health threatened chemicals [1]. Therefore, complex regulatory systems have been developed for reusing of biosolids with the intention of protecting human, animal and plant health, ground and surface water quality, enduring soil quality and soil biodiversity [5, 6, 7, 8]. These regulations encourage municipal wastewater treatment facilities to treat biosolids to a higher quality level and minimize constraints on use; and require relatively expensive management practices, further assuring clean and safe beneficial uses for biosolids [2, 7]. Such treatment should be designed to improve the characteristics of the biosolids for a disposal practice, increase the economic feasibility of using a particular practice and reduce the potential for public health, environmental and nuisance problems [1, 5]. Conventional technologies are usually not enough effective, time–consuming, expensive [1], and the processes that reduce trace pollutants have no effects on the level of pathogens [9]. Ergo, it is preferable to use technologies which upgrade biosolids chemically and biologically.

Application of low intensity direct electric field (LIDEF), electrokinetic (EK), is a novel approach which has been evaluated for its promising metal removal and disinfection effect on biosolids [9, 10, 11, 12, 13]. Electrokinetic technology has been used in soil remediation for many years [14]; however, in the last several years, the environmental engineering community has embraced an innovative application of this technology to treat biosolids [11]. This technology can be considered as a unique remediation method for simultaneous dewatering, metal removal and pathogen reduction in sewage sludge through oxidation and reduction zones [9]. EK has been used successfully for inactivation of fecal coliforms (FCs) [15, 16] and *Salmonella spp.* below detectable levels in different sewage sludge [16]. Also, EK enhanced by BIOXY S^{TM} (BS) and glutaraldehyde (GTA) has shown to sufficiently reduce the number of *C. perfringens* spores and Reovirus in anaerobically digested biosolids [10].

These significant reductions for two species of pathogenic bacteria, the bacterial spore and Reovirus suggested that the enhanced EK (EEK) is a promising alternative treatment for reduction of bacterial load in biosolids with the potential to decrease the amount of disinfectants used; however, aforementioned studies were conducted in 1D electric field EK reactors which needs long treatment times (3–10 days). This residence time is short when compared with other biosolids treatment methods, e.g., lime treatment and composting, yet could be ameliorated by altering electric field configurations. Furthermore, some of the previously applied enhancement agents such as GTA needs be replaced with safer compounds. Moreover, no work has been done so far on the disinfection mechanism of EEK in biosolids matrix through eradication of high resistant bacterial spores. Understanding how the mode of action of EEK is and the mechanisms of microbial response to this action are essential for the optimization of the disinfection process. Consequently, for microbiological safety and control of this emerging technology, it is essential to realize how the stressors applied by the EK process contribute to its role in eliminating bacterial spores.

The main objective of this study was the development of an enhanced 2D electric field process, BioElectro^{TM}, for the advance inactivation of spores in biosolids,

and application of analytical tools to clarify the mechanistic relationships during spore inactivation under BioElectro$^{\text{TM}}$ treatment. Using OD$_{600}$, plate count and transmission electron microscope (TEM) approaches, a fundamental assessment of spore inactivation mechanisms and non–linear log$_{10}$ reduction was performed. In line with this objective a research project entitled "L'étude sur l'application des processus électrocinétiques pour la désinfection des microorganismes dans le boue et les eaux usées" was proposed to Le Fonds Québécois de la Recherche sur la Nature et les Technologies (FQRNT) and granted to the author.

1.1   Contributions

The contributions of our research are as follows:

- Introducing an eco–friendly process to produce a high quality biosolids.
- Assessment of indigenous *C. perfringens* spores inactivation in biosolids matrix during the exposure to BioElectro$^{\text{TM}}$ treatment.
- Development of a mathematical model for the spore disinfection kinetics in biosolids matrix treated under EEK.
- Defining the coefficient of electrical conductivity of XAN + (1-X)BS system in biosolids matrix.
- Assessment of the demand and decay rate of peracetic acid (PAA) in biosolids.
- Providing reliable evidences on the proposed spore activation and germination effects of LIDEF.
- Ultrastructural evaluations of spores exposed to EEK treatment.

Chapter 2

Hypothesis based on the previous works

Although electrokinetic (EK) methods for biosolids dewatering exist commercially in the market, the enhanced EK (EEK) inactivation of spores in biosolids matrix, or as it is introduced throughout this treatise BioElectro$^{\mathrm{TM}}$, is a novel application of this technology which implements LIDEF enhanced with eco–green compounds. It has been revealed that an electric current passing through the contaminated matrix under treatment by means of suitable electrodes initiates electrokinetic phenomena (EKP) and is able to eradicate microorganisms [9, 11, 17, 18, 19, 20, 21, 22]. As compared with other biosolids disinfection processes, the advantages of EEK disinfection are evident: the disinfecting effect can be adjusted according to the on–site demand. EK disinfection shows a reservoir effect, is often more cost–effective and requires less maintenance than other disinfection methods. Furthermore, this technology permits biosolids dewatering and simultaneous removal of toxic metals. Therefore, the driving hypotheses behind the application of EEK as a promising and efficient method for the biosolids treatment can be interpreted as:

- multifunctional EK process produces a high quality biosolids,
- the combination of stressors provokes an interactive disinfection of bacterial spore and

- disinfection of spores in the biosolids matrix follows the heterogeneous kinetics.

2.1 EEK as a multifunctional process in treatment of biosolids

Electrokinetic technology has been used in soil remediation for many years [14, 23]; however, applications of this technology on biosolids treatment are more recent [11, 22]. EK can be considered as a unique remediation method for the simultaneous dewatering, heavy metal removal and pathogen inactivation in sludge matrix through a number of phenomena including oxidation and reduction reactions. In a dewatering study, EK process with electric field intensity ranging from 2.5–5.0 V/cm was used to generate the movement of bound water in the sludge specimen for a treatment time of 4-41 hours [24]. The fundings showed a removal efficiency of 62.6 percent at the applied electric field intensity of 5.0 V/cm for 41 hours. In another study, the EK process enhanced with processing fluids, sodium dodecylsulfate and citric acid was conducted for five days to remove metals from an industrial wastewater sludge [25]. Results showed the highest metal removal efficiency of 78 percent was achieved by using 0.024 M of citric acid and an electric field intensity of 1.25 V/cm.

The application of EK on industrial and municipal sludge was investigated by a number of researchers at the Concordia University under the supervision of Professor Maria Elektorowicz. In a study performed by [15], the EEK with a potential gradient (PG) regimes between 0.5 and 1.5 was applied for simultaneous removal of water, metal, organic compound and FCs in biosolids. The results of this investigation presented an average removal of 84 percent for zinc, 100 percent for Cd and Pb and 91 percent for iron [12, 15]. The fundings also confirmed a negative growth of FCs. A novel approach for treatment of petroleum oily sludge by combination of EK and bioremediation was employed by [26]. The observed results approved 35 and 81 percent reduction in the total petroleum hydrocarbons and aliphatic hydrocarbons content of oily sludge, respectively. In another study [16], five different combinations of sewage sludge, to wit: primary, combined primary and secondary,

attached growth secondary, waste activated and anaerobically digested were treated under the influence of 0.5 and 2 V/cm electric field intensity enhanced with an ammonium salt, for six to nine days. The treated sludges were assessed for the presence of FCs and *Salmonella spp.* No FCs and *Salmonella spp.* were detected at the end of treatment. The highest total solids (TS) content of 98 percent was achieved with the minimum electric field intensity (0.5 V/cm) in the presence of the enhancement agent. A pilot–plant study was conducted by [27] using an innovative system [28] to investigate dewatering, metal removal and organic matter reduction in biosolids using electrokinetic phenomena. This study demonstrated maximum Pb and Zn removal efficacies of about 75 and 90 percent, respectively under relatively low electric field intensity, and a maximum water removal capability of 70 percent TS using a higher PG. In a recent study, simultaneous dewatering, heavy metal removal and inactivation of helminth ova of combined primary and secondary sewage sludge was investigated using an EK system enhanced with ammonium nitrate (AN) [29]. The results presented that the applied EEK was able to deliver a product free of viable helminth ova. Moreover, 23 percent TS and mean removal levels of 54, 30 and 24 percent for Zn, Cd and Pb, respectively, after a period of three days exposure time was reported.

A comprehensive research [10, 17, 18, 19] was conducted by the author of the current work to assess physicochemical characteristics (10 properties) of EK treated biosolids as well as the optimal condition for the inactivation of *C. perfringens* spores and Reovirus in anaerobically digested biosolids by investigating the interactive effects of three various enhancement agents, viz, di–ammonium phosphate, GTA and BS in conjunction with EK technology in a 1D electric field configuration. Optimal inactivation results were selected with a 4.5 log reduction in *C. perfringens* spores and a complete inactivation of Reovirus. The optimal condition showed that electric field intensity (E) and the concentrations of BS and GTA were significantly ($p < 0.05$) important in biosolids disinfection experiments. The percent contribution of E, BS and GTA in the optimal condition was 21, 13, 62 percent, respectively [10].

A number of mechanisms have been suggested to explain for the multifunctional

effects of EK technology especially in the case of dewatering and heavy metal removal, however, little,if any, is known about the mechanism of pathogen inactivation through this technology. It is believed that many foregoing properties of EK technology are pertinent to application of external electric field; consequently generation of EKP which will be discussed in detail in the following sections.

2.1.1 Electrokinetic technology

Electrokinetic technology is based on operation of direct current (DC) within the contaminated matrix for removing pollutants through several physico–chemical reactions coined as electrokinetic phenomena (EKP) [30, 31]. External electric fields can be directly applied to the sludge matrices by the use of two charged electrodes (cathode and anode). Application of electric field involves three types of processes: *a*) Faradaic charge–transfer reactions, *b*) ohmic heating and *c*) electrokinetic phenomena.

2.1.1.1 Faradaic charge–transfer reactions

Faradaic reactions are oxidation or reduction reactions of electroactive species in solution [32]. For example, electrolysis is a Faradaic process where electrons are transported within the electrode–electrolyte interface leading to the transformation of chemical species [33]. Water undergoes both oxidation and reduction; therefore, in an aqueous solution electrolysis of water generates oxygen gas, hydrogen gas, as clearly evidenced by bubble generation [34], hydrogen ions (H^+) due to oxidation at the anode and hydroxyl (OH-) ions due to reduction at the cathode as shown by the following reactions.

At the anode side–oxygen evolution reaction (OER):

$$2\,H_2O \leftrightarrow\ O_2 \uparrow + 4H^+_{(aq)} +\ 4\,e^- \qquad\qquad E^0_R = 1 \cdot 229\,V \qquad\qquad [1]$$

At the cathode side–hydrogen evolution reaction (HER):

$$4\,H_2O + \ 4\,e^- \ \leftrightarrow \ 2\,H_2 \uparrow ^+ \ 4\,OH^-_{(aq)} \qquad E^0_R = -0.828V \qquad\qquad [2]$$
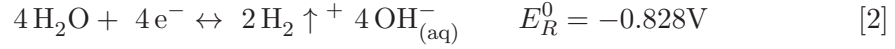
Essentially, acid is produced at the anode and alkaline is produced at the cathode; therefore, pH in the cathode is increased, while pH at the anode is decreased. The migration of H^+ from the anode and OH^- from the cathode leads to dynamic changes in pH during the initial stages of electric potential application [35]. Ultimately, H^+ ion will dominate the system chemistry since the ionic mobility of H^+ ions is 1.75 times that of the OH^- ions [36].

The rate of electrolysis reactions is related to the total current applied according to Farady's law. This can be calculated by following equation [37]:

$$J = \frac{I}{z_i F} \qquad\qquad (2.1)$$

where J = the rate of oxidation or reduction by electrolysis (MT^{-1}), I = the current (A), z = the charge of ion, F = Farady's constant (96,485 C/mole).

2.1.1.2   Ohmic heating

Ohmic heating also refereed to as electroconductive heating and Joule heating [38] is among the processes created due to passing a suitable intensity electrical current directly through the body of the material with sufficient water and electrolytes. The created heat is transferred by conduction mechanisms within and between bodies of matter and is then dissipated convectively. Ohmic heating brings about a fast and uniform means of heating liquids and particulates [39] via the transformation of electrical energy to thermal [38, 39]. Its associated energy equation in the liquid domain is presented by:

$$\rho C_p \left(\frac{\partial T}{\partial t} + v \cdot \nabla T \right) = \nabla \cdot \left[k_{(T)} \nabla \right] + \sigma_{(T)} E \cdot E \qquad\qquad (2.2)$$

where ρ = the density, C_P = the specific heat, T = the absolute temperature, t = the time, v the velocity vector of the electroosmosis flow (EOF), $k_{(T)}$ = the temperature–dependent thermal conductivity, $\sigma_{(T)}$ = the temperature–dependent electrical conductivity of the liquid and E = the intensity of the externally applied electric field [16]. The rate of produced heat is in direct correlation with field strength and constancy as well as the electrical conductivity [39, 40]. The electric field strength is adjustable through variation in the electrode distance or the applied electric field [40]. The electrical conductivity (κ or σ) of system's phases [39, 40] and its temperature dependence are the most governing factors of ohmic heating [40]. There are critical κ values below 0.01 S/m and above 10 S/m where ohmic heating is not feasible for the high voltage or amperage demand to generate the amount of heat needed to raise temperature substantially by the Joule effect, in case of very low or very large conductivity values, respectively [41, 42]. It is believed that ohmic heating results in destruction of microorganisms by a thermal effect and a mild electroporation mechanism [43]. The term "electrical breakdown" or "dielectric rupture"
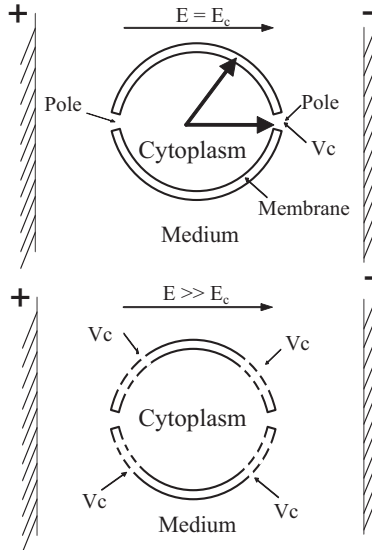
Figure 2.1: Schematic diagram of a cell exposed to the electric field intensity. The membrane potential V_m is created due to the external field. For membrane sites in perpendicular orientation to the field direction, the potential V_m is zero. The breakdown voltage V_c is hence first reached in field direction, E = E_c. It is only reached in membrane sites orientated at a certain angle to the field direction if supracritical field strengths (E $>>E_c$) are applied [44]

pertains to the primary event which subsequently leads to secondary alterations in the membrane characteristics (Figure 2.1) and changes in the cell interior [45]. A number of models have been suggested to explain the electrical breakdown, however the molecular mechanism leading to this event still has to be elucidated. One of the well–known is that the membrane can be presumed as a capacitor filled with a dielectric. External electric field created a membrane potential difference V across the membrane as a result of charge separation. Breakdown of the membrane and formation of transmembrane pores happens by a further increase in the external field strength. At supercritical field strengths or longer exposure times the size and number of pores become large in relation to the total membrane surface, irreversible breakdown and mechanical demolition of the cell takes place [44].

2.1.1.3 Electrokinetic phenomena

Electrokinetic is a generic term pertaining to the relative movement between two charged phases [46]. EKP are manifestations of the electrical properties of interfaces, which use electric fields to create forces that work on fluids or suspended particles and instigate them to move in astonishing ways [47]. These phenomea are often explained by the presence of the electric double layer (EDL), also called "electrical interfacial layer" [48]. The EDL is the spatial distribution of ions around the surface of a charged body (a solid particle, a gas bubble, a liquid droplet or a porous body) when it is placed in contact with an aqueous medium [47]. It is comprised of two parallel layers of charge: *a*) the first layer is the surface charge (either positive or negative); and *b*) the second layer forms from free ions in the fluid under the influence of electric attraction and thermal motion, and it electrically screens the first layer [49]. Electric double layer is generally the property of systems with a large ratio of surface area to volume, including colloid or porous bodies with particles or pores (respectively) on the scale of microns or even nanometers. Also, the electrochemical behavior of electrodes is based on EDL [50].

Electrokinetic phenomena arise from the differential migration of two phases of EDL due to shear off the mobile part [46, 50]. Among the several kinds of phe-

nomena that might take place four kinds: electrophoresis, electroosmosis, streaming potential and sedimentation potential are more frequently encountered [46].

- **Electrophoresis**: This is the motion of a charged surface or molecules, e.g., colloidal particle, relative to a stationary bulk liquid under the influence of an applied electric field [49]. Counter–ions of the surrounding bulk liquid are electrostatically attracted to the surface charge of the particle. As the particle moves through the liquid, the counter–ions travel in and out of the charged ion cloud or EDL surrounding the particle [46]. Figure 2.2 depicts a typical particle electrophoresis.
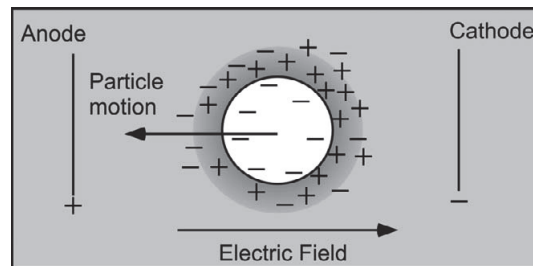
Figure 2.2: Electrophoresis of a charged particle in an external electric field [46]

- **Electroosmosis**: This shows the flow of the bulk liquid along a stationary charged surface under the influence of an applied electrical field [49]. A gra-
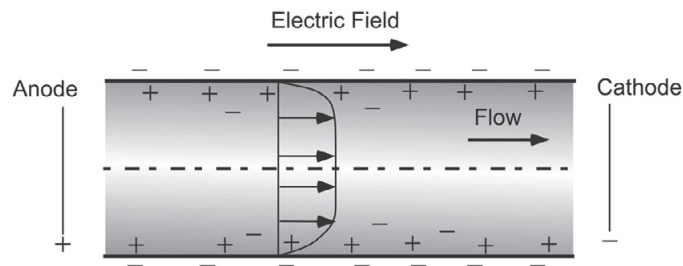
Figure 2.3: Electroosmotic flow in a capillary tube [46]

dient in electric potential applied peripheral to the electric double layer will create the mobile part of the EDL to move in the direction of the cathode or anode based on the polarity of the EDL. This electromigration of ions constituting the EDL results in viscous shearing of the adjacent bulk–liquid molecules, which eventually causes bulk–liquid motion [46]. Figure 2.3 rep-

resents a typical electroosmotic fluid flow in a capillary tube with negative charge.

- **Streaming potential**: A result of the electric field is generated when a bulk liquid is forced to flow past a charged surface. [49]. For instance, a streaming potential is set up when an electrolyte solution is pumped through a negatively charged capillary as shown in Figure 2.4 The streaming potential phenomenon is believed to be opposite of the electroosmosis [46].
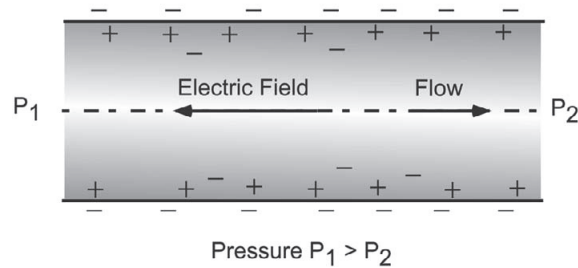
Figure 2.4: Development of streaming potential when an electrolyte is pumped through a capillary [46]

- **Sedimentation potential–Dorn effect or the migration potential**: This is the creation of an electric field due to migration of charged particles relative to a liquid [49]. The particles can move because of gravitational or centrifugal fields [46]. Figure 2.5 illustrates the sedimentation potential of a settling suspension of charged colloidal particles under the influence of a gravitational field.
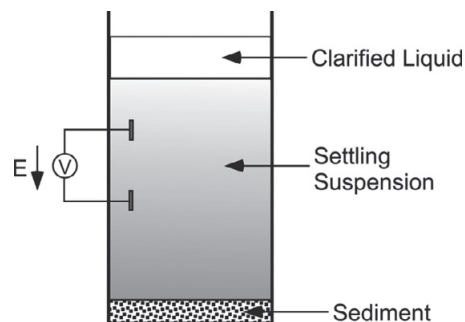
Figure 2.5: Sedimentation of charged colloidal particles under gravity setting up a sedimentation potential [46]

The overall performance of applied external electric field is determined by the com-

plex interplay of factors that may be optimized to achieve an effective treatment method. Some of these factors are as follows [51]:

- **Mass–transport regime**: It is a prominent factor in processes which are influenced by the solution velocity and agitation [52]. In general, a higher amount of mass–transport coefficient is found near the electrode surface [51].

- **Electrolysis medium**: The type of treated matrix and its ionic concentration, pH and temperature has great impact on the process [51]. Modifying electrolysis properties, e.g, adding iron, chlorine, manganese dioxide or using UV will enhance the treatment process.

- **Electrode materials**: The nature of the electrode material affects the selectivity and the efficacy of the process. The suitable electrode material should be economical, stable in electrolyte, with high activity for the desired purpose and low activity toward secondary reactions [51]. The choice of electrode material greatly depends on the useful potential range of the electrode in the particular electrolyte and purity of the material [32]. Solid metals including platinum, gold and stainless steel are among the most used material for electrodes. A common benefit of metal electrodes is that their high conductivity results in low background currents; however, they undergo corrosion or passivation, formation of a salt film on the surface, and other reactions. Carbon electrodes have high surface activity, nevertheless their electrochemical reactions are normally slower than metallic electrodes. This group of electrodes are very pH–sensitive due to formation of hydrogen, hydroxyl and carboxyl bonds. Different forms of carbon are employed as electrodes including glassy carbon, carbon fibers, carbon black, various forms of graphite and carbon paste [32, 51].

- **Reactor design**: The reactor dimension, design of electrodes and arrangement of electrodes in the reactor influence the eminent features of the process [51].

- **Current distribution**: It determines the spatial distribution of the consump-

13

tion of reactants [51]. Current distribution depends on the resistance of the solution and the strength of the current passing through it [53]. The electric field intensity vector, E (V/m), is defined as equation 1.7 [54]:

$$E = -\Delta\phi \qquad (2.3)$$

where ϕ = the electric potential (V). For steady state conditions, the electric field distribution is defined as follows [54]:

$$0 = -\Delta^2\phi \qquad (2.4)$$

- **Electrode potential and current density**: Important in controlling the type and rate of reactions which occur [55]. Electric current can be used to create 1D or 2D electric fields. For example, a 1D electric field could be generated using electrical sheets or non same–polarity electrodes in front of one another, while a 2D field is generally produced by square or hexagonal configuration in which one cathode is located in the center and four (possibility eight) anodes are surrounding the cathode. Electrode layout influences the distribution of electric fields [10, 56]. Considering the electric field distributions, the ineffective area for 1D or 2D reactors is in the shape of a curvilinear triangle, which its base is the distance between electrodes of the same–polarity. The height of it depends on processing time, electrode spacing and alignment [57]. Figure 2.6 depicts approximate distributions of the resulting inactive spots for 1D and 2D configurations.

Few experiments have been performed to use electric current as a killing agent [58]; however the standardizing of the procedures has incurred impediments related to the nonhomogeneous experimental conditions [32], and several factors that must simultaneously be taken into consideration (e.g., electric field intensity, current density, possible electrode use, medium composition, type of microorganism, physiological state of the microbial population and duration of treatment) [59, 60].
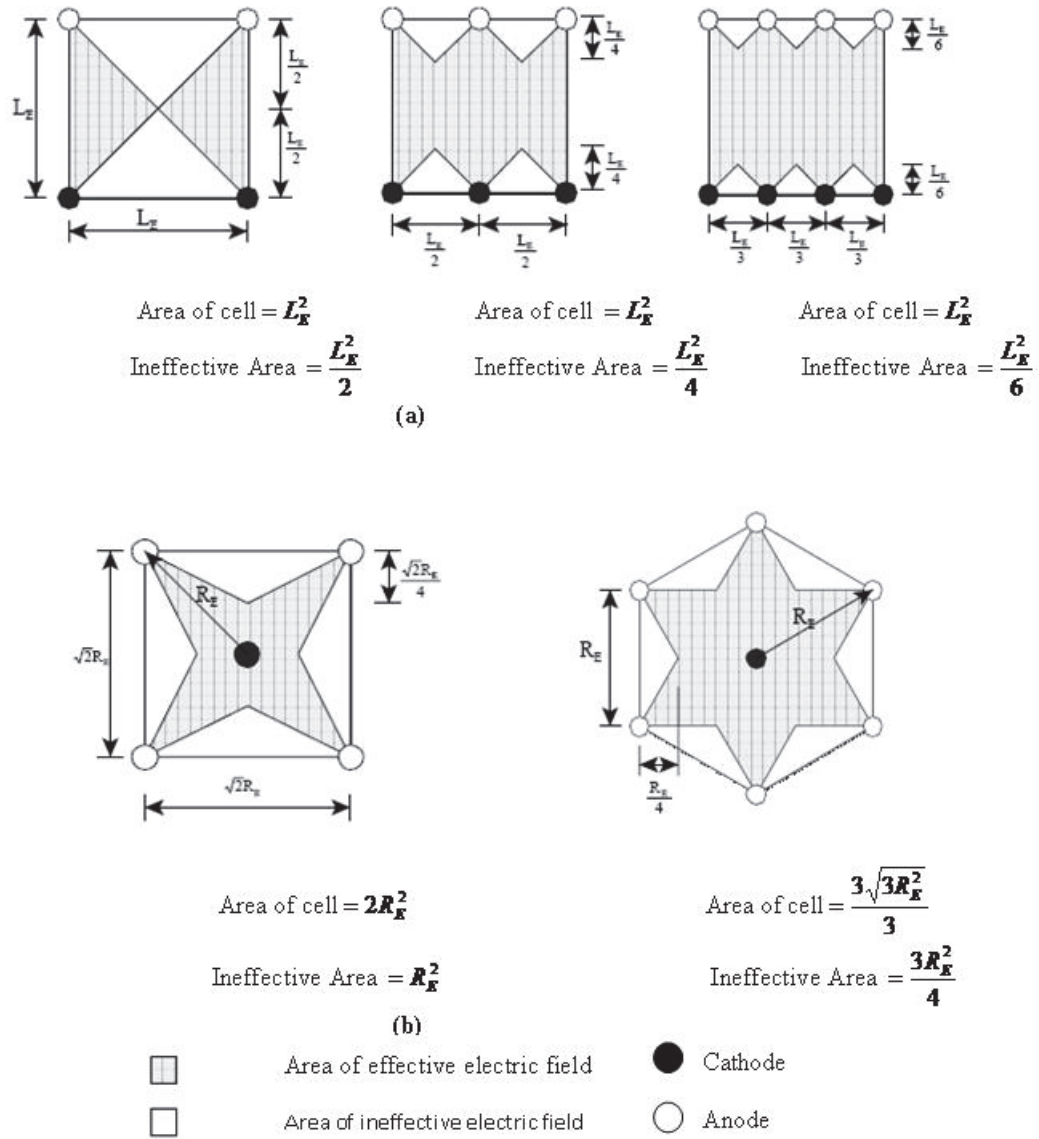
Figure 2.6: Approximate evaluation of ineffective areas for (a) 1D and (b) 2D electrode configurations [57]

Besides aforementioned factors, the medium composition and microorganism to be treated play an eminent role in efficiency of EK disinfection treatment. Therefore, some important characteristics of anaerobic digestion (AnD) biosolids and the bioindicator microorganism to be treated will be discussed in great detail henceforth.

2.1.2   Overview of source and characteristics of biosolids

Untreated wastewater comprises suspended solids, dissolved organic matter, insoluble trace elements and nutrients [8, 61]. In the process of wastewater treatment (WWT), solids are recovered from wastewater to generate what is identified as biosolids [62]. The physical and chemical characteristics of the biosolids alter from different places based on the residents and industrial sector served [61], degree of segregation between storm water and sanitary wastes, land applications, groundwater levels and treatments which it goes through [63]. It has been proven that biosolids has a high amount of both organic matter and important plant nutrients [5] and can act as a soil fertilizer via the contribution of organic matter [8]. Some early civilizations used their human waste for land application and soil amendment [3]; however, by increasing populations, beneficial use of waste was replaced with dumping this valuable source of nutrients into streams and rivers [3, 64]. Over the past decade increased public concern for environmental pollution of oceans, waterways and air has brought about the increase in beneficial application of biosolids once again [64]. Although biosolids is comprised of valuable nutrients, it also contains pathogenic organisms and pollutants, which are sources of concern for human health and the accumulation of toxic substances in soils [65]. Therefore, they must be protected from contamination and treated to avoid risks and be used safely in accordance with good practice [2].

According to regulations on the land application of biosolids released by government agencies worldwide biosolids must undergo proper treatment(s), referred to as "stabilization" processes and meet restricted criteria before applied to the land [65, 66]. Biosolids regulations generally specify limits on components applicable to environmental and human health protection including pollutant concentrations, the attraction of potential pathogen vectors and pathogens or indicator microorganism density [65]. These regulations typically classify biosolids as high or low quality based on meeting recommended trace element and pathogen quality standards as well as process requirements for pathogen and vector attraction reduc-

tion [8]. The pathogen standards identify two main levels of biosolids disinfection: P_1 in Québec classification (Class A in USEPA) and P_2 (Class B) biosolids [7, 65]. P_1 biosolids compel elimination of fecal coliform to less than 1,000 most probable number (MPN)/g TS or reduction of *Salmonella* spp. to non–detectable levels according to Bureau de normalisation du Québec (BNQ) standards [7]. It is also tentatively suggested that spores of *C. perfringens* should not be more than 3,000/g TS [6].

The process of biosolids treatment essentially involves a combination of several methods including [5]:

- Adjustment of pH (alkaline stabilization),
- Composting,
- Heat drying,
- Digestion.

Adding alkaline materials to raise the pH level is one of the stabilization methods which make conditions unsuitable for the growth of most of organisms [67]. Variation of alkaline stabilization processes can be used to produce either Class A or Class B disinfection [68]. Class A requirements can be accomplished either when the pH of mixture is retained above 12 for 72 hours, with a temperature of 52°C maintained for 12 hours for the same period of time [67] or by maintaining temperatures at or above 70°C for 30 minutes, while retaining the pH requirement of 12 [69].

Composting is another method for treating biosolids to generate Class A biosolids [70]. It is described as a function of microbial activity and can be determined by O_2 uptake rate, CO_2 production rate, or by the heat produced [71]. Three methods of composting wastewater residuals are common [70]. Each method is comprised of mixing dewatered wastewater solids with a bulking agent to supply carbon source and provide porosity. During the "active composting" period the temperature of mixture rises [72, 73]. The required temperatures that must be achieved and maintained for efficacious composting differ according to the method and the end product application [70].

17

Heat drying, in which heat from a direct or indirect source is applied to evaporate moisture from wastewater solids, is one of the means that can be employed to decrease the volume and better the quality of biosolids [74].

Digestion is the process of biochemical decomposition of organic solids to simpler and more stable substances [72, 75, 76]. It decreases the total mass of solids, obliterates pathogens and facilitates dewatering process of biosolids [72]. Biosolids digestion may be performed under aerobic or anaerobic conditions [76]. Aerobic digestion is comparable to the activated sludge process and usually applied in small, package–activated biosolids treatment systems [75]. During the aerobic digestion biosolids are aerated for 20 days or more to stabilize organic matter, reduce the volume and eliminate pathogens [76, 77]. Anaerobic digestion can be applied for the same purpose as aerobic digestion [75, 76]. However, it is mostly specific to large waste water treatment plants (WWTPs) [76, 77].

2.1.2.1 Anaerobically digested biosolids

Anaerobic digestion is a series of naturally occurring processes in which a number of families of anaerobic bacteria working in an assembly–line fashion to break down biodegradable material into methane (CH_4) and carbon dioxide (CO_2) (a mixture called biogas) in an oxygen free environment [78, 79]. Furthermore, the AnD process generates a stabilized liquid effluent (so–called digestate) that contains all the water, all the minerals and approximately half of the carbon from the incoming materials and can be used as soil conditioner to fertilize land [72]. Theoretically, AnD process can be split into three separate steps performed by five groups of microorganisms [78, 79]:

- **Hydrolysis, liquefaction and fermentation**: During which the proteins, cellulose, lipids, and other complex organics are converted to a size and form that can pass throughout bacterial cell walls [80]. Basically, no organic waste stabilization takes place during hydrolysis [78, 80]; it is needed that the organic matter is converted into a soluble form that can be used by the bacteria in the

next stage of treatment [79]. Hydrolysis and liquefaction are achieved through extracellular, hydrolytic enzymes generated [78, 80].

- **Volatile acid fermentation**: Upon hydrolysis of complex organics, they are converted through biochemical reactions to long chain, amino acids, sugars, organic acids and ultimately to smaller organic acids, e.g., propionic–, butyric–, and valeric–acid [78, 79]. Hydrogen plays an important role in controlling organic acid generation and consumption [78]. By increasing the partial pressure of hydrogen above 10^4 atm, methane production is hindered and the concentration of organic acids will surge [81].

- **Methane formation**: It is in this stage of the process that waste stabilization happens via conversion of the acetic acid into CH_4, a water insoluble gas which readily separates from the sludge and leaves the system [78]. The action of "methanogenic bacteria" also produces carbon dioxide [78, 80] which either escapes as gas or is converted to bicarbonate alkalinity [78], hydrogen sulfide (H_2S), nitrogen gas (N_2) and several other gases [74, 82]. The methanogenic bacteria are strictly anaerobic, and even low amounts of oxygen are detrimental to them [80].

Anaerobic digestion can be performed at two temperature regimes: mesophilic temperatures ($\approx 35°C$) and thermophilic temperatures ranging from 55 to 70°C [77]. Conventional AnD is accomplished at mesophilic temperatures, mostly due to the lower energy prerequisites and better stability of the process [83].

Pathogen reduction is an imperative characteristic of the anaerobic process [79, 84]. The level of disinfection attained by a particular anaerobic digester is affected by a range of interacting operational factors and conditions [85]. Mesophilic treatment is mainly used as a stabilizing process rather than a method of disinfecting [86]. Pathogen inactivation studies reveal that *E. coli* and *Salmonella* spp. are not injured by mesophilic temperatures, while rapid inactivation occurs by thermophilic digestion [6, 85].

A large group of pathogens are inactivated at temperatures higher than 70°C over a relatively short duration of time [79]. However, some that have further evolved structures as a means of survival in adverse conditions require higher temperatures for a complete kill [1]. Some worms, e.g., *Taenia* spp. and *Ascaris* spp. have developed an egg stage as a natural way to survive [6, 87]. Pathogenic protozoa such as *Cryptosporidium* and *Giardia* have evolved a cyst stage for the same reason [79]. Clostridium and Bacillus are the two most prominent types of endospore–forming bacteria. In this stage microorganisms are tremendously resistant to the stresses of the ambient environment [6]. Enteric viruses are another group of pathogens that show high resistance to inactivation [88]. The above mentioned groups of pathogens plus emerging bacteria such as *E. coli* O157:H7 and *Helicobacter pylori* are among pathogens of concern to evaluate the efficiency of biosolids treatment method [88, 89].

2.1.3   Studies on indicators in biosolids

Given a wide array of pathogens that might be found in biosolids [1], and also due to the innate restraints related to pathogen monitoring, indicator organisms are used as surrogates for pathogens [90]. Indicator organisms are selected groups of microorganisms believed to indicate the possibility of the presence of special case pathogens [10]. Several criteria governing the selection of indicator microorganisms such as: *a*) both the indicator and pathogenic organisms should respond to physical treatment and disinfection in a similar way, or else the indicator should conservatively be harder to treat; *b*) the indicator's detection method should be easy, and *c*) the indicator microorganism should be present at concentrations high enough to allow log reduction calculations to be executed [91]. In the 1970s, US environmental protection agency (USEPA) regulations recognized *Ascaris* eggs as the parasite indicator organism in biosolids, due to the ability to survive in very harsh environmental conditions, and to the easy recognition because of their size [1, 92]; however, a concern with using *Ascaris* eggs as indicator microorganims is that their existence in biosolids is not ubiquitous, as a result of a variable geographic distribution [92].

Furthermore, current regulations lack a timely procedure to monitor indirectly for the inactivation of *Ascaris* eggs, and instated *Ascaris* inactivation is employed to ascertain whether or not a disinfection method produces Class A biosolids [1]. The direct method of assessing *Ascaris* ova inactivation currently needs separating the eggs from biosolids, culturing them for three to four weeks and then inspecting the ova microscopically for viability [92]. This method is time–consuming and expensive [1, 92]. In addition, it has been found that *Ascaris* sp. considered by many investigators to be the most challenging organism to destroy, could be killed at 53°C in the period of 30 minutes [93]. *C. perfringens* spore has been proposed as another possible indicator organism to assess the efficiency of biosolids treatment methods and a good indicator organism for *Ascaris* inactivation by anaerobic digestion [1, 94]. It can be found in densities of 10^6 colony–forming units (CFUs)/g solids in raw or untreated biosolids [95].

2.1.3.1 Microbiology of *C. perfringens* spore

C. perfringens is a Gram–positive, endspore–forming, rod–shaped, non motile and anaerobic bacterium that can tolerate only 5 percent of oxygen, and is known to be the most widely distributed pathogen in nature [96, 97, 98]. It ferments lactose, sucrose and inositol with the production of gas, reduces sulfite to H_2S, hydrolyzes gelatin, reduces nitrate, and produces lecithinase and acid phosphatase [99]. *C. perfringens* is a ubiquitous organism and a normal flora of human and animal gastrointestinal (GI) tract. Its population in a healthy human is $<10^3$–10^5 CFU/ g feces, whereas a person with *C. perfringens* food poisoning has counts of 10^3–10^6 CFU/ g of feces [96]. This pathogen has the fastest growth rate of all microorganisms with a duplication time of 6.3–6.6 minutes at 43–47°C [100, 101, 102].

During extreme conditions, *C. perfringens* undergoes a differentiation process (in seven stages) and forms single oval subterminal spores with a diameter of $<1\mu$m [103, 104]. The endspore is a highly refractile body produced within the mother cell [103] with complex multi–layered structures that contain a spore coat and a cortex [105, 106]. The spore coat prevents penetration of chemicals into the cortex. Inside the

spore (in the core) there exists protein, deoxyribonucleic acid (DNA), ribonucleic acid (RNA), dipicolinic acid (DPA) (pyridine–2,6–dicarboxylic acid) and divalent cations [107]. Spore DNA is extremely protected against various sorts of damage via the saturation of the spore chromosome with small, acid–soluble proteins (SASPs) [108]. Also, the low amount of water in the spore contributes to its ability to survive under harsh conditions [107].

Spores are resistance to heat, drying, UV radiation and chemical disinfectants which would kill the vegetative cell [109]. Decimal reduction time at 100°C ($D_{100°C}$) varies between strains from 0.31 to >150 minutes [96].

It has been revealed that *C. perfringens* spores exposed to a five mg/L of free chlorine for four hours were inactivated only about 1.5 LR, while an electrochemically generated solution of mixed oxidants, at the amount of five mg/L, inactivated *C. perfringens* spores in pH 7 buffered water at 25°C, with 2.3 LR within the same period of time [110].

2.2 Interactive disinfection and provoking combination of stressors

It is presumed that disinfection effect of EEK is attributed to: *a*) a synergism between treatment parameters, e.g., electric field and enhancement agents, and *b*) application of multiples stressors. Multiple disinfectants have been employed with increasing frequency in recent years. Reports demonstrated that the application of combined disinfectants is more effective, e.g., for inactivating *Cryptosporidium*, than the added effect of the individual disinfectants [111, 112]. The researchers hypothesize that disinfection effect of combined disinfectants is due to a potential synergistic mechanism and generation of multiple stressors. The type of interactive effect can be determined using the mathematical model developed by [113, 114] and modified for disinfection kinetics by [115].

$$\sum_{i=1}^{n} \frac{x_i}{y_i} = 1 \qquad (2.5)$$

where x_i = concentration of the individual agent in the combination, y_i = concentration of the agents that individually would produce the same magnitude of effect as that of the combination, i = individual agent, n = total number of agents. When the sum is less than 1, it shows the synergistic interaction.

It is believed that for a disinfection technology to perform sufficiently, it must apply multiple stressors that result in several log reductions (LRs) for organisms including bacteria, viruses, worms and protozoa [93, 116]. The key stressors can be divided in three groups: physical, chemical and biological stressors [116, 117].

2.2.1 Effect of physical stressors on microorganisms

The most important physical agents are ionization radiation [118, 119], UV radiation [119], moist heat [118, 119], dry heat, inactivation by cold [120], desiccation, ultrasound [117] and hydrostatic pressure [121].

Ionization radiation is presumed to create single– or double–stranded breaks of DNA in the cell [122]; however, studies show that single–strand scission in spores may repair during post irradiation germination [123].

By exposing vegetative bacterial cells to UV light, thymine dimers are produced between adjacent thymine molecules in the same strand of DNA [124]. Other dimers are also likely to be formed, including a uracil–thymine heterodimer [120]. The induction of dimers is sufficient to explain the lethal nature of UV radiation. However, some bacteria are able to repair this damage [124]. Spore resistance to UV radiation is related to α, β–type SASPs, which protect DNA [125], and also the ability of the spore to remove 5–thyminyl–5,6 dihyrothymine (TDHT), thymine–containing photoproducts [126].

The moist heat causes RNA and DNA breakdown, scission of low–molecular–weight material, protein coagulation and changes in the shape of the cell [127]. The release of intracellular constituents and loss of DPA and calcium has been observed in bacterial spores exposed to lethal heat [120]. The water content of the spore has been shown to be a controlling factor in the spore's sensitivity to moist heat [128].

Dry heat is a much less efficient process than moist heat. Thus a much higher

temperature for a longer period of time is needed [120].

Cold shock, a process in which organisms are suddenly chilled without freezing, causes death of Gram–positive and Gram–negative bacteria but not yeasts [124].

Hydrostatic pressure has inactivation effects on vegetative cells and spores. Studies by Sale et al. (1970) showed that, within a certain pressure range and depending on the type of spore, increasing pressure reduces the survivors. Above this pressure range, increasing pressure has a reduced effect on inactivation [129]. The mechanism of action of pressure on spores is due to induction of germinate, and the germinate cells are then inactivated by other factors, e.g., temperature [130, 131]. Dipicolinic acid, calcium and hexosamine–containing material are freed from pressurized spores, and it becomes phase bright [129].

2.2.2 Effect of chemical stressors on microorganisms

The chemical stressors are those that are not generated by biological activity but are either added directly or produced via chemical reactions [117]. In this group are pH, oxidants and non–charged disinfectants such as nitrous acid and PAA [132]. Alkaline treatment, lime stabilization, ferrate (VI) oxidation [133], ozonation and chlorination are some treatments based on chemical stressors [116, 134]. Although an enormous amount of time and endeavour has been spent examining the impacts of chemical agents, the exact mechanism of action of many biocidal compounds still is unclear [120]. Different chemical groups such as alcohols, aldehydes, anilides, biguanides, peroxygens, quaternary ammonium compounds (QACs), etc. have been examined for their biocidal activity [106]. Studies on mechanisms of disinfection of these chemicals show that, whatever the type of microbial cell, most likely the inactivation procedure all follow a sequence of similar events [135]. This can be pictured as interaction of the disinfectant with the cell membrane, followed by penetration into the cell and action at the target site(s) [105]. As an example, GTA is a dialdehyde which has been used as a disinfectant since 1964 [105, 106]. Low concentrations (0.1%) of the GTA have inhibitory effects on germination, while much higher concentrations (2%) are sporicidal [136]. Its mechanism of action engages a strong

24

reaction with unprotonated amines on the cell surface [105]. The bacterial spore shows several sites at which interaction with GTA is likely; however, the interaction with a particular site does not necessarily lead to spore inactivation [137]. High concentrations of free ammonia at elevated pH have been presented to contribute to the inactivation of viruses and *Ascaris* ova [138, 139].

Peroxygens are another important group of chemical compounds applied as disinfectants [105, 106]. Peracetic acid (CH_3CO_3H) and hydrogen peroxide (HP) are two important peroxygens [106]. HP is an oxidant due to generation of hydroxyl free radicals ($^\bullet OH$) which attack critical cell constituents such as lipids, proteins and DNA in sulfhydryl groups and double bonds [105]. Peracetic acid is a more potent biocide than HP, showing sporicidal, bactericidal, virucidal and fungicidal activity at low concentrations (0.3%) [120]. Decomposition of PAA produces safe end–products such as acetic acid and oxygen [105]. Using electron spin resonance (ESR) and spin trapping (ST) to examine radical production of PAA and with relating radical production to the bacterial killing effect, it is presumed that PAA denatures proteins and enzymes and increases cell wall permeability by disturbing sulfhydryl (–SH) and sulfur (S–S) bonds [140]. A new compound with the trade name of BIOXY S^{TM} (BS) is a non–hazard way of producing PAA in a more stable form. BS is a biocide and strong oxidant composed of sodium percarbonate (a hydrogen peroxide (HP) precursor), tetraacetyl ethylene diamine (TAED) (peracid precursor) and sequestrants [141]. It has stronger oxidation potential than chlorine or chlorine dioxide [142] with neither corrosive effect nor formation of disinfection by–products (DBPs). Upon dissolving the BS in water, TAED, in presence of HP, undergoes fast perhydrolysis producing PAA and diacetyl ethylene diamine (DAED). Two molecules of PAA are released by nuclophilic attack of the OOH$^-$ ions on the instable imide bonds of the TAED molecules [141]. The reaction is a stepwise process through the intermediate Triacetylethylenediamine (TriAED). Studies show that TriAED only exists for a short time, and almost all TAED is transformed to

DAED which is readily biodegradable [143]. The reaction steps are as follows [144]:

$$H_2O + C_2H_6Na_4O_{12} \rightarrow 3\,H_2O_2 + 2\,Na_2(CO_3)HO \qquad [3]$$

$$H_2O_2 \leftrightarrow H^+ + OOH^- \xrightarrow{OH^-} H_2O + OOH^- \qquad [4]$$

$$C_{10}H_{16}N_2O_4 + OOH^- \rightarrow 2\,C_2H_4O_3 + C_6H_{12}N_2O_2 \qquad [5]$$

$$2\,C_2H_4O_3 \rightarrow 2\,C_2H_4O_3 + O_2 \qquad [6]$$
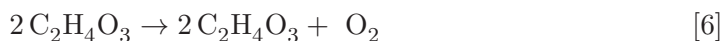
It is envisaged from the above reaction scheme that disinfection effect of BS is related to the available amount of sodium percarbonate, TAED and PAA.

2.2.3 Effect of biological stressors on microorganisms

The biological stressors can be grouped in two categories: *a*) biochemical byproducts of biological activity, such as ammonia, amines, organic acids, aldehydes, and ketones *b*) changes in physiological state of resistance cells, e.g., germination of spores, which make microorganisms more prone to harsh environmental conditions. Some of the treatment methods such as aerobic digestion, anaerobic digestion, composting, pulsed electric field (PEF) and high pressure and high temperature (HPHT) make use of biological stressors.

2.2.4 Mechanisms of disinfection and bacterial resistance to disinfectants

Disinfection is defined as "killing of pathogenic agents by chemical or physical means directly applied" [120]. Spaulding (1968) suggested three levels of disinfection action as: *1*) high–level (e.g., sporicidal) *2*) intermediate–level which kill vegetative cells, most viruses and some spores, *3*) low–level, which kill only vegetative cells and some

viruses [120]. Generally disinfectants target a range of cellular loci classified in three broad regions: *1*) the cell wall, *2*) cytoplasmic membrane (respiratory functions) and *3*) cytoplasm (enzymes and the genetic material) [145, 146]. Various bacteria respond to bactericides in different ways. This is either because of intrinsic differences such as unique cell envelope components and non-susceptible proteins or due to the development of resistance [147] created by adaptation or genetic exchange [145]. The nature and mechanism of the interaction between microorganisms and disinfectants has an important role in the kinetics of inactivation (Figure 2.7) [145, 147]. Knowledge about these interactions assists us in understanding the linear, concave, convex or combined behavior in semi–log inactivation curves, and, therefore, the kinetics of inactivation [148].
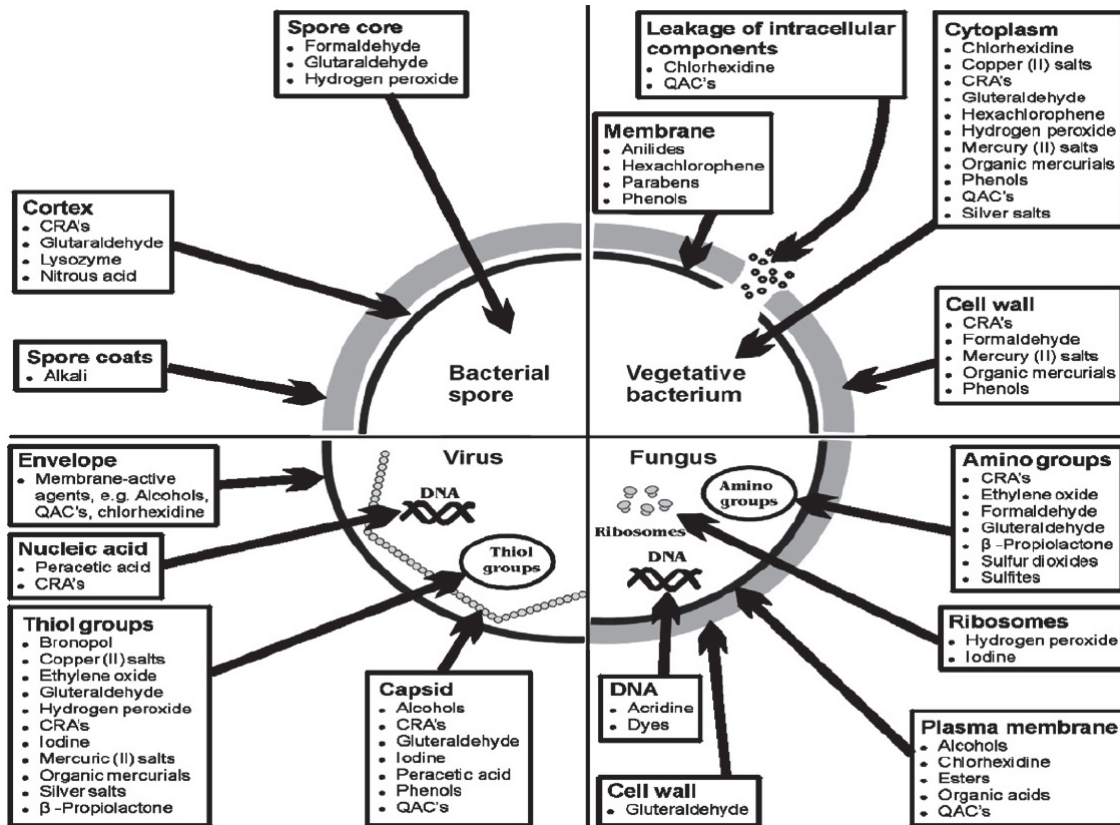
Figure 2.7: Mechanism of action of biocides on microorganisms [145]

2.2.4.1   Mechanisms of action of disinfectants

Defining the exact mechanism of action of a chemical, physical or biological stressors is not an easy task if not impossible. This could be due to the fact that more than one cell component may be influenced, and subsequently the problem is to differentiate the primary effect from the secondary effects, which may, though, contribute to cell death [120]. In general, cellular morphology and chemical composition, growth phase, extra–cellular substances and the nature of disinfection process are among the most imperative features that influence the access of disinfectant to cell wall, cytoplasmic membrane and cytoplasm [146]. Interaction of the disinfectant with the cell surface followed by penetration into the cell and action at the target site are the key mechanisms of disinfection [149]; however, they are not instantaneous and can be influenced by factors such as environmental conditions (e.g., temperature, pH, humidity, etc), type of microorganism and biocide concentrations [146]. Therefore, external factors may profoundly affect the kinetics and extent of inactivation without necessarily invoking direct consequences on the disinfection mechanism [150]. The target sites are usually located at the cell envelope or within the cytoplasmic region of the cell [151]. Cytoplasmic membrane, which has a rich matrix of phospholipids and enzymatic/structural proteins, control the selective permeability and the maintenance of intracellular homeostasis and vectorial transport/metabolism [146]. These vital functions and the large expanse for interaction make the cytoplasmic membrane more prone to biocide assault [146, 151]. Interaction at the cell membrane can cause a considerable effect on viability; however, most disinfectants seem to be active intracellularly [105]. Thus, maintenance of the folding proteins and the integrity of DNA are other important factors for cell survival [152]. Biocide chemistry and mode of action also changes the magnitude or rate of penetration of biocide through the cell envelope and damage to the cell [146, 148].

Although each disinfection process has its own precise mechanism of interaction, the ultimate outcomes present considerable similarity. The main observed damages are:

a) disruption of the transmembrane proton motive force leading to an un-coupling of oxidative phosphorylation and inhibition of active transport across the membrane, *b*) inhibition of respiration or catabolic/anabolic reactions, *c*) disruption of replication, *d*) loss of membrane integrity resulting in leakage of essential intracellular constituents such as potassium cation, inorganic phosphate, pentoses, nucleotides and nucleosides and proteins, *e*) lysis, *f*) coagulation of intracellular material [146].

The order of these injuries shows the increasing severity of damage from bacteriostatic to bactericidal [146]. Conventional theory revealed that death of a cell can arise from initial lesions if inimical condition last for sufficient duration or amount [153].

Studies on bacterial spores illustrate that disinfectants can be sporostatic but are not inevitably sporicidal [105]. Only a few antibacterial agents are actively sporicidal and even powerful disinfectants may be sporostatic, rather than sporicidal [105, 106]. Power and Russell (1989) demonstrated that 2 percent alkaline GTA sterilizes an inoculum of 10^8 CFU/mL of vegetative cells of *B. subtilis*, *E. coli* and *Staphylococcus aureus* within 10 minutes at 22°C, while *B. subtilis* spores entail several hours [154]. These fundings suggest that the efficiency of treatment is very much affected by the physiological state cell and its resistivity.

2.2.4.2   Bacterial resistance to biocides

Bacterial resistance has been described as the temporary or permanent ability of an organism and its progeny [145] to withstand the effect of biocides that are intended to destroy or control them [155]. Several mechanisms which bestow bacterial resistance to biocides are: *a*) alteration of the target [156, 157], *b*) reduction in target access [156, 158] and *c*) inactivation of the inhibitor [156, 159]. These resistance mechanisms can be obtained through intrinsic structural features of a microorganism [147, 160], or by selective mutations and/or via the acquisition of genetic material which encodes resistance mechanisms from another microorganism [155, 161].

2.2.4.3 Intrinsic resistance of bacterial spores

Intrinsic resistance is a natural, chromosomally managed characteristic of a bacterial cell that allows the cell to circumvent the action of a biocide [105, 161]. The most well known intrinsic resistance mechanism is changes in the permeability of the cell wall, also signified as "permeability barrier" [155, 161], which not only exists in spores, but also in vegetative bacteria, e.g., mycobacteria and Gram–negative bacteria [145, 161]. It has also been shown that changes in other constituents of the outer membrane ultrastructure such as proteins [162], fatty acid composition [163] and phospholipids decreases biocide efficiency [155].

In addition, the charge property of the cell surface plays an important role in bacterial resistance mechanisms to positively charged biocides, for example QACs [155, 164].

Sporulation, the process of conversion of vegetative cell into a spore, is another important form of intrinsic resistance which involves seven stages (Table 2.1) [105].

Table 2.1: Stages of sporulation process [165]

1	Initiation;
2	Pre–sporulation phase: DNA as an axial filament;
3	Septation:asymmetric cell formation;
4	Cortex formation between inner and outer forespore membranes commences;
5	Synthesis of spore coats and DPA: uptake of Ca^{2+};
6	Spore maturation: coat material becomes more dense, refractivity increases;
7	Lysis of mother cell and liberation of mature spore.

During this process, the vegetative cell (stage 0) goes through the first morphological changes [165] that culminate in the generation of the mother cell (stage I, II) [105]. Then (stage III), DNA is divided into two complete copies. The inner, forespore, section is surrounded by its membrane, which is in turn enclosed by a second membrane of opposite polarity [165]. Next, peptidoglycan is laid down (stage IV) between the outer (mother cell) membrane and inner membrane to form the cortex, a specialized peptidoglycan comprises of a spore–specific muramic lac-

tam [105, 166]. DPA is generated inside the developing spore, and calcium enters from the outside by active transport [167]. As calcium enters the spore, water is removed [105]. A protein coat is synthesized exterior to the cortex and ultimately assembled around the outer surface of the spore [105, 165]. The spore becomes mature at this stage (stage V) [167]. Some spores form an additional layer called the exosporium [165]. The mature spore becomes increasingly phase–bright and resistance to heat (stage VI) [105]. Finally, lytic enzymes destroy the mother cell compartment (stage VII) [167].

The ultimate product of the sporulation process is a mature, resistant spore [165]. The heat resistance of the spore is considered to be the result of the low water activity in the spore core [168]. The spore cortex has an important function in the dehydration of the core through applying physical or osmotic pressure [165] or possibly both [169, 170]. Calcium dipicolinate also plays a role in heat resistance; however its function is not clear yet [165]. There is a possibility that it acts as a secondary stabilizing agent [171]. Spore DNA is particularly well shielded against many diverse categories of damage, especially UV light, through the saturation of the spore chromosome with a group of DNA–binding proteins named α and β–SASPs, synthesized in the forespore [108, 171]. The spore coat layers are not necessary for dormancy or heat resistance, nevertheless they are imperative in the resistance of the spore to enzymatic attack [172].

The dormancy and resistance properties of the bacterial spore are extraordinary for a living cell [165]. They are invariably the most resistant of all types of bacteria [166] to desiccation, organic chemicals, enzyme action, UV irradiation and extremes of temperature and pH [173], which may remain dormant for extended periods [166]. This comportment is due to substantial structural specialization developed within a mother cell [165].

A typical bacterial spore is a complex system, that is composed of several different layers (Figure 2.8) [175, 176]. The interior–most compartment of the spore houses RNA, DNA and DPA [105], a significant amount of SASPs [105, 166], calcium, potassium, manganese and phosphorus which can be found in the spore [105].
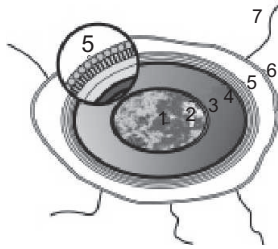
Figure 2.8: Typical bacterial spore structure. Structure of a *Bacillus* spore: spore core (1), inner membrane (2), cortex (3), outer membrane (4), spore coat (5), exosporium (6), and appendages (7) [174]

This compartment is surrounded by the cortex outside which are two membrane layers (the inner and denser outer spore coats) [106] stemmed from the septum formed at the commencement of sporulation [166]. Some types of spores contain a thin exosporium at the outermost layer too [105].

Biochemical studies show that the coat is mainly composed of proteins [105, 177], around 30 protein species which do not resemble one another [166], a low amount of lipids and carbohydrates [177]. The inner coat contains an alkali–soluble part built up of acidic polypeptides [105], which can be degraded to their unit parts via treatment with sodium dodecyl sulfate (SDS) [106]. An alkali–resistant fraction related to the presence of disulfide–rich bonds being found in the outer coat [178]. These features show that the role of spore coats and essential resistance factors in the interior of the spores is critical in protecting spores from a wide range of assaults [100, 105, 177].

All types of spores are not equally insusceptible to biocides [160]. Spores of *Bacillus* and *Clostridium* species are strikingly resistant to extreme environmental conditions, therefore, in many cases play as surrogate for *Giardia* cysts and *Cryptosporidium* oocysts [173]. Studies on the pattern of morphological and biochemical changes occurring during sporulation and its relationship with disinfection resistance divulge that resistance may be an early, intermediate or (very) late event [105, 160]. For example, an early resistance ensues to formaldehyde, whereas resistance to heat is an intermediate event, and GTA resistance being a late occurrence (Figure 2.9) [160].
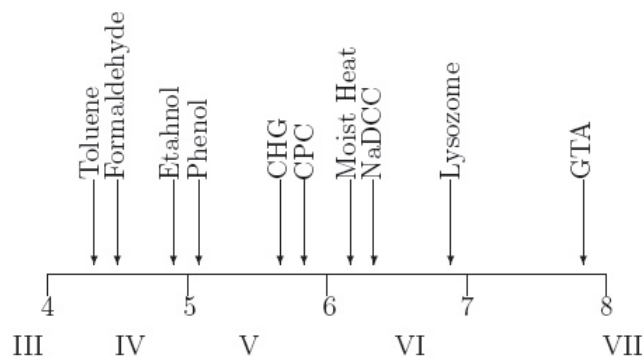
Figure 2.9: Development of resistance of *Bacillus subtilis* during sporulation. Roman numerals show the sporulation stage from III to VII. Arabic numbers represent the time (hours) following the onset of sporulation and the approximate times at which resistance develops against biocides. CHG, chlorhexidine; CPC, cetylpyridinium chloride; NaDCC, sodium dichloroisocyanurate [105]

Although resistance to harsh environmental condition and being metabolically latent, the spores can return to the active life in as little as 20 minutes via spore outgrowth and germination [179] which is of the utmost importance for sterilization methods and research for: *i*) spores provoke disease via germination and outgrowth in foodstuffs or in the body, and *ii*) germinated spores are eminently less invulnerable to different kinds of environmental stress than dormant spores are [180, 181]. Therefore, if a means could be found to effectively use the germination–inducing properties of spore, then the treatment processes could be carried out at a lower temperature or chemical concentrations with concomitant savings in both energy costs and product quality.

2.2.4.4   Spore germination characteristics

Spore germination is mainly a biophysical and degradative process. It is a series of events (activation, outgrowth and germination) leading to the loss of the spore–specific properties [179, 182] (Figure 2.10). One theory to describe the germination–associated alterations is that the first events in outgrowth would involve increasing the fluidity of spore′s inner membrane [179] and resuming efflux of monovalent cations (H^+, Na^+ and K^+), divalent cations (Ca^{2+}, Mg^{2+} and Mn^{2+}) and DPA [180, 182, 183]. A signal with unknown nature is conveyed to the outer layers

33

of the spore, simulating coat and cortex lytic enzymes [184, 185]; which consequently leads to the complete rehydration of the spore core [179]. ATP production and biochemical pathways resume [186], DNA repair routes act at the time of spore outgrowth to fix DNA damage created during their potentially long dormancy [125, 187], and the SASPs are dissociated from DNA [187], providing a supply of amino acids (AAs) [179].
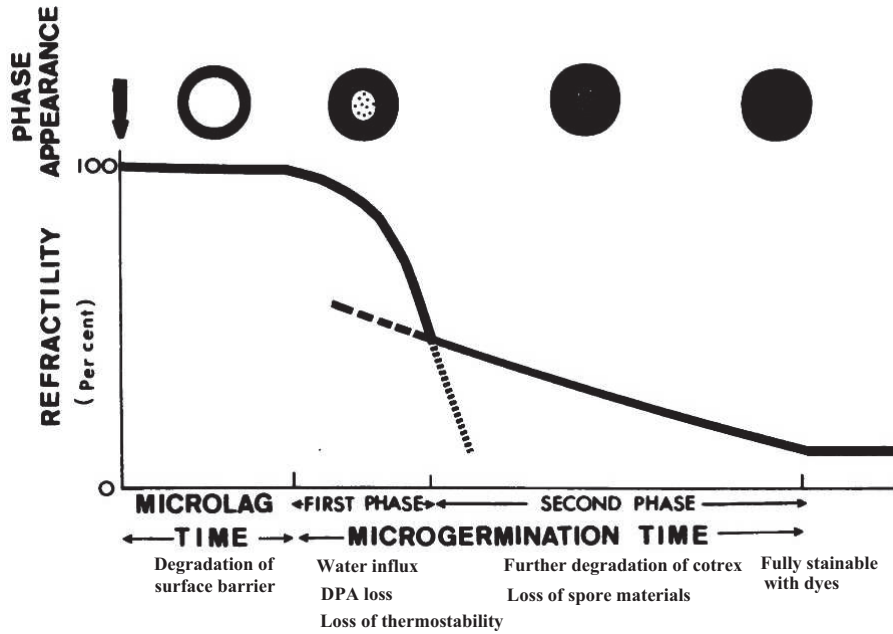
Figure 2.10: Change in refractility and other physiological adaptations evidently happening during different stages of germination in single spores. Broken lines in the germination curve are the proposed curves occurring autonomously of each other within a spore. The curve (solid line) reflecting experimental observations [188]

The physiological outgrowth of bacterial spore is invariably accompanied with the henceforward features: *a*) capability of forming colony in appropriate growth condition, *b*) increasing sensitivity to environmental stresses which do not influence the viability of the dormant spore [189], *c*) loss of translucency along with darkening of the spore cell when scrutinized under phase contrast microscopy [190], *d*) striking decrease in the optical density $(OD)_{580-610nm}$ of bacterial spore suspensions, *e*) a noticeable slight elongation of the cell, *f*) uniform stainabilty by methylene blue [191], *g*) almost 29–35 percent reduction in the dry weight of the ungerminated spore probably due to loss of Ca^{2+}–DPA, and nondialyzable polypeptide into the aqueous

environment [192] and h) oxidative metabolism of glucose [193]. Where each and every one of the preceding features can be observed, it represents that the process of germination has transpired.

Generally, spore germination can be considered as an irreversible and a triggered process initiated by either nutrients (a single AA, sugars and purine nucleosides), termed germinants, or non–nutrient (hydrostatic pressure, Ca^{2+}–DPA, cationic surfactant, dodecylamine, CO_2, lysozyme and heat) stimuli [180, 181]. Within seconds of contacting spores with triggers, the spore becomes empowered to germinate even after elimination of the tiger [180, 181]. However, partial germination seems to happen under suboptimal condition for germination, e.g., inadequate media, suboptimal temperature and the presence of inhibitors [194]. For a better distinction of nutrient and non–nutrient spore germination Setlow (2003) elucidated a reaction/interaction model [181] based on which nutrients stimulate the germinant receptors. This induces the release of ions including Ca^{2+}–DPA from the spore core, which consecutively activates cortex–lytic enzyme (CwlJ) action. SleB, another cortex–lytic enzyme, may be induced by germinant receptor activation through nutrient binding and/or alteration in the stress by the spore cortex as a result of the core hydration. SleB and/or CwlJ then catalyze the cortex hydrolysis. Non–nutrient germination may involve a different process from nutrient germination, or may activate the process at a later step in the pathway. For instance, high pressures either activate the germinant receptors or opens channels for the release of Ca^{2+}–DPA [195, 196], while alkylamines can activate Ca^{2+}–DPA release through affecting the spore′s inner membrane without interacting with any germinate receptors [181]. Extrinsic Ca^{2+}– DPA, released from other spore bodies or external sources, hydrolyzes spore cortex through activating CwlJ. This mechanism might be augmented by subsequential release of endogenous Ca^{2+}–DPA. Lysozyme treatment as well brings about cortex hydrolysis and the release of Ca^{2+}–DPA [181].

It has been described that high–intensity PEF (30 kV/cm, 1,000 μs) treatments could result in germination of bacterial spores [197] by altering physiological state of the spores, and hence, increase the susceptibility of spores to heat and electric

currents [43]. Based on this information, the author of the current work hypothesized that spore germination through LIDEF might also be possible by applying a much lower electric field (for instance, 2.5 V/cm) at longer exposure times, e.g., two hours.

2.3 Heterogeneous disinfection kinetics of spores in the biosolids matrix

It is hypothesized that the spore survival curves in the EEK disinfection system follow a heterogeous or sigmoidal inactivation pattern due to the application of multiple stressors. When inactivation of spores or vegetative microorganisms is considered, the log–linear shape of bacterial survival curves is a particular case among types of curves, however, a bacterial strain can produce different shapes of survival curves when the intensity of the stress or the cell physiological state varies. In such
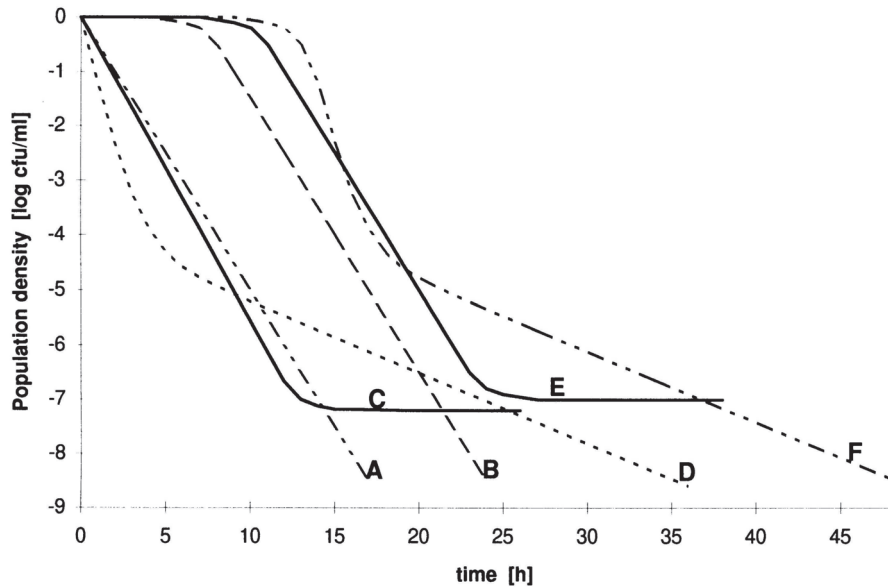
Figure 2.11: Graphic representations of different shapes of microbial survival curves. A: linear curves, B: curves with a shoulder, C and D: curves with a tailing (or biphasic curves), E and F: sigmoidal curves [198]

cases, curves with shoulders (convex), and tailing (concave), S shape (tailing–off + shoulder) and inverted S shape (shoulder + tailing–off) curves are expected (Figure 2.11) [120]. The development of mathematical models is tremendously complex

as inactivation kinetics rely on many defined and undefined factors [120, 199]. Regardless of these intricacies, models have been developed to picture the inactivation of microorganisms with rational precision [120, 200].

Early studies to explain the kinetics of the microbial inactivation deliberated the significance of essential variables including: *a*) chemical species and concentration of disinfectants, *b*) exposure time, *c*) temperature, *d*) type and concentration of microorganism, and *e*) pH [148]. Later studies have been proposed to describe the non–linear inactivation behavior [120]. Each model is inimitable to the microbial pathogen and disinfection process considered, as well as the requested quality standards for treated matrices [201]. Some of these models were derived from a best–fit mathematical model while some of them were based on assumed inactivation mechanisms [148]. The most frequently used disinfection models are Chick, Chick–Watson, Hom, Power Law, and Hom Power Law model [202]. These models can be derived from the following differential rate law:

$$\frac{dN}{dt} = -k \cdot m \cdot N^x \cdot C^n \cdot t^{m-1} \tag{2.6}$$

where $\frac{dN}{dt}$ = the rate of inactivation; N = the number of survival bacteria at contact time t; k = the reaction rate constant found experimentally; C is the concentration of the disinfectant; and m, n, and x are empirical constants [198, 199, 202].

Furthermore, other models have been introduced to fit the curves with a shoulder, curves with a tailing, and sigmoidal curves [202].

2.3.1 Chick's Law

Chick (1908), in her study of disinfection law, identified the analogy between a bimolecular elementary reaction and inactivation of the bacterium *Bacillus paratyphosus* [120]. She observed disinfection was first order where the rate of inactivation is similar to a chemical reaction and is given by [203]:

$$r_d = -\frac{dN}{dt} = k \cdot N \tag{2.7}$$

where r_d = the disinfection rate, k = the pseudo–first–order inactivation rate constant and N = the concentration of microorganisms at time t [120].

In a batch system, in which the rate of inactivation is equivalent to $\frac{\partial N}{\partial t}$, Eq. 2.8 results in an exponential decay in organisms, assuming that the rate constant, k, is in fact constant [200].

$$\log S = \log \frac{N}{N_0} = -k \cdot C \cdot t \tag{2.8}$$

Succeeding studies, conversely, have revealed that disinfection reactions are not simple bimolecular elementary reactions and cannot be entirely expressed by the simplest model in many cases.

2.3.2 Chick–Watson Law

Watson (1908) established the Chick–Watson Law where the pseudo–first–order inactivation rate constant, k, is related to the disinfectant concentration, C by [204]:

$$k = k' \cdot C^n \tag{2.9}$$

where n = the coefficient of dilution, k' = the pseudo first–order reaction rate constant (time^{-1}) and is presumed to be independent of disinfectant concentration and microorganism concentration [205]. The Chick–Watson Law expresses inactivation as a function of disinfectant concentration and contact time. The rate equation for the Chick–Watson Law is given by [148, 206]:

$$r_d = \frac{dN}{dt} = -k' \cdot C^n \cdot N \tag{2.10}$$

In a batch system, when C, n, and k are constant, the above rate law may be integrated so that the following relationship arises [205]:

$$\log S = \log \frac{N}{N_0} = -k' \cdot C^n \cdot t \tag{2.11}$$

where S, N and N_0 are the survival ratio, the concentrations of viable microorganisms at time t and 0, respectively. Watson also suggested an empirical logarithmic function to explain the effect of different disinfectant concentrations [120].

$$C^n \cdot t = constant \tag{2.12}$$

where t is the time needed to reach a given level of inactivation. If n >1, concentration is more important than time [206].

2.3.3 Hom model

Hom (1972) developed a mathematical model for expressing complex inactivation kinetics [120]. The theory proposed by Hom united the effect of time and concentration related to studies of chloride inactivation of bacteria [207]. For a continuous–flow system or a dynamically changing batch system, the Hom equation is obtained from the subsequent differential rate expression [208]:

$$r_d = \frac{dN}{dt} = -m \cdot N \cdot (kC^n)^{\frac{1}{m}} \cdot \left[-\ln \left(\frac{N}{N_0} \right) \right]^{(1-\frac{1}{m})} \tag{2.13}$$

where k = the inactivation rate constant, m = the m–order reaction rate constant and n = the coefficient of dilution.

Integration of this rate law with constant C gives [205]:

$$\log S = \log \left(\frac{N}{N_0} \right) = -k \cdot C^n \cdot t^m \tag{2.14}$$

If m = 1, Eq. 2.14 becomes the Chick–Watson relationship (Eq. 2.11). Concave and convex curves are obtained in semi-log plots of survival against time and/or C.t product when m >1 and when m<1, respectively [209].

Prior studies on inactivation of *Giardia* [210],*Cryptosporidium* [211], aerobic spore–forming bacteria [212] and heterotrophic plate count (HPC) bacteria [213] have shown that Hom′s model can give a satisfactory fitting curve to data.

2.3.4 Rational model (Power Law model)

A "rational" kinetics model developed by Majumdar et al. (1973) is applied to explain ozone inactivation of poliovirus in a completely mixed batch reactor (CMBR) and is written as [214]:

$$r_d = \frac{dN}{dt} = -k \cdot C^n \cdot N^x \tag{2.15}$$

where x is the empiric constant. Integrating of Eq. 2.15 gives:

$$\log S = \log\left(\frac{N}{N_0}\right) = \frac{-1}{x-1}\log\left[1 + (x-1)kC^n t N_0^{x-1}\right] \tag{2.16}$$

The Rational model can describe shoulder (x<1) and tailing–off (x>1) phenomena. Furthermore, it explains the effect of initial microbial density on disinfection. If x>1, the survival ratio will decline with increasing N_0 under the same disinfection conditions [120]. This equation reduces to the Chick–Watson model when x is equal to 1.

Roy et al. (1981) applied the Rational model to continuously stirred tank reactor (CSTR) studies on the inactivation of poliovirus1 with ozone in demand–free systems. Analysis of their study derived the following model [120]:

$$\frac{dN}{dt} = -k \cdot C \cdot N^{0.69} \tag{2.17}$$

Rational model illustrates a non–linear dependency of inactivation efficiency on viable microbial density. This model is capable of describing shoulders (x<1) or tailing–off (x>1) behavior [120, 215].

2.3.5 Hom Power Law (HPL)

Anotai (1996) introduced a kinetics model which includes subsets of both the Hom and Rational models and incorporates the parameters of both models [216]. The

rate of inactivation can be defined by the differential form of the model as:

$$r_d = \frac{dN}{dt} = mkC^n N^x \left[\frac{\left\{ \left(\frac{N^{1-x}}{N_0^{1-x}} - 1 \right) N_0^{1-x} \right\}^{1-\frac{1}{m}}}{(x-1)^{1-\frac{1}{m}} (kC^n)^{1-\frac{1}{m}}} \right] \tag{2.18}$$

Upon integration, it can be expressed as:

$$\log \left(\frac{N}{N_0} \right) = -\frac{1}{x-1} [1 + N_0^{x-1}(x-1)k'C^n t^m] \tag{2.19}$$

where the parameters k, m, n and x are the same parameters as those from the Hom and Rational model [216, 217].

2.3.6 Series Event model

The multi–hit or series–event model is another model to describe the shouldering phenomena of inactivation [120]. This model describes inactivation as a series of events taking place in a discrete stepwise manner [218]. Organisms pass from one event level to the next at a rate which is assumed to be first order with regard to the disinfectant concentration and independent of the event level [199]. According to this model, organisms survive the disinfection process if they receive hit numbers less than the required threshold number [120, 199]. The rate of obliteration of the ωth site in an organism is as follows [120]:

$$\frac{dN_\omega}{dt} = kCN_{\omega-1} - kCN_\omega \tag{2.20}$$

Solving for $\omega = 0$ to ℓ-1 results in the expression of the survival ratio in the series event model [199, 218]:

$$\log \frac{N}{N_0} = -kCt + \log \left(\sum_{\omega=0}^{\ell-1} \frac{(kCt)^\omega}{\omega!} \right) \tag{2.21}$$

where ω = the event level and ℓ = the threshold event.

Disinfection methods discussed so far were for chemical inactivation agents. Comparable kinetics models have been engendered for physical treatment processes such as irradiation and heat [120]. Some of these models will be discussed in detail in the following sections.

2.3.7   Multiple–target model

This model was developed for inactivation by radiation, except UV inactivation and was then applied to explain initial shoulders in survival curves of disinfection. The model is used due to its simple logic, mathematics and ability to fit batch data [199]. The basic assumption for this model is that a particle (organism or clumps of organisms) has a finite number (n_c) of discrete critical targets, and for complete destruction of the particle, all of the critical targets must be hit once [202]. The destruction rate of the target is expressed by first order kinetics:

$$\frac{dq}{dt} = -kCq \tag{2.22}$$

where q is concentration of targets (number per mL). Since the number of targets is finite, the probability of attaining the next hit is reduced as the inactivation continues [199]. A binomial probability of zero gives the probability of a specific target surviving,

$$P(0) = \frac{q}{q_c} \tag{2.23}$$

where q = the concentrations of targets at time t and q_c = critical concentration of targets.

For a closed–batch reactor, the rate of attaining the ith hit in a particle r_{Ni} is:

$$r_{Ni} = (n_c - i + 1)kCN_{i-1} - (n_c - i)kCN_i \tag{2.24}$$

where k represents the inactivation rate constant with unit [L/mg.s]; n_c is the targets number comprised in a particle; (n_c-i+1) and (n_c-i) are probability factors related to the raised difficulty or specificity in hitting the remaining targets as the reaction

proceeds [199].

The probability of inactivating a specific target is $1 - e^{-kCt}$, and the probability of a particle to survive with n_c critical targets is:

$$\frac{N}{N_0} = [1 - (1 - P(0))^{n_c}]$$

(2.25)

The probability of survival of a particle with n_c critical targets is obtained by [219]:

$$\log \frac{N}{N_0} = \log(P_i) = \log[1 - (1 - e^{-kCT})^{n_c}]$$

(2.26)

where k in this model, unlike the previous models, has units of L/(mg.min).

2.3.8 Modified multiple–target

With the same basic assumption as the Multiple target model, the Modified multiple–target was introduced to describe the destruction rate of particles by non–first order kinetics. This model was first used to express the disinfection behavior of ozone on *B. subtilis* spores. The probability of survival of a particle with n_c critical targets can be expressed as [220]:

$$\log \frac{N}{N_0} = \log(P_i) = \log \left\{ 1 - [1 - (e^{-kCT})]^{n_c} \right\}$$

(2.27)

In a continuous flow system, this model can be written as:

$$r = -kn_c C^n N_0 \left[1 - \left(1 - \left(\frac{N}{N_0} \right) \right)^{\frac{1}{n_c}} \right] \left[\left(1 - \left(\frac{N}{N_0} \right) \right)^{\frac{n_c-1}{n_c}} \right]$$

(2.28)

2.3.9 Empirical models

Besides mechanistic methods, statistical approaches are applied to derive empiric disinfection models. For example the inactivation of *E. coli* by ozone was modeled as:

$$\log \frac{N}{N_0} = a + bC + ct$$

(2.29)

where C and t are independent variables, and a, b, c are model parameters [120].

Clark et al. (1989) developed a regression model for 99.99% inactivation of *Giardia lambila* cysts as follows [221]:

$$t = RC^a pH^b temp^c \tag{2.30}$$

where pH = pH of contaminated matrix, temp = the temperature (°C), and a, b and c are constants.

Chapter 3

Experimental approach

The basic research paradigm was to perform studies which lead to an advance inactivation of bacterial spores in the AnD sewage sludge. Furthermore, it was intended to ascertain disinfection mechanism and to model kinetics of spore inactivation in the designed system. To satisfy these objectives the research was conducted in four experimental phases as follows:

- The first phase consisted of design and manufacture of the BioElectro^{TM} system (electrodes, the reactor vessel and the sealed cap) which would provide the optimum 2D electric field distribution. Also, the best enhancement agents for BioElectro^{TM} process were chosen based on the author previous work and published information [10, 16, 19, 20, 27, 29, 222].

- The second phase was the rudimentary assessment of the selected experimental variables of latter stage and delineation of optimum experimental conditions.

- The third phase implemented the optimal conditions of phase–II on a series of bench–scale experiments. The collected disinfection data were analyzed using multiple linear regression (MLR) to assess significance of experimental variables on the disinfection mechanism.

- The last phase of this study was attributed to the development of disinfection kinetics model. Observational data were modeled by a function which was a non–linear combination of the model parameters and experimental variables.

3.1 Phase I: System considerations and selection of enhancement agents

This phase was performed to provide the basic requirements of the BioElectro$^{\text{TM}}$ process, to wit: the reactor and enhancement agents.

As mentioned earlier (Chapter 1) one of the unique feature of the contemporary work was the application a 2D electric field system for disinfection of the biosolids. To this end, the reactor dimension and electrode configuration were designed in a way to assure the required electric field distribution. Architecture and selection of electrode material was another aspect in the BioElectro$^{\text{TM}}$ reactor to be considered in order to support the occurrence of desired electrochemical reactions.

Beside the reactor features, applied enhancement agents have profound effects on the efficiency of the process, the quality of the resultant product and the required treatment times. Hence, the selection of suitable enhancers was another critical issue to be investigated in this phase.

3.1.1 BioElectro$^{\text{TM}}$ reactor specifications

The laboratory scale prototype of BioElectro$^{\text{TM}}$ equipment consisted of a 3,100 mL Plexiglas rectangular reactor with internal dimensions of 214 mm length × 214 mm width × 74.1 mm height (Figure A.1). The reactor was equipped with four perforated (64 holes) 316L stainless steel (SS) electrodes (10 mm diameter cylinders, 102 mm long (Figure A.3) of which only 70 mm in contact with the matrix) coated with stainless steel mesh (200 μm) located at a distance of 172 mm surface to surface (182 mm center to center) from each other acting as the anode and cathode. The used SS is an iron-chromium alloy with the chemical composition detailed in Table 3.1.

Table 3.1: Chemical composition (w/w%) of tested SS detected by atomic adsorption

Steel	Fe	Cr	Ni	Mo	Mn	Si	N	P	C	S
316L	Bla	19.32	13.2	2.25	1.87	0.48	0.05	0.019	0.016	0.01

Underneath each electrode a 200 mL Nalgene bottle was installed to collect EOF when necessary. Four glass red–dye thermometers (0–100°C) were installed at the immediate vicinity (10 mm) of electrodes to monitor heating rate. The heat rate at the middle of the reactor was measured using a HACH probe (HQ40d Digital Multi–Parameter Meter). A Plexiglas seal was prepared to act as sealed cap for the the reactor (Figure A.2). To monitor electrical parameters, along the distance
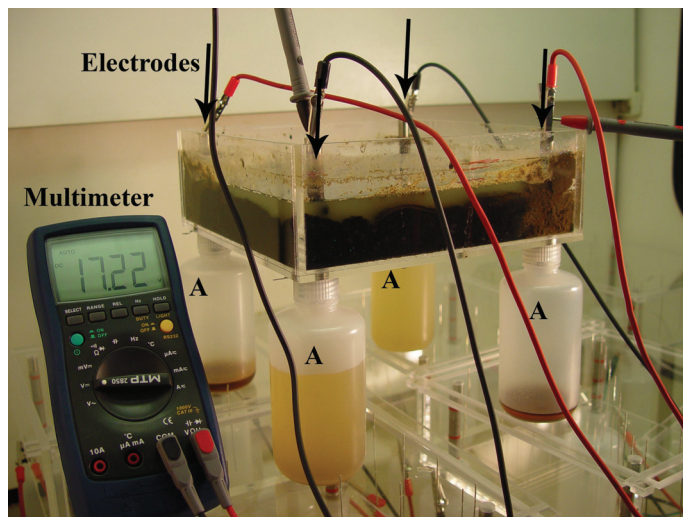
Figure 3.1: BioElectro$^{\text{TM}}$ system, Black arrows show the electrodes, "A" represents Nalgene bottle

between the cathodes and the anodes, a total of 16 silver probe–electrodes (five in each sides of the cap and six on one diagonal) with the length of 71 mm and diameter of 1 mm fixed into a fitted cover were used. Once fully assembled, the reactor was compacted and leak proofed. The system was connected to a regulated power supply (GENESYS 1500 W, TDK Lambda Americas Inc) with a maximum PG and current capacity of 120 V and 10.5 A, respectively. The connection was in the way that the electrodes at the same side of the reactor had different polarities while those on the diagonal direction had the same polarity. The power supply transforms altering current (AC) from a utility line (120–V, 60 Hz) into high voltage AC, then rectifies to DC signals. The electric field distribution between two electrodes was monitored by direct measurement of the potential difference between stainless steel electrodes and silver electrodes using a digital multimeter (MTB2850). BioElectro$^{\text{TM}}$ system

47

was installed in a laboratory hood with a continues positive airflow.

3.1.2 Selection of enhancement agents

In order to carry out the spore inactivation experiments by BioElectro^{TM}, key process variables needed to be determined. The nature of the process is based on the interactive disinfection in which synergistic/additive effects of electric field intensity (E) and enhancement agents play an eminent role. Therefore, the selection of enhancement agents had to been done based on their promising effect on providing multiple stressors on spore protective structures and a definite improvement in the inactivation. To this end, the author's previous works suggested a use of BIOXY S^{TM} (BS) and glutaraldehyde (GTA) [10, 17, 18, 19]. As explained earlier in Subsection 2.2.2, BS is a solid source of PAA and readily biodegradable. It has sporicidal properties with no adverse environmental effect [141]. Also, it increases conductivity of the biosolids, as investigated in the current work (Subsection 3.3.3). Therefore, BS could be considered as a reliable enhancement agent. As for GTA, the more careful studies on its characteristics showed that although it is a promising disinfectant, human exposure needs to be restricted due to its potential adverse health effects [223]. Hence, its application was abandoned. In a personal conversation with Maria Elektorowicz, Ph.D., Head of EK research group at Concordia University, the application of a mixture of ammonium and nitrate (AN) as a proxy for GTA was affirmed. AN has been widely used as an enhancement agent in previous EK research [16, 27, 29, 222] because of its valuable chemical properties in the EK system. For instance, the electrical conductivity of aqueous AN solutions escalates significantly with increasing concentration of salt (Subsection 3.3.3). This is attributed to the ionic nature of AN that substantially contribute to the electrolyte load in the sludge, and consequently, to its ability to conduct electric current. Also, it is known that the major factors that influence the equilibrium [224] (Reaction [7]) between unionized (NH_3) and ionized ammonia (NH_4^+) are pH and temperature [225]; hence under pH–high temperature conditions created in the EK reactor the disinfection efficiency of AN improves due to higher generation of toxic NH_3. The ammonia

conversion rate can be calculated by Eq. 3.1 [225].

$$\text{NH}_{3(g)} + n\text{H}_2\text{O} \leftrightarrow \text{NH}_3.n\text{H}_2\text{O}_{(aq)} \leftrightarrow \text{NH}_4^+ + OH^- + (n-1)\text{H}_2\text{O}_{(l)} \qquad [7]$$

$$f(\%) = \frac{1}{1 + 10^{(pK_a - \text{pH})}} \times 100 \qquad (3.1)$$

where f is fraction of total ammonia that is unionized and pK_a = dissociation constant from Eq. 3.2.

$$pK_a = 0.0901821 + \frac{2729.92}{T} \qquad (3.2)$$

where T = temperature in kelvin.

Typical physicochemical characteristics of the selected enhancement agents are listed in Table 3.2. The experiments then were carried out with three selected variables: E (V/cm), applied BS and AN doses (g/L).

Table 3.2: Typical physicochemical characteristics of the selected enhancement agents

Enhancer	Chemical Formula	%N	Solubility(g/L)	Appearance
BS	$C_2H_6Na_4O_{12} + C_{10}H_{16}N_2O_4$	–	55.6	Solid
AN	NH_4NO_3	27	1500	Solid

3.2 Phase II: Delineation of optimum experimental conditions

The main goal of this phase was to define the optimal experimental conditions under which a minimum 3 LRs of spores in AnD biosolids during BioElcetro^{TM} process is achievable. To this end, the work was codified in the two following sections.

3.2.1 Single–factor effect (SF) of experimental variables

To evaluate the disinfection effecincy of each experimental variable, namely E (V/cm) and applied concentrations of BS and AN individually, single–factor (SF) analyses were performed. Furthermore, the results of this step was used to ascertain the experimental variable levels in multi–factor effect experiments (Subsection 3.2.2) and the type of interaction between selected variables (Eq. 2.5). Table 3.3 shows the applied single–factor design for each experimental variable and references for the selection of variable levels. The experiments were performed with identical initial spore densities at the ambient temperature (23°C) for 24 hours.

Table 3.3: Single–factor (SF) design for each experimental variable

Code	Experimental variable	Variable value	Reference
SF1		0.7	[10, 17, 18, 19]
SF2	E (V/cm)	1.5	[17, 19, 20, 22]
SF3		2.5	[19, 29]
SF4		3.0	[20, 27]
SF5		0.2	[10, 141]
SF6		13	[19, 20]
SF7		25	[19, 20, 141]
SF8	BS (g/L)	50	[19, 20]
SF9		60	[19, 20]
SF10		100	[19, 20]
SF11		180	[19, 20]
SF12		240	[19, 20]
SF13		13	[19, 20, 29]
SF14	AN (g/L)	26	[19, 20]
SF15		30	[19, 20]
SF16		43	[12]

3.2.2 Multi–factor effects (MF) of experimental variables

Application of an enhancement agent, as a means to enhance the EK activity, evidently changes the disinfection efficiency of the process which can be expressed in terms of LR. In such a disinfection system the interaction between interactive factors and their ratios are vitally important for the correct effect; therefore, the studies were conducted to ascertain minimum values of each experimental variable in a combination by which a 3 LRs of spores was obtainable. To this end, the first selection step of experimental variable levels (Table 3.4) was performed based on the results of single–factor design (Subsection 3.2.1) and previous works [10, 15, 16, 29]. A screening mixture experiment was designed using the D–optimal approach with the aid of Design–Expert 6.0.4 (StatEase® Inc.2001) to identify the target variable levels. The corresponding design is shown in Table 3.5.

Table 3.4: Experimental variables and their levels in the first selection step

Experimental variable	Variable level				
	1	2	3	4	5
E (V/cm)	0	2.5	2.8	3	–
BS (g/L)	0	13	25	50	100
AN (g/L)	0	13	26	30	–

Table 3.5: Screening mixture experiment design in the first selection step

Code	E(V/cm)	BS(g/L)	AN(g/L)
MF1	3	13	0
MF2	3	50	13
MF3	3	50	26
MF4	3	25	26
MF5	3	13	30
MF6	3	100	26
MF7	3	0	13

Continued on next page

51

Table 3.5–continued from previous page

Code	E(V/cm)	BS(g/L)	AN(g/L)
MF8	3	0	30
MF9	3	25	30
MF10	3	50	30
MF11	3	25	0
MF12	3	0	0
MF13	3	100	13
MF14	2.8	50	0
MF15	2.8	25	13
MF16	2.8	50	13
MF17	2.8	0	26
MF18	2.8	13	0
MF19	2.8	13	26
MF20	2.8	0	30
MF21	2.8	25	30
MF22	2.8	100	13
MF23	2.8	100	0
MF24	2.8	100	30
MF25	2.5	0	13
MF26	2.5	25	26
MF27	2.5	50	26
MF28	2.5	100	30
MF29	2.5	13	30
MF30	2.5	100	0
MF31	2.5	50	0
MF32	2.5	0	26
MF33	2.5	13	26

Table 3.5–continued from previous page

Code	E(V/cm)	BS(g/L)	AN(g/L)
MF34	2.5	0	0
MF35	2.5	25	13
MF36	2.5	13	13

Inactivation experiments were performed based on the defined conditions in randomized order to offset any lurking variables such as sampling time, temperature, or the like. Each experiment was repeated three times to account for variability and to decrease experimental errors. For each test 14 samples were collected (detailed in Subsection 3.5.2) at the end of experiment (five hours exposure time). The results were reported as the geometric mean concentrations of the viable spores in all collected samples. The obtained results were investigated for fulfillment of the defined goal; a combination of minimum experimental variable levels by which a 3 LRs of spores is attainable. Bearing this in mind, a new selection of variable levels was selected as illustrated in Table 3.6. The D–optimal design procedure was carried out on newly selected variable levels to define the optimal series of experimental conditions. Seven conditional series (Table 3.7) were chosen as the selected experimental conditions to evaluate the mechanism and kinetics of disinfection in BioElectro^{TM} process.

Table 3.6: Experimental variables and their levels in the second step selection

Experimental variable	Variable level	
	1	2
E (V/cm)	2.5	2.8
BS (g/L)	13	25
AN (g/L)	13	26

Table 3.7: Selected experimental conditions

Series	Experimental variable		
	E (V/cm)	BS (g/L)	AN (g/L)
1	2.8	13	26
2	2.8	25	13
3	2.8	13	13
4	2.5	25	13
5	2.5	13	26
6	2.5	25	26
7	2.5	13	13

3.3 Phase III: Confirmatory disinfection experiments

This phase was set to provide analytical data to manifest the mechanism of disinfection during BioElectro^{TM} process. To achieve this purpose, the work performed was composed of six distinct sections.

3.3.1 Bench–scale disinfection experiments

Disinfection experiments were conducted based on the conditions defined in Table 3.7 for a period of two hours. To assess the reproducibility of the experimental method, the tests were run in quadruplicate (four replicates). The inactivation data collected from each 5–minute time interval were analyzed using MLR with the aid of STATISTICA 10 (StatSoft® Inc., 2011). The major purpose of using regression analysis was to describe the nature of the relations between the experimental variables, i.e., initial spore density (N_0), electric field intensity (E) and applied enhancement agents concentrations (BIOXY S^{TM} (BS) and ammonium nitrate (AN)) and the response variable (survival rate) in each time interval more accurately.

It is worth mentioning that the initial *C. perfringens* spore density (N_0) is one of the intrinsic features of biosolids which varied per test run in a range approximately from 3–25×10^6 CFUs /g TS (dry weight); therefore, it was considered as one of the experimental variables in regression analysis.

Results of MLR were employed to determine the significant factors during the disinfection process; consequently the mechanism of disinfection.

3.3.2 Kinetics analysis of enhancement agents residuals

The concentration of applied enhancement agents is likely to reduce during the contact time. Chemical demand–free condition is unlikely for oxidants. Decreases in chemical residuals are attributed to demand caused by particulates, reduced inorganic species, organic matter, microorganisms and reaction of the chemicals with water [217]. Therefore, it was necessary to determine the decay rate and instantaneous demand of PAA produced by BS.

3.3.3 Conductivity assessment of biosolids

The ionic nature of applied enhancers, namely BS and AN, increase the electrolyte load in the biosolids; and therefore, its ability to conduct electricity. To evaluate this effect, the biosolids was examined for conductivities at different temperatures (307.15–347.15K) with respect to enhancer type and concentration. Also, conductivity measurements were done for the mixture of enhancers at various mole fractions.

3.3.4 Numerical quantification of the electric field, current density and power dissipation

As seen in Chapter 2, several factors such as the reactor design, applied electric field intensity and system conductivity are affecting the overall performance of EK treatment system. Therefore, a series of numerical computation were performed to determine the effects of foregoing factors on local electric field distribution, current density norm (CDN) and total power dissipation density (TPDD) of the disinfection system.

3.3.5 Current impact on spore activation and germination

To examine the proposed hypothesis that LIDEF can act as an environmental trigger for spore germination several experiments were conducted. As explained in Subsection 2.2.4.4, measurement of the OD_{600}, eminently, the maximum rate of the fall off, is an easy and reliable method for quantitating and comparing rates of spore

germination. Hence, OD_{600} analyses along with colony count were done to evaluate the proposed hypothesis.

3.3.6 Physiological analysis of treated spores

To assess the physiological response of spores after treatment under electric field, AN, BS and combination of which the TEM technique was used. Defined understanding of spore morphological changes in response to applied environmental stimuli served as a model for inactivation mechanism and permitted to characterize, in a limited way, possible spore inactivation pathways during BioElectro$^{\text{TM}}$ process.

3.4 Phase IIII: Modeling of disinfection kinetics

The inactivation data from each experimental series defined in (Table 3.7) were analyzed using non–linear regression (NLR) method to mathematically model disinfection kinetics. In the NLR analysis, the relationship of survival with the experimental variables, namely E, BS, AN and N_0, was estimated by expressing survival as a non–linear function of experimental variables. The best–fit model for all series of disinfection experiments and corresponding best–fit parameters were obtained in the batch data analysis. A MATLAB® program (The Math Work, Inc., R2011a 7.12) using *fsolve* function was developed to predict the spore survival ratio during BioElectro$^{\text{TM}}$ process.

```
┌─────────────────────────────────────────────────────────────┐
  1. Design of bench reactor + selection of enhancers
├──────────────────────────────┬──────────────────────────────┤
│   Reactor specifications     │   Selection of enhancers     │
│      (Section 3.1.1 )        │      (Section 3.1.2 )        │
└──────────────────────────────┴──────────────────────────────┘
                              ↓
┌─────────────────────────────────────────────────────────────┐
        2. Delineation of experimental conditions
├──────────────────────────────┬──────────────────────────────┤
│     Single-factor effect     │     Multi-factor effects     │
│        experiments           │        experiments           │
│      (Section 3.2.1 )        │      (Section 3.2.2 )        │
└──────────────────────────────┴──────────────────────────────┘
                              ↓
┌─────────────────────────────────────────────────────────────┐
        3. Confirmatory disinfection experiments
├──────────────────────────────┬──────────────────────────────┤
│   Batch-scale disinfection   │     Kinetics analysis of     │
│                              │ enhancement agents residual  │
│      (Section 3.3.1 )        │      (Section 3.3.2 )        │
├──────────────────────────────┼──────────────────────────────┤
│  Conductivity assessment     │                              │
│       of biosolids           │   Numerical quantification   │
│      (Section 3.3.3 )        │      (Section 3.3.4 )        │
├──────────────────────────────┼──────────────────────────────┤
│      Germination tests       │    Physiological analysis    │
│      (Section 3.3.5 )        │      (Section 3.3.6 )        │
└──────────────────────────────┴──────────────────────────────┘
                              ↓
┌─────────────────────────────────────────────────────────────┐
    4. Mathematical modeling of disinfection kinetics
                  (Section 3.4 )
└─────────────────────────────────────────────────────────────┘
```

Figure 3.2: Outline of thesis methodology

3.5 Analytical methods

3.5.1 Initial biosoldis characteristics

BioElectro$^{\text{TM}}$ treatment was performed on anaerobically digested sewage sludge obtained from Robert O. Pickard environmental center (ROPEC)– wastewater treatment plant, Ottawa. Samples, collected between 10:30 to 11:30 A.M., were transferred to the Environmental Engineering laboratory in the Concordia University, Montréal.

Table 3.8: Characteristics of the biosolids sample before BioElectro$^{\text{TM}}$ treatment

Parameter	Unit	Value
C. perfringens spore	CFU/g TS	3–25×10^6
TS	%	2.60
TVS	%	0.56
pH	–	8.17
ORP	mV	-57.30
κ	mS/cm	4.37
A$_T$	mg CaCO$_3$/L	44
NH$_4^+$	mg/L	72.10
Cl$^-$	mg/g	7.79
η	mPa.s	287
Particle size distribution		
Geomean size	μm	38.87
Geo. StDev	μm	1.64
Mode size	μm	47.78

The collected biosolids samples were refrigerated and analyzed within eight hours after collection to determine initial characteristics (Table 3.8) such as *C. perfringens* spores density, TS, total volatile solids (TVS) (standard methods–2540 A, 2540 B, 2540 E, 2540 G), pH (HQ40d Digital Multi–Parameter Meter, HACH), oxidation–reduction potential (ORP) (ORPtest, 10 oakton EUTECH instruments), electrical conductivity (κ) (HQ40d Digital Multi–Parameter Meter, HACH), total alkalinity (A$_T$) (Brinkman Methrom 848 Titrino Plus), ammonia ion (Vernier LabQuest), chloride (HACH spectrophotometer DR2800), viscosity (η) (DV–E, Brookfield digital viscometer) and particle size distribution (*Partica*, laser scattering, HORIBA,

LA–950V0).

3.5.2 Performance of BioElectro™ experiments

The biosolids suspension was vigorously mixed for five to ten minutes. The obtained homogeneous suspension was mixed with BS (atomes company, Ville Saint Laurent, Québec) and AN (AGRO company, Montréal) at the predefined doses based on experimental conditions explained previously (Tables 3.5 and 3.7) to provide the required enhancement concentrations. The prepared menstruum was dispersed into BioElectro™ batch reactors with the working volume of 2,800 mL. Only for the experiments related to the disinfection kinetics (Subsection 3.3.1) the reactors were impermeable (no EOF was collected) by blocking electrode holes to maintain constant volume conditions of 2,800 mL of biosolids in each experimental run. Two distinct sampling regimes were carried out:

1. For the experiments in Subsection 3.2.2, 14 samples (Figure 3.3) were collected at the end of each trial (five hours exposure time) as follows: One sample from the center of the reactor, one sample from the middle point between anode and cathode (total of four samples), two samples from a distance of one cm around each electrode (total of eight samples) and one sample from the whole reactor after mixing at 250 rpm for two minutes.
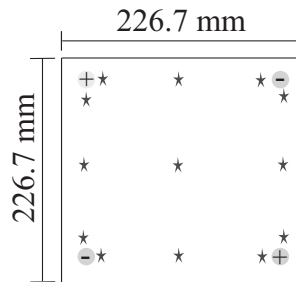
Figure 3.3: Diagram of EK reactor and sampling points (stars) in multi–factor effect experiments

2. In the bench–scale disinfection experiments (Subsection 3.3.1) one sample for every 5–minute time interval (total of 24 samples) was collected.

Samples were removed from the reactor by means of a 100–mL sterile HDPE syringe. The sample size was 10 mL and each was kept in 50 mL polypropylene centrifuge tubes (Coning, 05–538–67) for further assessments.

3.5.3   Enumeration of *C. perfringens* spores

To avoid further disinfection reaction, treated samples were examined without any delay (within two minutes) for *C. perfringens* density. Spores were counted based on method developed by [226]. Five mL of collected samples were transferred to round wide–mouth bottles (Fisher Scientific 1397–150) and diluted in 45 mL of dilution water. For spore activation and removing vegetative cells, the bottles were kept in water bath (Blue M, MAGNI–WHIRL # MW–1130–A) at 75°C for 20 minutes and cooled to room temperature in the ice water. The decimal dilutions of samples were obtained by the addition of one mL sample to pre–sterilized dilution tubes containing nine mL dilution water. Similarly, further decimal dilutions were prepared using aseptic technique. The dilution tubes were vortexed at each step and kept at room temperature for not more than 30 minutes.

Pour plating technique was applied to culture heat treated samples onto tryptos–sulfite–cycloserine (TSC) medium (Oxoid^{TM}, CM00587) with TSC supplement (Oxoid, SR0088E) and egg yolk emulsion (Oxoid^{TM}, SR0047). The plates were incubated in anaerobic conditions using an anaerobic culture system (VWR, 29446–290) for 20–24 hours at 35±0.5°C. Plates showing estimated 20–200 black colonies with apparent halos (luminous radiance, crown of light) were selected. Five presumptive *C. perfringens* colonies from each enumeration agar were stab–inoculated into supplement buffered nitrate–mobility (S–BNM) and lactose gelatine (LG) medium and incubated at 35±0.5°C over night. The S–BNM cultures were tested for presence of nitrite by adding 0.5 mL of solution A and 0.2 mL of solution B to test tubes. Development of orange color within 15 minutes indicated the presence of nitrites. If no color developed, a few grains of zinc (Zn) metal powder (40 mesh, ACROS, 36726000) was added and let stand for 10 minutes. No color change after addition of Zn signified inability of organism to reduce nitrates. The colonies were examined

in LG medium for gas production and color change. The color change from red to yellow indicated the fermentation of lactose with production of acid. After incubation period, culture tubes were chilled for one hour at 4°C and checked for gelatin liquefaction. If the medium was solidified, an additional 24 hour re–incubation at 35±0.5°C was performed. Non–motile, Gram–positive bacilli that produced black colonies on TSC agar, reduced nitrates to nitrites, produced acid and gas from lactose and liquefied gelatin within 48 hours were confirmed as *C. perfringens*. Once confirmed as *C. perfringens*, a loop of growth from the LG medium was transferred into 10 mL of fluid thioglycollate medium (FTG) (Oxoid[TM], CM0023) containing 0.1 g $CaCO_3$ and dispersed by gentle shaking. The medium was heated at 75°C for 20 minutes, cooled and incubated at 37±0.5°C for 16–18 hours. One mL of this culture was transferred to 10 mL of deoxygenated (freshly heated to 103°C for 10 minutes to repel oxygen and cooled to 37±0.5°C) FTG medium and incubated overnight. The culture was added at one percent concentration to Duncan–Strong (DS) sporulation medium and incubated at 37±0.5°C for 24 hours. Five mL of a 24 h–sporulating culture was then heated for 20 minutes at 75°C) in a capped tube, followed by cooling, dilution and enumeration on TSC agar. The plates were counted after 24 hours of incubation at 35±0.5°C in an anaerobic system. The Number of *C. perfringens* spores in the sample was calculated based on the percentage of colonies confirmed as *C. perfringens*. For example, if geometric mean plate count of 10^{-4} dilution was 105 and 6 of 10 colonies tested were confirmed as *C. perfringens*, the number of *C. perfringens* spores or CFU per mL is $105 \times \frac{6}{10} \times 10^4 = 630,000$. The concentration of the spores in dry solids was computed by:

$$N = \frac{Nc_i \cdot V_i}{\text{Dry solids}} \tag{3.3}$$

where Nc_i and V_i are the number of colonies in each culture dish and equivalent volume (mL) of sample in a particular replicate analysis, respectively. The results were tabulated as CFU /g TS and recorded in spreadsheet files. All values reported are the geometric mean for four experiments performed with four independent biosolids.

3.5.4 Effects of enhancement agents on electrical conductivity of biosolids

To examine the effect of enhancement agents on electrical conductivity of biosolids the conductivity measurements were done in three groups: *a*) various concentrations of AN, *b*) various concentrations of BS and *c*) mixtures of enhancers at various mole fractions. The conductivity measurements were conducted using a conductivity probe (HQ40d Digital Multi–Parameter Meter, HACH) at the temperature range of 307.15 to 347.15 K.

3.5.4.1 Effects of type and concentrations of enhancement agents on electrical conductivity of biosolids

The collected data (raw data are presented in Appendix B) for different concentration of enhancement agents were evaluated using least–squares method. Table 3.9 presents the least–squares fitted values for conductivity of AN and BS in biosolids matrix at different temperatures.

Table 3.9: Least–squares fitted values of the parameters of Eq. 3.4 for conductivity of AN and BS in biosolids matrix

Compound	T(K)	a	b	c	r^2
	307.15	4.7045	97.762	45.518	0.9970
AN	317.15	4.7822	98.668	47.442	0.9967
	327.15	5.0500	97.180	42.776	0.9972
	337.15	5.2150	97.170	41.886	0.9972
	347.15	5.2237	99.352	46.768	0.9971
	307.15	4.0997	65.306	66.664	0.9963
BS	317.15	4.1170	66.395	68.697	0.9954
	327.15	4.2438	65.023	65.238	0.9954
	337.15	4.2981	64.871	56.121	0.9951
	347.15	4.3440	64.797	54.419	0.9951

Furthermore, isotherms of specific electric conductivity (EC) (κ vs. g/L) for various concentrations of AN and BS in biosolids matrix at two different temperatures

(307.15 and 347.15 K) are shown in Figure 3.4. Based on the presented data the improvement in electrical conductivity of biosolids was evident by application of BS and AN. For example, by increasing the concentrations of BS and AN from 3 to 30 g/L the κ values were increased by about a factor of three and four respectively.
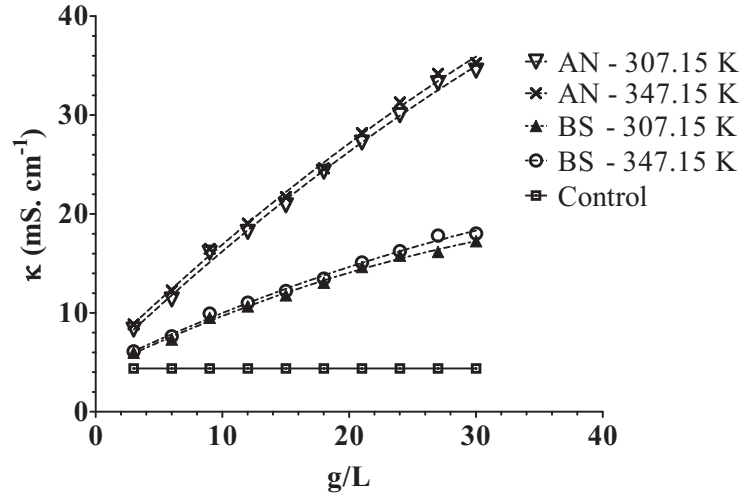
Figure 3.4: Isotherms of electrical conductivity of AN and BS at two different temperatures

3.5.4.2 Effects of XAN + (1-X)BS system on electrical conductivity of biosolids

The specific EC was also determined for the [XAN + (1-X)BS] system in the composition range $0 < X < 1$, where X denote AN mole ratio. In Figure 3.5 the experimental conductivity isotherms at five different temperatures were plotted against X. The κ–X isotherms increased by increasing X. The experimental conductivity, (κ), was well represented by the following equation:

$$\kappa = A + B(T/K) + C(T/K)^2 \tag{3.4}$$

where κ = specific conductivity, T = the absolute temperature, and A, B and C = coefficients determined by the least–squares method. The values of the coefficients at typical temperatures are listed in Table 3.10. The EC values of biosolids

for each experimental series were then calculated based on the developed equation (Table 3.12).
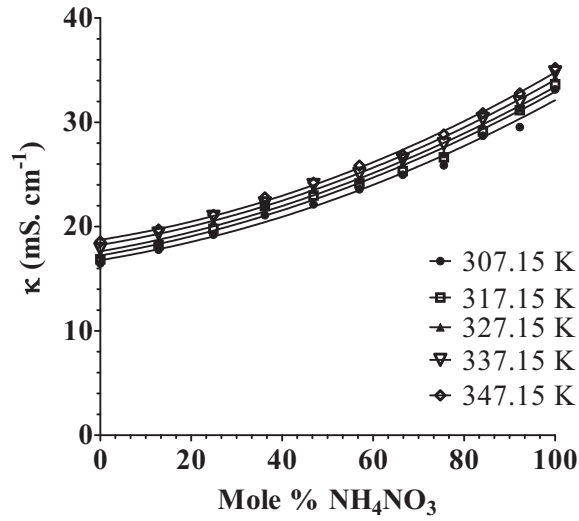
Figure 3.5: Isotherms of conductivity (κ) vs. mole of AN

Table 3.10: Least–square fit equations of the conductivity data for AN+BS system

X	T(K)	Data pt	A(mS/cm)	B(mS/cm.K^2)	C(mS/cm)	r^2
0.00	307–348	15	1359.80	177.07	4.4802	0.9940
0.13	307–348	15	887.66	76.86	2.5048	0.9772
0.25	307–348	15	2581.40	243.67	6.5261	0.9968
0.36	307–348	15	1764.00	155.57	2.7728	0.9984
0.47	307–348	15	318.13	21.56	0.2309	0.9998
0.57	307–348	15	2905.10	237.63	4.3079	0.9613
0.67	307–348	15	2843.40	214.26	4.5237	0.9846
0.76	307–348	15	390.26	38.35	0.4383	0.9915
0.84	307–348	15	390.02	23.28	0.7128	0.9992
0.92	307–348	15	1809.70	107.83	1.9337	0.9968
1.00	307–348	15	2258.50	133.59	1.6965	0.9959

Table 3.11: Empirical parameter of the conductivity–concentration equations ($\kappa =$ a + bX + cX^2)

T(K)	Data pt	a(mS/cm)	b(mS/cm.K^2)	c(mS/cm)	StDev
307.15	33	16.800	0.0707	0.0008	0.1549
317.15	33	17.232	0.0758	0.0008	0.0983
327.15	33	17.629	0.0763	0.0008	0.1190
337.15	33	18.245	0.0714	0.0009	0.1259
347.15	33	18.736	0.0691	0.0009	0.1084

Table 3.12: Summary of EC values in each experimental series

Series	E(V/cm)	BS(g/L)	AN(g/L)	Data pt	κ(mS/cm)
1	2.8	13	26	56	27
2	2.8	25	13	56	23
3	2.8	13	13	56	25
4	2.5	25	13	56	23
5	2.5	13	26	56	27
6	2.5	25	26	56	25
7	2.5	13	13	56	25

3.5.5 Kinetics analysis of PAA residuals

To measure the decay rate of PAA produced by BS, samples from each experimental series (Table 3.7) were collected at predetermined times and instantly titrated using a peracetic acid kit (LaMotte, 7191–01) to measure either PAA in 15 ppm increments or peroxide concentrations in 50 ppm increments. The values of k and D were estimated for each experimental series separately. In many cases, following any initial disinfectant demand being satisfied, the rate oxidants decay in aqueous solution can generally be described by first–order kinetics [205]. In other words, if the applied dose of chemicals is equal to C_a, then the residual at time t (C_t, in batch systems) can be written as:

$$C_t = (C_a - D) \exp(-k \cdot t) \tag{3.5}$$

where C_a is the applied chemical dose (g/L), D is the instantaneous chemical demand (g/L), k is the first order chemical decay rate (time^{-1}) in time t. The term initial residual (C_0) is used for the chemical concentration right after the instantaneous demand being satisfied (C_a–D). In the cases when there is no significant demand the initial residual (C_0) is equal to the applied dose (C_a). The values of the first order chemical decay rate (k) and the instantaneous demand (D) were determined by non–linear least–squares regression using Prism 5 (GraphPad Inc. 1992–2010). In this approach, the best–fit values of k and D were estimated as the values that minimized the sum of squares of the difference between predicted and observed chemical residual:

$$\text{RSS} = \text{minimum} \sum \left[C_{\text{predicted}} - C_{\text{observed}} \right]^2 \tag{3.6}$$

where C_{observed} is the actual disinfectant concentration measured (g/L) and $C_{\text{predicted}}$ is the corresponding concentration (g/L) predicted using Eq. 3.5.

3.5.6 Measurement of germination

For this experiments, spores were exposed to electric field intensity of 2.5 and 2.8 (V/cm). Ten samples were collected over a period of 80 minutes and monitored for OD_{600} using PerkinElmer spectrophotometer (Lambda 40). Experiments were run in triplicate and the maximum rate in the fall of the OD_{600} was determined graphically from the plot of OD_{600} values versus time.

3.5.7 COMSOL Multiphysics simulations

Numerical computations for local electric field distribution, CDN and TPDD were performed by means of finite element method (FEM) using COMSOL Multiphysics **GmbH** 4.2, 2011. The biosolids was assumed to be homogeneous, and the Laplace′s equation was used for the 2D model steady current calculations. The E(x,y) was analyzed for configuration of four probe electrodes as represented in Figure 3.6. In this model the electrodes were positioned inside a square (214 mm × 214 mm) representing BioElectro^{TM} reactor. The radius of all probe electrodes was 5 mm. The distance d, defined as the surface to surface distance between the positive and the negative electrode, 172 mm. The Plexiglass reactor wall was assumed nonconductive. Constant potential gradient was assigned to the grid points in regions where electrodes were located, while insulation boundary conditions were set on the remaining boundaries. Model geometries were meshed by triangular finite elements. The computations were performed for conditions defined in Table 3.13.
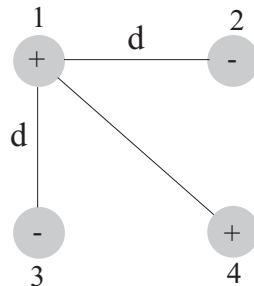
Figure 3.6: Probe electrode configuration (not to scale) used for numerical computations

Table 3.13: Conditions used for numerical calculations using COMSOL

κ (mS/cm)	E (V/cm)
4.37[*]	2.5
	2.8
23[**]	2.5
	2.8
25[**]	2.5
	2.8
27[**]	2.5
	2.8

[*] Initial EC of biosolids
[**] EC of biosolids in BioElectro[TM] system

3.5.8 Preparation of *C. perfringens* spores for TEM analyses

To have pure suspension of spores one mL of anaerobically digested biosolids were cultured onto TSC using "pure plate" method. The plates were incubated under anaerobic conditions for 20–24 hours at 35°C. The produced black colonies with apparent halos (luminous radiance, crown of light) were transferred into 10 mL FTG broth for growth at 37°C as explained previously [227]. Sporulating culture was then added, at 1% concentration, to raffinose–modified DS sporulation medium supplemented with 0.5 mM caffeine [228] and incubated at for 24 hours at 37°C. Spores were harvested by centrifugation (MISC–CAEQUIP Heraeus General Purpose Tabletop) at 3,000 rpm for 10 minutes and cleaned of cells and vegetative debris after harvest [229]. Removal of vegetative debris was accomplished by a method suggested by [230]. Soluble components were removed by two washings in distilled water (4,000 rpm, 10 minutes). Spores and debris were subsequently pelleted in two layers by low–speed (1,000 rpm), long–time (20 minutes) centrifugation. The bottom was composed of an adherent, tightly packed layer of clean spores, and the upper layer was gelatinous and composed of spores and vegetative debris. The upper layer removed by a gentle rocking motion in 5 to 10 mL of distilled water [231]. Spores were purified by repeated washing in sterile distilled water until they were >99% free of cell debris and germinated spores. The final suspension contained 10^5–10^8

spores/mL.

The spore suspension was then centrifuged at 2,000 rpm for five minutes to concentrate the spores in eppendorf tubes. The spore pellets were resuspended in 2.5% (v/v) glutaraldehyde fixative solution. The suspension was collected, transferred into 1.5 mL eppendorf test tube and centrifuged at 5,000 rpm for eight minutes. The fixative solution was decanted, and the tube was refilled with the fixative solution without disturbing the pellet. The pellet was stored in refrigerator overnight at 4°C. Thereafter, samples were washed with washing buffer three times for the total of maximum one hour. A final fixation was performed with a solution containing 1% aqueous Osmium tetroxide (OsO_4) and 1.5% aqueous ferrocyanide ($K_4[Fe(CN)_6] \cdot 3H_2O$) for two hours. Subsequently, samples were washed with washing buffer three times for a total of 15 minutes. Dehydration followed by using a graded ethanol series of 30%, 50%, 70%, 90%, 95% and 100% (three times), each for 15 minutes. This was followed by infiltration with Epon/acetone 1:1 (overnight), 2:1 (whole day), 3:1 (overnight) and pure Epon for four hours (two hours on rotator and two hours under vacuum). Next, the samples were embedded with an appropriate label and polymerized in 60°C oven for 48 hours. Ultrathin sections (90–100 nm) were made using an ultramicrotome stained with uranyl acetate, Reynolds lead citrate and micrographed under FEI Tecnai–12 transmission electron microscope (courtesy of Department of dentistry, McGill University), operating at an accelerating voltage of 120 kV equipped with an XR–80C AMT, 8 megapixel CCD camera. An environmental scanning electron microscope (ESEM) (courtesy of Le département de génie chimique de École Polytechnique de Montréal) (Quanta 200 FEG field emission gun with Everhart–Thornley secondary electron detector, CCD camera) was also used at 20kV working distance of 5 mm and a spot size of three.

3.6 Material preparation

3.6.1 Dilution water

In order to prepare decimal dilutions of spores prior to enumeration, phosphate buffered dilution water was prepared according to standard methods [232]. The stock phosphate buffer solution was prepared by dissolving 34 g potassium dihydrogen phosphate (KH_2PO_4) in 500 mL of Milli–Q® water. Its pH then was adjusted to 7.2 ± 0.5 with a 1N solution of sodium hydroxide (NaOH) and diluted to 1 L with Milli–Q® water. Dilution water was prepared by adding 1.25 mL of stock phosphate buffer solution and 5 mL of magnesium chloride solution (81.1 g $MgCl_2 \cdot 6\,H_2O$/L Milli–Q® water) to one liter of Milli–Q® water. It was dispensed in amounts providing 9 ± 0.2 mL after autoclaving for 15 minutes.

3.6.2 Duncan–Strong (DS) sporulation medium

Duncan–Strong medium was formed by mixing 15 g/L protease peptone, 4 g/L yeast extract, 1 g/L sodium thioglycollate, 4 g/L raffinose, 10 g/L $Na_2HPO_4 \cdot 7\,H_2O$ and 1 L Milli–Q® water. Seventy–five mL of the suspension were dispersed into 100 mL erlenmeyer flasks with screw caps and sterilized by autoclaving for 20 minutes.

3.6.3 Lactose gelatine (LG) medium

It is a mixture of 10 g/L tryptose, 10 g/L yeast extract, 10 g/L lactose, 5 g/L Na_2HPO_4, 0.05 g/L phenol red and 120 g/L gelatine. First, 950 mL of Milli–Q® water was heated to 50°C while gelatine in small quantities was added. The solution was cooled down and then yeast extract and Na_2HPO_4 was added. Mixed thoroughly and pH was adjusted to 7.5 ± 0.5 with a 6N solution of NaOH before adding lactose and phenol red. The suspension was dispensed into (100 mm $\times$12 mm) culture tubes and sterilized for 20 minutes at 121°C.

3.6.4 Laboratory water

The water used in the laboratory (conductivity of 18.2 MΩ) was produced by a Milli–Q® water system (Millipore–Advantage A10).

3.6.5 Glutaraldehyade %2.5 fixative solution

Sodium cacodylate (1.05 g) was added to 40 mL Milli–Q® water in a beaker. The solution was stirred using magnetic stir until sodium cacodylate completely was dissolved. The pH was adjusted to 7.3 ± 0.5 with a 6N solution of HCl according to SOP EQP–1.0. Glutaraldehyde (50%) in the amount of 2.5 mL was the added and final volume was adjusted to 50 mL using Milli–Q®.

3.6.6 Supplement buffered nitrate–mobility (S–BNM) medium

It contains 3 g/L beef extract, 5 g/L peptone, 5 g/L KNO_3, 2.5 g/L Na_2HPO_4, 5 g/L D–galactose, 5 g/L glycerol and 3 g/L agar. Mixture powder (28.5 g) was suspended in 1 L Milli–Q® water. Then the suspension was warmed up to 85°C and dispersed into glass tubes (150 mm×16 mm) with plastic caps and sterilized by autoclaving for 20 minutes.

3.6.7 Solution A

Eight grams of sulfanilic acid were dissolved in 1 L of a 5N solution of CH_3COOH.

3.6.8 Solution B

Five grams of alpha–naphtol or N–(1–naphthyl) ethylene diamine dihydrochloride were added to 1 L of a 5N solution of CH_3COOH.

Chapter 4

Results

This chapter presents the data obtained from the measurements and analyses conducted along the course of this investigation. It is divided into three parts: *a*) the results from selection of optimum disinfection conditions, *b*) the results from bench–scale disinfection BioElectro^{TM} experiments and kinetics of disinfection and *c*) the results of chemical, physical and biological impact of BioElectro^{TM} process.

4.1 Selection of optimum disinfection conditions

4.1.1 Single–factor (SF) effects

As outlined in Subsection 3.2.1, the single–step experiments on inactivation of *C. perfringens* spore were carried out for various electric field intensity (E) (V/cm) and concentrations (g/L) of enhancement agents, namely BIOXY S^{TM} (BS) and ammonium nitrate (AN), as define in Table 3.3. The results of 48 distinct spore viability analyses are illustrated in Table 4.1. Inactivation results of the exposure to a direct electric field under the studied conditions showed high resistance of the spores to electric field. These results were compatible with those of author previous work [10] with a slight increase (9 percent) in efficiency which can be attributed to the effect of a 2D EK system over a 1D system. Also, it was observed that exposure to a higher level electric field of 3 V/cm increased spore reduction; however this did not have a significant (P >0.05) impact on its mean viability result compared to

the condition with electric intensity of 2.5 V/cm. Accordingly, two higher electric field intensities, namely 2.5 and 3 V/cm were chosen for further study. Electric field intensity of 2.8 V/cm also was selected as the middle point.

Table 4.1: Single–factor (SF) experimental variable disinfection results

Code	Experimental variable	Variable value	LR[*]
SF1		0.7	0.14
SF2	E (V/cm)	1.5	0.21
SF3		2.5	0.33
SF4		3.0	0.36
SF5		0.2	ND[**]
SF6		13	0.35
SF7		25	0.62
SF8	BS (g/L)	50	1.02
SF9		60	1.13
SF10		100	2.65
SF11		180	3.08
SF12		240	3.71
SF13		13	ND
SF14	AN (g/L)	26	ND
SF15		30	ND
SF16		43	ND

Total exposure time = 24 hour
[*]Geometric mean of triplicate
[**]Non–detected

Single–factor effect examinations of BS showed the impact of increasing concentration on disinfection efficiency. The required concentration of BS to achieve minimum 3 LRs was 180 g/L under the studied conditions. This was much lower than previously reported concentration for PAA (550 mg/ mL) [233]. From these results, four concentrations, viz, 13, 25, 50, 100 g/L were selected for the next step of experiments.

The biosolids samples subjected to various concentrations of AN did not show significant reduction in spore numbers compared to those of control samples. It seems therefore that under the experimental conditions herein described AN does not behave as a disinfectant. However, as presented in Subsection 3.5.4, AN has a great impact on conductivity of biosolids and consequently the disinfection effects

of electric field. Also, its disinfection action on spores might be improved in the vicinity of the cathode due to the elevated pH. Three concentrations of AN, 13, 26 and 30 g/L were applied towards multi–factor effect examinations.

4.1.2 Multi–factor (MF) effects

A screening mixture experiment was designed to define the optimum disinfection conditions by which a minimum 3 LRs of spores is obtainable under a combination of experimental variables at their minimum levels. The results of LR of spores, TS%, maximum and minimum measured pH at the cathode and anode, respectively, are summarized in Table 4.2, as geometric means of triplicate experiments with 95% confidence intervals around the geometric mean.

Table 4.2: Screening mixture experiment results: LR, TS% and pH

Code	E(V/cm)	BS(g/L)	AN(g/L)	LR	TS%	pH	
						C	A
MF1	3	13	0	1.5	4.78	13.31	2.54
MF2	3	50	13	8.4	8.7	12.89	3.54
MF3	3	50	26	8.7	8.8	12.91	3.25
MF4	3	25	26	8.5	7.3	13.23	2.67
MF5	3	13	30	8.5	4.98	13.67	2.31
MF6	3	100	26	8.5	13.2	11.21	3.21
MF7	3	0	13	0.98	4.21	13.32	2.19
MF8	3	0	30	6.12	6.4	13.65	0.98
MF9	3	25	30	8.3	7.5	13.13	3.12
MF10	3	50	30	8.3	8.2	12.87	3.71
MF11	3	25	0	8.3	6.3	13.23	3.56
MF12	3	0	0	0.37	2.5	12.98	3.23
MF13	3	100	13	8.3	16.2	9.12	4.56

Table 4.2–continued from previous page

Code	E(V/cm)	BS(g/L)	AN(g/L)	LR	TS%	pH	
						C	A
MF14	2.8	50	0	7.5	7.54	12.43	3.45
MF15	2.8	25	13	7.7	6.58	12.87	3.15
MF16	2.8	50	13	8.4	6.31	12.12	3.34
MF17	2.8	0	26	0.99	7.12	13.13	2.87
MF18	2.8	13	0	1.2	3.89	13.15	2.98
MF19	2.8	13	26	7.1	4.98	13.76	2.1
MF20	2.8	0	30	3.14	5.73	13.23	2.43
MF21	2.8	25	30	7.5	6.97	12.97	2.87
MF22	2.8	100	13	8.4	14.87	9.13	5.2
MF23	2.8	100	0	8.3	15.25	8.98	7.13
MF24	2.8	100	30	8.4	15.3	9.56	4.76
MF25	2.5	0	13	0.71	3.16	13.12	2.34
MF26	2.5	25	26	5.11	6.54	12.78	3.1
MF27	2.5	50	26	5.16	8.4	12.24	3.34
MF28	2.5	100	30	7.12	13.12	8.99	7.41
MF29	2.5	13	30	3.52	4.56	12.54	3.32
MF30	2.5	100	0	6.87	13.2	8.32	7.89
MF31	2.5	50	0	6.13	5.12	9.12	6.78
MF32	2.5	0	26	0.89	3.24	12.98	4.21
MF33	2.5	13	26	3.46	3.78	12.78	4.56
MF34	2.5	0	0	0.33	2.11	12.56	4.13
MF35	2.5	25	13	4.21	6.42	12.87	3.1
MF36	2.5	13	13	3.56	3.67	12.45	3.20

It was found that combinations of experimental variables at selected levels, in most of the cases (80 percent), were successfully capable of achieving >3 LRs of spores. To examine whether further decrease in variable levels would provide the required spore reduction two complementary tests (CT) were designed as in Table 4.3. The experiments were run in triplicate, and the results showed no satisfactory reduction of spores in either cases.

Table 4.3: Complementary tests disinfection results

Code	E(V/cm)	BS(g/L)	AN(g/L)	LR	StDev
CT1	2.5	9	9	0.85	0.021
CT2	2	13	13	0.97	0.012

Total exposure time = five hours

Therefore, based on the data collected from the screening mixture experiments and to fulfill the purpose of this section the new levels of experimental variables were selected as: E = 2.8 and 2.5 V/cm, BS = 13 and 25 g/L and AN = 13 and 26 g/L. The D–optimal experimental design was performed on newly selected variables and ultimate seven series of the experimental conditions were defined (Table 4.4).

Table 4.4: BioElectro^{TM} process experimental conditions

Series	Experimental variable		
	E (V/cm)	BS(g/L)	AN(g/L)
1	2.8	13	26
2	2.8	25	13
3	2.8	13	13
4	2.5	25	13
5	2.5	13	26
6	2.5	25	26
7	2.5	13	13

4.2 Bench–scale BioElectro^{TM} disinfection experiments

As discussed in Chapter 3.3, the main purpose of disinfection experiments was to investigate the effect of experimental variables, to wit: electric field intensity (E), BIOXY S^{TM} (BS) and ammonium nitrate (AN) concentrations, defined under ex-

perimental conditions of Table 4.4, on the spore survival rate and mechanism of disinfection during BioElectro$^{\text{TM}}$ process. Furthermore, it was intended to develop a mathematical relationship between foregoing variables and final spore densities for the designed system. To this end, a series of analytical and statistical techniques were carried out, which their results are discussed in the following sections.

4.2.1 Impact of disinfection experiments on spore viability

BioElectro$^{\text{TM}}$ disinfection experiments were performed under the optimal composition of the experimental variables (Table 3.7) at the average initial temperature, pH and ORP of 18°C, 8.17 and -57.3 mV, respectively. The disinfection results (geometric mean of quadruplicates) are displayed in Table 4.5. The results of 28 (7×4) runs were evaluated and indicated that all BioElectro$^{\text{TM}}$ processed biosolids samples tested for microbiological performance criteria exceeded the regulatory requirements for biosolids pathogen control; that is, the treated biosolids samples met the minimum 3 LRs of *C. perfringens* spores; however, with a slight difference in the exposure time. For example, 3.66 LRs were observed after 70 minutes of treatment under the first experimental condition (Table 4.5), while the last conditional series (#7) represented 3.17 LRs after 120 minutes. Additionally, the results showed that experimental series with higher electric field intensity (E = 2.8 V/cm), videlicet the first, second and third, reached greater LR at the shorter period of time (70 minutes) compared with those treated under lower field intensity (E = 2.5 V/cm), namely 4$^{\text{th}}$ through 7$^{\text{th}}$. This fact can be seen more clearly in the survival curves depicted in Figure 4.1. Furthermore, the BioElectro$^{\text{TM}}$ survival curve of spores was found to be triphasic, comprising a short linear part at low treatment times, a very large shoulder and a second linear section. The large shoulder presumably indicates several factors: *a*) some threshold values of damage that must be exceeded before inactivation occurs; *b*) multi–hit inactivation process; *c*) activation of dormant spores; *d*) trimodal behavior of spore populations and *e*) effects of multiple stressors. All raw data obtained from experimental series are given in Appendix C. The experimental inactivation data from each series was analyzed together (at each time slot) and

separately, using multiple linear regression (MLR) and non–linear regression (NLR) methods. The basic purpose of these methods was to investigate the independent variables and the significance of their effect on disinfection efficiency.

It should be mentioned that due to the importance of instantaneous demand and substantial decay of PAA produced by BS on disinfection mechanism the results of kinetic analyses of PAA residuals is discussed in the following section (Subsection 4.2.2), and then MLR and NLR evaluations of disinfection experiments will be covered.

Table 4.5: Summary of spore inactivation results of BioElectro^{TM} disinfection process

Series	$\mathbf{E}^a$	$\mathbf{BS}^b$	$\mathbf{AN}^c$	$\mathbf{N_0}^d$	Data pt^e	t^f	LR^g
1	2.8	13	26	5 083 450	60	70	3.66
2	2.8	25	13	12 057 669	60	70	3.22
3	2.8	13	13	5 373 954	60	70	3.51
4	2.5	25	13	6 216 577	68	80	3.10
5	2.5	13	26	6 592 598	64	75	3.01
6	2.5	25	26	5 102 523	64	75	3.09
7	2.5	13	13	8 744 801	100	120	3.17

^{a} Electric field intensity–(V/cm)
^{b} BIOXY S^{TM}–(g/L)
^{c} Ammonium nitrate–(g/L)
^{d} Initial spore densities–(CFU/ g TS)
^{f} Data point
^{f} time–(min)
^{g} Log reduction
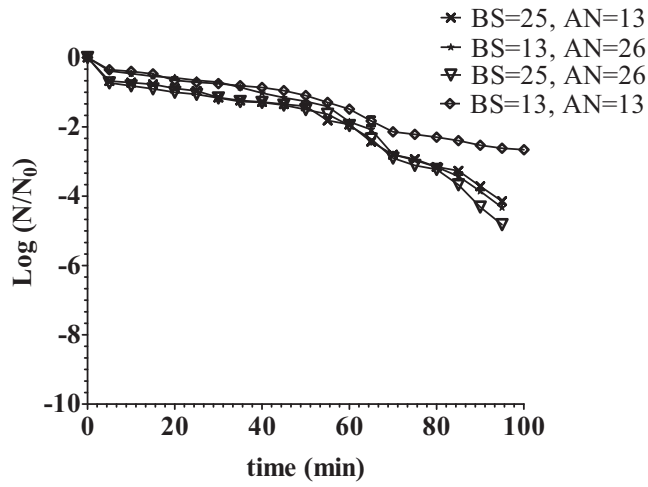
(a) E = 2.5 V/cm
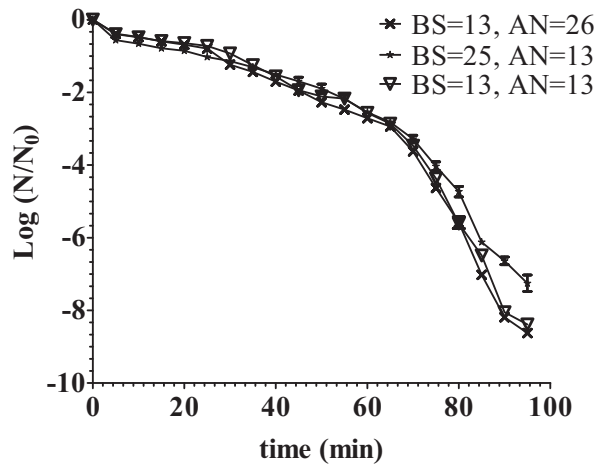
(b) E = 2.8 V/cm

Figure 4.1: Spore survival curve at each experimental series

4.2.2 Kinetic analyses of PAA residuals

As explained earlier (Chapter 3), one of the effects of BS in BioElectro$^{\text{TM}}$ process is related to production of peracetic acid (PAA). Therefore, it was necessary to determine PAA demand and decay rate and its outcome on mechanism of inactivation. The summary of PAA kinetic analysis for each experiment is given in Table 4.6. In this table, the adj. r^2 of each model fit were calculated using Eq. 4.1.

$$\text{Adjusted r}^2 = 1 - \frac{\text{RSS}/(n-p)}{\text{TSS}/(n-1)} \tag{4.1}$$

Table 4.6: Summary of PAA decay rates in each experimental series

E(V/cm)	BS(g/L)	AN(g/L)	D*(g/L)		k** (min^{-1})		Adj. r^2
			Geomean	**StDev**	**Geomean**	**StDev**	
2.8	13	26	5.0237	0.1008	0.2930	0.0014	0.9998
2.8	25	13	4.5727	0.6121	0.2947	0.0035	0.9995
2.8	13	13	5.0218	0.1414	0.2927	0.0019	0.9997
2.5	25	13	4.7703	1.0862	0.2940	0.0014	0.9995
2.5	13	26	5.0134	0.0957	0.2932	0.0019	0.9997
2.5	25	26	4.8027	0.6035	0.2934	0.0013	0.9999
2.5	13	13	4.9594	0.2690	0.2906	0.0025	0.9993
All			4.7870	0.4967	0.2931	0.0023	–
Number of points					708		

* Demand
** Decay rate

In addition, the regression plots for each of the experimental series are given in Figure 4.2 through Figure 4.8. The instantaneous demands (D) data for each experiment are presented in Appendix D.

The kinetic analysis of disinfectant residuals showed that there was a substantial decay of PAA, decay rate of 0.293 (geometric mean) min^{-1}. Figure 4.9 represents the related curve–fitting plot using Eq. 3.5. The model is consistent with the data and provided a good predication of the PAA concentration values. Based on these results the disinfection effects of PAA in BioElectro$^{\text{TM}}$ process is only expected for the first 10–13 minutes of the process.
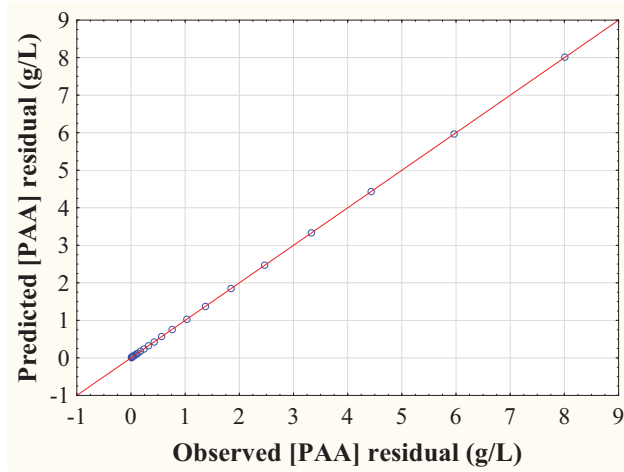
Figure 4.2: Plot of observed and fitted PAA residuals in the 1st experimental series
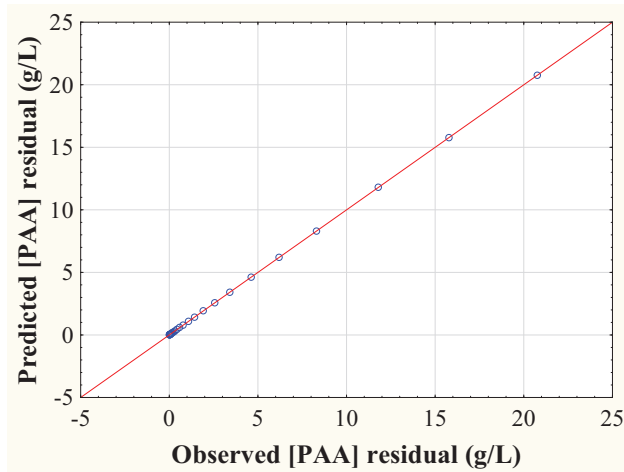
Figure 4.3: Plot of observed and fitted PAA residuals in the 2nd experimental series
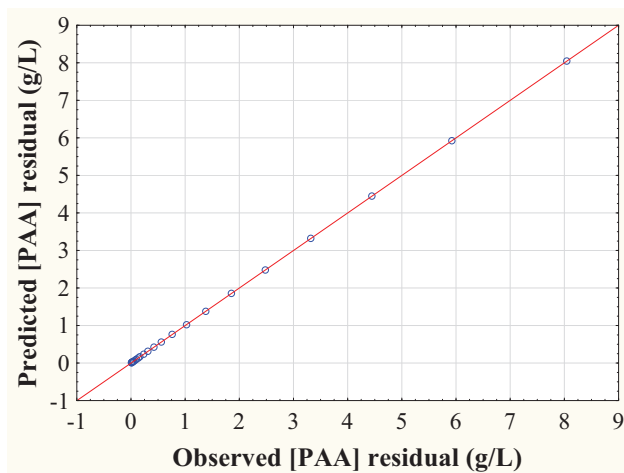
Figure 4.4: Plot of observed and fitted PAA residuals in the 3rd experimental series
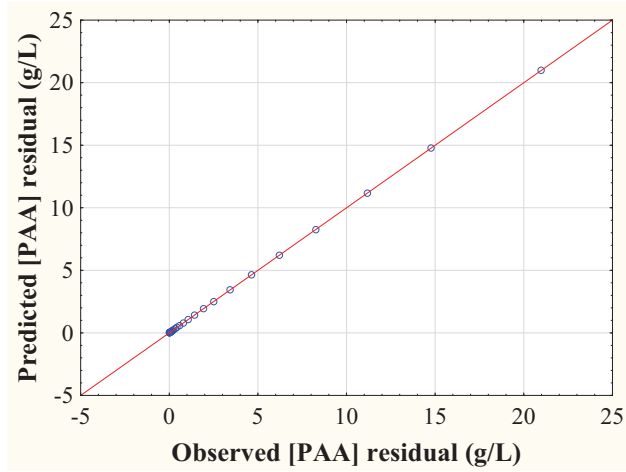
Figure 4.5: Plot of observed and fitted PAA residuals in the 4th experimental series
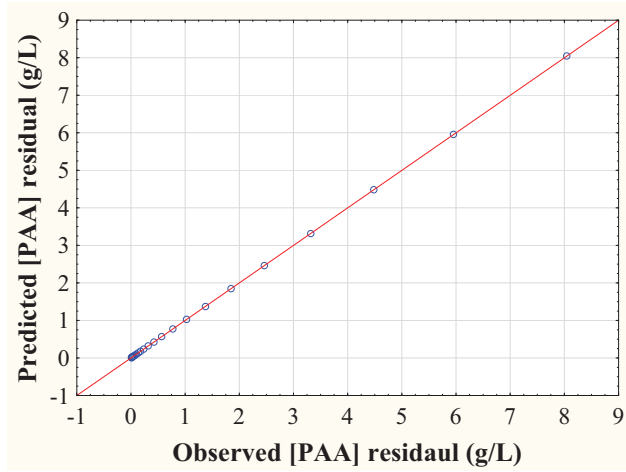
Figure 4.6: Plot of observed and fitted PAA residuals in the 5th experimental series
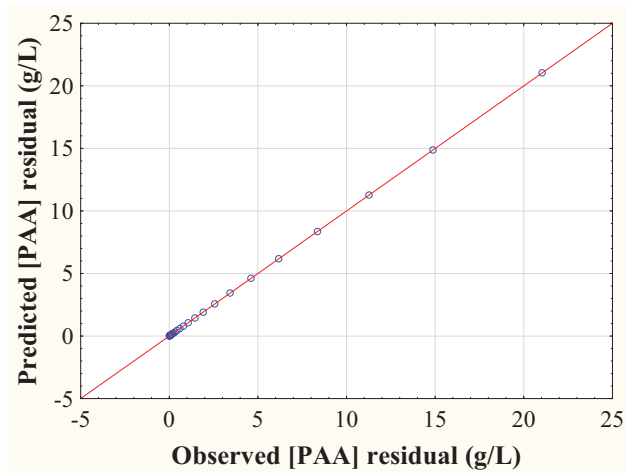
Figure 4.7: Plot of observed and fitted PAA residuals in the 6th experimental series
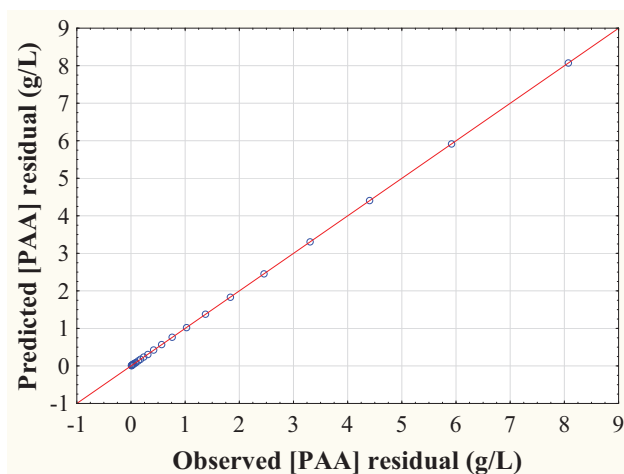
Figure 4.8: Plot of observed and fitted PAA residuals in the 7$^{\text{th}}$ experimental series
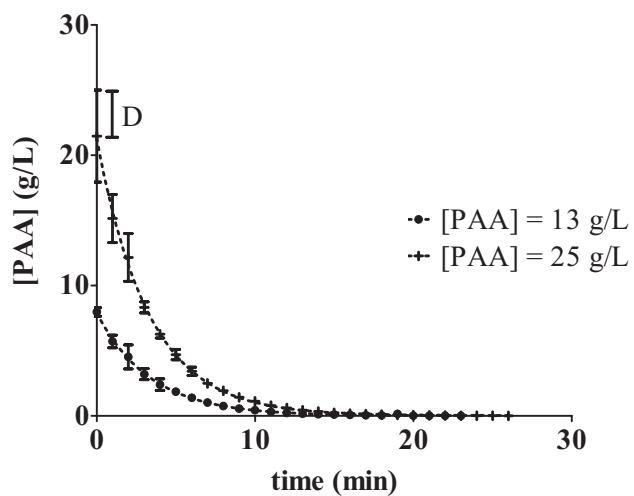
Figure 4.9: PAA consumption curve. Dotted lines refer to the 1$^{\text{st}}$ order model with $D \neq 0$ (bars indicate minimum and maximum PAA concentration values)

4.2.3 Regression analysis of spores survival data

The experimental inactivation data from each series of experiments were analyzed, employing MLR and nonlinear regression methods. The main purpose of using regression analysis was to denote the nature of the relations between the independent variables and the response variable more accurately. In multiple linear regression and non–linear regression analysis, the relationship of survival with the experimental variables (time (t), initial spore densities (N_0), electric field intensity (E) and applied enhancement agents concentrations (BIOXY S^{TM} (BS) and ammonium nitrate (AN))) was estimated by expressing survival as a linear and a non–linear function of experimental variables, respectively. In addition, the regression was used to predict the survival in terms of time, E, BS, AN and/or initial microbial densities (N_0).

4.2.3.1 Multiple linear regression

The regression analysis was conducted to ascertain the quantitative dependency between the experimental variables (t, N_0, E, BS and AN), and the response variable (survival ratio (S)). With the use of MLR, the mathematical form of equation relating survival ratio in each t–interval with applied enhancement agents doses (BS and AN), electric field intensity (E) and initial microbial density (N_0) was developed.

During MLR analysis, BS, AN, E and N_0 were considered as predictors. Also, to include the relationships between survival ratio and effects of enhancement agents with electric field, interactions of which in pairs (E×BS and E×AN) and ensemble (E×BS×AN) as independent predictors were used.

A total of seven predictors (E, BS, AN, N_0, (E×BS), (E×AN) and (E×BS×AN)) were used to obtain the best combination of predictors that explain the inactivation data. With seven predictors, there were 128 possible models. Ergo, it was not feasible to fit the data to each possible multiple linear model. Stepwise procedures were applied to develop the model that included the predictors that had statistically significant ($P < 0.05$) effects on the dependent variable. The logarithmic transfor-

mation of survival ratio was the response variable in the regression process. Only the data with non–zero survival was employed in the regression analysis. A stepwise forward selection was conducted using statistical software, STATISTICA 10 (StatSoft® Inc., 2011). Forward selection involves starting with no variables except constant in the model, trying out the predictors one by one and including those with great F statistics. If the addition of the parameter creates significant improvement in the fit ($P < 0.05$) then the model with that variable is accepted. The process continues by adding one more predictor until a predictor with a non–significant ($P < 0.05$) partial regression slope is reached or all predictors are included [234].

The predictors that had meaningful effects on logarithmic transformation of survival ratio at each t–interval are given in Table 4.7.

Table 4.7: Subsets of the predictors in the best–fit MLR

t(min)	Predictors								
	Adj. r^2	RSS	E	BS	AN	E×BS	E×AN	E×BS×AN	N_0
5	0.9620	0.0218		✓					✓
10	0.9760	0.0135		✓				✓	✓
15	0.3570	0.8294	✓	✓					
20	0.8942	0.0572	✓		✓		✓	✓	✓
25	0.8986	0.0593	✓	✓	✓	✓	✓	✓	✓
30	0.9290	0.0746	✓	✓	✓		✓		✓
35	0.9817	0.0213	✓	✓	✓	✓	✓		✓
40	0.9687	0.0566	✓	✓		✓	✓	✓	✓
45	0.9912	0.0246	✓	✓	✓	✓	✓	✓	✓
50	0.9862	0.0572	✓	✓	✓		✓		✓
55	0.9897	0.0367	✓	✓	✓	✓	✓	✓	✓
60	0.9963	0.0140	✓	✓	✓	✓	✓	✓	✓
65	0.9289	0.2581	✓	✓	✓	✓		✓	✓
70	0.9308	0.3730	✓	✓	✓				✓
75	0.9637	0.5991	✓	✓	✓				✓
80	0.9649	1.2859	✓	✓	✓				✓
85	0.9891	0.7711	✓	✓	✓				✓
90	0.9719	2.9837	✓	✓	✓				✓

E = Electric field intensity
BS = Bioxy S
AN = Ammonium nitrate
N_0 = Initial number of spores

Since stepwise regression commences with a constant without any variables, the

constant was included in the stepwise regression model whether it is significant or not.

Subsequently, the normality of errors and the significance of correlation between errors and the predictors were examined. Based on the normal distribution of regression residuals, only the errors of regression of 20 min data were normally distributed. The residuals of the rest of the MLR were not normally distributed. The histograms of regression residuals are given in Figure 4.10 through Figure 4.27. In these plots, the solid line represents the normal distribution. None of the predictors had any significant ($P < 0.05$) correlation with regression residuals.
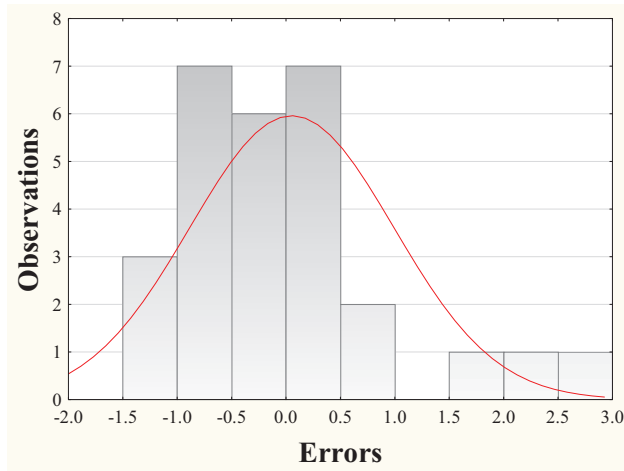
Figure 4.10: Distribution of MLR residuals of t–interval 5 min
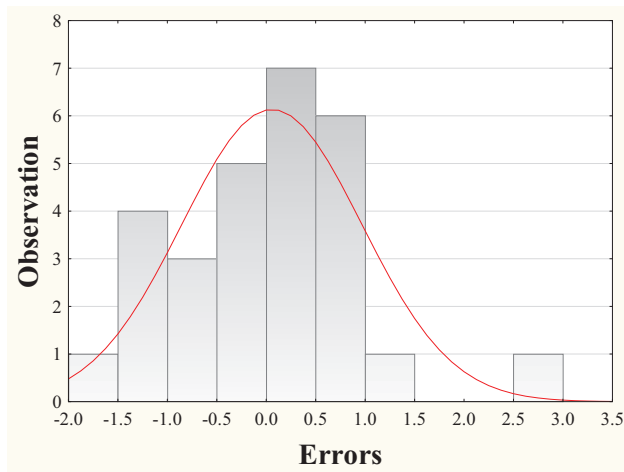
Figure 4.11: Distribution of MLR residuals of t–interval 10 min
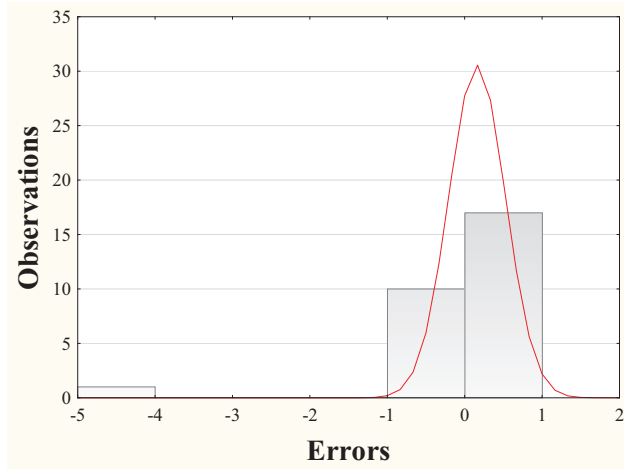
Figure 4.12: Distribution of MLR residuals of t–interval 15 min
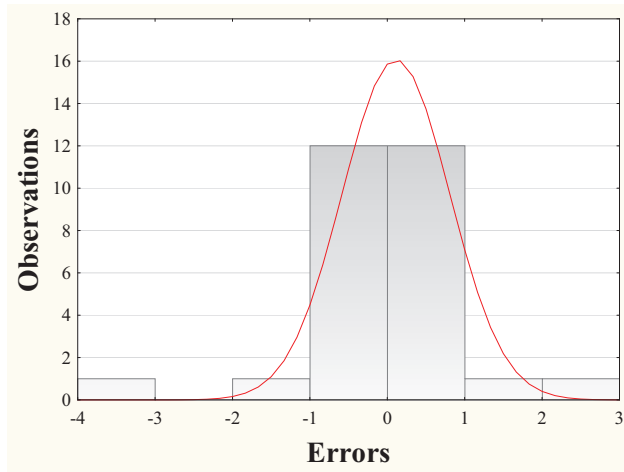
Figure 4.13: Distribution of MLR residuals of t–interval 20 min
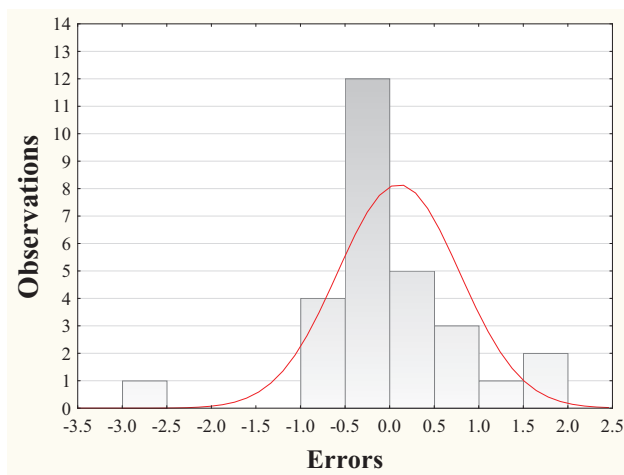
Figure 4.14: Distribution of MLR residuals of t–interval 25 min
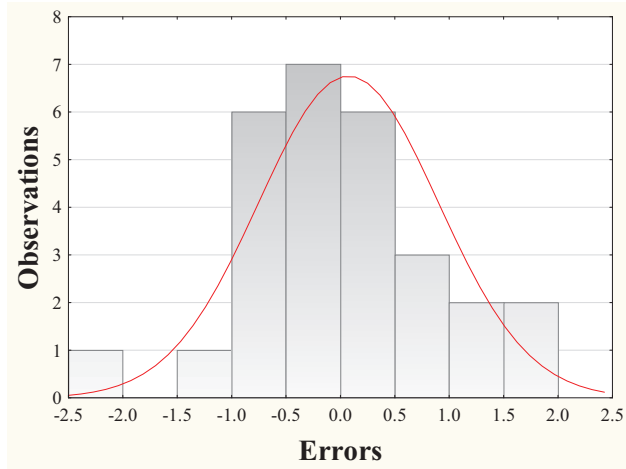
Figure 4.15: Distribution of MLR residuals of t–interval 30 min
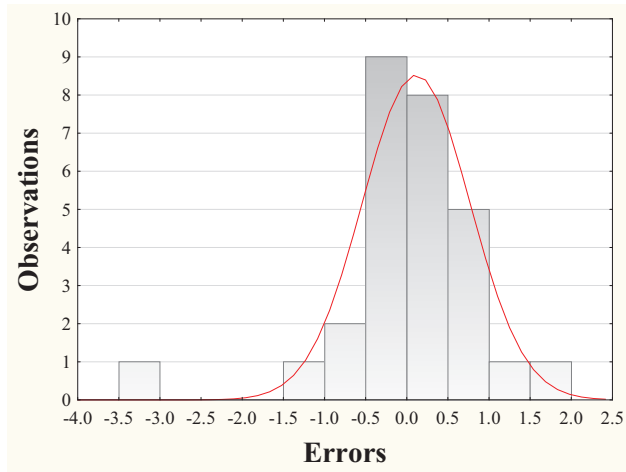
Figure 4.16: Distribution of MLR residuals of t–interval 35 min
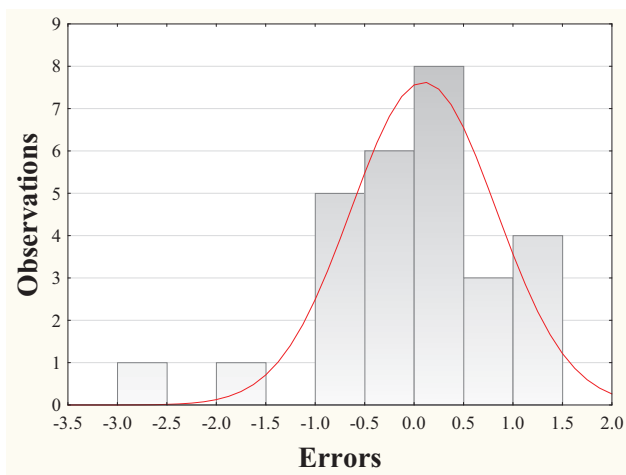
Figure 4.17: Distribution of MLR residuals of t–interval 40 min
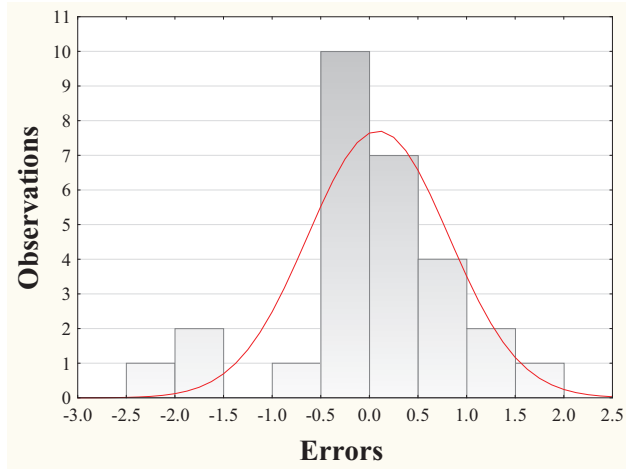
Figure 4.18: Distribution of MLR residuals of t–interval 45 min
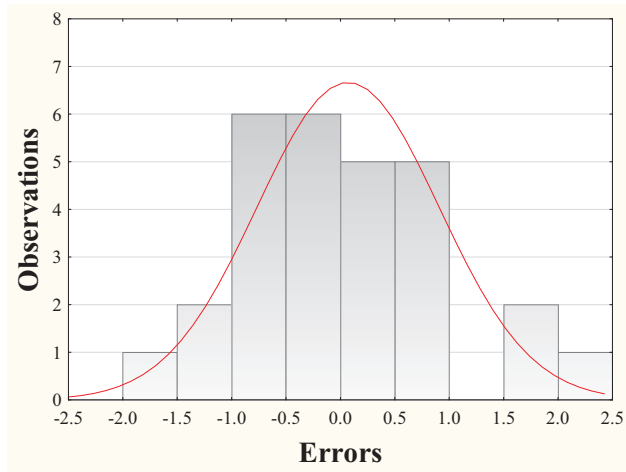
Figure 4.19: Distribution of MLR residuals of t–interval 50 min
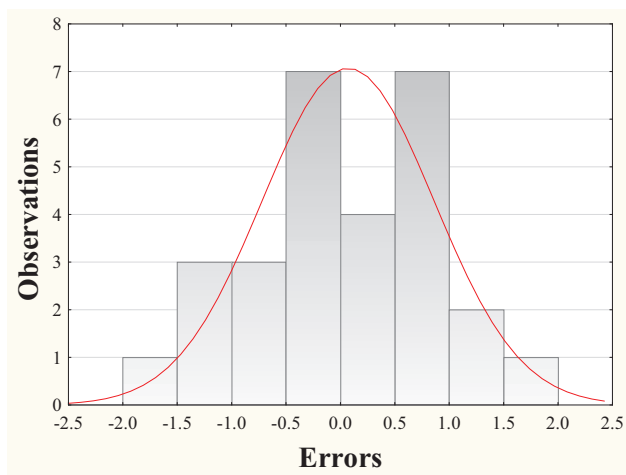
Figure 4.20: Distribution of MLR residuals of t–interval 55 min
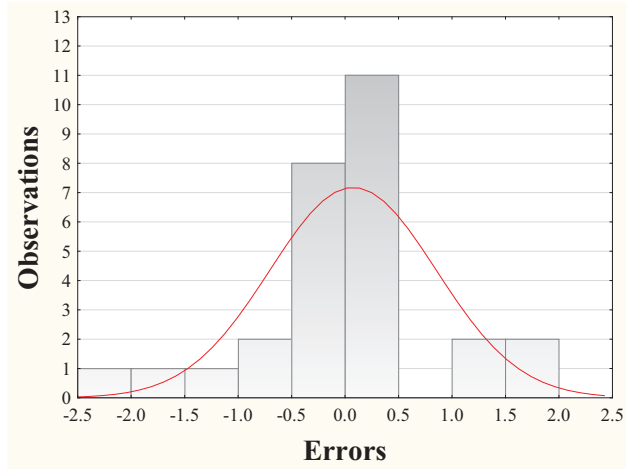
Figure 4.21: Distribution of MLR residuals of t–interval 60 min
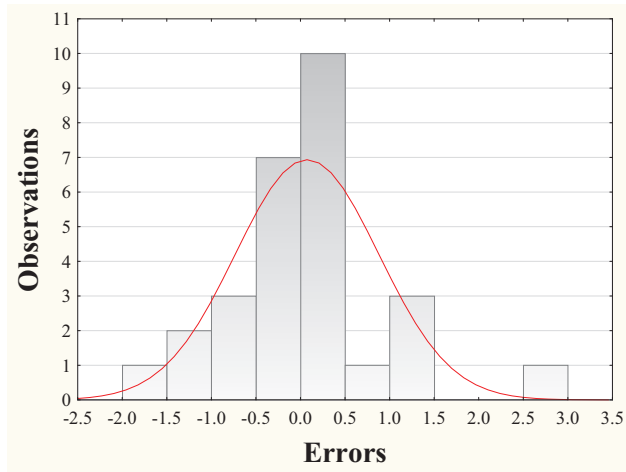
Figure 4.22: Distribution of MLR residuals of t–interval 65 min
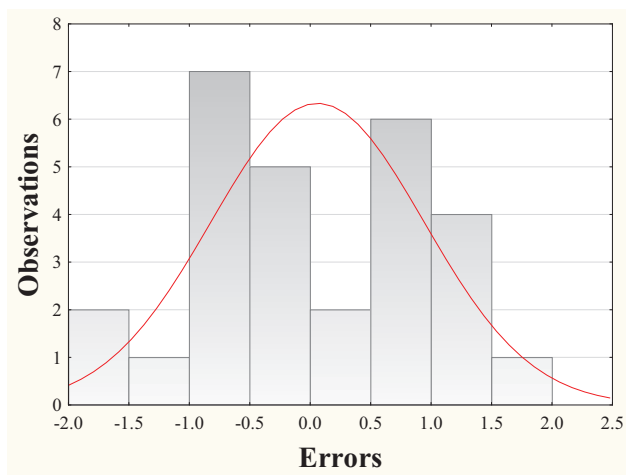
Figure 4.23: Distribution of MLR residuals of t–interval 70 min
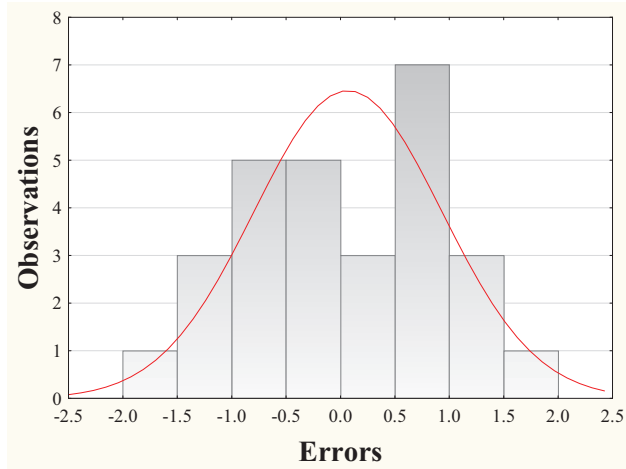
Figure 4.24: Distribution of MLR residuals of t–interval 75 min
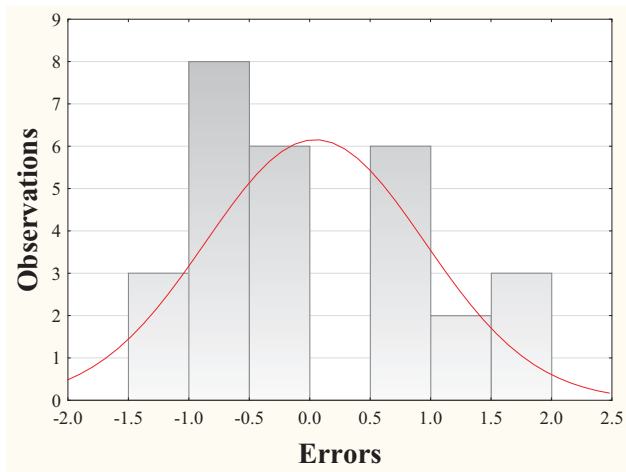
Figure 4.25: Distribution of MLR residuals of t–interval 80 min
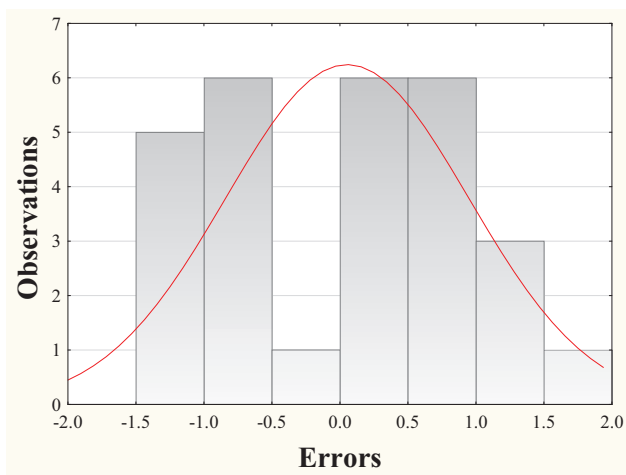
Figure 4.26: Distribution of MLR residuals of t–interval 85 min
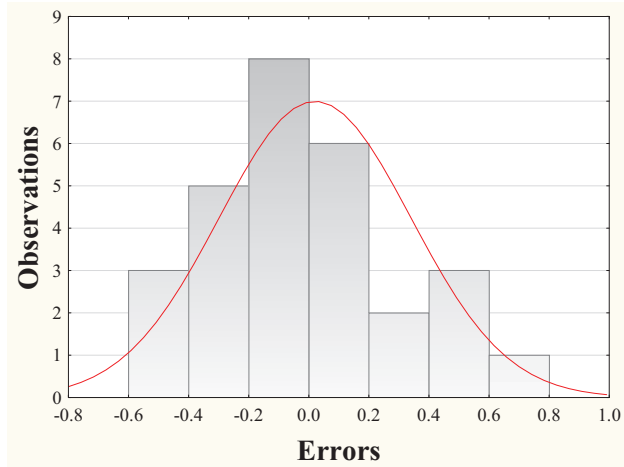
Figure 4.27: Distribution of MLR residuals of t–interval 90 min

The purpose of MLR was to ascertain the subset of predictors that provided the best–fit to the observed survival ratio data in each time increment. The survival ratios predicted by the models are given in Table 4.8 and the observed survival ratios are plotted in Figure 4.28 through Figure 4.45. The solid line shows equal observed and predicted density of surviving organisms. In a perfect fit, all observations should be on this line, i.e., all the predicted data would be equal to observed data. STATISTICA 10 output of regression is provided in Appendix E.

Multiple linear regression analysis of inactivation data show that significant effects of parameters on inactivation efficacy changed during treatment time. In other words, survival ratio at different time intervals was a function of some parameters at that specific period. For example, at lower treatment times (5–10 minutes) the disinfection effect of BS was more evident, however, at the prolonged treatment time inactivation efficiency was a multi–factor function in which E, BS, AN and N_0 were significantly ($P < 0.05$) important.

Table 4.8: MLR models for each inactivation time interval conditions of Table 4.4 developed using stepwise regression

t–interval(min)	
5	$\log S = -0.128 - BS + 0.391\ N_0$
10	$\log S = 0.1836 - 0.94\ BS - 0.15\ E \times BS \times AN$
15	$\log S = -0.35\ E - 0.66\ BS$
20	$\log S = -2.107 + 0.486\ E + 3.85\ AN - 2.8\ E \times AN - 1.3\ E \times BS \times AN + 0.245\ N_0$
25	$\log S = -5.4690 + 1.6\ BS + 5.01\ AN - 4.3\ E \times AN - 6.6\ E \times BS - 0.98\ E \times BS \times AN + 0.49\ N_0$
30	$\log S = -2.67 + 0.588\ E - 0.95\ BS + 7.37\ AN - 7.5\ E \times AN + 0.432\ N_0$
35	$\log S = -0.46\ E - 2.3\ BS + 3.87\ AN + 1.53\ E \times BS - 4\ E \times AN + 0.468\ N_0$
40	$\log S = 6.58 - 1.4\ E - 3.9\ BS + 3.03\ E \times BS - 0.48\ E \times AN + 0.471\ E \times BS \times AN + 0.343\ N_0$
45	$\log S = 9.67 - 1.7\ E - 3.6\ BS - 1.2\ AN + 3\ E \times BS + 0.885\ E \times AN + 0.364\ E \times BS \times AN + 0.36\ N_0$
50	$\log S = 4.38 - 0.78\ E - 0.25\ BS + 1.43 AN - 1.5\ E \times AN + 0.389\ N_0$
55	$\log S = 4.7 - 0.78\ E - 2.4\ BS + 2.73\ AN + 1.59\ E \times BS - 3.2\ E \times AN + 0.607\ E \times BS \times AN + 0.293\ N_0$
60	$\log S = 11.38 - 1.7\ E - 3.1\ BS - 2\ AN + 2.35\ E \times BS + 1.26\ E \times AN + 0.7\ E \times BS \times AN + 0.158\ N_0$
65	$\log S = 9.40 - 1.5\ E - 3.9\ BS - 0.54\ AN + 3.03\ E \times BS + 0.636\ E \times BS \times AN + 0.261\ N_0$
70	$\log S = 5.81 - 0.99\ E - 0.26\ AN - 0.32\ BS + 0.367\ N_0$
75	$\log S = -3.46 - 0.866\ E - 0.159\ BS - 0.167\ AN + 0.228\ N_0$
80	$\log S = 18.34 - E - 0.1\ BS - 0.09\ AN + 0.283\ N_0$
85	$\log S = 27.91 - E - 0.11\ BS - 0.17\ AN + 0.144\ N_0$
90	$\log S = 33.38 - E - 0.09\ BS - 0.14\ AN + 0.230\ N_0$

$\log S = LR = \log \frac{N_t}{N_0}$

N_0= initial number of spores

E = electric field intensity (E); BS = BIOXY S$^{\text{TM}}$ (BS); AN = ammonium nitrate (AN)
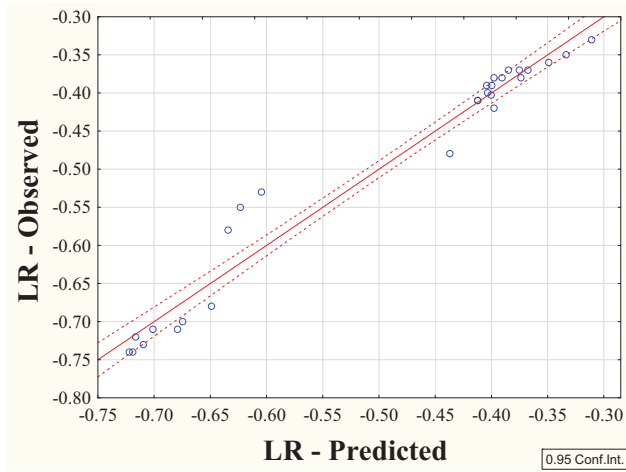
Figure 4.28: Observed vs. predicted LR by MLR in t–interval 5 min
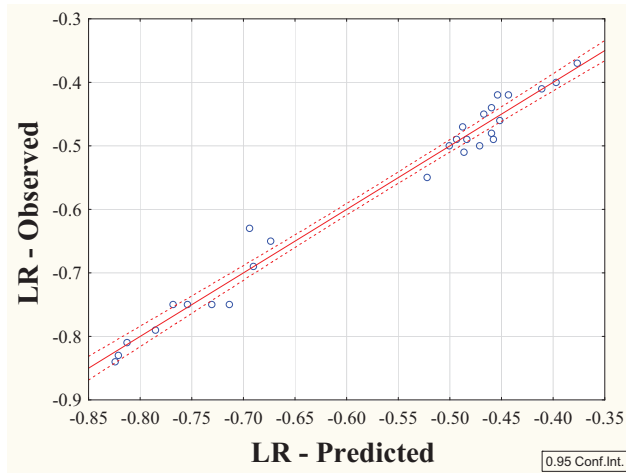
Figure 4.29: Observed vs. predicted LR by MLR in t–interval 10 min
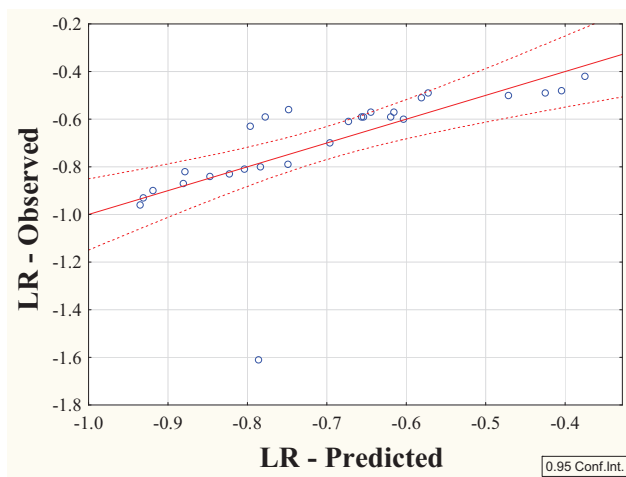
Figure 4.30: Observed vs. predicted LR by MLR in t–interval 15 min
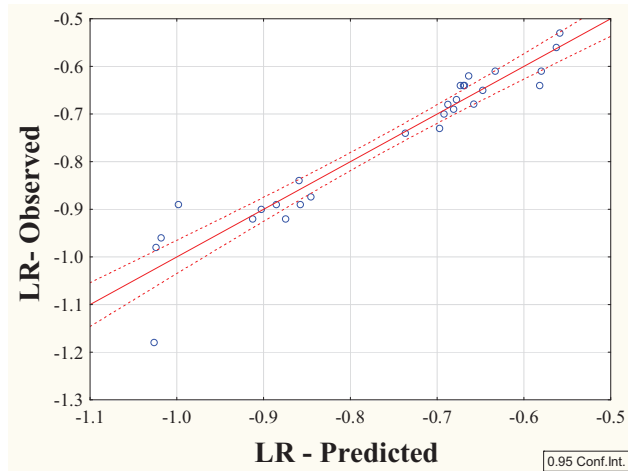
Figure 4.31: Observed vs. predicted LR by MLR in t–interval 20 min
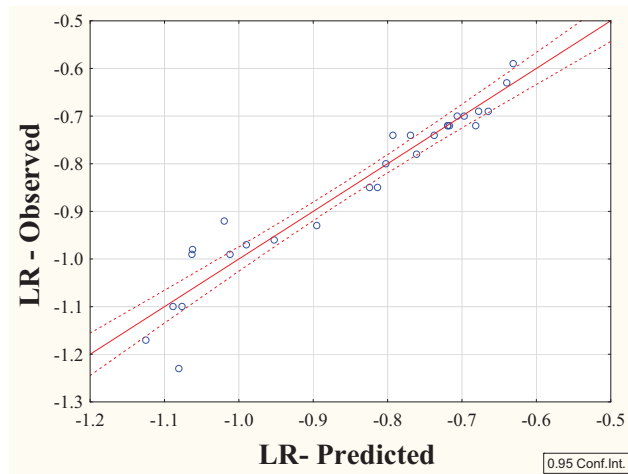
Figure 4.32: Observed vs. predicted LR by MLR in t–interval 25 min
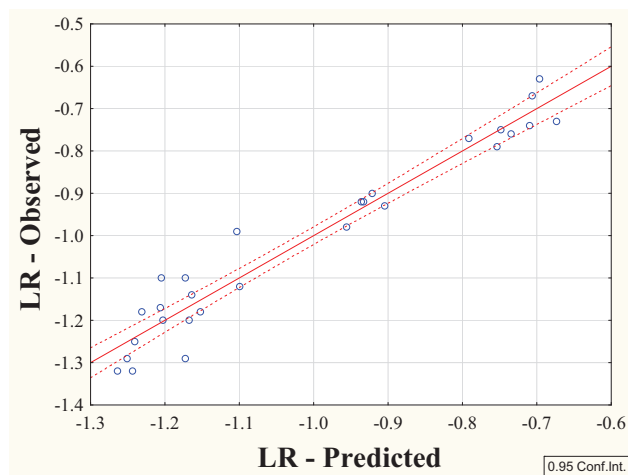
Figure 4.33: Observed vs. predicted LR by MLR in t–interval 30 min
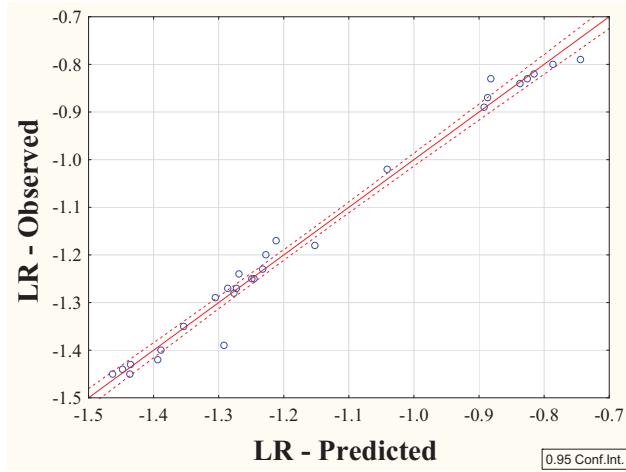
Figure 4.34: Observed vs. predicted LR by MLR in t–interval 35 min
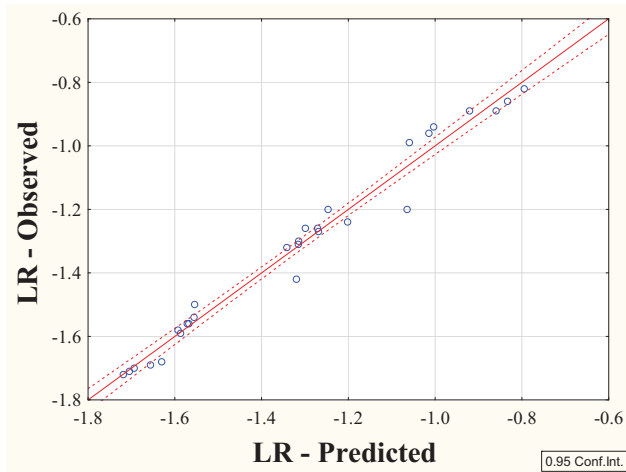
Figure 4.35: Observed vs. predicted LR by MLR in t–interval 40 min
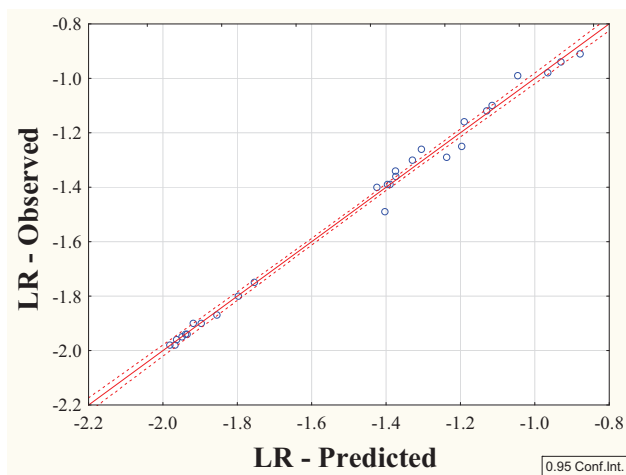
Figure 4.36: Observed vs. predicted LR by MLR in t–interval 45 min
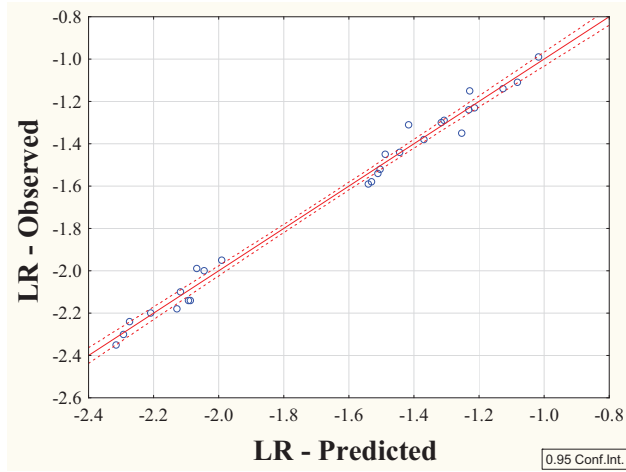
Figure 4.37: Observed vs. predicted LR by MLR in t–interval 50 min
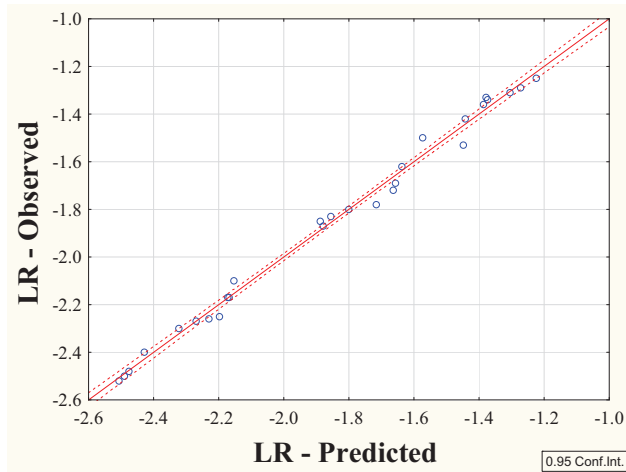
Figure 4.38: Observed vs. predicted LR by MLR in t–interval 55 min
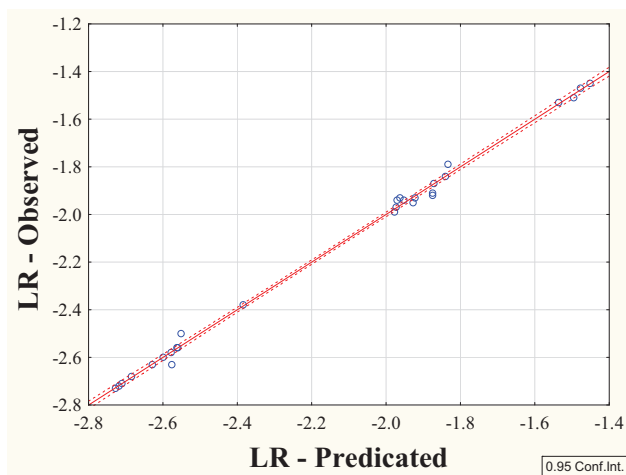
Figure 4.39: Observed vs. predicted LR by MLR in t–interval 60 min
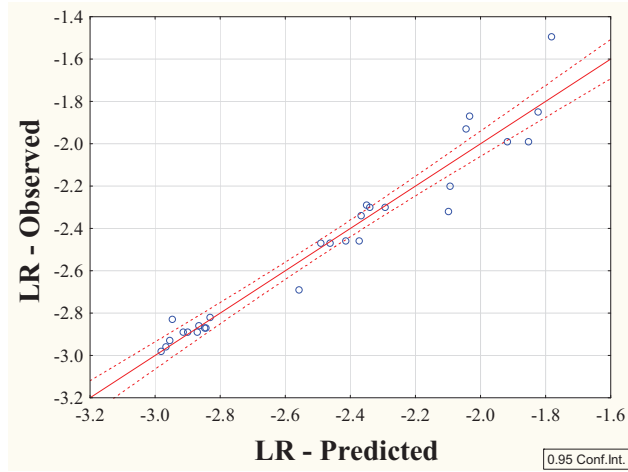
Figure 4.40: Observed vs. predicted LR by MLR in t–interval 65 min
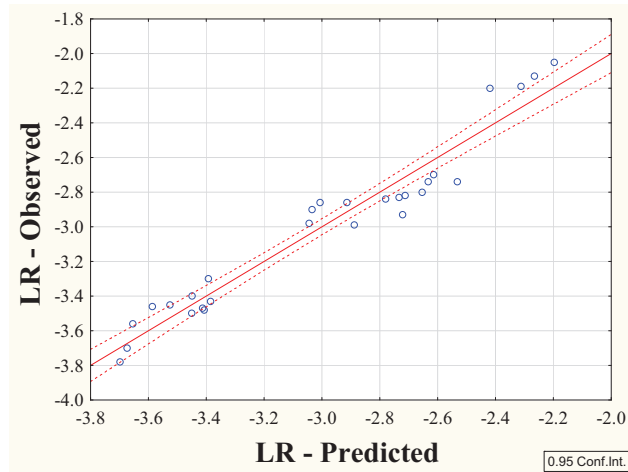
Figure 4.41: Observed vs. predicted LR by MLR in t–interval 70 min
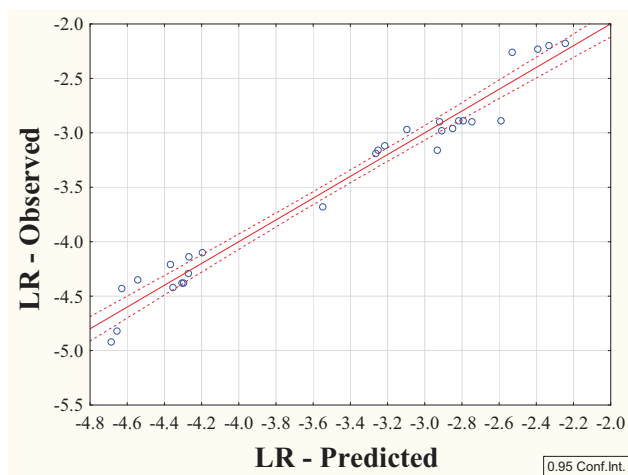
Figure 4.42: Observed vs. predicted LR by MLR in t–interval 75 min
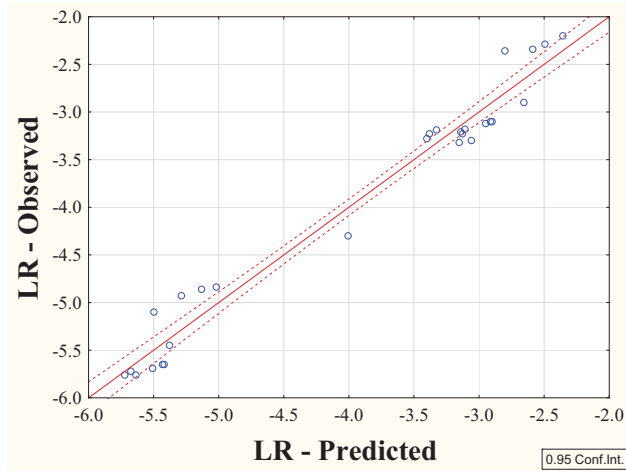
Figure 4.43: Observed vs. predicted LR by MLR in t–interval 80 min
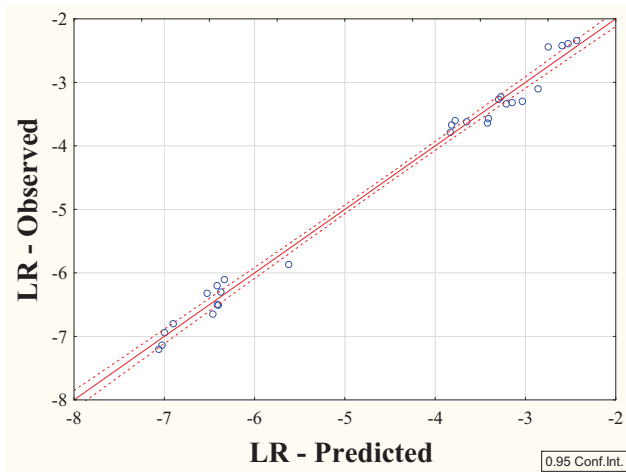
Figure 4.44: Observed vs. predicted LR by MLR in t–interval 85 min
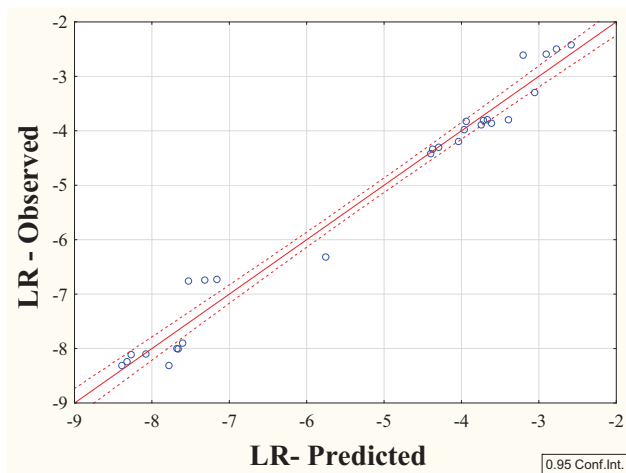
Figure 4.45: Observed vs.predicted LR by MLR in t–interval 90 min

4.2.3.2 Non–linear least–squares regression

To quantify the overall inactivation mechanism mathematical models were suggested. The underlying basic assumption was that, a homogeneous suspension of spores is exposed to BioElectro$^{\text{TM}}$ system at zero time. It was further assumed that the bulk solution concentration of BS and AN remains practically constant throughout the course of the experiment. Six empirical models (Table 4.9) were then developed.

Table 4.9: Developed disinfection kinetic models for BioElectro system

Model name	Model
BE1	$\log\left(\frac{N}{N_0}\right) = \left(b_1 + a_1 \cdot BS^{n_1} \cdot t^{k_1}\right)\left(b_2 + a_2 \cdot AN^{n_2} \cdot t^{k_2}\right)\left(b_3 + a_3 \cdot E^{n_3} \cdot t^{k_3}\right) \cdot N_0^{m_1}$
BE2	$\log\left(\frac{N}{N_0}\right) = (b_1 + a_1 \cdot N_0^{m_1} \cdot BS^{n_1} \cdot t^{k_1})(b_2 + a_2 \cdot N_0^{m_2} \cdot AN^{n_2} \cdot t^{k_2})(b_3 + a_3 \cdot N_0^{m_3} \cdot E^{n_3} \cdot t^{k_3})$
BE3	$\log\left(\frac{N}{N_0}\right) = \frac{-1}{(b_1 - 1)} \log\left(d_1 + (b_1 - 1) \cdot a_1 \cdot BS^{n_1} \cdot AN^{n_2} \cdot E^{n_3} \cdot t^{k_1} \cdot N_0^{(b_1-1)}\right)$
BE4	$\log\left(\frac{N}{N_0}\right) = (b_1 + a_1 \cdot BS^{n_1} \cdot t^{k_1})(b_2 + a_2 \cdot AN^{n_2} \cdot t^{k_2})(b_3 + a_3 \cdot E^{n_3} \cdot t^{k_3})$
BE5	$\log\left(\frac{N}{N_0}\right) = \frac{-N_0^{(b_1-1)}}{(b_1-1)(b_2-1)(b_3-1)} \cdot (1 + (b_1 - 1) \cdot a_1 \cdot BS^{n_1} \cdot t^{k_1}) \cdot (1 + (b_2 - 1) \cdot a_2 \cdot AN^{n_2} \cdot t^{k_2}) \cdot (1 + (b_3 - 1) \cdot a_3 \cdot E^{n_3} \cdot t^{k_3})$
BE6	$\log\left(\frac{N}{N_0}\right) = \frac{-N_0^{(b_1-1)}}{(b_1-1)(b_2-1)(b_3-1)} \cdot \exp\left(1 + (b_1 - 1) \cdot a_1 \cdot BS^{n_1} \cdot t^{k_1}\right) \cdot \exp\left(1 + (b_2 - 1) \cdot a_2 \cdot AN^{n_2} \cdot t^{k_2}\right) \cdot \exp\left(1 + (b_3 - 1) \cdot a_3 \cdot E^{n_3} \cdot t^{k_3}\right)$

N: Spore densities at time t–(CFU/ g TS)
N_0: Initial spore density–(CFU/ g TS)
AN: Applied ammonium nitrate dose–(g/L)
BS: Applied BIOXY S$^{\text{TM}}$dose–(g/L)
E: Applied electric field intensity–(V/cm)
t: Exposure time–(min)
a_i, b_i, d_i, k_i, m_i: Rate parameters

The inactivation model analyses of experiments were performed by fitting the experimental data to the newly developed inactivation models applying ordinary non–linear least–squares (NLLS) regression. Survival data from all data set were fit to each of the developed inactivation model at the same time (Section F.1). The best–fit inactivation model incorporated explicit dependence on the independent variables that had significant effects on disinfection efficiency. The best–fit model and its estimated parameters showed the type of dependency on electric field intensity (E), BIOXY S$^{\text{TM}}$ (BS) and ammonium nitrate (AN) concentrations and/or the initial spore density. In this case, the best–fit parameters were the ones that resulted in minimum sum of squares of differences in predicted and observed log survival:

$$\text{RSS} = \min \sum \left[\log \left(\frac{N}{N_0} \right)_{\text{predicated}} - \log \left(\frac{N}{N_0} \right)_{\text{observed}} \right]^2 \qquad (4.2)$$

where, $\log \left(\frac{N}{N_0} \right)_{\text{observed}}$ is the actual survival ratio of spores and $\log \left(\frac{N}{N_0} \right)_{\text{predicted}}$ is the survival ratio predicted through the equations in Table 4.9.

The goal for estimating the kinetic parameters was to ascertain the values in the most applicable rate expression that described disinfection performance. The first part of parameter estimation of inactivation models was done for all data sets at the same time. Each data set comprised of initial spore density (N_0), density of surviving spores (N), exposure time (t), electric field intensity (E) and applied enhancement agents doses (BS, AN). Only observations with non–zero values of surviving spore were used in the analysis. Therefore, the NLR of the inactivation data for each model was done using ordinary least squares regression. These computations were conducted using a non–linear optimization in MATLAB®(The Math Work, Inc., R2011a 7.12). Parameters were estimated for a single inactivation model for all data set; hence, the overall estimation process was repeated to check all of the six kinetic models for seven data sets. The residual sum of squares (RSS) of each fit along with the estimated parameters are given in Table 4.10. In addition, the adjusted

coefficient of determination (adj. r^2) for each model fit was calculated using Eq. 4.3.

$$\text{Adjusted r}^2 = 1 - \frac{\text{RSS}/(n-p)}{\text{TSS}/(n-1)} \tag{4.3}$$

where, n = the number of observations, p = the number of parameters where separate parameters were used for each experiment, RSS is residual sum of squares, and TSS is total sum of squares. In the usual r^2, the value of r^2 increases with an addition of a parameter. However, the adj. r^2 takes into account the number of predictors in the model and can decrease or increase as new parameters are added to the model [234].

Table 4.10: Summary of least–squares regression of developed models

Parameters	Model					
	BE1	BE2	BE3	BE4	BE5	BE6
a_1	0.0012	0.0003	0.0403	1.2495	0.0020	0.0030
b_1	0.0160	0.6600	0.8463	3.2458	0.6843	0.9076
d_1	–	–	0.9919	–	–	–
n_1	0.4290	0.4023	0.2176	0.3820	0.4130	4.0198
a_2	0.00001	0.00001	–	0.00003	263.4766	23.1124
b_2	0.0004	0.0001	–	1.6928	0.9999	1.0066
n_2	1.8220	0.6374	0.0328	0.4168	0.0019	0.0338
a_3	0.0001	28.3565	–	0.4933	1.1598	0.00001
b_3	579.5920	12.7959	–	0.4945	0.0125	0.0028
n_3	13.7691	5.9328	2.8343	0.2593	0.2625	17.1313
k_1	1.2454	3.2878	0.8413	0.3346	2.9092	17.1313
k_2	3.2077	3.6780	–	2.6482	0.0044	0.1323
k_3	2.5840	0.3596	–	0.0463	0.0430	2.2089
m_1	0.3085	0.2770	–	–	–	–
m_2	–	0.2567	–	–	–	–
m_3	–	0.0184	–	–	–	–
RSS	10.40	16.699	17.0983	33.1725	12.4223	28.4192
Adj. r^2	0.9765	0.9617	0.9630	0.9200	0.9701	0.9362

After fitting the inactivation data, the best–fit model was chosen. The primary criteria was to avoid "overfitting", where the addition of an extra parameter may result in lower RSS, howbeit, this extra parameter may add very little to the explanatory power [234]. For the sake of simplicity, first models were segregated into

subgroups based on the number of parameters they had. Then the models with the lowest RSS in each subgroup were compared with each other (Table 4.11). In a pairwise comparison, BE4 and BE6 did not presented any improvement in the fit over the BE5 model with the same number of parameters. In other words, the RSS from BE4 and BE6 was greater than that of the BE5 model. Accordingly, the application of the partial F–test to ascertain the significance of improvement was not pertinent in this case.

Table 4.11: Illustration of hierarchy and selection of models

Model	No. of parameters	RSS	1$^{\text{st}}$ step selection	Final selection
BE3	7	17.0983	BE3	
BE4	12	33.1725		BE3 vs. BE5
BE5	12	12.4122	BE5	
BE6	12	28.4192		
BE1	13	10.4003	BE1	BE3 vs. BE1
BE2	15	16.6986	BE2	BE3 vs. BE2

Next, the fairly simpler model was compared with a fairly more complex model (with an additional parameter) to examine whether the extra parameter ameliorates the fit reasonably. Models with more parameters generally have lower RSS, nevertheless, the improvement in the fit may not be compelling. Ergo, the statistical significance of improvement in fit was checked by partial F–test, where the F value was calculated as follows:

$$F = \frac{(\text{RSS}_{\text{Simple model}} - \text{RSS}_{\text{Complex model}})/(\text{df}_{\text{Simple model}} - \text{df}_{\text{Complex model}})}{\text{RSS}_{\text{Complex model}}/\text{df}_{\text{Complex model}}} \quad (4.4)$$

The corresponding probability was calculated applying the inverse F distribution function in Microsoft Excel 2007®, where the null hypothesis (H$_0$) was that the partial slope {F(Model with added parameter | Previous model)} equaled zero.

$$\text{Probability} = \text{P} = \text{F}_{\text{dis}}(\text{F}, \text{df}_{\text{Simple model}} - \text{df}_{\text{Complex model}}, \text{df}_{\text{Complex model}}) \quad (4.5)$$

where, df = degrees of freedom.

The significance level chosen in this process was 0.05. Probability, P, lower than the significance level attests the statistical significance of improvement in fit of the more complex model over the simpler model. In this way, statistical significance after the addition of parameter was examined. The pairwise F–test comparisons are given in Table 4.12. The comparison of the BE3 against the BE5, BE1 and BE2, which are more complex models, revealed that there was no statistically significant improvement in the fit of BE5, BE1 and BE2 even though the regression of which had lower RSS. Consequently, it was affirmed that the BE3 provided superior fit compared to other inactivation models.

Table 4.12: Probabilities for pairwise comparison of model fits with partial F–test

Simpler model		More complex model	Probability
BE3	vs.	BE1	0.4017
BE3	vs.	BE5	0.6342
BE3	vs.	BE2	6.4183

The 95% confidence intervals for each parameter of the best–fit model (BE3) was computed using the following F ratio test [235]:

$$\frac{\text{RSS}(\beta_p)/(n-df)}{\text{RSS}_0/(n-df)} \leq (1 + \text{F}^{df}_{n-p(1-\alpha)} \cdot \frac{p}{n-p}) \tag{4.6}$$

$$\text{RSS}(\beta_p) = \text{RSS}_0(1 + \text{F}^{df}_{n-p(1-\alpha)} \cdot \frac{p}{n-p}) \tag{4.7}$$

where β_p = the vector of parameters for the bound of confidence region, df = the degrees of freedom, n = the number of observations, and p = the number of parameters. F is the F statistic estimated through the inverse F probability distribution function in Microsoft Excel® 2007. For 95% confidence interval, α is 0.05, with a numerator degrees of freedom of p, and denominator degrees of freedom of (n - p). Eq. 4.7 was solved by altering one parameter at a time. This equation had at least two solutions for each parameter, and the upper and lower solutions closest to the optimum parameter were found by using "Goal Seek" add–in in Microsoft Excel® 2007. The estimated 95% confidence intervals for each parameter are given in Table 4.13.

Table 4.13: 95% confidence intervals for each parameter of each best–fit model

Model	Parameter	Optimum	Lower limit	Upper limit
BE3	a_1	0.0403	0.0362	0.0444
	b_1	0.8463	0.8038	0.8888
	d_1	0.9919	0.9489	1.0349
	n_1	0.2176	0.2026	0.2326
	n_2	0.0328	0.0307	0.0349
	n_3	2.8343	2.7829	2.8857
	k_1	0.8413	0.8033	0.8793

The main purpose of regression analysis was to ascertain the values of parameters in the most applicable inactivation model that supported the best prediction of observed LRs of spores. Regression plots can provide visual aspect on how well the model fits the observed data and the presence of any unusual observations that might be outliers. The regression plots of the best–fit model (BE3) for each experimental series are given in Figure 4.46 through Figure 4.52. In these regression plots, the predicted and observed LRs were graphed to see how well the predictions came true. The solid line represents equally predicted and observed LR. The smaller the spread around this line, the better the fit is. In most of the regression plots, the data points are grouped around this line.
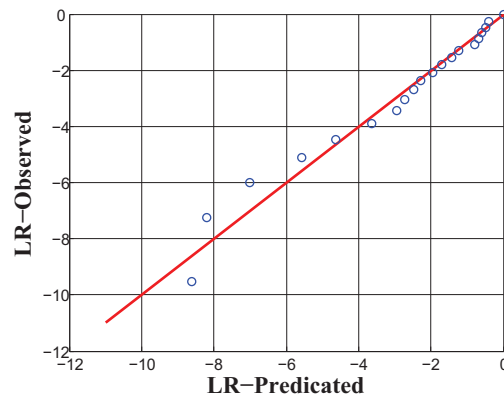
Figure 4.46: Observed LR vs. LR predicted by BE3 in the 1$^{\text{st}}$ experimental series
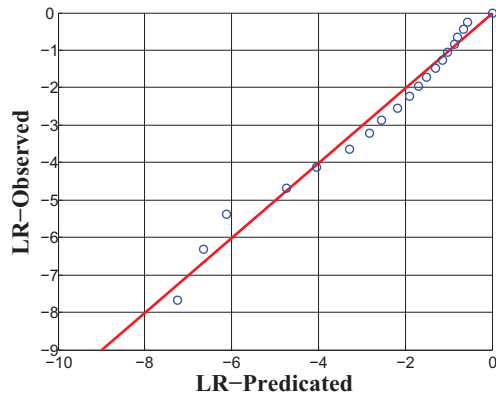
Figure 4.47: Observed LR vs. LR predicted by BE3 in the 2nd experimental series
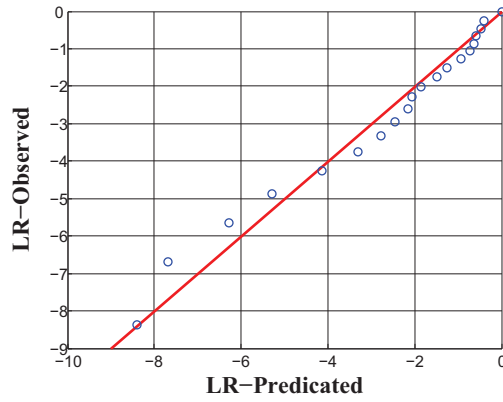
Figure 4.48: Observed LR vs. LR predicted by BE3 in the 3rd experimental series
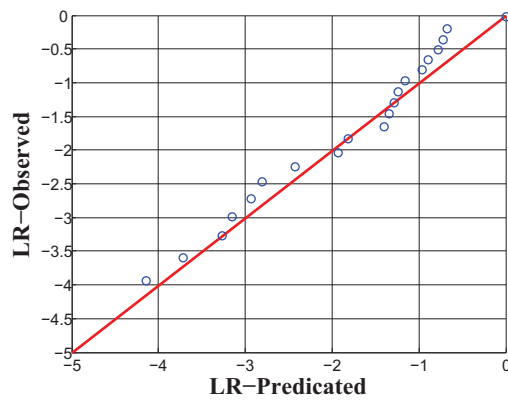
Figure 4.49: Observed LR vs. LR predicted by BE3 in the 4th experimental series
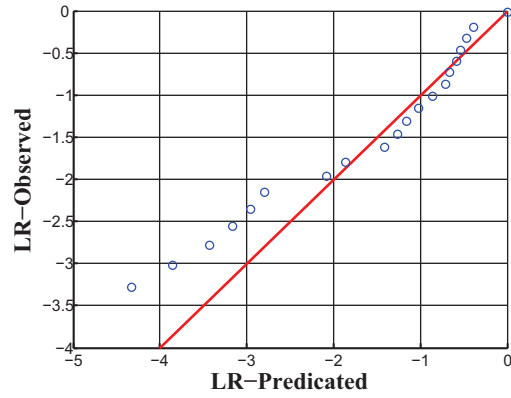
Figure 4.50: Observed LR vs. LR predicted by BE3 in the 5th experimental series
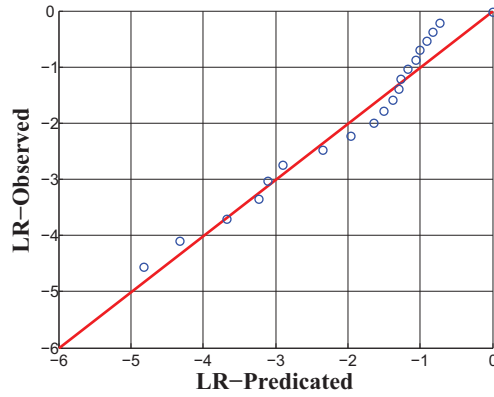
Figure 4.51: Observed LR vs. LR predicted by BE3 in the 6th experimental series
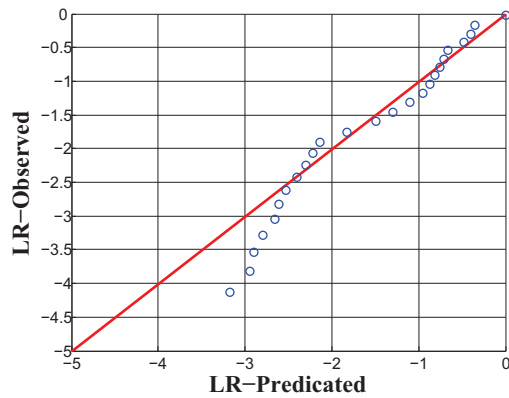
Figure 4.52: Observed LR vs. LR predicted by BE3 in the 7th experimental series

4.3 Chemical, physical and biological impact of Bio-Electro process

The following subsections detail the results of the bench–scale studies and evaluate the chemical, physical and biological effects of the disinfection process. Chemical analyses were pH, ammonium ion and total alkalinity. The physical parameters of interest are local field distribution, current norm distribution, power dissipation and temperature. The biological factors to be studied were germination state and ultrastructural changes.

4.3.1 pH and ion distribution

It is important to track the acid-base equilibria (including pH) across the EK reactor since these acid-base equilibria determine local ion mobilities and conductivities of the electrolyte and are strongly affected by the rate and nature of electrolytic reactions. In other words, reactions occurring at the electrode surfaces are intimately coupled to local chemistry and electrokinetic phenomena. The measured pH values for BioElectro^{TM} process at the vicinity of cathode, anode and overall reactor are presented in Table 4.14. The biosolids′ pH values of the most sections diverge from the initial value of pH 8.17 to maximum and minimum pH values of 13.87 and 1.98, respectively; achieved by treatment (E = 2.8, BS = 13, AN = 26). It is evident that biosolids treated under higher electric field intensity, E = 2.8, showed a greater deviation from the initial value compared with those treated by E = 2.5. The pH profile of the system depicted in Figure 4.53 demonstrate a sharp increase in pH between the anode and cathode. This could be due to several factors: *a*) concentrations and mobilities of other ions exist in the solution influence the location of the pH jump via affecting the distribution of the electric field and forming complexes with hydroxyl ions and protons; *b*) the pH buffer capacity, cation exchange capacity of the biosolids and interactions of the solution with the biosolids may alter the speed of the advancement of the acidic and the basic front and the location of the pH jump.

Table 4.14: Summary of pH values in each experimental series

E(V/cm)	BS(g/L)	AN(g/L)	Data pt	pH		
				C*	A**	Overall***
2.8	13	26	560	13.87	1.98	7.80
2.8	25	13	560	13.65	3.12	8.29
2.8	13	13	560	13.56	3.02	8.15
2.5	25	13	560	12.87	3.10	8.15
2.5	13	26	560	12.54	3.32	8.12
2.5	25	26	560	12.78	3.10	8.16
2.5	13	13	560	12.45	3.23	8.29

*Max measured pH in the Cathode area

**Min measured pH in the Anode area

***Max measured pH in the whole reactor
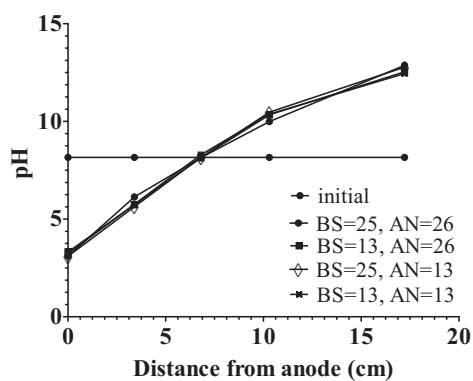
(a) E = 2.5 V/cm
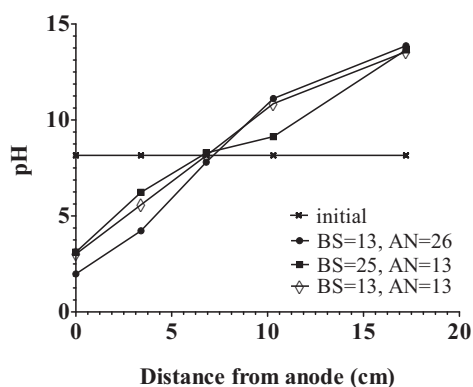
(b) E = 2.8 V/cm

Figure 4.53: pH profile of BioElectro^{TM} process

As the BioElectro$^{\text{TM}}$ process take advantage of some concentrations of BS and AN, it was necessary to ascertain the effect of this two salts on concentrations of total alkalinity (A_T) and total ammonia, $(NH_3)_t$. The measured alkalinity was in the range between 52 and 79 mg $CaCO_3$/L. It was evident that application of BS influenced A_T of the system. For instance, an increase in the concentration of BS from 13 to 25 g/L brought about a 42 percent surge in A_T. This effect could be related to the presence of $NaCO_3$ in BS formulation as explained earlier (Subsection 2.2.2). A similar but more pronounced association was determined between applied concentrations of AN and the rise in $(NH_3)_t$ amounts. Essentially, by duplicating the applied concentration of AN the measured amount of $(NH_3)_t$ showed a 78 percent increase. The data in Table 4.15 also show a 99 percent decrease in viscosity of the processed biosolids stored at room temperature (21–23°C).

Table 4.15: Total alkalinity, total ammonia and viscosity results in each experimental series

E(V/cm)	BS(g/L)	AN(g/L)	A_T(mg $CaCO_3$/L)	$(NH_3)_t$(mg/L)	η^*(mPa.s)
2.8	13	26	52	489	3.0
2.8	25	13	79	274	2.7
2.8	13	13	78	218	3.1
2.5	25	13	77	194	2.7
2.5	13	26	55	470	3.1
2.5	25	26	78	440	2.7
2.5	13	13	52	256	3.0
Blank			44	72.1	287

*At the room temperature

(a) E = 2.5 V/cm   (b) E = 2.8 V/cm
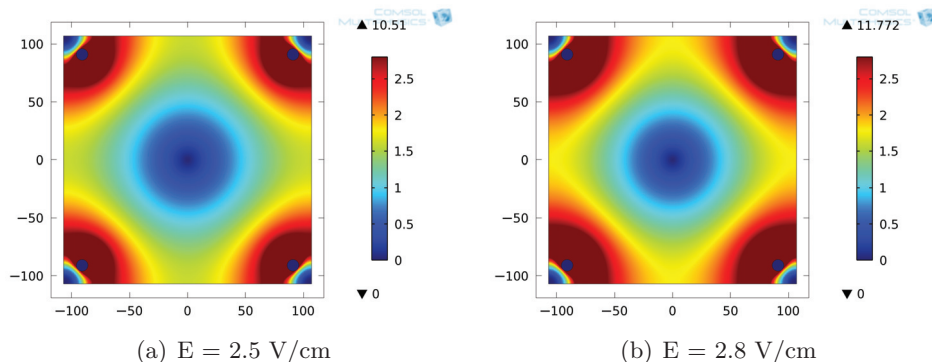
Figure 4.54: Calculated electric field distribution for BioElectro[TM] system. The values of electric field strength are displayed by color scale legend with the maximum value E = 2.8 V/cm

4.3.2 Local electric field distribution in BioElectro[TM] system

As explained in Subsection 3.5.7, the electric field distribution in BioElectro[TM] system was studied using the FEM model consists of 2,700 triangle elements. The 2D model was used, corresponding to the cross section of the EK reactor. The conductivities of the bulk biosolids was defined based on Table 3.13.

The final results of this modeling Figure 4.54 showed that the electric field distribution is nonhomogeneous and mainly governed by the reactor shape and electrode configuration. On the basis of the modeling results, it was observed that biosolids electrical conductivity does not influence the distribution of the electric field within the reactor. Although the BioElectro[TM] treatment may alter the uniformity of biosolids electrical conductivity to some extent, the electric field distribution still reflects the effects of the electrode configuration. The highest electric field strength occurs in the vicinity of electrodes; the higher the distance from the current electrodes, the lower current density. This leads to stronger electrochemical reactions and generation of oxidizing agents at the electrode (electron conductor) and bisolids (ionic conductor) interface. Also, it was evident that with increasing the applied E from 2.5 to 2.8 V/cm the electric field strength inside the reactor became higher.

4.3.3 Current density norm in BioElectro^{TM} system

Numerical computations were also conducted by means of FEM for current density norm. It can be clearly seen (Figure 4.55) that both applied electric field and conductivity of the system are the major determinant of the maximum current density in the distribution profile. For example, increasing conductivity of the system from 4.37 to 27 mS/cm at the applied E = 2.5 V/cm brought about a surge in CDN by a factor of about 5. The same increase in conductivity at the applied E = 2.8 V/cm begot an increase by a factor of about 6. Also, comparable to the electric field distribution, the highest current density was observed in the proximity of electrodes.

4.3.4 Total power dissipation density in BioElectro^{TM} system

The results of numerical calculation on TPDD in BioElectro^{TM} system revealed its dependency on applied E and conductivity of the system. Applying greater electric field or increasing electrical conductivity of the system brought about smaller cold (blue) area or greater radial distribution of power dissipation (Figure 4.56). This will be more evident, by comparing conditions with the same conductivity and different applied electric field intensities (e.g., Figure 4.56(a) and Figure 4.56(b)) or conditions of similar electric field intensity at various conductivities (e.g., Figure 4.56(d) and Figure 4.56(f)). Likewise electric field distribution and CDN, the higher degree of potential drop was detected in the electrode neighborhood due to the resistance of the solution near the electrode surface and higher rate of electrochemical reactions. Table 4.16 presents the effect of different electric field intensity and EC on TPDD and volumetric energy (Q_v). These results suggest that electric field used in BioElectro^{TM} process exceeded the decomposition voltage of water. This implies that the EK reactor exhibits an ohmic loss as explained in Subsection 2.1.1.2.

(a) E=2.5 V/cm, κ=4.37 mS/cm

(b) E=2.8 V/cm, κ=4.37 mS/cm

(c) E=2.5 V/cm, κ=23 mS/cm

(d) E=2.8 V/cm, κ=23 mS/cm

(e) E=2.5 V/cm, κ=25 mS/cm

(f) E=2.8 V/cm, κ=25 mS/cm

(g) E=2.5 V/cm, κ=27 mS/cm

(h) E=2.8 V/cm, κ=27 mS/cm
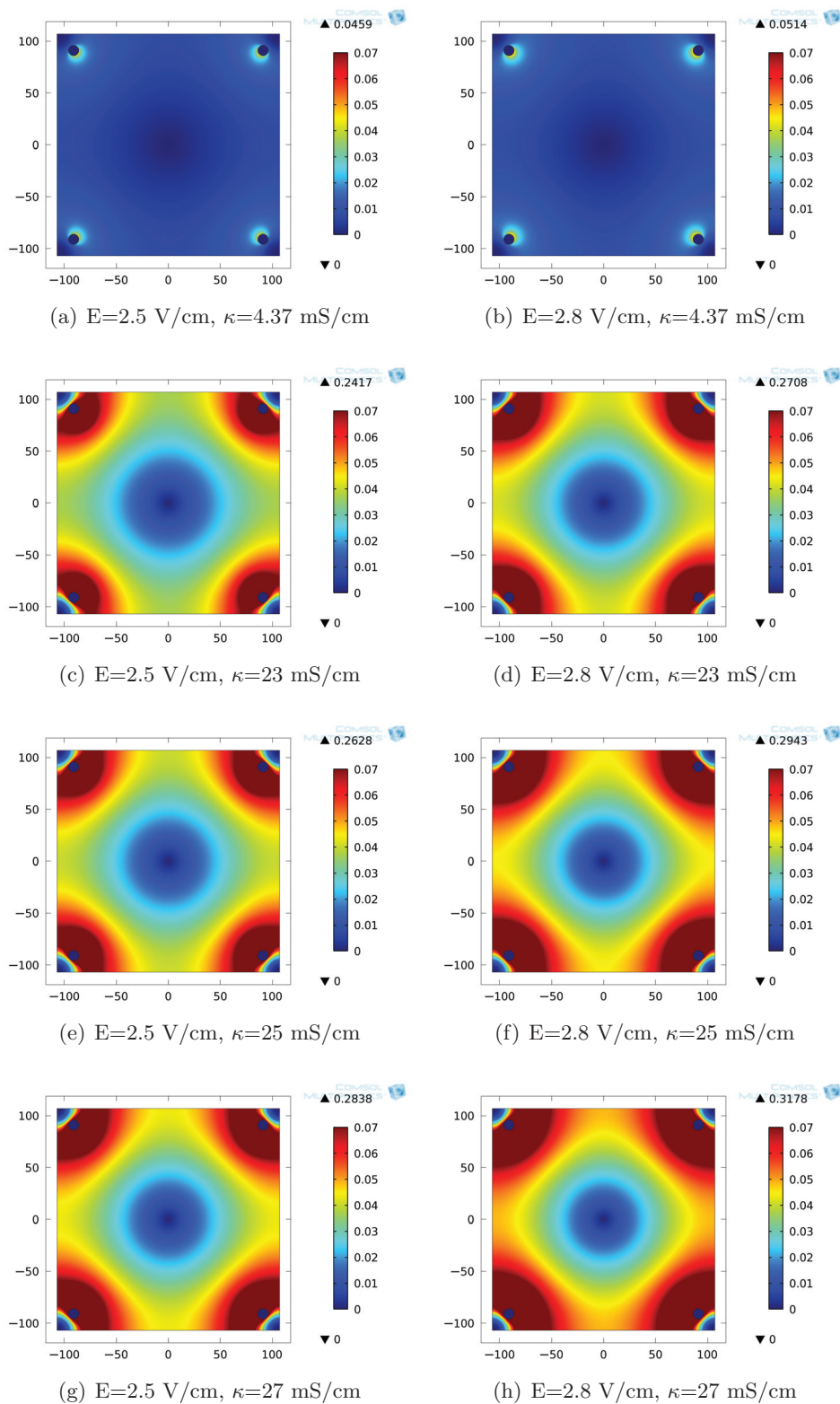
Figure 4.55: Calculated current norm distribution for BioElectro™ system at different E and conductivities

(a) E=2.5 V/cm, κ=4.37 mS/cm

(b) E=2.8 V/cm, κ=4.37 mS/cm

(c) E=2.5 V/cm, κ=23 mS/cm

(d) E=2.8 V/cm, κ=23 mS/cm

(e) E=2.5 V/cm, κ=25 mS/cm

(f) E=2.8 V/cm, κ=25 mS/cm

(g) E=2.5 V/cm, κ=27 mS/cm

(h) E=2.8 V/cm, κ=27 mS/cm

Figure 4.56: Calculated total power dissipation density for BioElectro$^{\text{TM}}$ system at different E and conductivities

Table 4.16: Calculated TPDD and volumetric energy

κ(mS/cm)	E(V/cm)	PG (V)	Current(A)	TPDD average(W/cm^3)	Q_v*
4.37	2.5	43	0.6307	0.0170	27
	2.8	48	0.7063	0.0213	34
23	2.5	43	3.3185	0.0894	144
	2.8	48	3.7167	0.1121	180
25	2.5	43	3.6071	0.0972	156
	2.8	48	4.0399	0.1219	196
27	2.5	43	3.8956	0.1049	168
	2.8	48	4.3631	0.1316	212

* Q_v = Volumetric energy a.k.a Joule heating

4.3.5 Impact of ohmic heating on temperature rates in BioElectro process

To investigate the ohmic heating impact, thermometers were introduced to the reactor, as explained in Subsection 3.1.1, to measure the temperatures. The temperature

Table 4.17: Summary of maximum recorded temperatures in each experimental series

E(V/cm)	BS(g/L)	AN(g/L)	T(°C)				
			C*	at t(min)	A**	at t(min)	ave.***
2.8	13	26	97.0	74	98	74	97.5
2.8	25	13	97.0	60	97	60	96.0
2.8	13	13	96.0	62	97	71	96.2
2.5	25	13	95.5	73	96	91	95.5
2.5	13	26	95.0	92	96	96	94.6
2.5	25	26	92.0	99	92	87	91.0
2.5	13	13	97.0	110	97	95	96.3
2.8	0	0	56.0	173	29	173	30.6
2.5	0	0	55.0	198	27	198	29.8

* Max measured T in the Cathode area

** Max measured T in the Anode area

*** Max measured T in the center of the reactor

log (Table 4.17) showed an increase in temperature in all seven experimental conditions (Table 4.17). Ohmic heating effect was particularly stronger at the presence of enhancement agents due to increasing conductivity. The temperature rise from
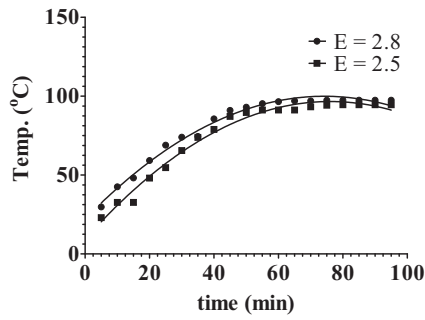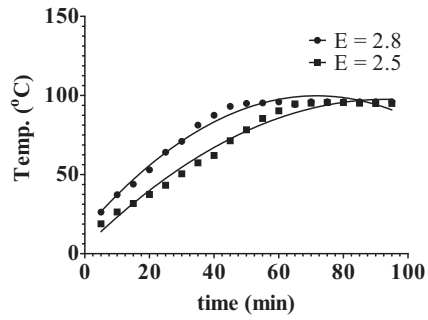
(a) BS=13, AN=26 (g/L)　　　　　(b) BS=25, AN=13 (g/L)
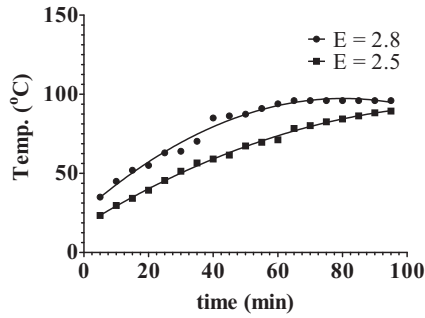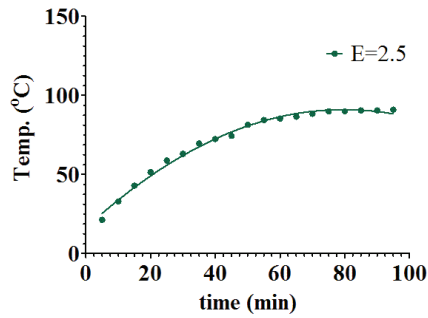
(c) BS=13, AN=13 (g/L)　　　　　(d) BS=25, AN=26 (g/L)

Figure 4.57: Heating rates in biosolids as a function of the applied electric field intensity

the power dissipated as heat due to electric resistance of the biosolids is observed to follow Joule's law $(P = V^2/R)$, whereby the increase in heating rate is coupled to the increased applied electric field intensity (E). This relationship is made apparent in Figure 4.57 where increasing applied electric field, while the concentrations of enhancement agents are constant, generated greater heat.

4.3.6 Impact of BioElectro process on germination of *C. perfringens* spores

To assess the proposed hypothesis about the effect of low intensity electric field (LIEF) on spore activation (Subsection 2.2.4.4), the time–course of the spore germination was followed by observing the changes in OD_{600} of treated samples. The loss of OD_{600} was observed in electric field–treated spores as stated in Table 4.18. All raw data are provided in Appendix G.

Table 4.18: Loss of OD for *C. perfringens* spores during exposure to LIEF

E (V/cm)	Mean[a] %decrease (±StDev) in OD_{600} in 60 min
2.5	54 ± 0.19
2.8	56 ± 0.33
Data pt	78

[a] Values are geomean of quadruplicate experiments

As shown in Figure 4.58, both curves (E = 2.5 and 2.8 V/cm) presented a sigmoidal decline preceded by an interval of constant absorbance, called the lag period, however, reduction in OD_{600} was faster for those spore treated with 2.8 V/cm than those of 2.5 V/cm.
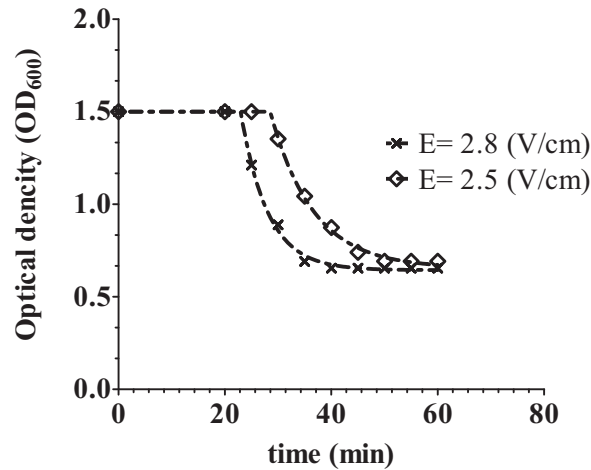
Figure 4.58: Rate of loss in OD_{600} values of *C. perfringens* spores during exposure to LIEF

Also, to estimate the extent of electric field–induced germination of *C. perfringens* spores, the biosolids was examined for viable counts before and after exposure to E = 2.5 and 2.8 V/cm, for one hour. As shown in Figure 4.59, the differences in viable spore counts between before (A) and after (B, D) LIEF treatment indicated a meager spore reduction. However, this decline was significant for the same suspension of spores after 40 minutes incubation at 45°C (C, E). These results proffer that although spores are highly resistant to LIEF treatment, they can be activated and germinate under the influence of electric field. The incubation time was necessary for the spore to pass the activation, outgrowth and germination stage. It was also observed that the spore germination was slightly (4%) higher for E = 2.8 V/cm than 2.5 V/cm.
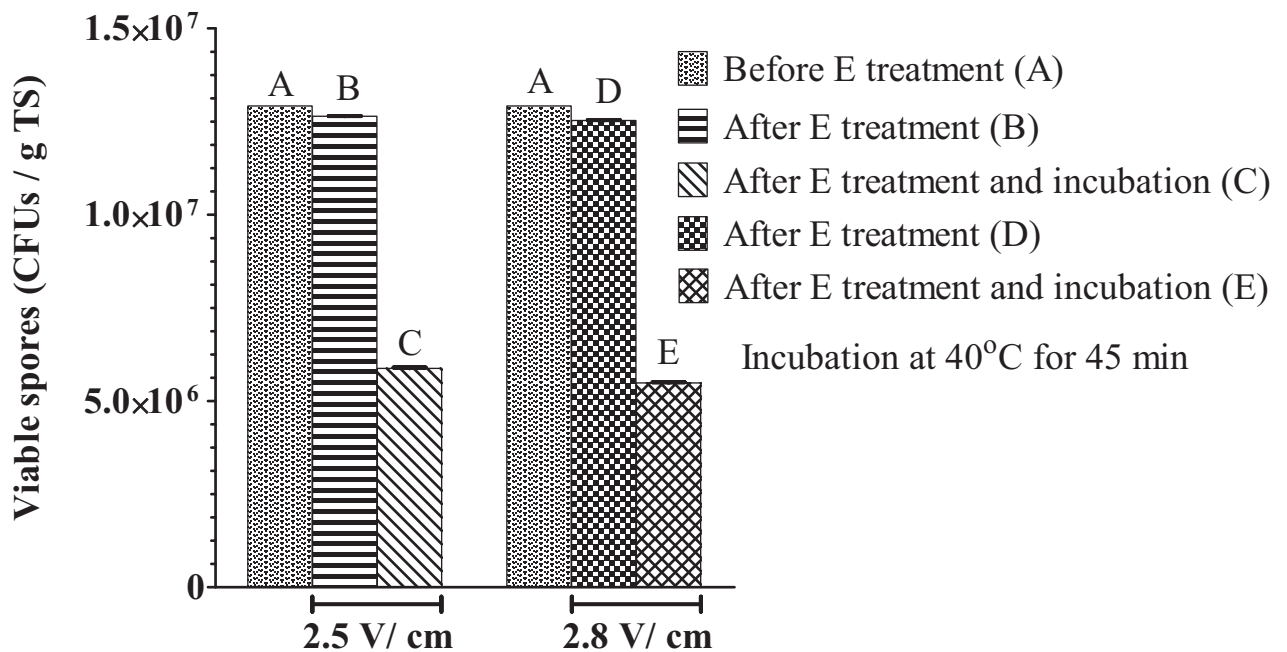
Figure 4.59: Viable–spores count of *C. perfringens* before and after exposure to LIEF (2.5 and 2.8 V/cm), and after subsequent incubation at 40°C

4.3.7 Impact of BioElectro^{TM} process on ultrastructure of the spore

Representative micrographs of thin sections of *C. perfringens* spore reveals a number of cortical integuments surrounding the spore core. It was, therefore, essential

to define which of these are present in the intact spore and to compare the morphological changes after exposure to AN, BS, LIEF and a combination of which in BioElectro^{TM} system.

Ultrathin sections of intact *C. perfringens* spores divulge the dark spore core surrounded by a thick, electron–transparent cortex and a multi–layered spore coat (Figure 4.60). Flanked by the spore core and cortex, an electron–translucent germ cell wall (GCW) is typically descried (Figure 4.60b). The cortex shows dark stained granules (G) at its exterior edges (Figure 4.60b). The ≈ 25–50 nm thick spore coat (Ct) is constructed by a 4–8 nm dark layer (Da) facing the cortex, a second 5–8 nm dark layer (Dr) and a 8–12 nm grey layer (Gr) sandwiched in between. As seen in Figure 4.60c, the spore is surrounded by a 70–90 nm layer of the exosporium (Ex) which is made by two main layers: A ≈ 60–80 nm dark outer layer (Na) decorated by a nap of hair–like projections that irregularly arise from an intermediate covering and a ≈ 4–10 nm light inner basal layer (Ba).

4.3.7.1 Effect of AN on spore ultrastructure

Electron micrograph (EM) of AN treated (2.6% w/v) *C. perfringens* spores (Figure 4.61) appeared very similar to that of intact spore for it possesses a featureless and dark core enclosed by a thick (50–130 nm), electron–transparent cortex (Figure 4.61b) and a multi–layered spore coat (Figure 4.61c). Sandwiched between the spore core and cortex, the translucent germ cell wall was identified. Dark stained granules were also recognized at the cortex outer border (G). The spore coat resembles that of intact spore for having two dark layers flanking an 8–11 nm grey layer. Spores are delimited by a dense exosporium layer (60–85 nm) which is made of a hair–like (50–60 nm), outer layer and a light inner layer (3–7 nm). Ultrastructural analyses, as well as colony–forming ability of treated spores revealed no indication of inactivation due to exposure to AN.
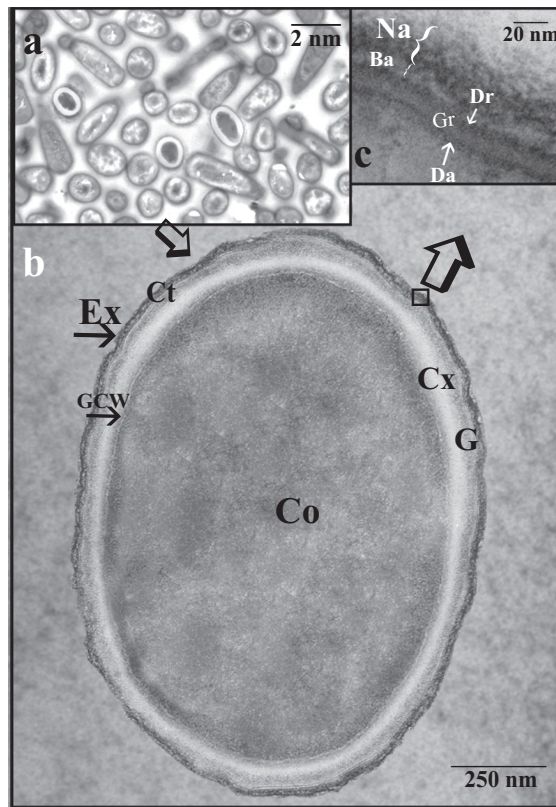
Figure 4.60: EM sections of *C. perfringens* spore suspension. (a) Overview showing spores with dark core and white cortex. (b) Between the core (Co) and cortex (Cx), a lightly stained germ cell wall (GCW, black arrow) is typically observed. The light staining cortex (Cx) has dark stained granules at its outer edges (G). (c) Detail of the spore coat, showing three coat layers (Da, Gr and Dr), as well as a dark outer layer (Na) and a light inner basal layer (Ba) forming the exosporium
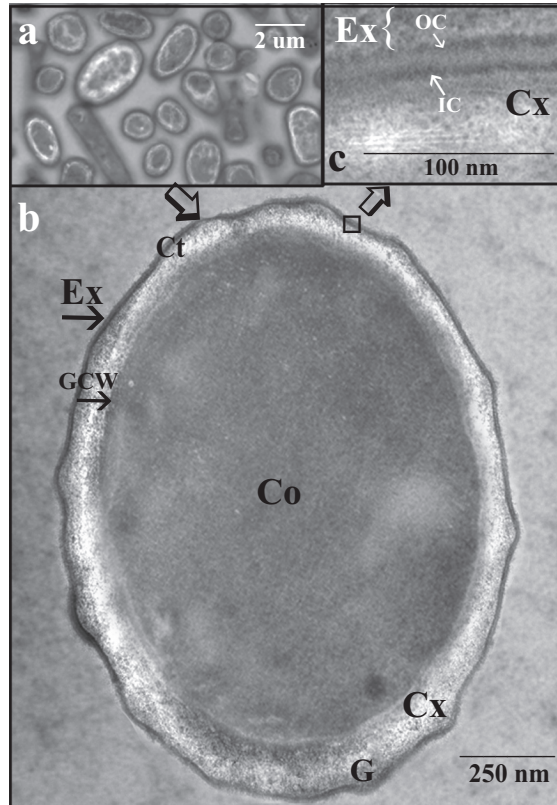
Figure 4.61: TEM micrograph of *C. perfringens*spore after treatment with 2.6% (w/v) AN. (a) General view of spores with electron dense core and white cortex. (b) The light staining cortex (Cx) with dark stained granules (G) at its border with spore coat. A lightly stained germ cell wall (GCW, black arrow) is located between the core (Co) and cortex (Cx). (c) Feature of the spore coat, representing inner coat layer (IC) and outer coat layer (OC)

4.3.7.2 Effect of BS on spore ultrastructure

A 15 minute exposure to BS primarily created nicks in the inner, narrow, electron dense coat (Figure 4.62a: black arrows) with noticeably changing the ultrastructure of the exosporium, the outer coat and the internal structure. The cortex layer was not easily detectable. Treated spores exhibited morphological features distinct from intact spores, e.g., spores showed polygon shapes, and they shrank. A 30 minute exposure led to destruction of the spore integuments (exosporium, spore coats and cortex) (Figure 4.62b: black circles) and ultimately brought about the dissolution of ulcerated spores (Figure 4.62b: black arrow).
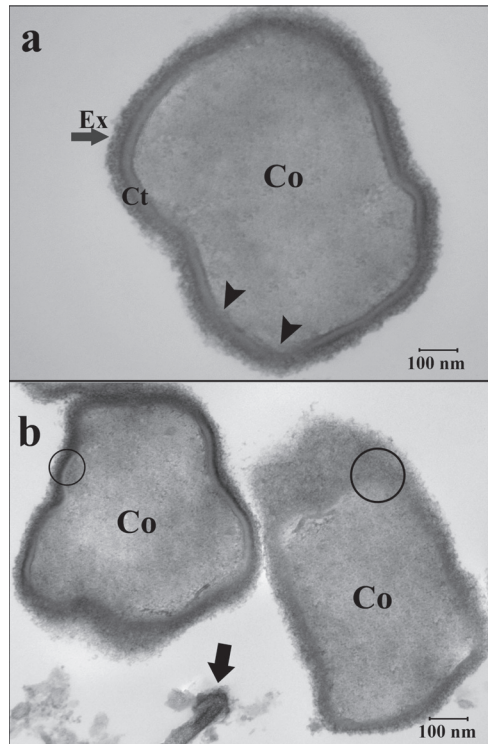
Figure 4.62: Ultrastructure *C. perfringens* spores treated with BS. (a) Note creation of nicks (black arrows) and deformation of the spore body. (b) Black circles showing the destruction of exosporium, spore coats and cortex. The debris of a hydrolyzed spore (black arrow)

4.3.7.3 Effect of LIEF on spore ultrastructure

After a 30 minute exposure to LIEF the structural components discerned in the intact spore were more discernible, in addition to several others not easily observed

in intact spores. The core membrane (CM), germ cell wall (GCW), cortex (Cx) and coat layers (Ct) were evident. Compact spore cytoplasm changed into a spongy structure represents the protoplast (P). Vesicular bodies (V) can be differentiated at the edge of the protoplasmic core (Figure 4.63(a)). Nicks became visible in the fine striated inner spore coat (Figure 4.63(a): white arrow) accompanied by a thinning of the outer spore coat (Figure 4.63(a): black square). As shown in Figure 4.63(b) (black circle), the inner and outer spore coats were almost completely disintegrated, and the spore possesses a distinctly fibrillar nucleoplasm (N) surrounded by a cytoplasm (C). The conspicuous features in Figure 4.63(c) are the breakdown of the cortex along with the development of young cell. The cell wall (CW) was also well defined. The overall pattern of ultrastructural changes was followed by loss of OD_{600} of the spore suspension (Subsection 4.3.6).

4.3.7.4 Effect of BioElectro^{TM} on spore ultrastructure

After a 60 minute treatment of spores by BioElectro^{TM} system a series of spores with different morphologies characteristics was discerned (Figure 4.64). While some spores have a distinct fibrillar nucleoplasm delimited by a granulated cytoplasm, the lamellated mesosome and the cell wall, which are a representation of the germinated spore (Figure 4.64a), others developed certain emblematic characteristics of gradual disintegration that include progressive lightening of the spore core, destruction of the exosporium, spore coat and cortex. With prolonged treatment (two hours) the integuments become progressively thinner and led to complete dissolution of the spores and naked sporeplasts (Figure 4.64b).
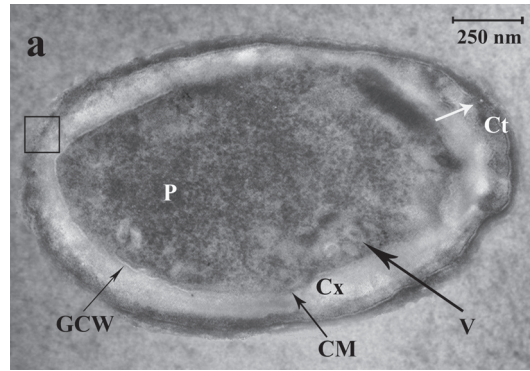
(a)
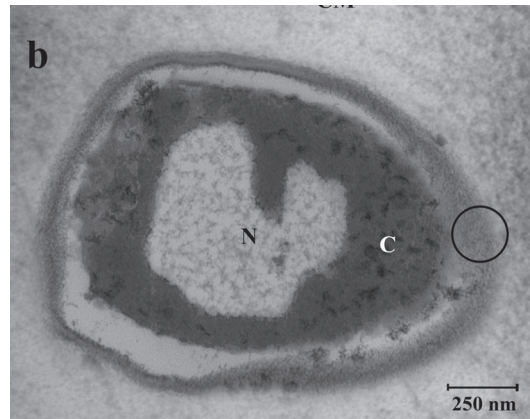
(b)
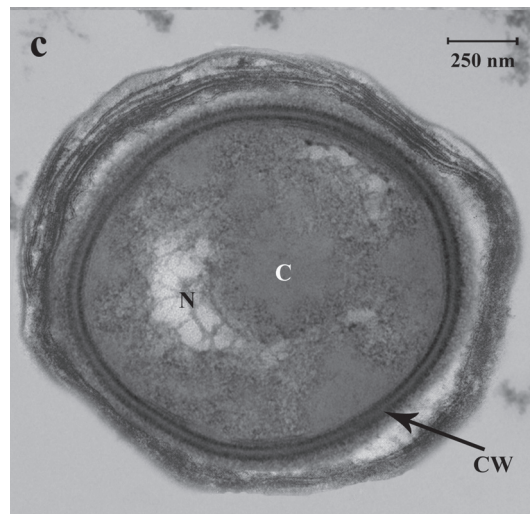
(c)

Figure 4.63: Effect of exposure to LIEF on *C. perfringens* spore. (a) Appearance of core membrane (CM), germ cell wall (GCW), cortex (Cx) and coat layers (Ct), protoplast (P) and Vesicular bodies (V). Break in inner spore coat (white arrow) and thinning of the outer spore coat (black square). (b) Disintegration of coat layers (black circle). Fibrillar nucleoplasm (N) surrounded by a cytoplasm (C). (c) Well defined cell wall (CW)
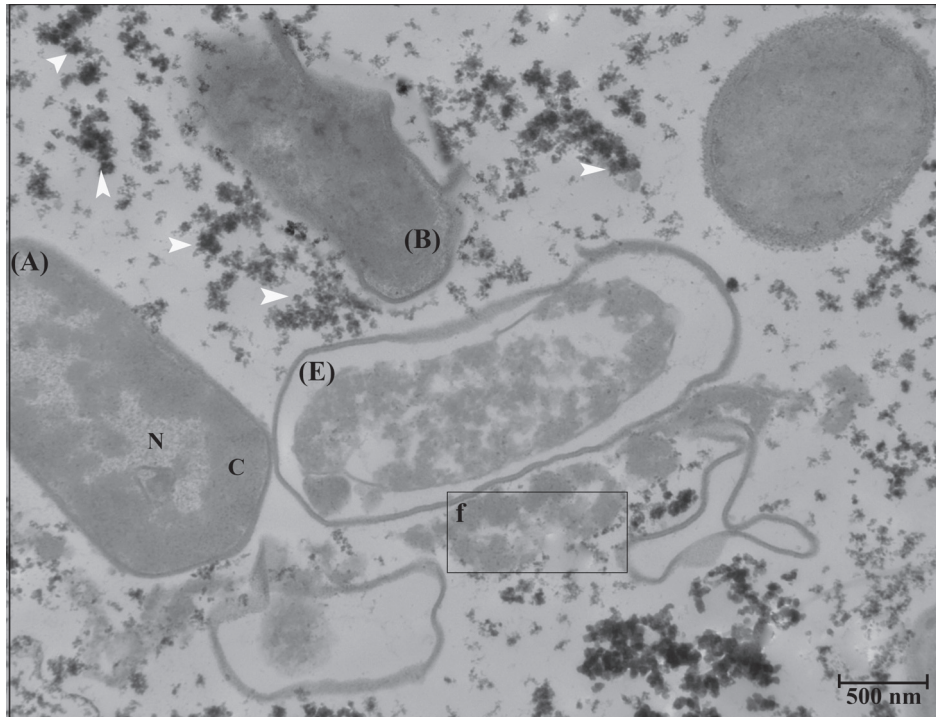
Figure 4.64: Ultrastructure of *C. perfringens* spores after treatment by BioElectro^{TM}. Compare Spore (A) with the spore in Figure 4.63(b). The nucleoplasm (N) and granulated cytoplasm are evident in both cases. Note to the spore (B). The spore coat layers and cortex have been hydrolyzed similar to that of Figure 4.62. Disintegrated spores (E), naked sporeplasts (inset f) and spore debris (white arrows) are easily detectable

Chapter 5

Discussion on mechanism of disinfection

The objective of this study was to ascertain the optimal conditions for pathogen inactivation in anaerobically digested sewage sludge using an enhanced 2D electric field process, BioElectro$^{\text{TM}}$. Furthermore, it was intended to ascertain disinfection kinetic and mechanism of spore inactivation in the designed system. Several screening tests were conducted to determine these optimum conditions; while bench–scale disinfection testes were implemented to verify their impact on physical, chemical and biological parameters through which the mechanism of disinfection was explained. Mathematical models were developed to describe the precise relationship between experimental variables and disinfection efficiencies.

In general, the results from this work showed that there are high numbers of *C. perfringens* spores in anaerobically digested biosolids and BioElectro$^{\text{TM}}$ process was effective in significantly eradicating (>3 LRs) the number of this bioindicator (Table 4.5) in the AnD biosolids matrix. This can be observed evidently by comparing samples before and after treatment through BioElectro$^{\text{TM}}$ process (Figure 5.1). The results and review of the data affirmed process reliability and product quality that exceeds the P_1 (Class A) regulatory compliance. This process offer advantages over conventional methods by providing an interactive disinfection system and ap-

(a) Before treatment (b) After treatment
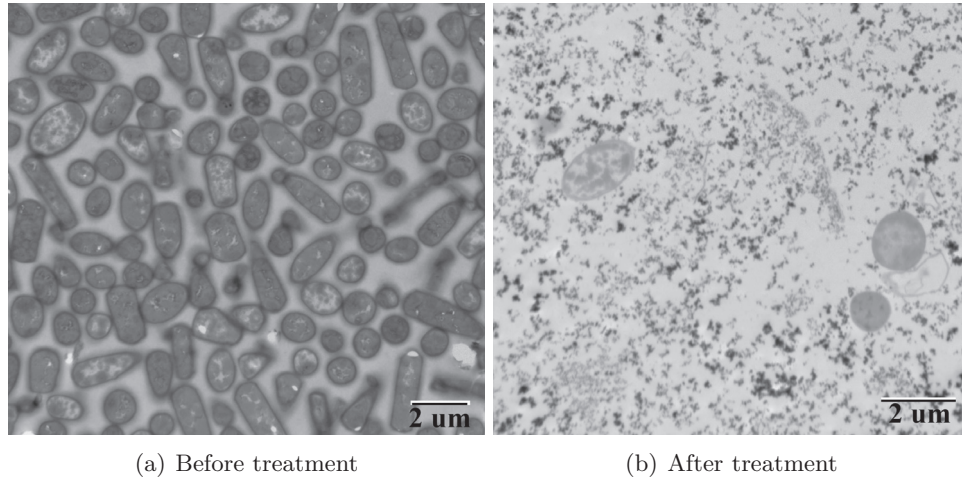
Figure 5.1: Comparison of spores before and after BioElectro$^{\text{TM}}$ treatment

plying multiple stressors. Combination of stressors can lead to cost reductions and a superior quality biosolids product.

An interesting feature observed in BioElectro$^{\text{TM}}$ treatment of spore was its triphasic survival curves, comprising a short linear segment, followed by a very large shoulder and finally a first–order inactivation kinetics. It was suggested that this pattern is due to the nature of the treatment and effect of multiple stressors. The results of MLR analysis confirmed combination effect of several stressors on disinfection efficiency of BioElectro$^{\text{TM}}$. At the beginning of procedure, t = 10 minutes, applied BS concentrations showed (Table 4.7) more pronounced effects compared with other factors, namely E and AN. This stage was identified with 60 percent reduction in number of spores and appearance of linear phase in the spore survival curves. As observed from ultrastructural investigations (Figure 4.62), BS first produced breaks in spore coat along with destructions in the cortex and spore shape, and finally the ulcerated spore began dissolution. The chemical composition of BS implies that its sporicidal activity is allied to the concentrations of hydrogen peroxide and a much greater extent to peracetic acid (PAA) (Reaction [3] through Reaction [6]). PAA is a rather small molecule that should easily traverse cross the exosporium and coats of bacterial spore [236]. Seemingly, PAA molecules can penetrate the cortex space but may not be able to cross the inner spore membrane which is believed to be a

condense state [237]. Oxygen–based free radicals could then be generated in the environment outside of the coats or in the cortex space. They would have to diffuse to targets within the protoplast, possibility in the core membrane. However, at present, there is no information on the targets for the lethal action of BS. It does seem reasonable to conclude that oxygen–centered free radicals are involved in killing. No signs of germination in treatments with BS were detected. Subsequently, it is believed that oxidative killing by BS did not entail germination of spores and consequent killing of sensitive germinated cells. Moreover, BS inactivation is akin to heat killing in that spores are killed completely before any major deprivations in refractivity or release of dipicolinic acid (DPA) [129]. Sufficient ($\geq$3 LRs) sporicidal effect of BS in biosolids matrix is only detectable in concentrations greater than 18 percent (w/v) (Table 3.3). This low efficiency is associated with instantaneous demands (5 g/L) (Table 4.6) for PAA in biosolids matrix and its substantial decay (decay rate of 0.293 min^{-1}) (Figure 4.9) to carbon dioxide and water.

At higher exposure times, the period of time beginning at 15 minutes and expanding up around 60 minutes, the effect of E and its interactions with BS and AN was more evident (Table 4.7). This interval time is characterized with the presence of an extensive shoulder in the survival curve (Figure 4.1). To explain shoulder formation, Shull et al. (1963) suggested that the spore suspension contained an initial activated and dormant population of spores which has to be activated prior to be destroyed [238]. In the performed experiments this possibility was examined by determining physiological state or "fitness" of treated spores. The fitness of cells described as both structural (i.e., alterations in cortex and membrane) and functional (i.e., capability to be recovered by culture) factors as defined in [239]. Exposure to electric fields might alter the physiological state of the spores, and therefore, increase the sensitivity of spores to heat and electric currents [43]. Ultrastructural analyses (Figure 4.63) revealed several interesting cytological aspects of the spore after treatment with low intensity electric field (LIEF). Through LIDEF exposure, the dense spore core changed to a typical spongy structure similar to that of vegetative cells, the nuclear apparatus was clearly visible in the less dense dumbbell–shaped

nuclear site, and vesicular bodies were distinct. Spore coat layers, along with the cortex, were disintegrated. Degradation of coat layers proteins signified that somehow proteolytic enzymes which exist near the surface of spore coats [240] might be triggered during exposure, so that a swift attack on these outer layers proceeded. The cortex attained a loose fibrillar appearance as the result of the breakdown of the peptidoglycan of the cortex [241]. The observed ultrastructural changes were in agreement with those reported during the activation and germination process of the spore [241, 242]. In line with these observations, meaningful reductions in spore survival was obtained (Figure 4.59) by the application of LIEF conditions for germination and inactivation. One of the other nimble and adequate reference methods to inspect spore germination with the maximum detection range of two $\log_{10}$ is the measurements of the loss of refractility and optical density [243]. The OD_{600} experiments showed around 57 percent reduction in OD (Table 4.18, Figure 4.58).

The following two possibilities can be envisioned for the effect of LIEF on the spore activation and germination: *a*) sublethal heat (62–95°C) [244] generated during the treatment, time interval 20–50 minutes (Table C.8 through Table C.14), begets alterations in the permeability of the spore coat and opening of a chemical bond between DPA and spore enzymes; *b*) electrokinetically deployed reduction state at the cathodic side of BioElectro^{TM} reactor ruptures disulfide bonds in the spore coat and brings about hydrolysis of cortex. As a consequence of cortex hydrolysis, rehydration of the spore core and lose of Ca_2^+–DPA happens. Harrell and Mantini (1957) [245] suggested a correlation between DPA exudation and degree of activation [245]. They determined a relationship between the amount of the released DPA and a raise in metabolism of glucose. Other authors [246] presumed that reducing agents alter the tertiary structure of a coat protein responsible for the maintenance of the dormant state by reducing the disulfide linkages which stabilize the protein in a specific configuration resulting in partial unfolding of the protein.

Furthermore, it was speculated that destruction of spores by BS at the earlier exposure times induces the germination in BioElectro^{TM} process. It has been shown that Ca^{2+}–DPA released by some spores in a population triggers the germination

129

of others [247, 248]. After exposure to Ca^{2+}–DPA an immediate decrease in OD_{600} with loss of refractility occurs [241]. DPA release is followed by degradation of the spores cortex, and cortex hydrolysis is initiated either indirectly or directly by DPA release [247, 249]. The capability of DPA to induce the germination of spores proposes that this chelate does not require the GerA family of germinant receptors. Ca^{2+}–DPA might either activate an effector that locates downstream of the germinant receptors or trigger a parallel line of the germination pathway [247].

Although the precise mechanism of spore germination by LIEF remains obscure, obtained data from contemporary work proposed a tentative working model to explain the effects of BioElectro^{TM} on *C. perfringens* spore germination (Figure 5.2). The whole assumptions are based on the germination model for *C. perfringens* due
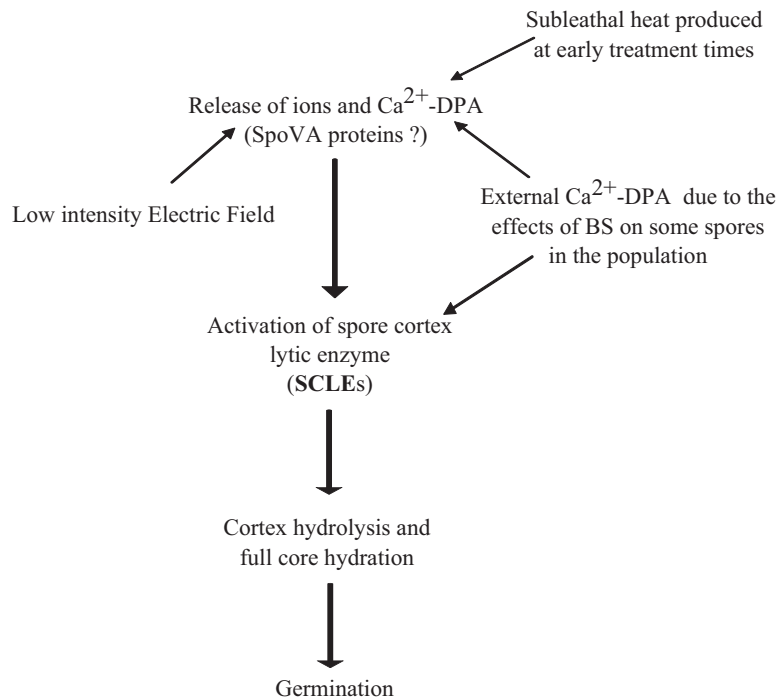
Figure 5.2: Hypothesized model for BioElectro^{TM} germination of *C. perfringens* spores

to the effects of nutrient and nonnutrient germinants [180] and literature data in Chapter 2 as follows: Opening of Ca^{2+}–DPA channels [247] is the beginning, where a germination reaction without nutrients is attainable. Manifestly, the pivotal factor for full cortex destruction as well as core hydration and hence loss of resistance

is the activation of the main eminent spore cortex lytic enzymes (SCLEs). External Ca^{2+}–DPA induces germination through a mechanism that requires the GerKA and GerKC receptor to fully activate downstream germination events. Electric field triggers DPA release by ultimately opening a DPA channel in the spores inner membrane. SCLEs are then activated by the Ca^{2+}–DPA release triggered by LIEF and promote cortex hydrolysis and completion of spore germination. Another theory from the biophysical point of view on curvilinear (shoulder) sections of survival curve explains its relationship with the effect of spore agglomeration [250], an activation process due to the outer proteinaceous coat and/or the spore exosporium and consequently the specific hydrophobicity [251, 252], which counteracting the inactivation process [253, 254, 255]. Generally, the greater the relationship between separative forces and adhesive forces is, the greater the density of the agglomerates is. In aqueous solutions van der Waals adhesive forces are smaller than in gas atmosphere. Consequently, agglomerates in aqueous solutions have a denser packaging or lower porosity. However, in aqueous solutions the main effects on separative forces are the zeta potential and Debye length based on the electrostatic double–layer [256] which can be affected by application of external electric field. Therefore, agglomeration is unlikely under BioElectro$^{\text{TM}}$ conditions. Figure 5.3 shows the largest observed
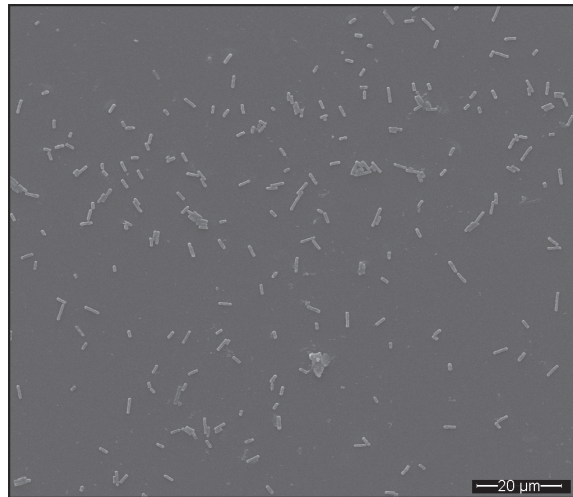
Figure 5.3: Largest observed agglomerations after screening of spore suspensions with approximately 10^8 CFU/ mL under ESEM

agglomeration of spores in BioElectro$^{\text{TM}}$ system. As it can be seen clearly, no large

131

agglomerates were observed in the suspension. An increase in the bubble density at the electrode surface as a result of electrolysis reactions as well as bubbles released into the electrolyte solution (Figure 5.4) due to hydrolysis of BS (Reaction [6]) can also contribute, though to a lesser degree, to formation of shoulder in inactivation curve. Bubbles clinging to the electrodes' surface decrease the effective surface area which consecutively increase the effective current density. This leads to a surge in the activation polarization, the voltage overpoteintial needed to surpass energy of the electrochemical reaction on the catalytic surface, at both the anode and cathode and interruption of electrochemical reactions [257].

Figure 5.4: Bubble creation in BioElectro^{TM} system

The third phase of the BioElectro^{TM} survival curve is characterized by the second sharp reduction in the number of spores (Figure 4.1). Based on the MLR analysis (Table 4.7) disinfection kinetic of this section is associated with a synergism among E, BS and AN (Table 4.8). The combination effects of erstwhile factors generates several related processes which assume to be responsible for the third phase of disinfection kinetics. The most eminent of these processes are: a) ohmic heating (Subsection 2.1.1), b) electropermeabilization and c) electrochemical reactions. Cho et al. postulated that principal mechanisms of spore inactivation during ohmic heating is essentially due to the thermal effect [43]. The rate of heating is directly proportional to the square of the electric field intensity (E^2) and the electrical conductivity

(Eq. 2.2). The electric field intensity can be altered by adjusting the electrode distance or the applied PG. This effect was observed in this study when increasing E from 2.5 V/cm (PG = 43 V) to 2.8 V/cm (PG = 48.16 V) brought about a surge in produced heat under examined conditions (Table 4.16). Another dominant factor affecting ohmic heating is the electrical conductivity of the matter and its temperature dependence. In current study, this was achieved by enhancing conductivity of biosolids through application of BS and AN (Figure 3.4 and Figure 3.5) which in turn increased degree of produced ohmic heating (Table 4.16, Table 4.17 and Figure 4.57). The electrical conductivity rises with increasing temperature, vindicating that ohmic heating becomes more efficient as temperature rises, which could theoretically contribute to runaway heating. Several authors [43, 258, 259] studied the killing effect of ohmic heating and high temperature on spores. Studies have shown that a protein subunit in the cytoplasmic membrane is the imperative target in the thermal inactivation of bacterial spore. It was suggested that degradation of the protein subunit makes the membrane dysfunctionally permeabilized, causing death of the cell [258]. Black and Gerhardt [260] demonstrated that the protoplast membrane is disintegrated in heat–killed spores. The disruption of membrane was also confirmed in this work as it is evident in Figure 4.64.

Along with the heating promotion, research data strongly suggest that the applied electric field creates a mild non–thermal cellular damage through the so–called dielectric rupture theory. Germinated spores under BioElectro^{TM} system develop vegetative cells surrounded by a bilayer lipid membrane (BLM) made of lipid with specific conductance of 10^{-3} S/cm^2 or smaller. Under the influence of an intense transmembrane electric field higher than the dielectric strength of a cell membrane the specific conductance of membrane increase dramatically which in turn causes a charge separation in the cell membrane. When the external electric field is equal to or slightly greater than the critical value of one volt, the permeability of the membrane is enhanced and material diffusion throughout the membrane is achieved through the reversible pores. By increasing the electric field or longer exposure times the pores will become irreversible and cell membrane are destroyed [44, 261]. Mem-

brane breakdown and formation of pores under the influence of BioElectro$^{\text{TM}}$ system was observed in *C. perfringens* (Figure 5.5) which confirms the results of previous studies.
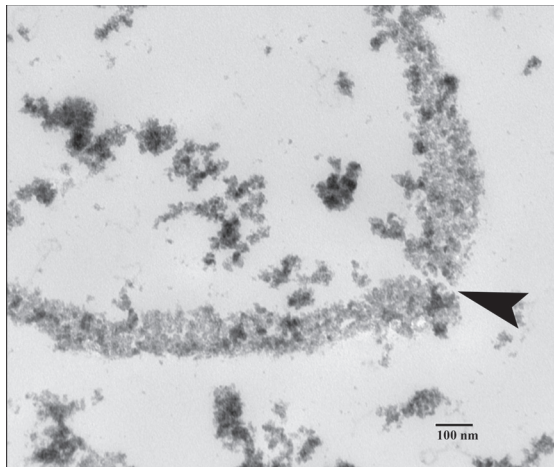
Figure 5.5: Pore created in cell membrane due to dielectric rupture in BioElectro$^{\text{TM}}$ system, the black arrow shows the pore

It has been shown that breakdown voltage across the membrane is not affected by the pH of the solution. However, other membrane and system parameters, strikingly temperature may play an eminent role [44, 262]. For instance, direct breakdown experiments on planar lipid BLM and on algal cells have presented that the breakdown voltage of a unit lipid–protein membrane is around 2 V at 4°C, 1 V at 20°C and about 0.5 V at 30–40°C [44]. Therefore, it can be postulated that in the systems such as BioElectro$^{\text{TM}}$ the presence of ohmic heating might intensify the influence of electric field on creation of pores and increase the rate of electropermeabilization, consequently leading to excess exudation and cell death.

Another factor affecting disinfection mechanism of BioElectro$^{\text{TM}}$ is pertinent to electrochemical and chemical reactions which have shown promising inactivation results on different microorganisms [263, 264]. The extent of electrochemical reactions rely on many parameters, such as the nature of electrolyte [265]. Several authors proposed that the major contribution to the electrochemical disinfection effect is made by the formation of short–lived and high–energy intermediate electrochemical products such as $^{\bullet}O_2^-$, $^{\bullet}OH^-$ and ClO_2^- [266, 267, 268]. Figure 5.6 depicts the tenta-

tive chemical reactions taking place at BioElectro^{TM} process. The condition exists
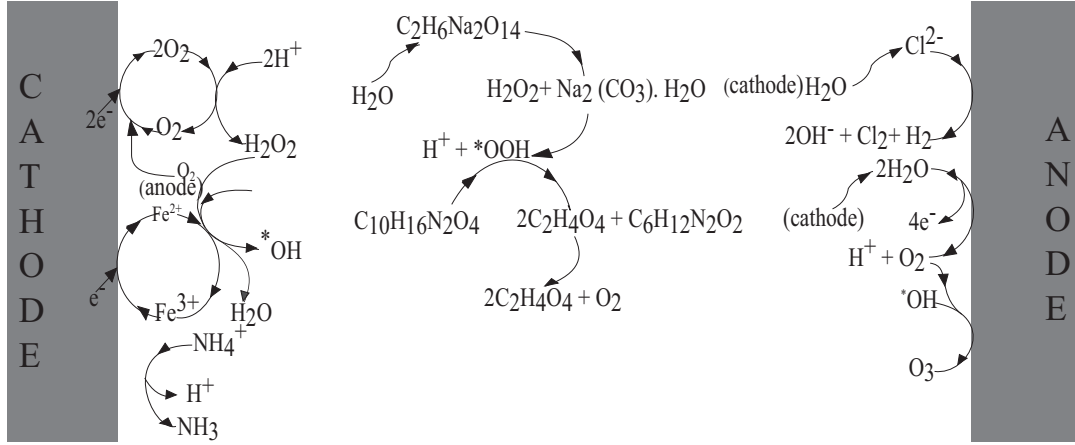
Figure 5.6: Schematic representation of the main electrochemical and chemical reactions involved in the BioElectro^{TM} process

in the BioElectro^{TM} reactor significantly influences the electrochemical and chemical generation of oxidant species within the device. For instance, several reactions (Reaction [3] through Reaction [6]) take place in the system which are solely related to the application of BS and not electrochemical reactions. These reaction lead to formation of HP, Na_2CO_3 and O_2. Furthermore, 316L stainless steel (SS) electrodes used in BioElectro^{TM} reactor exhibit pronounced hydrogen generation and pH alterations of the heating biosolids compared with other type of electrodes, e.g., carbon electrodes. Based on the observations, predominant electrochemical reactions can be assigned as detailed below. Under acidic conditions (i.e., at pH 2.5–3.5), the cathodic reaction (Reaction [2]) could couple following reaction (Reaction [8]) which happens in anodic side resulting in more hydrogen production compared to those at higher pH.

$$M_s \leftrightarrow M^{2+}_{(aq)} + 2\,e^- \tag{8}$$

where M = Fe, Cr, Ni, Mo. The overall reaction is:

$$M_s + 2\,H^+_{(aq)} \leftrightarrow M^{2+}_{(aq)} + H_{2(g)} \tag{9}$$
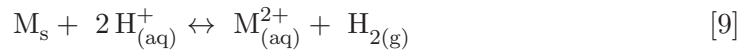
When M = Fe, the tested 316L SS electrode contains around 66 percent Iron

(Table 3.1), the equilibrium constant value (log K = 14.86) and standard potential ($E^0 = 0.44$ V) affirm the occurrence of Reaction [8]. The rise of pH (Figure 4.53) can be due to the loss of $H^+_{(aq)}$ ions as the hydrogen gas, and Fenton's reaction (Haber–Weiss reaction) which releases $OH^-_{(aq)}$ ions into the heating biosolids [269].

$$Fe^{2+}_{(aq)} + H_2O_2 \leftrightarrow Fe^{3+}_{(aq)} + {}^\bullet OH + HO^-_{(aq)} \qquad [10]$$

The needed H_2O_2 for the Reaction [10] is produced by cathodic reaction as follows:

$$O_{2(g)} + 2\,e^- \leftrightarrow H_2O_2 \qquad E^0 = -0.68V \qquad [11]$$
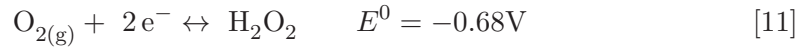
This enhances the destruction of cells in the biosolids. Under mildly acidic conditions, pH changes related to hydrogen formation can be due to the following reaction (Reaction [12]), which can be accompanied by generation of chloride gas (Reaction [13] and Reaction [14]).

$$M_{(s)} + 2\,H_2O_{(liq)} \leftrightarrow M^{2+}_{(aq)} + H_{2(g)} + 2\,OH^-_{(aq)} \qquad M = Fe, \qquad E^0 = -0.39V$$
$$[12]$$

$$2\,Cl^-_{(aq)} \leftrightarrow Cl_{2(g)} + 2\,e^- \qquad E^0 = -1.37V \qquad [13]$$

$$2\,H_2O_{(liq)} + 2\,Cl^-_{(aq)} \leftrightarrow Cl_{2(g)} + H_{2(g)} + 2\,OH^-_{(aq)} \qquad E^0 = -2.19V \qquad [14]$$
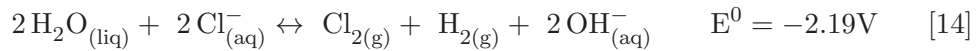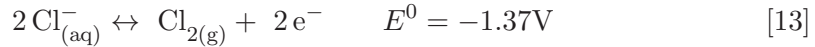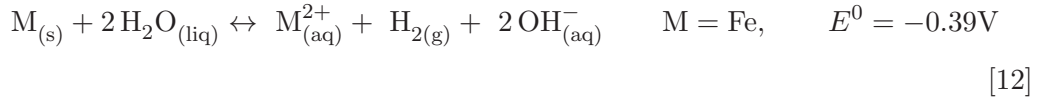
At the pH values above nine (cathodic side) the presence of chlorine will be exclusively limited to the hypochlorite anion (ClO^-) and will favor the generation of the ${}^\bullet OH$ radical over the ${}^\bullet Cl$ and ${}^\bullet Cl^-_2$ radicals [270]. Oxygen evolution always happens concurrently with ozone formation. Obviously, not all O_2 formed produces O_3. Indeed, O_3–generation is very much dictated by the effective encounter of O_2 and ${}^\bullet O$ [271]. Generation of ferrate(VI) is another possible reaction which may take place at the anodic side. Although above mention electrochemical reactions are expected to occur in BioElectro^{TM} reactor, it was not feasible to measure the

produced amount of each ion and radical due to their low stability and continues
conversion from one form to another.

Given the use of AN, the generated ammonia during the BioElectro^{TM} process
may also contribute to spore inactivation.

Table 5.1: Computed pK$_a$ and NH$_3$ in each experimental conditions of
BioElectro^{TM} process

Series	T($°$C)	pK$_a$	pH	f^a	(NH$_3$)$_t$(mg/L)	NH$_3$(mg/L)
1	97.5	7.46	7.80	0.69	489	337
2	96.0	7.49	8.29	0.86	274	237
3	96.2	7.48	8.15	0.82	218	180
4	95.5	7.50	8.15	0.82	194	159
5	94.6	7.51	8.12	0.80	470	377
6	91.0	7.59	8.16	0.79	440	347
7	96.3	7.48	8.29	0.86	256	228

^{a} Fraction of total ammonia that is unionized

The toxicity of ammonia is usually considered to be provoked by the unionized
molecule (NH$_3$) rather than by the ionized fraction (NH$_4^+$) which coexist in equilib-
rium in ammonia–in–water systems (Reaction [7]) [272]. The NH$_3$ species is more
lipophilic compared to NH$_4^+$ and can easily permeate through the inner microbial
cellular membranes. The greatly enhanced diffusion of NH$_3$ is accountable for the
more effective pathogen eradications. Furthermore to be considered is the impact of
temperature on ammonia effectiveness. As represented in Eq. 3.1 (Subsection 3.1.2)
at the elevated temperatures, the pK$_a$ of ammonia is reduced (pK$_a$ = 9.25 at 25$°$C,
pK$_a$ = 7.5 at 97$°$C) making it easier to reach a higher concentration of unionized
ammonia at lower pH levels (less than 10). Table 5.1 shows the NH$_3$ generated in
each experimental conditions of BioElectro^{TM} process. It is evident that although
the overall pH of the system did not exceed 8.5, NH$_3$ was the primary form of ammo-
nia due to the elevated temperature. The high temperatures of the system reached
in the system reduced level of pH needed to achieve a high concentration of free

ammonia. The effect of temperature on the toxicity of ammonia was also confirmed by [273]. He found that the ammonia concentration needed for *Ascaris* inactivation was directly associated to temperature. For example, at 25°C a 0.1% ammonia concentration achieved a 100 percent inactivation of *Ascaris* within 180 days, however when temperature was risen to 52°C the same ammonia dose expressed sufficient inactivation within one day. Moreover, at higher temperatures, the pathogens are more susceptible to ammonia disinfection; therefore, the rate of inactivation was faster as it is evident in Table 5.2.

Table 5.2: Electric field related temperature rise and LR changes during BioElectro process

t (min)	E (2.5 V/cm)		E (2.8 V/cm)		Extent of inactivation
	LR	T (°C)	LR	T (°C)	
20	0.9	53–40	1	45–50	Disinfection
40	1	45–55	2	60–70	
60	2	65–75	3	80–90	Pasteurization
80	3	85	6	95	
100	5	95	8	97	Sterilization

Another related factor in the close system of this study was vapor pressure. As elucidated by Henry's Gas Law, a rise in temperature in concurrence with the presence of ammonia increases the vapor pressure of the ammonia gas within the biosolids. For instance, the vapor pressure of ammonia at 50°C is about five times that found at ambient temperatures [274]. This raise in vapor pressure serves to raise the diffusion of the ammonia into the biosolids, consequently permitting greater contact with pathogens and higher inactivation effects.

The results and discussion covered so far propose hypothesized lethal pathways of multiple stressors in BioElectro$^{\text{TM}}$ process as depicted in Figure 5.7.

It was also ascertained that initial number of spores (N_0) is one of the affecting factor in regression analysis. This factor is among the biosolids intrinsic specification, and its amount could not be preassigned as desired. According to the models developed by MLR (Table 4.8) inactivation of *C. perfringens* spores showed some
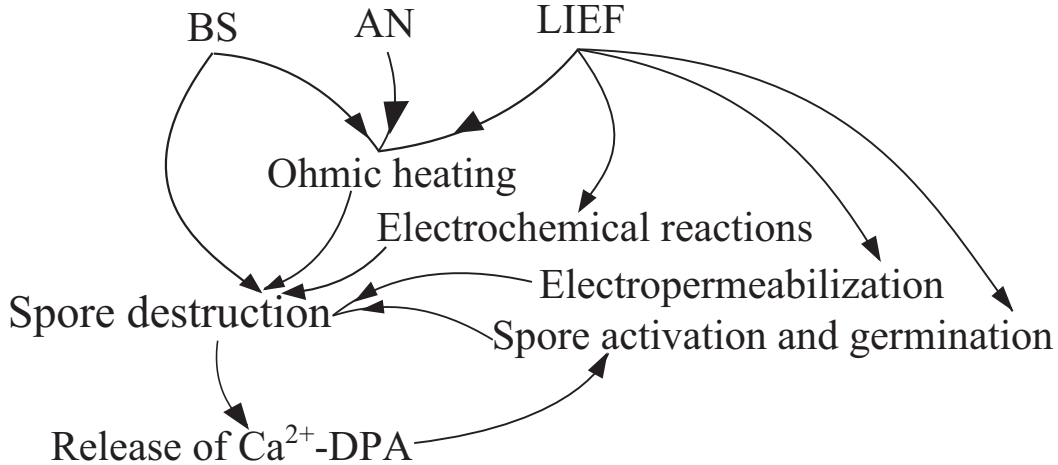
Figure 5.7: Putative lethal pathways of multiple stressors in BioElectro$^{\text{TM}}$ process

kind of dependency on initial spore density. The reason for this is that initial spore values (N_0) compared to other input variables (E, BS and AN) are significantly higher (up to 3–4 order of magnitude) and therefore show greater effect on regression analysis. Furthermore, this may be explained through quorum sensing (QS), cell density–dependent signaling through the use of autoinducers. However, because spores of *C. perfringens* are highly dormant, and they survive under harsh conditions, it is unlikely to expect QS mechanism. Moreover, it is possible that the observed cell density dependency was due to dynamic conditions and heterogeneity of spore populations. In other words, presence of sub–populations of differing resistance influence the inactivation efficiency.

To explain the overall mechanism of *C. perfringens* spore inactivation in Bio-Electro process kinetic models were defined. Chick–Watsons model (Eq. 2.11) of disinfection [203] predicts a linear inactivation curve, however the data from this study affirmed that this model would be unable to describe the totality of the observed survival curve shapes in BioElectro$^{\text{TM}}$ process. Because the complexity of BioElectro$^{\text{TM}}$ process restricts developing complete theoretically based kinetics model, empirical models were developed (Table 4.9). The goodness of the fit of the models was assessed by RSS and the Adj.r^2 between the experimental and predicted values with the MATLAB® program using NLR. It was found that all proposed models were effective in modeling the different shapes of the survival curves (Ta-

ble 4.10 and Appendix F) of all seven experimental series. The highest Adj.r^2 (0.9765) and the smallest RSS value (10.40) was related to BE1 model. Yet, it had a high number of parameters (13). By having greater number of parameters some degree of improvement in fit was obtained, but at the same time parameter estimates were worse because of having less data per parameter. Based on the pairwise F–test comparison BE3 model (Eq. 5.1) was selected as the simple complete model of choice.

$$\log\left(\frac{N}{N_0}\right) = \frac{-1}{(b_1 - 1)} \log d_1 + (b_1 - 1) \cdot a_1 \cdot BS^{n_1} \cdot AN^{n_2} \cdot E^{n_3} \cdot t^{k_1} \cdot N_0^{(b_1 - 1)} \quad (5.1)$$

BE3 is similar to the empirical power function model (Subsection 2.3.4) which can describe shoulder phenomena. The model defines the relationship between predictors, to wit: E, BS, AN and time, and the response variable (spore survival). Furthermore, it explains the effect of initial microbial density on disinfection. If b_1 >1, the survival ratio will decrease with increasing N_0 under the same disinfection conditions.

Chapter 6

Conclusion and future work

6.1 Conclusion

Organic and nutrient content of biosolids suggest its application as fertilizer and soil amendment [2, 3]. However, besides nutrient biosolids contains pathogens with fecal source which threaten human health if not being used safely in accordance with good practice [1, 2]. In this study a method of treating biosolids by destruction of *C. perfringens* to meet more stringent standards for protecting public health and safety was developed. The currently available biosolids treatment methods are not generally effective enough and/or eco–friendly. The introduced technology gets benefit of low intensity electric field (LIEF) effects enhanced with BIOXY S^{TM} (BS) and ammonium nitrate (AN). To represent both the application and its nature the technology was coined "BioElectro", a name derived from biosolids and electrokinetic.

In this study the optimum range and combination of affecting factors in Bio-Electro treatment, to wit: electric field intensity (E), BS and AN, were ascertained (Table 3.7). Based on the defined conditions it was plausible to conclude that the bioelectric effect reduces the required concentrations of applied sporecides, as it was observed in the case of BS (Table 4.1).

The results of this study showed a significant reduction (>3 LRs) in the number of spores after two hours treatment under BioElectro^{TM} process (Section 4.2). In

other words, the treated product exceeded the minimum legislative requirements in term of pathogens. Furthermore, the resultant product had a lower viscosity compared with the initial biosolids sample (Table 4.15). This is an added bonus of the process which makes the processed biosolids fully compatible with conventional equipment being used for land application of biosolids and liquid manure.

The current study showed impacts of multiple stressors on spore inactivation. This was represented by triphasic survival curves (Figure 4.1). Several authors [275, 276, 277] found similar pattern in the destruction of *C. botulinum* after treatment with a combination of UV and gamma ray, but there are different hypotheses to explain this phenomenon.

It was found that the fast reduction of spores at lower treatment times (the first phase of spore survival curves) was related to disinfection effects of PAA generated from hydroloysis of BS (Table 4.7). However, its applied concentration was not enough to destruct the entire spore population. Also, kinetic analyses of PAA residuals exhibited instantaneous demand and substantial decay of PAA in the biosolids matrix (Table 4.6). Ultrastructural examination using TEM revealed the creation of nicks and changes in the structure of spore due to the oxidation properties of PAA (Figure 4.62). It was shown that the lag phase found in spore inactivation (shoulder formation) can sufficiently be described by activation and germination of spores for inducing effect of LIEF and Ca^{2+}–DPA released from PAA–lysed spores. On the basis of the TEM examinations (Figure 4.63), OD_{600} measurements (Table 4.18 and Figure 4.58) and plate count (Figure 4.59) a plausible explanation (Figure 5.2) was supplied on the mechanism of germination under the influence of BioElectro^{TM} system. It was suggested that germination reactions are initiated by opening of the Ca^{2+}–DPA channels at E >1 V/cm. Consequently, SCLEs are activated and promote cortex hydrolysis and completion of spore germination. There is no doubt that these mechanisms still need to be more deeply studied, especially the Ca^{2+}–DPA release, the specific SCLEs in the spore matrix and the partial core hydration. Acquisition of this information would lead to a better understanding of the spore inactivation mechanism(s) and may improve sterilization concepts of

BioElectro$^{\text{TM}}$ process.

The current work also acknowledged the inactivation efficiency of the system is related to electrochemical reactions and production of oxidants such as H$_2$O$_2$, Cl$_2$ and O$_3$. It was concluded that conditions in BioElectro$^{\text{TM}}$ system such as electrode materials, pH and temperature significantly affect the type and rate of electrochemical reaction and therefore, formation of radicals, ions and gases such as NH$_3$. It was apparent that ohmic heating played an eminent role in the formation of the last section of spore survival curve (the first–order inactivation). The elevated temperature brought about spore injury, activation of spores and finally degradation of cytoplasmic membrane and spore death. It was noticed that the electrical conductivity of the biosolids determines the rate of ohmic heating (Figure 4.56 and Table 4.16), therefore enhancing the conductivity of system by adding BS and AN significantly improved internal thermal energy and generation of ohmic heating. Moreover, it was speculated that irreversible breakage of protoplast membrane, also known as electropermeabilization, is another important factor in destroying bacterial spore. Elevated temperatures such as conditions in BioElectro$^{\text{TM}}$ process enhance dielectric breakdown of membrane and rate of disinfection. An hypothesized lethal pathway of BioElectro$^{\text{TM}}$ disinfection process was introduced (Figure 5.7). It was furthermore concluded that the process should work for raw municipal sludge too.

Also, inactivation kinetics of *C. perfringens* spores during BioElectro$^{\text{TM}}$ process was modeled by an empirical model (Eq. 5.1). The model was able to predict the spore inactivation of all seven experimental conditions very precisely.

6.2   Future work

Although the developed technology was successfully able to produce biosolids that meet and exceed the most stringent regulatory compliance requirements, the following recommendations for future studies are proposed.

- *C. perfringens* spore was used as the bioindicator to examine the efficiency of the treatment method; however this evaluation can be validated by using

other surrogates, e.g., Prion proteins, the infectious agent in bovine spongiform encephalopathy (BSE).

- Disinfection efficacy test methods using *C. perfringens* spore are very labour intensive, sensitive and time consuming and it would be more practical to develop/use new methods which are easier, faster and more precise. One of the suggested methods would be flow cytometer (FCM) which can characterize up to thousands of particles per second.

- Studies should be performed to evaluate the impacts of initial densities of spores on disinfection mechanism.

- Examinations has to been performed to evaluate permanent stabilization of the final products.

- The quality of produced biosolids needs to be tested for agricultural purposes.

- Pilot plant studies are suggested to assess production and budgetary requirements of the full scale system.

References

[1] Committee on Toxicants and National Research Council Pathogens in Biosolids Applied to Land. *Biosolids Applied to Land: Advancing Standards and Practices.* The National Academic Press, Washington, DC, USA, 2002. 1, 20, 21, 141

[2] R.J. LeBlanc, P. Matthews, and R.P. Richard. Global atlas of excreta, wastewater sludge, and biosolids management: Moving forward the sustainable and welcome uses of a global resource. Technical report, Greater Moncton sewage Commission, 2006. 1, 16, 141

[3] D. Barraoui. *Dynamique et biodisponibilitie des éléments nutritifs et métalliques dans les boues décontaminée.* PhD thesis, Université du Québec, Québec, Canada, 2006. 1, 16, 141

[4] P.R. Ponugoti, M.F. Dahab, and R. Surampalli. Effects of different biosolids treatment systems on pathogen and pathogen indicator reduction. *Water Environment Federation*, 69(7):1195–1206, 1997. 1

[5] USEPA US Environmental Protection Agency. Biosolids technology fact sheet land application of biosolids. Technical Report EPA 832-F-00-064, United States Environmental Protection Agencies, Washington, DC, USA, 2000. 1, 16, 17

[6] E.G. Carrington. Evaluation of sludge treatments for pathogen reduction. Technical Report ISBN 92-894-1734-X, European Communities, 2001. 1, 17, 19, 20

[7] M. Hébert. Guidelines for the beneficial use of fertilizing residuals. Technical report, Ministére du Développement durable, de l' Environnement et des Parcs, 2008. 1, 17

[8] 2000. `www.compost.org/Biosolids_Composting_FAQ.pdf`. 1, 16, 17

[9] M. Elektorowicz, E. Safaei, H. Abdoli, J. Huang, and A. Badawieh. Treatment of sludge to exceptional quality before its application as a soil amendment: EKDIM system. *7th Symposium on Electrokinetic Remediation (EREM)*, 7, 2008. 1, 2, 4

[10] E. Safaei Takhtehfouladi. Enhanced electrokinetic (EK) technology: A comparative study for inactivation of *Clostridium perfringens* spores and reovirus in anaerobically digested biosolids. Master's thesis, Concordia University, Montréal, QC, Canada, 2007. 2, 6, 14, 20, 45, 48, 50, 51, 72

[11] M. Elektorowicz, J. Oleszkiewicz, J. Huang, E. Safaei, H. Abdoli, and A. Habel. EKDIM–an electrokinetic process treats municipal wastewater sludge for safe land application. *XX–TH Jubille–National, VIII–TH International Scientific and Technological Conference*, 7:276–287, 2008. 2, 4, 5

[12] A. Esmaeily, M. Elektorowicz, S. Habibi, and Oleszkiewicz J.A. Dewatering and coliform inactivation in biosolids using electrokinetic phenomena. *Journal of Environmental Science and Technology*, 5(3):197–202, 2006. 2, 5, 50

[13] J. Huang, M. Elektorowicz, and J.A. Oleszkiewicz. Dewatering and disinfection of aerobic and anaerobic sludge using an elektrokinetic (EK) system. *Water Science and Technology*, 57(2):231–236, 2008. 2

[14] K. Tomoyuki and T. Shun'itsu. Removal of organochlorine compounds in contaminated soil by electrokinetic remediation combined with iron reaction wall. *Journal of Japan Society on Water Environment*, 29(2):101–105, 2006. 2, 5

[15] A. Esmaeily. *Deatering, metal removal, pathogen elimination, and organic matter removal in biosolids using electrokinetic phenomena.* PhD thesis, Concordia University, Montréal, QC, Canada, 2002. 2, 5, 51

[16] K.-D. Huang and R.-J. Yang. Numerical modeling of the joule heating effect on electrokinetic flow focusing. *Electrophoresis*, 27:1957–1966, 2006. 2, 5, 9, 45, 48, 51

[17] E. Safaei, M. Elektorowicz, J. Oleszkiewicz, and R. Reimers. Response of Clostridium perfringens to electrokinetic disinfection process of biosolids. *14th Annual Conference McGill Civil Engineering Graduate Students' Society*, 2007. 4, 6, 48, 50

[18] E. Safaei, M. Elektorowicz, J. Oleszkiewicz, and R. Reimers. Enhanced electrokinetic technology (EEKT) for inactivation of Clostridium perfringens spores in anaerobically digested biosolids. *23rd EASTERN Canadian Symposium on Water Quality Research*, 2007. 4, 6, 48, 50

[19] E. Safaei and M. Elektorowicz. Bench–scale trial of electrokinetic treatment on anaerobically digested biosolids; microbial inactivation. *8th World Congress of Chemical Engineering*, 2009. 4, 6, 45, 48, 50

[20] E. Safaei. Inactivating Clostridium perfringens spores in anaerobically digested biosolids using enhanced elektrokinetics. *University of Waterloo Graduate Student Research Conference*, 2011. 4, 45, 50

[21] M. Elektorowicz, J. Huang, J. Oleszkiewicz, R. Reimers, E. Safaei, and K. Coombs. Response of different types of biosolids to simultaneous dewatering and pathogens inactivation by electrokinetic system. *80th Annual Water Environment Federation*, 2007. 4

[22] M. Elektorowicz, E. Safaei, J. Oleszkiewicz, and R. Reimers. Electrokinetic remediation of biosolids through inactivation of Clostridium perfringens spores. *6th Symposium on Electrokinetic Remediation (EREM)*, 2007. 4, 5, 50

[23] M. Elektorowicz. Technical requirement related to the electrokinetic removal of contaminants from soils. *ASCE/CSCE Joint Conference on Environmental Engineering*, 1995. 5

[24] C. Yuan and C.-H. Weng. Sludge dewatering by electrokinetic technique: effect of processing time and potential gradient. *Advances in Environmental Research*, 7:727–732, 2003. 5

[25] C. Yuan and C.-H Weng. Electrokinetic enhancement removal of heavy metals from industrial wastewater sludge. *Chemosphere*, 65:88–96, 2006. 5

[26] M. Said. Novel technology for sustainable petroleum oily sludge management: bio–neutralization by indigenous fungal–bacterial co–counters. Master's thesis, Concordia University, Montréal, QC, Canada, 2004. 5

[27] H. Abdoli. A pilot scale study for dewatering, metal removal and organic matter reduction in biosolids using electrokinetic phenomena. Master's thesis, Concordia University, Montréal, QC, Canada, 2009. 6, 45, 48, 50

[28] M. Electorowicz and J.A. Oleszkiewicz. Method of treating sludge material using electrokinetic, EKDIM, 2009. 6

[29] A. Habel. Electrokinetic management of biosolids for the inactivation of Helminth ova. Master's thesis, Concordia University, Montréal, QC, Canada, 2010. 6, 45, 48, 50, 51

[30] L. Qishi, H. Wang, X. Zhang, and Y. Qian. Effect of direct electric current on the cell surface properties of phenol–degrading bacteria. *Applied and Environmental Microbiology*, 71(1):423–427, 2005. 7

[31] M.A. Wills, J.C. Haley, G.L. Fabian, and R.M. Bricka. Electrokinetic remediation of metals–contaminated sediments: A technology demonstration involving former waste lagoons. *Enviromental Management and Health*, 10:31–36, 1999. 7

[32] C.M.A. Bertt and A.M.O. Brett. *Electrochemistry: Principles, Methods, and Applications.* Oxford University Press, Great Britain, 1993. 7, 13, 14

[33] P.H. Rieger. *Electrochemistry.* Chapman & Hall, Inc., New York, NY, USA, 2nd edition, 1993. 7

[34] M.Z. Bazant and T.M. Squires. Induced–charge electrokinetic phenomena. *Current Opinion in Colloid and Interface Science*, Article in Press, 2010. `doi: 10.1016/j.cocis.2010.01.003`. 7

[35] A. Kraft. Electrochemical water disinfection: A short review. *Platinum Metals Review*, 52:177–185, 2008. 8

[36] B. Narasimhan and R. Sri Ranjan. Electrokinetic barrier to prevent subsurface contaminant migration: theoretical model development and validation. *Journal of Contaminant Hydrology*, 42:1–17, 2000. 8

[37] Z. Ahmad. *Principles of corrosion engineering and corrosion control.* Elsevier's Science and Technology, Burlington, MA, USA, 1st edition, 2006. 8

[38] D. Anderson. Ohmic heating as an alternative food processing technology. Technical report, Kansas State University, Manhattan, Kansans, USA, 2008. 8

[39] M.C. Knirsch, C.A. dos Santos, A.A.O. Soares Vicente, and T.C.V. Penn. Ohmic heating–a review. *Trends in Food Science & Technology*, 21:436–441, 2010. 8, 9

[40] P. Richardson. *Thermal technologies in food processing.* CRC Press LLC, Boca Raton, FL 33431, USA, 2001. 9

[41] G. Piette, M.L. Buteau, D. De Halleux, L. Chiu, Y. Raymond, and H.S. Ramaswamy. Ohmic heating of processed meat and its effects on product quality. *Journal of Food Science*, 69(2):FEP71–FEP77, 2004. 9

[42] G. Piette, M. Dostie, and H.S. Ramaswamy. Ohmic cooking of processed meats–state of art and prospects. *Procedures of the International Congress of Meat Science and Technology*, 47:62–67, 2001. 9

[43] H.-Y. Cho, A.E. Yousef, and S.K. Sastry. Kinetics of inactivation of Bacillus subtilis spores by continuous or intermittent ohmic and conventional heating. *Biotechnology and Bioengineering*, 62(3):368–372, 1999. 9, 36, 128, 132, 133

[44] U. Zimmermann. Electrical breakdown, electropermeabilization and electro-fusion. *Reviews of Physiology, Biochemistry & Pharmacology*, 105:175–256, 1986. 9, 10, 133, 134

[45] U. Zimmermann, J. Vienken, and G. Pilwat. Development of drug carrier systems: electrical field induced effects in cell membranes. *Bioelectrochemistry and Bioenergetics*, 7:553–574, 1980. 10

[46] J.H. Masliyah and S. Subir Bhattacharjee. *Electrokinetic and Colloid Transport Phenomena*. John Wiley & Sons, Inc., New Jersey, USA, 2005. 10, 11, 12

[47] Á.V. Delgado, F. González-Caballero, R.J. Hunter, L.K. Koopal, and J. Lyklema. Measurement and interpretation of electrokinetic phenomena. *Journal of Colloid and Interface Science*, 309:194–224, 2007. 10

[48] Á.V. Delgado. *Interfacial electrokinetics and electrophoresis*. Marcel Dekker, Inc., New York, NY, USA, 2002. 10

[49] P.C. Hiemenz and R. Rajagopalan. *Principles of Colloids and Surface Chemistry*. Marcel Dekker, Inc., New York, NY, USA, 3rd edition, 1997. 10, 11, 12

[50] P. Somasundaran. *Encyclopedia of surface and colloid science*, volume 3. CRC Press, Boca Raton, FL, USA, 2nd edition, 2006. 10

[51] C. Comninellis and G. Chen. *Electrochemistry for the Environment*. Springer, New York, NY, USA, 2010. 13, 14

[52] R.G. Kelly, J.R. Scully, D.W. Shoesmith, and R.G. Buchheit. *Electrochemical Techniques in Corrosion Science and Engineering*. Marcel Dekker, Inc., New York, NY, USA, 2003. 13

[53] J.O'M. Bockris, A.K. N. Reddy, and M. Gamboa-Aldeco. *Modern electrochemistry*, volume 2. Kluwer Academic/ Plenum Publishers, New York, NY, USA, 2 edition, 1998. 14

[54] A. Rittirong, J.Q. Shang, M.A. Ismail, and M.F. Randolph. Effect of electric field intensity on electro–cementation of caissons in calcareous sand. *International Journal of Offshore and Polar Engineering*, 17(9):74–79, 2007. 14

[55] D. Pletcher and F.C. Walsh. *Industrial electrochemistry*. Springer, New York, NY, USA, 2nd edition, 1990. 14

[56] D.L. Wise, D.J. Trantolo, E.J. Cichon, H.I. Inyang, and U. Stottmeister. *Remediation Engineering of Contaminated Soils*. Marcel Dekker, Inc., New York, NY,USA, 2000. 14

[57] A.N. Alshawabkeh. Basic and application of electrokinetic remediation, 2001. `http://www1.coe.neu.edu/~aalsha/shortcourse.pdf`. 14, 15

[58] A. Pareilleux and N. Sicard. Lethal effects of electric current on Escherichia coli. *Applied Microbiology*, 19:421–424, 1970. 14

[59] H. Huelsheger, J. Potel, and E.-G. Niemann. Electric field effects on bacteria and yeast cells. *Radiation and Environmental Biophysics*, 22(2):149–162, 1983. 14

[60] A. Valle, E. Zanardini, P. Abbruscato, P. Argenzio, G. Lustrato, G. Ranalli, and S. Sorlini. Effects of low electric current (LEC) treatment on pure bacterial cultures. *Journal of Applied Microbiology*, 103(5):1376–1385, 2007. 14

[61] P. Keller and Karina Rubenis. Biosolids treatment and disposal options report. Technical report, Opus International Consultants Limited, 2005. 16

[62] C.C. Wang, C.W. Chang, C.P. Chu, D.J. Lee, B.-V. Chang, C.S. Liao, and J.H. Tay. Using filtrate of waste biosolids to effectively produce bio–hydrogen by anaerobic fermentation. *Water Research*, 37(11):2789–2793, 2003. 16

[63] 2002. `http://www.atl.ec.gc.ca/epb/issues/wstewtr.html`. 16

[64] E. Epstein. *Land application of sewage sludge and biosolids.* Lewis, Boca Raton, FL, USA, 2002. 16

[65] R. Iranpour, H.H.J. Cox, R.J. Kearyney, J.H. Clark, A.B. Pincince, and G.T. Daigger. Regulations for biosolids land application in us and european union. *Journal of Residuals Science & Technology*, 1(4):209–222, 2004. 16, 17

[66] U. Krogmann, M. Qu, L.S. Boyles, and C.J. Martel. Biosolids and sludge management. *Water Environment Research*, 70(4):557–580, 1998. 16

[67] USEPA US Environmental Protection Agency. Biosolids technology fact sheet–alkaline stabilization of biosolids. Technical Report EPA 625/R-92-013, United States Environmental Protection Agencies, Washington, DC, USA, 2000. 17

[68] G.W. Foess and D. Fredericks. Comparison of class A and class B private biosolids stabilization technologies. *Florida Water Resources Joournal*, May:28–31, 1995. 17

[69] I.A. Zasada, T. loagan, F. Avendano, H. Melakeberhan, Y.C. Li, S.R. Koenning, and G.L. Tylka. Potential of an alkaline–stabilized biosolids to manage nematodes: Case studies on soybean cyst and root–knot nematodes. *Plant Disease*, 92(1):4–13, 2008. 17

[70] USEPA US Environmental Protection Agency. Biosolids technology fact sheet–use of composting for biosolids management. Technical Report EPA 832-F-02-024, United States Environmental Protection Agencies, Washington, DC, USA, 2002. 17

[71] L. Wu, L.Q. Ma, and G.A. Martinez. Comparison of methods for evaluating stability and maturity of biosolids compost. *Journal of Environmental Quality*, 29(2):424–429, 2000. 17

[72] F.R. Spellman. *Wastewater biosolids to compost.* Technomic Publishing Company, Inc., Basel, Switzerland, 1997. 17, 18

[73] USEPA US Environmental Protection Agency. Biosolids technology fact sheet–in vessel composting of biosolids. Technical Report EPA 832-F-00-061, United States Environmental Protection Agencies, Washington, DC, USA, 2000. 17

[74] USEPA US Environmental Protection Agency. Biosolids technology fact sheet–heat drying. Technical Report EPA 832-F-06-029, United States Environmental Protection Agencies, Washington, DC, USA, 2006. 18, 19

[75] F.R. Spellman. *Mathematics manual for water and wastewater treatment plant operators.* CRC Press LLC, Boca Raton, Florida, USA, 2004. 18

[76] F.R. Spellman. *Handbook of water and wastewater treatment plant operations.* CRC Press LLC, Boca Raton, FL, USA, 2008. 18

[77] C.N. Mulligan. *Environmental Biotreatment: Technologies for Air, Water, Soil, and Wastes.* Government Institutes, Rockville, MD, USA, 2002. 18, 19

[78] G.F. Parkin and W.F. Owen. Fundamentals of anaerobic digestion of wastewater sludges. *Journal of Environmental Engineering*, 112:867–920, 1986. 18, 19

[79] USEPA US Environmental Protection Agency. Biosolids technology fact sheet–multi-stage anaerobic digestion. Technical Report EPA 832-F-06-031, United States Environmental Protection Agencies, Washington, DC, USA, 2006. 18, 19, 20

[80] P.L. McCarty. Anaerobic waste treatment fundamentals. *Public Work*, 92(9):107–112, 1964. 18, 19

[81] F.E. Mosey. Mathematical modelling of the anaerobic digestion process: Regulatory mechanisms for the formation of short–chain volatile acids from glucose. *Water Science and Technology*, 15:209, 1983. 19

[82] M.H. Gerardi. *The microbiology of anaerobic digesters*. John Wiely & Sons Inc., Hoboken, NJ, USA, 2003. 19

[83] T. Forster-Carneiro, M. Pérez, and L.I. Romero. Anaerobic digestion of municipal solid wastes: Dry thermophilic performance. *Bioresource Technology*, 99(15):8180–8184, 2008. 19

[84] P. Abdul and D. Lloyd. Pathogen survival during anaerobic digestion: Fatty acids inhibit anaerobic growth of Escherichia coli. *Biotechnology Letters*, 7(2):125–128, 1985. 19

[85] S.R. Smith, N.L. Lang, K.H.M. Cheung, and K. Spanoudaki. Factors controlling pathogen destruction during anaerobic digestion of biowastes. *Waste Management*, 25(4):417–425, 2005. 19

[86] P.L. McCarty. Anaerobic waste treatment fundamentals. *Public Work*, 92(10):123–126, 1964. 19

[87] L. Mocé-Llivina, M. Muniesa, H. Pimenta-Vale, F. Lucena, and J. Jofre. Survival of bacterial indicator species and bacteriophages after thermal treatment of sludge and sewage. *Applied and Environmental Microbiology*, 69(3):1452–1456, 2003. 20

[88] J.P.S. Sidhu and S.G. Toze. Human pathogens and their indicators in biosolids: A literature review. *Environment International*, 35:187–201, 2009. 20

[89] W.A. Yanko. Occurrence of pathogens in distribution and marketing municipal sludge. Technical Report EPA/600/1-37/014, United States Environmental Protection Agencies, Washington, DC, USA, 1988. 20

[90] V.J. Harwood, A.D. Levine, T.M. Scott, V. Chivukula, J. Lukasik, S.R. Farrah, and J.B. Rose. Validity of the indicator organism paradigm for pathogen

reduction in reclaimed water and public health protection. *Applied and Environmental Microbiology*, 71:3163–3170, 2005. 20

[91] S. Verhille, R. Hofmann, C. Chauret, and R. Andrews. Indigenous bacterial spores as indicators of Cryptosporidium inactivation using chlorine dioxide. *Journal of Water and Health*, 1:91–100, 2003. 20

[92] C. Bean. Evaluation of Clostridium perfringens as an indicator organism to assess the efficiency of biosolids disinfection processes. Technical report, University of New Hampshire, 2007. `http://www.wrrc.unh.edu/pubs/annual%20reports/fy03.htm`. 20, 21

[93] J.E. Smith Jr., R.Y. Surampalli, R.S. Reimers, R.D. Ryagi, and B.N. Lohani. Disinfection processes and stability refinements to biosolids treatment technologies. *Practice Periodical of Hazardous, Toxic, and Radioactive Waste Management*, 12(1):10–17, 2008. 21, 23

[94] USEPA US Environmental Protection Agency. Environmental regulations and technology-control of pathogens and vectors in sewage sludge. Technical Report EPA-625/R-92/013, United States Environmental Protection Agencies, Washington, DC, USA, 1999. 21

[95] R.S. Reimers, M.D. Little, A. Lopez, and K.K. Mbela. Final testing of the synox municipal sludge treatment for PFRP approval–phase II. Technical report, School of Public Health and Tropical Medicine, Tulane University, New Orleans, LA, 1991. 21

[96] A.E.I. de Jong. *Clostridium perfringens: spores & cells & media & modeling.* PhD thesis, Wageningen University, Wageningen, The Netherlands, 2003. 21, 22

[97] B.P. Dey, C.P. Lattuada, A.M. McNamara, R.P. Mageau, and S.S. Green. *USDA/FSIS Microbiology Laboratory Guidebook*, volume 1,2. United State Department of Agriculture, USA, 3rd edition, 1998. 21

155

[98] D. Raju, M. Waters, P. Setlow, and M.R. Sarker. Investigating the role of small, acid–soluble spore proteins (SASPs) in the resistance of Clostridium perfringens spores to heat. *BMC Microbiology*, 6(50):1–13, 2006. 21

[99] A.W. Boadley and B.J. Dutka. *Bacterial Indicators/health Hazards Associated with Water*. Number 77–78026. American Society for testing and Material, Fla, USA, 1977. 21

[100] M. Dworkin, S. Falkow, E. Rosenberg, K.-H. Schleifer, and E. Stackebrandt. *The Prokaryotes: A Handbook on the Biology of Bacteria: Bacteria: Firmicutes, Cyanobacteria*, volume 4. Springer Science+Business Media, LLC, New York, NY, USA, 3rd edition, 2006. 21, 32

[101] R.G. Labbe and T.H. Huang. Generation times and modeling of enterotoxin–positive and enterotoxin–negative strains of Clostridium perfringes in laboratory media and ground beef. *Journal of Food Protection*, 58:1303–1306, 1995. 21

[102] T. Shimizu, K. Ohtani, H. Hirakawa, K. ohshmia, A. Yamashita, T. Shiba, N. Ogasawara, M. Hattori, and S.K. Hideo. 21

[103] USEPA US Environmental Protection Agency. ICR microbial laboratory manual. Technical Report EPA/600/R-95/178, United States Environmental Protection Agencies, Washington, DC, USA, 1996. 21

[104] Environmental Science & Research (ESR). Clostridium perfringens. Technical report, Ministry of Health, Wellington, New Zealand, 2001. 21

[105] G. McDonnell and A.D. Russell. Antiseptics and disinfectants: Activity, action, and resistance. *Clinical Microbiology Reviews*, 12(1):147–179, 1999. 21, 24, 25, 28, 29, 30, 31, 32, 33

[106] A.D. Russell. Bacterial spores and chemical sporicidal agents. *Clinical Microbiology Reviews*, 3(2):90–119, 1990. 21, 24, 25, 29, 32

[107] A.H.W. Hauschild and K.L. Dodds. *Clostridium botulinum: ecology and control in foods.* MACEL DEKKER, INC, New York, NY, USA, 1992. 22

[108] B. Setlow and P. Setlow. Small, Acid-Soluble Proteins bound to DNA protect Bacillus subtilis spores from killing by dry heat. *Applied and Environmental Microbiology*, 61(7):2787–2790, 1995. 22, 31

[109] D. Paredes-Sabja, B. Setlow, P. Setlow, and M.R. Sarker. Characterization of Clostridium perfringens spores that lack SpoVA proteins and dipicolinic acid. *Journal of Bacteriology*, 190(13):4648–4659, 2008. 22

[110] L.V. Venczel, M. Arrowood, M. Hurd, and M.D. Sobsey. Inactivation of Cryptosporidium parvum oocysts and Clostridium perfringens spores by a mixed–oxidantdisinfectant and by free chlorine. *Applied and Environmental Microbiology*, 63(4):1598–1601, 1997. 22

[111] G.R. Finch, E.K. Black, and L.L. Gyurek. Ozone and chlorine inactivation of Cryptosporidium. *Conference proceedings, Water Quality Technology Conference*, pages San Francisco, CA, USA, 1994. 22

[112] G.R. Finch. Control of Cryptosporidium through chemical disinfection: Current stateof–the–art. *Proceedings of AWWARF Technology Transfer Conference*, pages Portland, Oregon, USA, 1997. 22

[113] C.M. Bernbaum. Criteria for analyzing interactions between biologically active agents. *Advances in Cancer Research*, 35:269–335, 1981. 22

[114] C.M. Bernbaum. The expected effect of a combination of agents: the general solution. *Journal of Theoritical Biology*, 114(3):413–431, 1985. 22

[115] Y. Kouame and C.N. Haas. Inactivation of E. coli. by combined action of free chlorine and monochloramine. *Water Research*, 25(9):1027–1032, 1991. 22

[116] B.A. Acquisto, R.S. Reimers, and J.E. Smith. Factors affecting disinfection and stabilization of sewage sludge. *6th WEFTEC*, pages 1259–1277, 2006. 23, 24

[117] R.S. Reimers, S.D. Pillai, D.D. Bowman, K.B. Fitzmorris, and L.S. Pratt. Stressors influencing disinfection in residuals. *Disinfection 2005*, 15:658–672, 2005. 23, 24

[118] G.W. Gould. *Mechanism of action of food preservation procedure.* Elsvier Applied Science, London, 1989. 23

[119] A.D. Russell, W.B. Hugo, and A.G.J. Ayliffe. *Principles and practice of disinfection, preservation and sterilization.* Blackwell Scientific, London, 3rd edition, 1999. 23

[120] S.S. Block. *Disinfection sterilization and preservation.* Lippincott Williams & Wilkins, Philadelphia, PA, USA, 5th edition, 2000. 23, 24, 25, 26, 27, 28, 36, 37, 38, 39, 40, 41, 42, 44

[121] F.A. Skinner and W.B. Hugo. *Inhibition and Inactivation of Vegetative Microbes.* Academic Press, London, 1976. 23

[122] D.W. Ribbons and J.R. Norris. *Methods in Microbiology*, volume 8. Academic Press, London, 1973. 23

[123] H. Terano, H. Tanooka, and H. Kadota. Germination–induced repair of single–strand breaks of DNA in irradiated Bacillus subtillis spores. *Biochemical and Biophysical Research Communications*, 37:66–71, 1996. 23

[124] T.G.R. Gray and J.R. Postage. *The Survival of Vegetative Microbes.* Number 2. Cambridge University Press, Cambridge, UK, 1976. 23, 24

[125] P. Setlow. I will survive: protecting and repairing spore DNA. *Journal of Bacteriology*, 174:2737–2741, 1992. 23, 34

[126] J.E. Donnellan and R.B. Setlow. Thymine photoproducts but not thymine dimers found in ultraviolent–irradiatd bacteria spores. *Science*, 149:308–310, 1965. 23

[127] R.V. Lechowich and Z.J. Ordal. Influence of the sporulation temperature on the heat resistance and composition of bacterial spores. *Canadian Journal of Microbiology*, 8(3):287–295, 1962. 23

[128] J.C. Lewis, N.S. Snell, and H.K. Burr. Water permeability of bacterial spores and the concept of a contractile cortex. *Science*, 132:544–545, 1960. 23

[129] A.J.H. Sale, G.W. Gould, and W.A. Hamilton. Inactivation of bacterial spores by hydrostatic pressure. *Journal of General Microbiology*, 60:323–334, 1970. 24, 128

[130] P.A. Clouson, J.G. annd Wills. Kinetic of initiation of germination of Bacilus pumilus spores by germination. *The Journal of Bacteriology*, 103:140–143, 1969. 24

[131] J.G. Clouston and P.A. Wills. Initiation of germination and inactivation of Bacillus pumilus spores by hydrostatic pressure. *The Journal of Bacteriology*, 97:684–690, 1970. 24

[132] USEPA US Environmental Protection Agency. Control of pathogens and vector attraction in sewage sludge. Technical Report EPA/625/R-92/013, United States Environmental Protection Agencies, Washington, DC, USA, 2003. 24

[133] R.S. Reimers, S.K. Virender, S.D. Pillai, and D.R. Reinhart. Application of ferrates in biosolids and manure management with respect to disinfection and stabilization. *Wef proceedings*, 1:185, 2005. 24

[134] S.J. de Luca, C.N. Idle, and A.C. Chao. Quality improvement of biosolids by ferrate(VI) oxidation of offensive odour compounds. *Water Science and Technology*, 33(3):119–130, 1996. 24

[135] M.R.W. Brown and P. Gilbert. Sensitivity of biofilms to antimicrobial agents. *Journal of Applied Bacteriology–Symposium Supplement*, 74:87S–97S, 1993. 24

[136] S. Thomas and Russell A.D. Temperature–induced changes in the sporicidal activity and chemical properties of glutaraldehyde. *Journal of Applied Microbiology*, 28:331–335, 1974. 24

[137] E.G.M. Power, B.N. Dancer, and A.D. Russell. Effect of sodium hydroxide and two proteases on the revival of aldehyde–treated spores of Bacillus subtilis. *Letters in Applied Microbiology*, 10:9–13, 1990. 25

[138] M.D. Aitken, M.D. Sobsey, K.E. Blauth, M. Shehee, P.L. Crunk, and Walters G.W. Inactivation of ascaris suum and poliovirus in biosolids under thermophilic anaerobic digestion conditions. *Environmental Science and Technology*, 39(15):5804–5809, 2005. 25

[139] B.M. Pecson and K.L. Nelson. Inactivation of Ascaris suum eggs by ammonia. *Environmental Science and Technology*, 39:7909–7914, 2005. 25

[140] M.G.C. Baldry and J.A.L. Fraser. Temperature–induced changes in the sporicidal activity and chemical properties of glutaraldehyde. *Critical Reports on Applied Chemistry*, 22:91–116, 1988. 25

[141] F. Dagher and D. Dagher. Powdered composition for the generation of peracetic acid and use thereof to sanitize surface, 2006. 25, 48, 50

[142] M. Kitis. Disinfection of wastewater with peracetic acid: a review. *Environment International*, 30:47–55, 2004. 25

[143] HERA. Human & environmental risk assessment on ingredients of european household cleaning products. Technical report, HERA Environmental Task Force and the HERA Human Health Task Force, B–1160 Brussels, Belgium, 2002. 26

[144] A. El Shafei, M.M.G Fouda, and M. Hashem. One–step process for bioscouring and peracetic acid bleaching of cotton fabric. *Carbohydrate polymer*, 78:302–308, 2009. 26

[145] T.E. Cloete. Resistance mechanisms of bacteria to antimicrobial compounds. *International Biodeterioration & Biodegradation*, 51:277–282, 2003. 27, 29, 30

[146] S.P. Denyer and G.S.A.B. Stewart. Mechanisms of action of disinfectants. *International Biodeterioration and Biodegradation*, 41:261–268, 1998. 27, 28, 29

[147] C.K. Bower and M.A. Daeschel. Resistance responses of microorganisms in food environments. *International Journal of Food Microbiology*, 50:33–44, 1999. 27, 29

[148] C.J. Hurst. *Modeling disease transmission and its prevention by disinfection.* Cambridge University Press, New York, NY, USA, 1996. 27, 28, 37, 38

[149] R.G. Board, M.C. Allwood, and J.G. Banks. *Preservatives in the Food, Pharmaceutical and Environmental Industries.* Blackwell Scientific Publications, London, 1987. 28

[150] R.M.E. Richards, D.K.L. Xing, and T.P. King. Activity of p-aminobenzoic acid compared with other organic acids against selected bacteria. *Journal of Applied Bacteriology*, 78:209–215, 1995. 28

[151] O. Reichart. Modelling the destruction of Escherichia coli on the base of reaction kinetics. *International Journal of Food Microbiology*, 23:449–465, 1994. 28

[152] I.R. Booth. Stress and the single cell: Intrapopulation diversity is a mechanism to ensure survival upon exposure to stress. *International Journal of Food Microbiology*, 78(1-2):19–30, 2002. 28

[153] C.E.R. Dodd, R.L. Sharman, S.F. Bloomfield, I.R. Booth, and G.S.A.B. Stewart. Inimical processes: bacterial self–destruction and sub–lethal injury. *Trends in Food Science & Technology*, 8:238–241, 1997. 29

[154] E.G.M. Power and A.D. Russell. Glutaraldehyde: its uptake by sporing and non–sporing bacteria, rubber, plastic and an endoscope. *Journal of Applied Bacteriology*, 67:329–342, 1989. 29

[155] SCENIHR. Assessment of the antibiotic resistance effects of biocides. Technical report, European Commission–Health & Consumer Protection DG, Brussels, Belgium, 2009. 29, 30

[156] J.S. Chapman. Characterizing bacterial resistance to preservatives and disinfectants. *International Biodeterioration & Biodegradation*, 41:241–245, 1998. 29

[157] B.G. Spratt. Resistance to antibiotics mediated by target alterations. *Science*, 264:388–393, 1994. 29

[158] H. Nikaido. Prevention of drug access to bacterial targets: permeability barriers and active efflux. *Science*, 264:382–387, 1994. 29

[159] J. Davies. Inactivation of antibiotics and the dissemination of resistance genes. *Science*, 264:375–382, 1994. 29

[160] A.D. Russell. Bacterial resistance to disinfectants: present knowledge and future problems. *Journal of Hospital Infection*, 43(Spplement):S57–S68, 1998. 29, 32

[161] R. Beumer, S.F. Bloomfield, M. Exner, G.M. Fara, K.J. Nath, and E. Scott. Microbial resistance and biocides. Technical report, International Scientific Forum on Home Hygiene (IFH), International, 2000. 29, 30

[162] L. Guérin-Méchin, F. Dubois-Brissonnet, B. Heyd, and J.Y. Leveau. Quaternary ammonium compounds stresses induce specific variations in fatty acid composition of Pseudomonas aeruginosa. *International Journal of Food Microbiology*, 55:157–159, 2000. 30

[163] C.L. Winder, I.S. Al-Adham, S.M. Abdel Malek, T.E. Buultjens, A.J. Horrocks, and P.J. Collier. Outer membrane protein shifts in biocide–resistant

Pseudomonas aeruginosa PAO1. *Journal of Applied Microbiology*, 89:289–295, 2000. 30

[164] G.M. Bruinsma, M. Rustema-Abbing, H.C. van der Mei, C. Lakkis, and H.J. Busscher. Resistance to a polyquaternium–1 lens care solution and iso-electric points of Pseudomonas aeruginosa strains. *Journal of Antimicrobial Chemotherapy*, 57(4):764–766, 2006. 30

[165] A. Moir and D.A. Smith. The genetics of bacterial spore germination. *Annual Review Microbiology*, 44:531–553, 1990. 30, 31

[166] A. Driks. Maximum shields: the assembly and function of the bacterial spore coat. *TRENDS in Microbiology*, 10(6):251–254, 2002. 31, 32

[167] R.Y. Stanier, H.J. Rogers, and J.B. Ward. *Relations between structure and function in the prokaryotic cell: twenty-eighth symposium of the Society for General Microbiology held at the University of Southampton.* Cambridge University Press, New York, USA, 1978. 31

[168] J.C. Chambliss, G. Vary. *Spore VII.* American Society for Microbiology (ASM), Washington, DC, USA, 1978. 31

[169] G.J. Dring, D.J. Ellar, and G.W. Gould. *Fundamental and Applied Aspects of Bacterial Spores.* Academic Press, London, 1st edition, 1985. 31

[170] A. Hurst and G.W. Gould. *Spore VII*, volume 2. Academic Press, London, 1984. 31

[171] J.M. Mason and P. Setlow. Essential role of small, acid–soluble spore proteins in resistance of Bacillus subtilis spores to UV light. *The Journal of Bacteriology*, 167:174–178, 1986. 31

[172] A . Crafts-Lighty and D.J. Ellar. The structure and function of the spore outer membrane in dormant and germinlating spores of Bacillus megaterium. *Journal of Applied Bacteriology*, 48:135–145, 1980. 31

[173] K.S. Lee, D. Bumbaca, J. Kosman, P. Setlow, and M.J. Jedrzejas. Structure of a protein-DNA complex essential for DNA protection in spores of Bacillus species. *Proceedings of the National Academy of Sciences PNAS*, 105(8):2806–2811, 2008. 31, 32

[174] M. Plomp, T.J. Leighton, K.E. Wheeler, and A.J. Malkin. Architecture and high–resolution structure of Bacillus thuringiensis and Bacillus cereus spore coat surfaces. *Langmuir*, 21:7892–7898, 2005. 32

[175] C.E. Bayliss, W.M. Waites, and N.R. Kin. Resistance and structure of spores of Bacillus subtilis. *Journal of Applied Bacteriology*, 50:379–390, 1981. 31

[176] S.J. Foster. The role and regulation of cell wall structural dynamics during differentiation of endoscope-forming bacteria. *Applied Bacteriology symposium*, 79:25S–39S, 1994. 31

[177] A.L. Sonenshein, J.A. Hoch, and R. Losick. *Bacillus subtilis and its Closest Relatives*. American Society of Microbiology (ASM), Washington, DC, USA, 2002. 32

[178] L. Kenar, M. Ortatatli, H. Yaren, T. Karayilanoglu, and H. Aydogan. Comparative sporicidal effects of disinfectants after release of a biological agent. *Military Medicine*, 172(6):616–621, 2007. 32

[179] A. Moir, B.M. Corfe, and J. Behravan. Spore germination. *CMLS, Cellular and Molecular Life Sciences*, 59:403–409, 2002. 33, 34

[180] D. Paredes-Sabja, J.A. Torres, P. Setlow, and M.R. Sarker. Clostridium perfringens spore germination: Characterization of germinants and their receptors. *Journal of Bacteriology*, 190(4):1190–1201, 2008. 33, 35, 130

[181] P. Setlow. Spore germination. *Current Opinion in Microbiology*, 6:550–556, 2003. 33, 35

[182] A. Moir. How do spores germinate? *Journal of Applied Microbiology*, 101:526–530, 2006. 33

[183] J.F. Skomurski, F.M. Racine, and J.C. Vary. Steady–state fluorescence anisotropy changes of 1,6–diphenyl–1,3,5–hexatriene in membranes from Bacillus megaterium spores. *Biochimica et Biophysica Acta*, 731:428–436, 1983. 33

[184] A. Atrih, P. Zoellner, A. Guenter, M.P. Willamson, and S.J. Foster. Peptidoglycan structural dynamics during germination of Bacillus subtilis 168 endospores. *Journal of Bacteriology*, 180(17):4603–4612, 1998. 34

[185] A. Atrih, G. Bacher, R. Koener, A. Guenter, and S.J. Foster. Structural analysis of Bacillus megaterium KM spore peptidoglycan and its dynamics during germination. *Microbiology*, 145:1033–1041, 1999. 34

[186] M. Otani, N. Ihara, C. Umezawa, and K. Sano. Predominance of gluconate formation from glucose during germination of Bacillus megaterium QMB 1551 spores. *Journal of Bacteriology*, 167:148–152, 1986. 34

[187] P. Setlow. I will survive: DNA protection in bacterial spores. *TRENDS in Microbiology*, 15(4):172–180, 2007. 34

[188] T. Hashimoto, W.R. Frieben, and S.F. Conti. Germination of single bacterial spores. *Journal of Bacteriology*, 98(3):1011–1020, 1969. 34

[189] O.B. Williams, C. Lamanna, G. Knaysi, E.S. Wynne, C.F. Schmidt, H.R. Curran, M. Levine, H. Sugiyama, H. Reynolds, H. Lichtenstein, and C.R. Phillips. Symposium on the biology of bacterial spores. *Bacteriological Reviews*, 16:89–104, 1952. 34

[190] R.J.V. Pulvertaft and J.A. Hynes. Adenosine and spore germination; phase–contrast studies. *Journal of General Microbiology*, 5:657–663, 1951. 34

[191] J.F. Powel. Factors affecting the germination of thick suspensions of Bacillus suhtilis spores in L–Alanine solution. *Journal of General Microbiology*, 4:330–338, 1950. 34

[192] J.F. Powel and R.E. Strange. Biochemical changes occurring during the germination of bacterial spores. *Biochemical Journal*, 54:205–209, 1953. 35

[193] L.J. Rode and J.W. Foster. Mechanical germination of bacterial spores. *Proceedings of the National Academy of Sciences of the United States of America*, 46:118–128, 1960. 35

[194] N. Grecz and L.H. Arvay. Effect of temperature on spore germination and vegetative cell growth of Clostridium botulinum. *Applied and Environmental Microbiology*, 43(2):331–337, 1982. 35

[195] D. Margosch, M.A. Ehrmann, R. Buckow, V. Heinz, and M.G. Vogel, R.F.and Gaenzle. High–pressure–mediated survival of Clostridium botulinum and bacillus amyloliquefaciens endospores at high temperature. *Applied and Environmental Microbiology*, 72(5):3476–3481, 2006. 35

[196] H. Zhang and G.S. Mital. Effect of high–pressure processing (HPP) on bacterial spores: An overview. *Food Reviews International*, 24:330–351, 2008. 35

[197] W.A. Hamilton and A.J.H. Sale. Effects of high electric fields on microorganisms II: Mechanism of action of the lethal effect. *Biochimica et Biophysica Acta–BBA*, 148:789–800, 1967. 35

[198] R. Xiong, G. Xie, A.E. Edmondson, and M.A. Sheard. A mathematical model for bacterial inactivation. *International Journal of Food Microbiology*, 46:45–55, 1999. 36, 37

[199] B.F. Severin, M.T. Suidan, and R.S. Engelbrecht. Kinetic modeling of UV-disinfection of water. *Water Research*, 17(11):1669–1678, 1983. 37, 41, 42, 43

[200] C.N. Haas. Maximum likelihood analysis of disinfection kinetics. *Water Research*, 22:669–677, 1988. 37, 38

[201] C. Chauret. Disinfection principles. *Chlorine Dioxide: The state of science, regulatory, environmental issues, and case historic*, page 87, 2001. 37

[202] C.W. Hiatt. Kinetics of the inactivation of viruses. *Bacteriological Reviews*, 28(2):150–163, 1964. 37, 42

[203] H. Chick. An investigation of the laws of disinfection. *Bulletin of Environmental Contamination and Toxicology*, 8:92–158, 1908. 37, 139

[204] H.E. Watson. A note on the variation of the rate of disinfection with change in the concentration of the disinfection. *Journal of Hygiene*, 8:536–542, 1908. 38

[205] C.N. Haas and S.B. Karra. Kinetics of microbial inactivation by chlorine–1. *Water Research*, 18:1443–1449, 1984. 38, 39, 66

[206] A. Jessen, A. Randall, D. Reinhart, and L. Daly. Effectiveness and kinetics of ferrate as a disinfectant for ballast water. *6th WEFTEC*, pages 1259–1277, 2006. 38, 39

[207] J.C. Fair, G. andMorris, S.L. Chang, I. Weil, and R.P. Burden. The behavior of chlorine as a water disinfectant. *Journal AWWA*, 40:1051–1061, 1948. 39

[208] C.N. Haas, M.S. Heath, J. Jcangelo, J. Joffe, U. Anmangandla, J.C. Hornberger, and J. Glicker. *Development and Validation of Rational Design Methods of Disinfection*. American Water Works Association, USA, 1995. 39

[209] C. N. Haas and J. Joffe. Disinfection under dynamic conditions: Modifications of Hom model for decay. *Environmental Science and Technology*, 7(28):1367–1369, 1994. 39

[210] U. Anmangandla. Nonlinear regression analysis of bench–scale microbial disinfection kinetics. Master's thesis, Drexel University, Philadelphia, PA, USA, 1993. 39

[211] A. Driedger, E. Staub, U. Pinkernell, B. Marinas, W. Koster, and U.V. Gunten. Inactivation of Bacillus subtilis spores and formation of bromate during ozonation. *Water Research*, 35(12):2950–2960, 2001. 39

[212] B. Barbeau, L. Boulos, R. Desjardins, J. Coallier, and M. Prevost. Examining the use of aerobic spore-forming bacteria to assess the efficiency of chlorination. *Water Research*, 33(13):2941–2948, 1999. 39

[213] D.J. Pernitsky, G.R. Finch, and P.M. Huck. Disinfection kinetics of heterotrophic plate count bacteria in biologically treated potable water. *Water Research*, 5(29):1235–1241, 1995. 39

[214] S.B. Majumdar, W.H. Ceckler, and O.J. Sproul. Inactivation of poliovirus in water by ozonation. *Journal of the Water Pollution Control Federation*, 45(12):2433–2443, 1973. 40

[215] D. Roy, E.S.K. Chian, and R.S. Engelbrecht. Kinetics of enteroviral inactivation by ozone. *Journal of the Environmental Engineering Division*, 107:887–901, 1981. 40

[216] J. Anotai. *Effect of Calcium Ion on Chemistry and Disinfection of Free Chlorine at pH 10*. PhD thesis, Drexel University, Philadelphia, PA, USA, 1996. 40, 41

[217] C.N. Haas and G.R. Finch. *Methodologies For the Determination of Disinfection Effectiveness*. AWWA Research Foundation, USA, 1999. 41, 55

[218] L.L. Gyurék and G.R. Finch. Modeling water treatment chemical disinfection kinetics. *Journal of Environmental Engineering*, 124(9):783–793, 1998. 41

[219] L.L. Gyurék, H. Li, M. Belosevic, and G.R. Finch. Ozone inactivation kinetics of Cryptosporidium in phosphate buffer. *Journal of Environmental Engineering*, 125(10):913–924, 1999. 43

[220] B. Kaymak. *Effects of Initial Microbial Density on Disinfection Efficiency and Explanatory Mechanisms*. PhD thesis, Drexel University, Philadelphia, PA, USA, 2003. 43

[221] R.M. Clark, E.J. Read, and J.C. Hoff. Analysis of inactivation of Giardia lamblia by chlorine. *Journal of Environmental Engineering*, 115:80–90, 1989. 44

[222] H.M. Raihan. Application of electrokinetic to control metal transports in biosolids in a cold climate. Master's thesis, Concordia University, Montréal, QC, Canada, 2006. 45, 48

[223] R.O. Beauchamp Jr., M.B.G. St. Clair, T.R. Fennell, D.O. Clarke, and K.T. Morgan. A critical review of the toxicology of glutaraldehyde. *Critical Reviews in Toxicology*, 22(3,4):143–174, 1992. 48

[224] J.N. Butler. *Ionic Equilibrium*. Addison–Wesley Inc., New York, NY, USA, 1964. 48

[225] K. Emerson, R.E. Lund, R.V. Thurston, and R.C. Russo. Aqueous ammonia equilibrium calculations: effect of pH and temperature. *Journal of the Fisheries Research Board of Canada*, 32:2379–2383, 1975. 48, 49

[226] R.S. Reimers, J.A. Oleszkiewicz, D.D Bowman, and E.L. Faulmann. PEC application for the national classification of the J–Vap process to the category of PFRP. Technical Report Unpublished, Paradigm International, Inc, Metairie, Louisiana, USA, 2002. 60

[227] J.F. Kokai-Kun, J.G. Songer, J.R. Czeczulin, F. Chen, and B.A. McClane. Comparison of western immunoblots and gene detection assays for identification of potentially enterotoxigenic isolates of Clostridium perfringens. *Journal of Clinical Microbiology*, 32:2533–2539, 1994. 68

[228] V.K. Juneja, J.E. Call, and A.J. Miller. Evaluation of methylxanthines and related compounds to enhance Clostridium perfringens sporulation using a modified Duncan and Strong medium. *Journal of Rapid Methods and Automation in Microbiology*, 2:203–218, 1993. 68

[229] L.K. Chen and C.L. Duncan. Sporangial autolysis in Clostridium perfringens type A. *Biochim. Biophys. Acta*, 338:605–618, 1974. 68

[230] S.K. Long and O.B. Williams. Method for removal of vegetative cells from bacterial spore preparations. *Journal of Bacteriology*, 76:332–332, 1958. 68

[231] D.E. Gombas and R.F. Gomez. Sensitization of Clostridium perfringens spores to heat by Gamma radiation. *Applied and Environmental Microbiology*, 36(3):403–407, 1978. 68

[232] A. D. Eaton and M.A.H. Franson. *Standard Methods for the Examination of Water and Wastewater.* American Public Health Association (APHA), American Water Works Association (AWWA) & Water Environment Federation (WEF), Alexandria, VA, USA, 21 edition, 2005. 70

[233] R. Reimers. Hedging your bets for effective treatment–the case of multiple stressors. *W209 Controlling Pathogens and meeting Regulatory Requirements for Application of Biosolids*, 2010. 73

[234] G.P. Quinn and M.J. Keough. *Experimental design and Data Analysis for Biologists.* Cambridge University Press, Cambridge, UK, 2002. 85, 102

[235] M.D. Bates and D.G. Watts. *Nonlinear Regression Analysis and its Applications.* John Wiely & Sons, INC., New York, N.Y., USA, 1988. 104

[236] R. Scherrer, T.C. Beaman, and P. Gerhardt. 1971. *Journal of Bacteriology*, 108:868–873, Macromolecular sieving by the dormant spore of Bacillus cereus. 127

[237] G.S.A.B. Setwart, M.W. Eaton, K. Johnstone, M.D. Barrett, and D.J. Ellar. An investigation of membrane fluidity changes during sporulation and germination of Bacillus megaterium k.m. measured by electron spin and nuclear magnetic resonance spectroscopy. *Biochimica et Biophysica Acta*, 600:270–290, 1980. 128

[238] J. J. Shull, G. T. Cargo, and R. R. Ernst. Kinetics of heat activation and of thermal death of bacterial spores. *Applied Microbiology*, 11:485–487, 1963. 128

[239] C.J. Bunthof. *Flow cytometry, fluorescent probes, and flashing bacteria.* PhD thesis, Wageningen University, The Netherlands, 2002. 128

[240] H.L. Bishop and Doi. R.H. Isolation and characterization of ribosomes from Bacillus subtilis spores. *Journal of Bacteriology*, 91:695–701, 1966. 129

[241] G.W. Gould and A. Hurst. *The Bacterial Spore.* Academic Press INC., London, UK, 1969. 129, 130

[242] A. Propst and J.R. Mdse. Sporulation und Germination beim Clostridium butyricum M55. *Elektronenmikroskopische Untersuchung. Zentr Bakteriol Parasitenk. Abt I Orig*, 201:373–396, 1966. 129

[243] J.C. Vary and H.O. Halvorson. Kinetics of germination of Bacillus spores. *Journal of Bacteriology*, 89(5):1340–1347, 1965. 129

[244] N. Finley and M.L. Fields. Heat activation and heat–induced dormancy of Bacillus stearothermophilus spores. *Applied and Environmental Microbiology*, 10(3):231–236, 1962. 129

[245] W.K. Harrell and E. Mantini. Studies on dipicolinic acid in the spores of Bacillus cereus var. terminalis. *Canadian Journal of Microbiology*, 3(5):735–739, 1957. 129

[246] A. Keynan, Z. Evenchik, H.O. Halvorson, and J.W. Hastings. Activation of bacterial endospores. *Journal of Bacteriology*, 88(2):313–318, 1964. 129

[247] M. Paidhungat, K. Ragkousi, and P. Setlow. Genetic requirements for induction of germination of spores of Bacillus subtilis by Ca^{2+}–dipicolinate. *Journal of Bacteriology*, 183(16):4886–4893, 2001. 130

[248] M. Paidhungat and P. Setlow. Role of ger proteins in nutrient and nonnutrient triggering of spore germination in Bacillus subtilis. *Journal of Bacteriology*, 182(9):2513–2519, 2000. 130

[249] B. Setlow, E. Melly, and P. Setlow. Properties of spores of Bacillus subtilis blocked at an intermediate stage of spore germination. *Journal of bacteriology*, 183:4894–4899, 2002. 130

[250] S. Aiba and K. Toda. Some analysis of thermal inactivation of bacterial–spore clump. *Journal of Fermentation Technology*, 44:301–304, 1966. 131

[251] R. J. Doyle, F. Nedjat-Haiem, and J. S. Singh. Hydrophobic characteristics of Bacillus spores. *Current Microbiology*, 10:329–332, 1984. 131

[252] K.M. Wiencek, N.A. Klapes, and P.M. Foegeding. Hydrophobicity of Bacillus and Clostridium spores. *Applied and Environment Microbiology*, 56(9):2600–2605, 1990. 131

[253] A. Briggs. The resistances of spores of the genus Bacillus to phenol heat and radiation. *Journal of applied Bacteriology*, 9:490–504, 1966. 131

[254] K. Fox and B.D. Eder. Comparison of survivor curves of Bacillus suibtilis spores subjected to wet and dry heat. *Journal of Food Science*, 34:518–521, 1969. 131

[255] S. K. Navani, J. Scholefield, and M.R. Kibby. A digital computer program for the statistical analysis of heat resistance data applied to Bacillus stearothermophilus spores. *Journal of Applied Bacteriology*, 33:609–620, 1970. 131

[256] U. Broeckel, W. Meier, and G. Wagner. *Product Design and Engineering: Best Practices.* Wiley–VCH Verlag GmbH, Weinheim, Germany, 2007. 131

[257] M.M. Mench. *Fuel cell engines.* John Wiley & Sons, Inc., Hoboken, NJ, USA, 2008. 132

[258] B.H. Belliveau, T.C. Beaman, H.S. Pankratz, and P. Gerhardt. Heat killing of bacterial spores analyzed by differential scanning calorimetry. *Journal of Bacteriology*, 174(13):4463–4474, 1992. 133

[259] J. Farrell and A. Ros. Temperature effects on microorganisms. *Annual Review in Microbiology*, 21:101–120, 1967. 133

[260] S.H. Black and P. Gerhardt. Permeability of bacterial spores. III. permeation relative to germination. *Journal of Bacteriology*, 83:301–308, 1962. 133

[261] D. Knorr, M. GeulEn, T. Grahl, and W. Sitzmann. Food application of high electric field pules. *Trends in Food Science and Technology*, 5:71–75, 1994. 133

[262] R. Benz, F. Beckers, and U. Zimmermann. Reversible electrical breakdown of lipid bilayer membranes: A charge–pulse relaxation study. *Journal of Membrane Biology*, 48:181–204, 1979. 134

[263] K.P. Drees, M. Abbaszadeganb, and R.M. Maier. Comparative electrochemical inactivation of bacteria and bacteriophage. *Water Research*, 37(10):2291–2300, 2003. 134

[264] M.I. Kerwick, S.M. Reddyb, A.H.L. Chamberlain, and Holt. D.M. Electrochemical disinfection, an environmentally acceptable method of drinking water disinfection? *Electrochimica Acta*, 50:5270–5277, 2005. 134

[265] N.N. Barashkov, D. Eiseinberg, S. Eisenberg, G.Sh. Shegebaeva, I.S. Irgibaeva, and I.I. Barashkova. Electrochemical chlorine–free AC disinfection of water contaminated with Salmonella typhimurium bacteria. *Russian Journal of Electrochemistry*, 46(3):306–311, 2010. 134

[266] G. Patermarakis and Fountoukidis E. Disinfection of water by electrochemical treatment. *Water Research*, 24:1491–1496, 1990. 134

[267] X.Y. Li, H.F. Diao, F.X.J. Fan, J.D. Gu, F. Ding, and A.S.F. Tong. Electrochemical wastewater disinfection: Identification of its principal germicidal actions. *Journal of Environmental Engineering*, 130:1217–1221, 2004. 134

[268] M.A. Oturan. An ecologically effective water treatment technique using electrochemically generated hydroxyl radicals for in situ destruction of organic pollutants: Application to herbicide 2,4–D. *Journal of Applied Electrochemistry*, 30(4):475–482, 2000. 134

[269] R. Tomat and A. Rigo. Oxidation of polymethylated benzenes promoted by oh radicals. *Journal of Applied Electrochemistry*, 9:301–305, 1979. 136

[270] M. Hepel and J. Luo. Photoelectrochemical mineralisation of textile diazo dye pollutants using nanocrystalline WO3 electrodes. *Electrochimica Acta*, 4:729–740, 2001. 136

[271] L.M. Da Silva, L.A. De Faria, and J.F.C. Boodts. Green processes for environmental application. electrochemical ozone production. *Pure and Applied Chemistry*, 73:1871–1884, 2001. 136

[272] R.V. Thurston, R.C. Russo, and G.A. Vinogradov. Ammonia toxicity to fishes. effect of ph on the toxicity of the unionized ammonia species. *Environmental Science and Technology*, 15(7):837–840, 1981. 137

[273] W.C. Yang. Abiotic factors in biosolids processing that influence pathogen disinfection (nitrous acid and ammonia studies). Master's thesis, Tulane University, New Orleans, Louisiana, USA, 1996. 138

[274] C.L. Yaws. *Physical Properties: A Guide to the Physical, Thermodynamic, and Transport Property Data of Industrially Important Chemical Compounds*. McGraw Hill Co., New York, NY, USA, 1977. 138

[275] E. Durban and N. Gercz. Resistance of spores of Clostridium botulinum 33A to combinations of ultraviolet and gamma rays. *Applied microbiology*, 18(1):44–50, 1969. 142

[276] M. Peleg. Calculation of the non–isothermal inactivation patterns of microbes having sigmoidal isothermal semi–logarithmic survival curves. *Critical Reviews in Food Science and Nutrition*, 43(6):645–658, 2003. 142

174

[277] R.E. Zirkle, D.F. Marchbank, and K.D. Kuck. Exponential and sigmoid survival curves resulting from alpha and X irradiation of aspergillus spore. *Journal of Cellular and Comparative Physiology*, 39:75–85, 1952. 142

Appendix A

BioElectro^{TM} reactor layout
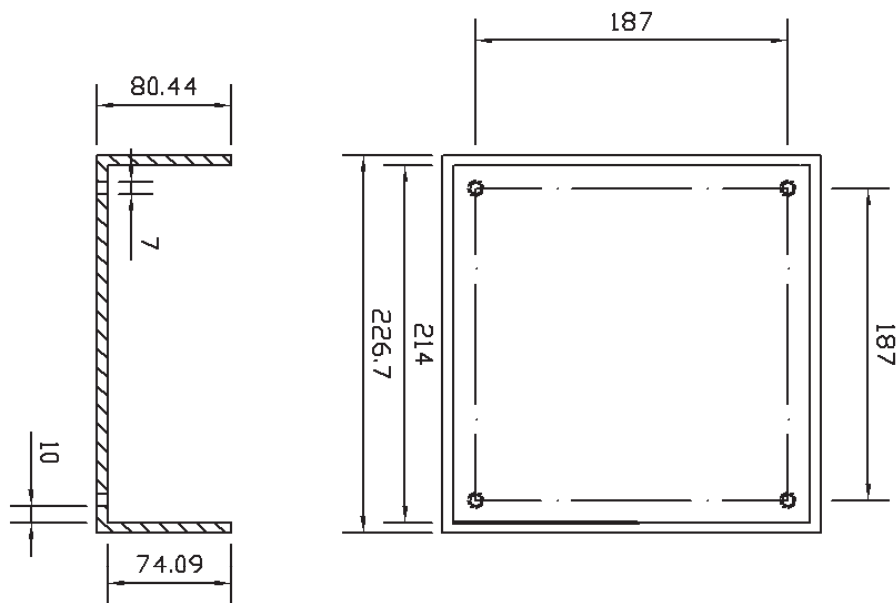
Figure A.1: BioElectro^{TM} reactor–vessel layout
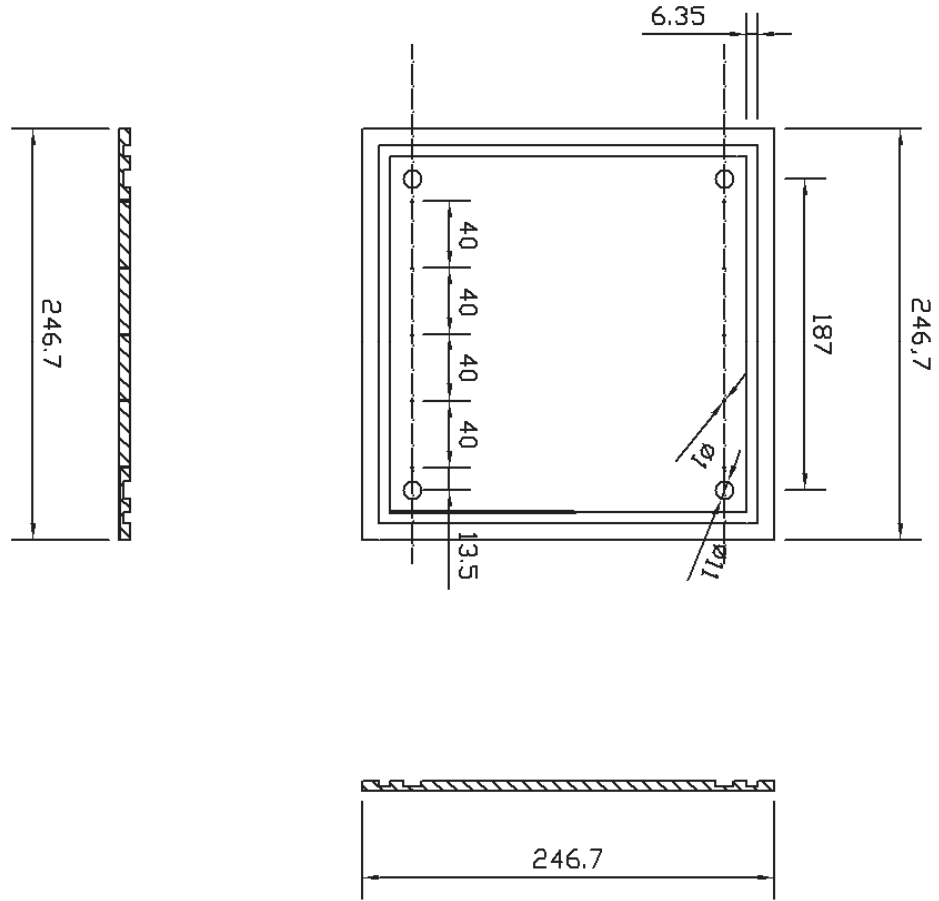
Figure A.2: BioElectro^{TM} reactor–sealed cap layout
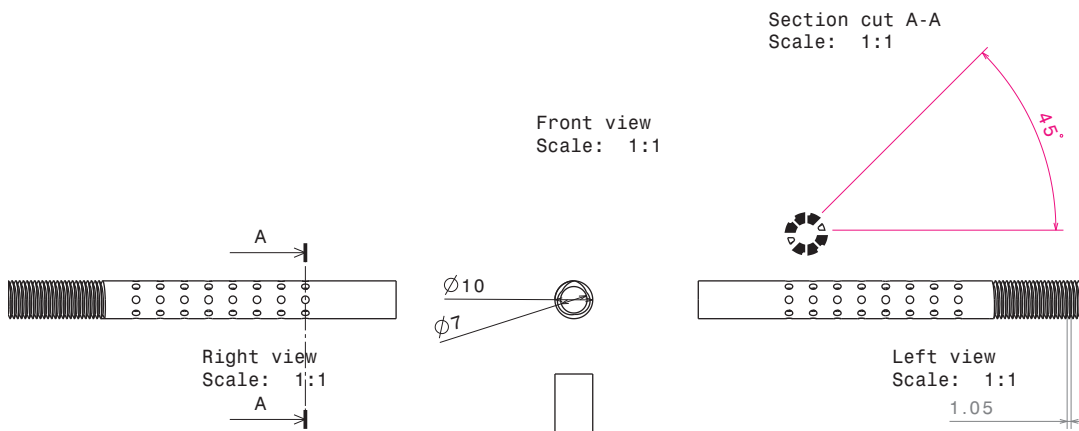
Figure A.3: BioElectro^{TM} electrode layout

Appendix B

Experimental data–Electrical conductivity

Table B.1: Conductivity data for AN at different concentrations and temperatures

Code	AN(g/L)	Mole	κ(mS/cm)				
			307.15K	317.15K	327.15K	337.15K	347.15K
1a	3	0.0375	8.31	8.42	8.52	8.69	8.83
2a	6	0.0750	11.36	11.54	11.91	12.14	12.27
3a	9	0.1124	16.07	16.12	16.27	16.30	16.46
4a	12	0.1500	18.18	18.52	18.68	18.93	19.03
5a	15	0.1874	20.88	20.92	21.13	21.33	21.72
6a	18	0.2249	24.26	24.36	24.42	24.51	24.61
7a	21	0.2623	27.12	27.50	27.63	27.85	28.15
8a	24	0.2998	29.98	30.11	30.52	30.91	31.30
9a	27	0.3372	33.22	33.52	33.68	33.97	34.10
10a	30	0.3748	34.48	34.53	34.96	35.17	35.26
1b	3	0.0375	8.32	8.43	8.54	8.70	8.84
2b	6	0.0750	11.35	11.54	11.87	12.12	12.23

Code	AN(g/L)	Mole	κ(mS/cm)				
			307.15K	317.15K	327.15K	337.15K	347.15K
3b	9	0.1124	16.08	16.13	16.29	16.33	16.45
4b	12	0.1500	18.18	18.53	18.67	18.96	19.02
5b	15	0.1874	20.86	20.93	21.13	21.35	21.69
6b	18	0.2249	24.27	24.35	24.43	24.53	24.62
7b	24	0.2623	27.27	27.53	27.63	27.84	28.14
8b	24	0.2998	29.98	30.12	30.51	30.92	31.20
9b	27	0.3372	33.23	33.52	33.67	33.96	34.30
10b	30	0.3748	34.47	34.54	34.97	35.18	35.23
1c	3	0.0375	8.32	8.47	8.50	8.71	8.83
2c	6	0.0750	11.34	11.52	11.98	12.13	12.29
3c	9	0.1124	16.09	16.13	16.28	16.32	16.48
4c	12	0.1500	18.16	18.52	18.69	18.94	19.02
5c	15	0.1874	20.87	20.90	21.12	21.34	21.70
6c	18	0.2249	24.28	24.37	24.42	24.52	24.60
7c	21	0.2623	27.23	27.52	27.62	27.82	28.20
8c	24	0.2998	29.97	30.12	30.50	30.90	31.30
9c	27	0.3372	33.21	33.50	33.68	33.97	34.10
10c	30	0.3748	34.47	34.56	34.98	25.19	35.25

Table B.2: Conductivity data for BS at different concentrations and temperatures

Code	BS(g/L)	Mole	κ(mS/cm)				
			307.15K	317.15K	327.15K	337.15K	347.15K
1a	3	0.0283	5.99	6.03	6.06	6.08	6.12
2a	6	0.0566	7.31	7.36	7.50	7.54	7.62
3a	9	0.0849	9.51	9.62	9.72	9.88	9.92
4a	12	0.1132	10.67	10.75	10.86	10.95	11.03
5a	15	0.1415	11.76	11.98	12.03	12.16	12.22
6a	18	0.1698	13.06	13.09	13.14	13.32	13.45
7a	21	0.1981	14.62	14.85	14.98	15.02	15.09
8a	24	0.2264	15.79	15.97	16.06	16.18	16.25
9a	27	0.2547	16.16	16.24	16.43	17.65	17.81
10a	30	0.2831	17.24	17.46	17.78	17.86	18.02
1b	3	0.0283	5.98	6.03	6.05	6.09	6.11
2b	6	0.0566	7.31	7.35	7.49	7.56	7.63
3b	9	0.0849	9.50	9.63	9.74	9.87	9.93
4b	12	0.1132	10.65	10.74	10.86	10.94	11.02
5b	15	0.1415	11.78	11.97	12.05	12.18	12.21
6b	18	0.1698	13.05	13.09	13.15	13.34	13.46
7b	21	0.1981	14.63	14.87	14.97	15.01	15.08
8b	24	0.2264	15.78	15.98	16.04	16.17	16.23
9b	27	0.2547	16.17	16.25	16.45	17.64	17.82
10b	30	0.2831	17.25	17.45	17.76	17.86	18.01
1c	3	0.0283	5.98	6.02	6.06	6.08	6.11
2c	6	0.0566	7.30	7.36	7.50	7.56	7.62
3c	9	0.0849	9.52	9.62	9.73	9.86	9.92
4c	12	0.1132	10.63	10.76	10.84	10.96	11.02

Code	BS(g/L)	Mole	κ(mS/cm)				
			307.15K	**317.15K**	**327.15K**	**337.15K**	**347.15K**
5c	15	0.1415	11.76	11.98	12.04	12.17	12.22
6c	18	0.1698	13.06	13.10	13.14	13.33	13.45
7c	21	0.1981	14.64	14.86	14.98	15.02	15.09
8c	24	0.2264	15.77	15.97	16.05	16.17	16.22
9c	27	0.2547	16.16	16.23	16.42	17.65	17.8
10c	30	0.2831	17.23	17.43	17.75	17.87	18.01

Table B.3: Conductivity data for the systems XAN + (1-X) BS with different mole ratios of AN (X) and temperatures

Code	AN(g/L)	BS(g/L)	X	κ(mS/cm)				
				307.15K	317.15K	327.15K	337.15K	347.15K
1a	0	30	0.0000	16.51	16.98	17.27	17.81	18.56
2a	3	27	0.1283	17.23	18.32	18.54	19.34	19.76
3a	6	24	0.2487	18.45	19.89	20.43	20.87	21.12
4a	9	21	0.3620	20.87	21.98	22.12	21.87	22.58
5a	12	18	0.4688	22.13	23.34	23.54	23.98	23.75
6a	15	15	0.5697	23.67	24.13	24.43	24.56	25.23
7a	18	12	0.6651	24.23	25.09	25.98	26.23	26.67
8a	21	9	0.7555	25.76	26.57	26.97	27.83	28.54
9a	24	6	0.8412	28.61	29.12	29.72	30.20	30.70
10a	27	3	0.9226	28.98	29.84	31.35	31.92	32.38
11a	30	0	1.0000	33.25	33.68	34.23	34.98	35.54
1b	0	30	0.0000	16.46	16.87	17.44	17.87	18.54
2b	3	27	0.1283	17.78	18.21	18.91	19.25	19.76
3b	6	24	0.2487	19.23	19.79	20.68	20.78	21.42
4b	9	21	0.3620	21.10	21.97	22.12	22.39	22.69
5b	12	18	0.4688	22.14	22.98	23.25	23.98	24.14
6b	15	15	0.5697	23.58	24.15	25.02	25.34	25.12
7b	18	12	0.6651	24.98	25.32	25.95	26.42	26.72
8b	21	9	0.7555	25.87	26.64	26.98	27.97	28.69
9b	24	6	0.8412	28.72	29.13	29.62	30.78	30.85
10b	27	3	0.9226	29.54	31.16	30.82	31.88	32.53
11b	30	0	1.0000	33.16	33.64	34.11	34.78	35.34
1c	0	30	0.0000	16.24	16.67	17.56	17.89	18.56

Code	AN(g/L)	BS(g/L)	X	κ(mS/cm)				
				307.15K	317.15K	327.15K	337.15K	347.15K
2c	3	27	0.1283	17.14	18.18	19.34	19.43	19.72
3c	6	24	0.2487	18.87	19.97	20.98	21.16	21.11
4c	9	21	0.3620	20.65	21.98	22.36	22.43	22.79
5c	12	18	0.4688	22.10	22.78	23.56	24.04	24.20
6c	15	15	0.5697	23.54	23.98	25.13	25.32	25.84
7c	18	12	0.6651	24.47	25.53	25.83	26.65	26.89
8c	21	9	0.7555	26.15	26.55	26.98	27.99	28.83
9c	24	6	0.8412	28.43	28.97	29.65	29.98	30.87
10c	27	3	0.9226	29.14	29.78	31.23	31.93	32.78
11c	30	0	1.0000	33.13	33.54	34.10	34.63	35.21

Appendix C

Experimental data–Inactivation, pH and temperature

C.1 Experimental data–Inactivation

Table C.1: Inactivation data of the 1st experimental series

Code	t(min)	E(V/cm)	BS(g/L)	AN(g/L)	N_0(CFU/g TS)	$N_{Observed}$(CFU/g TS)
1A	5	2.8	13	26	6767466	2886862
1A	10	2.8	13	26	6767466	2401188
1A	15	2.8	13	26	6767466	1863915
1A	20	2.8	13	26	6767466	1550337
1A	25	2.8	13	26	6767466	1123120
1A	30	2.8	13	26	6767466	537559
1A	35	2.8	13	26	6767466	257292
1A	40	2.8	13	26	6767466	138173
1A	45	2.8	13	26	6767466	85197
1A	50	2.8	13	26	6767466	42700
1A	55	2.8	13	26	6767466	26942
1A	60	2.8	13	26	6767466	14139

Table C.1–continued from previous page

Code	t(min)	E(V/cm)	BS(g/L)	AN(g/L)	N_0(CFU/g TS)	$N_{Observed}$(CFU/g TS)
1A	65	2.8	13	26	6767466	8718
1A	70	2.8	13	26	6767466	2347
1A	75	2.8	13	26	6767466	302
1A	80	2.8	13	26	6767466	54
1A	85	2.8	13	26	6767466	1
1B	5	2.8	13	26	4098276	1594415
1B	10	2.8	13	26	4098276	1295989
1B	15	2.8	13	26	4098276	960730
1B	20	2.8	13	26	4098276	763135
1B	25	2.8	13	26	4098276	578897
1B	30	2.8	13	26	4098276	196156
1B	35	2.8	13	26	4098276	145412
1B	40	2.8	13	26	4098276	78091
1B	45	2.8	13	26	4098276	42914
1B	50	2.8	13	26	4098276	18306
1B	55	2.8	13	26	4098276	12377
1B	60	2.8	13	26	4098276	7631
1B	65	2.8	13	26	4098276	4291
1B	70	2.8	13	26	4098276	680
1B	75	2.8	13	26	4098276	49
1B	80	2.8	13	26	4098276	7
1B	85	2.8	13	26	4098276	1
1C	5	2.8	13	26	4678540	1905945
1C	10	2.8	13	26	4678540	1513946
1C	15	2.8	13	26	4678540	1148445
1C	20	2.8	13	26	4678540	933491

Table C.1–continued from previous page

Code	t(min)	E(V/cm)	BS(g/L)	AN(g/L)	N_0(CFU/g TS)	$N_{Observed}$(CFU/g TS)
1C	25	2.8	13	26	4678540	741499
1C	30	2.8	13	26	4678540	239944
1C	35	2.8	13	26	4678540	169868
1C	40	2.8	13	26	4678540	91224
1C	45	2.8	13	26	4678540	51300
1C	50	2.8	13	26	4678540	23449
1C	55	2.8	13	26	4678540	14795
1C	60	2.8	13	26	4678540	8915
1C	65	2.8	13	26	4678540	5130
1C	70	2.8	13	26	4678540	934
1C	75	2.8	13	26	4678540	71
1C	80	2.8	13	26	4678540	9
1C	85	2.8	13	26	4678540	1
1D	5	2.8	13	26	5146318	2145342
1D	10	2.8	13	26	5146318	1743800
1D	15	2.8	13	26	5146318	1322807
1D	20	2.8	13	26	5146318	1075218
1D	25	2.8	13	26	5146318	936476
1D	30	2.8	13	26	5146318	289399
1D	35	2.8	13	26	5146318	191204
1D	40	2.8	13	26	5146318	102683
1D	45	2.8	13	26	5146318	57743
1D	50	2.8	13	26	5146318	29614
1D	55	2.8	13	26	5146318	17041
1D	60	2.8	13	26	5146318	10035
1D	65	2.8	13	26	5146318	6046

Table C.1–continued from previous page

Code	t(min)	E(V/cm)	BS(g/L)	AN(g/L)	N_0(CFU/g TS)	$N_{Observed}$(CFU/g TS)
1D	70	2.8	13	26	5146318	1417
1D	75	2.8	13	26	5146318	191
1D	80	2.8	13	26	5146318	9
1D	85	2.8	13	26	5146318	1

Table C.2: Inactivation data of the 2nd experimental series

Code	t(min)	E(V/cm)	BS(g/L)	AN(g/L)	N_0(CFU/g TS)	$N_{Observed}$(CFU/g TS)
2A	5	2.8	25	13	9725159	2031875
2A	10	2.8	25	13	9725159	1729405
2A	15	2.8	25	13	9725159	1311888
2A	20	2.8	25	13	9725159	1169221
2A	25	2.8	25	13	9725159	657501
2A	30	2.8	25	13	9725159	465474
2A	35	2.8	25	13	9725159	345062
2A	40	2.8	25	13	9725159	203187
2A	45	2.8	25	13	9725159	131189
2A	50	2.8	25	13	9725159	77250
2A	55	2.8	25	13	9725159	48741
2A	60	2.8	25	13	9725159	22798
2A	65	2.8	25	13	9725159	14385
2A	70	2.8	25	13	9725159	3444
2A	75	2.8	25	13	9725159	600
2A	80	2.8	25	13	9725159	114
2A	85	2.8	25	13	9725159	5
2A	90	2.8	25	13	9725159	2
2B	5	2.8	25	13	11568433	3260427
2B	10	2.8	25	13	11568433	2361971
2B	15	2.8	25	13	11568433	1672147
2B	20	2.8	25	13	11568433	1490303
2B	25	2.8	13	26	11568433	918913
2B	30	2.8	13	26	11568433	729919
2B	35	2.8	13	26	11568433	460548

Table C.2–continued from previous page

Code	t(min)	E(V/cm)	BS(g/L)	AN(g/L)	N_0(CFU/g TS)	$N_{Observed}$(CFU/g TS)
2B	40	2.8	13	26	11568433	297355
2B	45	2.8	13	26	11568433	183347
2B	50	2.8	13	26	11568433	115684
2B	55	2.8	13	26	11568433	62126
2B	60	2.8	13	26	11568433	29059
2B	65	2.8	13	26	11568433	14903
2B	70	2.8	13	26	11568433	4606
2B	75	2.8	13	26	11568433	838
2B	80	2.8	13	26	11568433	160
2B	85	2.8	13	26	11568433	7
2B	90	2.8	13	26	11568433	2
2C	5	2.8	25	13	12918660	3812568
2C	10	2.8	25	13	12918660	2892128
2C	15	2.8	25	13	12918660	1910810
2C	20	2.8	25	13	12918660	1726363
2C	25	2.8	25	13	12918660	1352750
2C	30	2.8	25	13	12918660	1026166
2C	35	2.8	25	13	12918660	577055
2C	40	2.8	25	13	12918660	408524
2C	45	2.8	25	13	12918660	229730
2C	50	2.8	25	13	12918660	144950
2C	55	2.8	25	13	12918660	70993
2C	60	2.8	25	13	12918660	33980
2C	65	2.8	25	13	12918660	17831
2C	70	2.8	25	13	12918660	6475
2C	75	2.8	25	13	12918660	1026

Table C.2–continued from previous page

Code	t(min)	E(V/cm)	BS(g/L)	AN(g/L)	N_0(CFU/g TS)	$N_{Observed}$(CFU/g TS)
2C	80	2.8	25	13	12918660	188
2C	85	2.8	25	13	12918660	10
2C	90	2.8	25	13	12918660	2
2D	5	2.8	25	13	25000000	8287278
2D	10	2.8	25	13	25000000	7045957
2D	15	2.8	25	13	25000000	6279716
2D	20	2.8	25	13	25000000	4549252
2D	25	2.8	25	13	25000000	3531344
2D	30	2.8	25	13	25000000	2937244
2D	35	2.8	25	13	25000000	2387481
2D	40	2.8	25	13	25000000	1342580
2D	45	2.8	25	13	25000000	1091290
2D	50	2.8	25	13	25000000	721009
2D	55	2.8	25	13	25000000	337241
2D	60	2.8	25	13	25000000	104218
2D	65	2.8	25	13	25000000	51044
2D	70	2.8	25	13	25000000	25582
2D	75	2.8	25	13	25000000	5223
2D	80	2.8	25	13	25000000	1253
2D	85	2.8	25	13	25000000	34
2D	90	2.8	25	13	25000000	12
2D	95	2.8	25	13	25000000	3

Table C.3: Inactivation data of the 3rd experimental series

Code	t(min)	E(V/cm)	BS(g/L)	AN(g/L)	N_0(CFU/g TS)	$N_{Observed}$(CFU/g TS)
3A	5	2.8	13	13	5657459	2358421
3A	10	2.8	13	13	5657459	1961649
3A	15	2.8	13	13	5657459	1522725
3A	20	2.8	13	13	5657459	1357130
3A	25	2.8	13	13	5657459	1128811
3A	30	2.8	13	13	5657459	712232
3A	35	2.8	13	13	5657459	333136
3A	40	2.8	13	13	5657459	163163
3A	45	2.8	13	13	5657459	71223
3A	50	2.8	13	13	5657459	57892
3A	55	2.8	13	13	5657459	44939
3A	60	2.8	13	13	5657459	17890
3A	65	2.8	13	13	5657459	8563
3A	70	2.8	13	13	5657459	2102
3A	75	2.8	13	13	5657459	290
3A	80	2.8	13	13	5657459	20
3A	85	2.8	13	13	5657459	3
3B	5	2.8	13	13	5149853	1957920
3B	10	2.8	13	13	5149853	1666460
3B	15	2.8	13	13	5149853	1323717
3B	20	2.8	13	13	5149853	1179763
3B	25	2.8	13	26	5149853	981283
3B	30	2.8	13	26	5149853	619149
3B	35	2.8	13	26	5149853	289598
3B	40	2.8	13	26	5149853	141839

Table C.3–continued from previous page

Code	t(min)	E(V/cm)	BS(g/L)	AN(g/L)	N_0(CFU/g TS)	$N_{Observed}$(CFU/g TS)
3B	45	2.8	13	26	5149853	59128
3B	50	2.8	13	26	5149853	37307
3B	55	2.8	13	26	5149853	34817
3B	60	2.8	13	26	5149853	14184
3B	65	2.8	13	26	5149853	6947
3B	70	2.8	13	26	5149853	1705
3B	75	2.8	13	26	5149853	215
3B	80	2.8	13	26	5149853	12
3B	85	2.8	13	26	5149853	2
3C	5	2.8	13	13	5006448	2039528
3C	10	2.8	13	13	5006448	1657791
3C	15	2.8	13	13	5006448	1286855
3C	20	2.8	13	13	5006448	1146911
3C	25	2.8	13	13	5006448	953959
3C	30	2.8	13	13	5006448	601907
3C	35	2.8	13	13	5006448	281533
3C	40	2.8	13	13	5006448	137889
3C	45	2.8	13	13	5006448	57482
3C	50	2.8	13	13	5006448	36269
3C	55	2.8	13	13	5006448	33848
3C	60	2.8	13	13	5006448	13789
3C	65	2.8	13	13	5006448	6754
3C	70	2.8	13	13	5006448	1696
3C	75	2.8	13	13	5006448	209
3C	80	2.8	13	13	5006448	11
3C	85	2.8	13	13	5006448	2

Table C.3–continued from previous page

Code	t(min)	E(V/cm)	BS(g/L)	AN(g/L)	N_0(CFU/g TS)	$N_{Observed}$(CFU/g TS)
3D	5	2.8	13	13	4105360	1597171
3D	10	2.8	13	13	4105360	1298229
3D	15	2.8	13	13	4105360	1007747
3D	20	2.8	13	13	4105360	877711
3D	25	2.8	13	13	4105360	747053
3D	30	2.8	13	13	4105360	429884
3D	35	2.8	13	13	4105360	220471
3D	40	2.8	13	13	4105360	107982
3D	45	2.8	13	13	4105360	42988
3D	50	2.8	13	13	4105360	27124
3D	55	2.8	13	13	4105360	23086
3D	60	2.8	13	13	4105360	9624
3D	65	2.8	13	13	4105360	5289
3D	70	2.8	13	13	4105360	1299
3D	75	2.8	13	13	4105360	156
3D	80	2.8	13	13	4105360	8
3D	85	2.8	13	13	4105360	1

Table C.4: Inactivation data of the 4th experimental series

Code	t(min)	E(V/cm)	BS(g/L)	AN(g/L)	N_0(CFU/g TS)	N_{Observed}(CFU/g TS)
4A	5	2.5	25	13	7879523	1572172
4A	10	2.5	25	13	7879523	1401199
4A	15	2.5	25	13	7879523	1277909
4A	20	2.5	25	13	7879523	1015079
4A	25	2.5	25	13	7879523	863973
4A	30	2.5	25	13	7879523	570821
4A	35	2.5	25	13	7879523	497164
4A	40	2.5	25	13	7879523	433012
4A	45	2.5	25	13	7879523	394912
4A	50	2.5	25	13	7879523	328473
4A	55	2.5	25	13	7879523	124882
4A	60	2.5	25	13	7879523	92576
4A	65	2.5	25	13	7879523	27321
4A	70	2.5	25	13	7879523	12488
4A	75	2.5	25	13	7879523	9920
4A	80	2.5	25	13	7879523	6259
4A	85	2.5	25	13	7879523	3949
4A	90	2.5	25	13	7879523	1249
4A	95	2.5	25	13	7879523	497
4B	5	2.5	25	13	5983518	1166693
4B	10	2.5	25	13	5983518	1064037
4B	15	2.5	25	13	5983518	948324
4B	20	2.5	25	13	5983518	75328
4B	25	2.5	25	26	5983518	641146
4B	30	2.5	25	26	5983518	404535

Table C.4–continued from previous page

Code	t(min)	E(V/cm)	BS(g/L)	AN(g/L)	N_0(CFU/g TS)	$N_{Observed}$(CFU/g TS)
4B	35	2.5	25	26	5983518	314020
4B	40	2.5	25	26	5983518	2930601
4B	45	2.5	25	26	5983518	243757
4B	50	2.5	25	26	5983518	217248
4B	55	2.5	25	26	5983518	88503
4B	60	2.5	25	26	5983518	68700
4B	65	2.5	25	26	5983518	20275
4B	70	2.5	25	26	5983518	8850
4B	75	2.5	25	26	5983518	6561
4B	80	2.5	25	26	5983518	2999
4B	85	2.5	25	26	5983518	2864
4B	85	2.5	25	26	5983518	826
4B	85	2.5	25	26	5983518	321
4C	5	2.5	25	13	4869177	927803
4C	10	2.5	25	13	4869177	865876
4C	15	2.5	25	13	4869177	754147
4C	20	2.5	25	13	4869177	585404
4C	25	2.5	25	13	4869177	498260
4C	30	2.5	25	13	4869177	321703
4C	35	2.5	25	13	4869177	249721
4C	40	2.5	25	13	4869177	233053
4C	45	2.5	25	13	4869177	193845
4C	50	2.5	25	13	4869177	172765
4C	55	2.5	25	13	4869177	68779
4C	60	2.5	25	13	4869177	55906
4C	65	2.5	25	13	4869177	16499

Table C.4–continued from previous page

Code	t(min)	E(V/cm)	BS(g/L)	AN(g/L)	N_0(CFU/g TS)	$N_{Observed}$(CFU/g TS)
4C	70	2.5	25	13	4869177	7038
4C	75	2.5	25	13	4869177	5099
4C	80	2.5	25	13	4869177	2331
4C	85	2.5	25	13	4869177	2226
4C	90	2.5	25	13	4869177	628
4C	95	2.5	25	13	4869177	238
4D	5	2.5	25	13	10799230	2840487
4D	10	2.5	25	13	10799230	2531587
4D	20	2.5	25	13	10799230	2154730
4D	25	2.5	25	13	10799230	1560964
4D	30	2.5	25	13	10799230	1268799
4D	35	2.5	25	13	10799230	819205
4D	40	2.5	25	13	10799230	713498
4D	45	2.5	25	13	10799230	621431
4D	50	2.5	25	13	10799230	553851
4D	55	2.5	25	13	10799230	482384
4D	60	2.5	25	13	10799230	179223
4D	65	2.5	25	13	10799230	132860
4D	70	2.5	25	13	10799230	54124
4D	75	2.5	25	13	10799230	19651
4D	80	2.5	25	13	10799230	13595
4D	85	2.5	25	13	10799230	8578
4D	90	2.5	25	13	10799230	5412
4D	95	2.5	25	13	10799230	1712

Table C.5: Inactivation data of the 5th experimental series

Code	t(min)	E(V/cm)	BS(g/L)	AN(g/L)	N_0(CFU/g TS)	$N_{Observed}$(CFU/g TS)
5A	5	2.5	13	26	4746795	1889733
5A	10	2.5	13	26	4746795	1466900
5A	15	2.5	13	26	4746795	1220114
5A	20	2.5	13	26	4746795	1087428
5A	25	2.5	13	26	4746795	904483
5A	30	2.5	13	26	4746795	769840
5A	35	2.5	13	26	4746795	611506
5A	40	2.5	13	26	4746795	299503
5A	45	2.5	13	26	4746795	266932
5A	50	2.5	13	26	4746795	237903
5A	55	2.5	13	26	4746795	140088
5A	60	2.5	13	26	4746795	57069
5A	65	2.5	13	26	4746795	22720
5A	70	2.5	13	26	4746795	5577
5A	75	2.5	13	26	4746795	3284
5A	80	2.5	13	26	4746795	2795
5A	85	2.5	13	26	4746795	1087
5A	90	2.5	13	26	4746795	497
5A	95	2.5	13	26	4746795	140
5B	5	2.5	13	26	6874257	2865667
5B	10	2.5	13	26	6874257	2495892
5B	15	2.5	13	26	6874257	2124349
5B	20	2.5	13	26	6874257	1893328
5B	25	2.5	13	26	6874257	1611483
5B	30	2.5	13	26	6874257	1469690

Table C.5–continued from previous page

Code	t(min)	E(V/cm)	BS(g/L)	AN(g/L)	N_0(CFU/g TS)	$N_{Observed}$(CFU/g TS)
5B	35	2.5	13	26	6874257	993632
5B	40	2.5	13	26	6874257	753747
5B	45	2.5	13	26	6874257	521465
5B	50	2.5	13	26	6874257	395572
5B	55	2.5	13	26	6874257	300072
5B	60	2.5	13	26	6874257	99363
5B	65	2.5	13	26	6874257	80766
5B	70	2.5	13	26	6874257	12510
5B	75	2.5	13	26	6874257	8856
5B	80	2.5	13	26	6874257	5215
5B	85	2.5	13	26	6874257	3692
5B	90	2.5	13	26	6874257	1065
5B	95	2.5	13	26	6874257	387
5C	5	2.5	13	26	4965069	1963023
5C	10	2.5	13	26	4965069	1606665
5C	15	2.5	13	26	4965069	1336366
5C	20	2.5	13	26	4965069	1218780
5C	25	2.5	13	26	4965069	1013737
5C	30	2.5	13	26	4965069	882928
5C	35	2.5	13	26	4965069	669769
5C	40	2.5	13	26	4965069	508072
5C	45	2.5	13	26	4965069	343499
5C	50	2.5	13	26	4965069	254639
5C	55	2.5	13	26	4965069	188767
5C	60	2.5	13	26	4965069	66977
5C	65	2.5	13	26	4965069	31328

Table C.5–continued from previous page

Code	t(min)	E(V/cm)	BS(g/L)	AN(g/L)	N_0(CFU/g TS)	$N_{Observed}$(CFU/g TS)
5C	70	2.5	13	26	4965069	7515
5C	75	2.5	13	26	4965069	6251
5C	80	2.5	13	26	4965069	3280
5C	85	2.5	13	26	4965069	1336
5C	90	2.5	13	26	4965069	734
5C	95	2.5	13	26	4965069	238
5D	5	2.5	13	26	7321489	3123197
5D	10	2.5	13	26	7321489	2783553
5D	15	2.5	13	26	7321489	2369187
5D	20	2.5	13	26	7321489	2160725
5D	25	2.5	13	26	7321489	1881913
5D	30	2.5	13	26	7321489	1716325
5D	35	2.5	13	26	7321489	1082928
5D	40	2.5	13	26	7321489	840619
5D	45	2.5	13	26	7321489	581567
5D	50	2.5	13	26	7321489	431121
5D	55	2.5	13	26	7321489	334657
5D	60	2.5	13	26	7321489	118741
5D	65	2.5	13	26	7321489	98764
5D	70	2.5	13	26	7321489	14608
5D	75	2.5	13	26	7321489	9432
5D	80	2.5	13	26	7321489	5816
5D	85	2.5	13	26	7321489	4311
5D	85	2.5	13	26	7321489	1160
5D	85	2.5	13	26	7321489	451

Table C.6: Inactivation data of the 6$^{\text{th}}$ experimental series

Code	t(min)	E(V/cm)	BS(g/L)	AN(g/L)	N_0(CFU/g TS)	N_{Observed}(CFU/g TS)
6A	5	2.5	25	26	7559200	1473926
6A	10	2.5	25	26	7559200	1225959
6A	15	2.5	25	26	7559200	1144131
6A	20	2.8	13	13	7559200	973814
6A	25	2.8	13	13	7559200	908816
6A	30	2.8	13	13	7559200	773528
6A	35	2.8	13	13	7559200	511065
6A	40	2.8	13	13	7559200	476953
6A	45	2.8	13	13	7559200	415409
6A	50	2.8	13	13	7559200	370234
6A	55	2.8	13	13	7559200	239043
6A	60	2.8	13	13	7559200	84816
6A	65	2.8	13	13	7559200	37886
6A	70	2.8	13	13	7559200	10435
6A	75	2.8	13	13	7559200	8100
6A	80	2.8	13	13	7559200	4661
6A	85	2.8	13	13	7559200	1813
6A	90	2.8	13	13	7559200	477
6A	95	2.8	13	13	7559200	151
6B	5	2.8	13	13	5349555	996134
6B	10	2.8	13	13	5349555	828548
6B	15	2.8	13	13	5349555	673470
6B	20	2.8	13	13	5349555	586567
6B	25	2.8	13	26	5349555	547416
6B	30	2.8	13	26	5349555	353442

Table C.6–continued from previous page

Code	t(min)	E(V/cm)	BS(g/L)	AN(g/L)	N_0(CFU/g TS)	$N_{Observed}$(CFU/g TS)
6B	35	2.8	13	26	5349555	307835
6B	40	2.8	13	26	5349555	293980
6B	45	2.8	13	26	5349555	244522
6B	50	2.8	13	26	5349555	161554
6B	55	2.8	13	26	5349555	128327
6B	60	2.8	13	26	5349555	62852
6B	65	2.8	13	26	5349555	27436
6B	70	2.8	13	26	5349555	7385
6B	75	2.8	13	26	5349555	4058
6B	80	2.8	13	26	5349555	3454
6B	85	2.8	13	26	5349555	1344
6B	90	2.8	13	26	5349555	268
6B	95	2.8	13	26	5349555	83
6C	5	2.8	13	13	4451370	810016
6C	10	2.8	13	13	4451370	643419
6C	15	2.8	13	13	4451370	488083
6C	20	2.8	13	13	4451370	294100
6C	25	2.8	13	13	4451370	262116
6C	30	2.8	13	13	4451370	228294
6C	35	2.8	13	13	4451370	181340
6C	40	2.8	13	13	4451370	169236
6C	45	2.8	13	13	4451370	144044
6C	50	2.8	13	13	4451370	114418
6C	55	2.8	13	13	4451370	84819
6C	60	2.8	13	13	4451370	45551
6C	65	2.8	13	13	4451370	15435

Table C.6–continued from previous page

Code	t(min)	E(V/cm)	BS(g/L)	AN(g/L)	N_0(CFU/g TS)	$N_{Observed}$(CFU/g TS)
6C	70	2.8	13	13	4451370	4661
6C	75	2.8	13	13	4451370	2874
6C	80	2.8	13	13	4451370	2336
6C	85	2.8	13	13	4451370	722
6C	90	2.8	13	13	4451370	169
6C	95	2.8	13	13	4451370	55
6D	5	2.8	13	13	4683377	852235
6D	10	2.8	13	13	4683377	692722
6D	15	2.8	13	13	4683377	550249
6D	20	2.8	13	13	4683377	490410
6D	25	2.8	13	13	4683377	372014
6D	30	2.8	13	13	4683377	295501
6D	35	2.8	13	13	4683377	251512
6D	40	2.8	13	13	4683377	234725
6D	45	2.8	13	13	4683377	190792
6D	50	2.8	13	13	4683377	123185
6D	55	2.8	13	13	4683377	95622
6D	60	2.8	13	13	4683377	50183
6D	65	2.8	13	13	4683377	21407
6D	70	2.8	13	13	4683377	5896
6D	75	2.8	13	13	4683377	3240
6D	80	2.8	13	13	4683377	2758
6D	85	2.8	13	13	4683377	1001
6D	90	2.8	13	13	4683377	214
6D	95	2.8	13	13	4683377	65

Table C.7: Inactivation data of the 7th experimental series

Code	t(min)	E(V/cm)	BS(g/L)	AN(g/L)	N_0(CFU/g TS)	$N_{Observed}$(CFU/g TS)
7A	5	2.5	13	13	6078122	2592802
7A	10	2.5	13	13	6078122	2310837
7A	15	2.5	13	13	6078122	1922071
7A	20	2.5	13	13	6078122	1240993
7A	25	2.5	13	13	6078122	1106036
7A	30	2.5	13	13	6078122	1032213
7A	35	2.5	13	13	6078122	899020
7A	40	2.5	13	13	6078122	783014
7A	45	2.5	13	13	6078122	621970
7A	50	2.5	13	13	6078122	430298
7A	55	2.5	13	13	6078122	284295
7A	60	2.5	13	13	6078122	179378
7A	65	2.5	13	13	6078122	62197
7A	70	2.5	13	13	6078122	38350
7A	75	2.5	13	13	6078122	33402
7A	80	2.5	13	13	6078122	26532
7A	85	2.5	13	13	6078122	22068
7A	90	2.5	13	13	6078122	14920
7A	95	2.5	13	13	6078122	13297
7A	100	2.5	13	13	6078122	11851
7A	105	2.5	13	13	6078122	9200
7A	110	2.5	13	13	6078122	7308
7A	115	2.5	13	13	6078122	6220
7A	120	2.5	13	13	6078122	3498
7B	5	2.5	13	13	9765463	4362072

Table C.7–continued from previous page

Code	t(min)	E(V/cm)	BS(g/L)	AN(g/L)	N_0(CFU/g TS)	$N_{Observed}$(CFU/g TS)
7B	10	2.5	13	13	9765463	3887701
7B	15	2.5	13	13	9765463	3233649
7B	20	2.5	13	13	9765463	2186215
7B	25	2.5	13	13	9765463	1948466
7B	30	2.5	13	13	9765463	1777022
7B	35	2.5	13	13	9765463	1547722
7B	40	2.5	13	13	9765463	1348010
7B	45	2.5	13	13	9765463	1121225
7B	50	2.5	13	13	9765463	758041
7B	55	2.5	13	13	9765463	500833
7B	60	2.5	13	13	9765463	330897
7B	65	2.5	13	13	9765463	137941
7B	70	2.5	13	13	9765463	72392
7B	75	2.5	13	13	9765463	61616
7B	80	2.5	13	13	9765463	50083
7B	85	2.5	13	13	9765463	39783
7B	90	2.5	13	13	9765463	30881
7B	95	2.5	13	13	9765463	25101
7B	100	2.5	13	13	9765463	22893
7B	105	2.5	13	13	9765463	16970
7B	110	2.5	13	13	9765463	13480
7B	115	2.5	13	13	9765463	12294
7B	120	2.5	13	13	9765463	7408
7C	5	2.5	13	13	11396011	5330315
7C	10	2.5	13	13	11396011	4861305
7C	15	2.5	13	13	11396011	4332643

Table C.7–continued from previous page

Code	t(min)	E(V/cm)	BS(g/L)	AN(g/L)	N_0(CFU/g TS)	$N_{Observed}$(CFU/g TS)
7C	20	2.5	13	13	11396011	2797289
7C	25	2.5	13	13	11396011	2326767
7C	30	2.5	13	13	11396011	2122037
7C	35	2.5	13	13	11396011	1848217
7C	40	2.5	13	13	11396011	1724856
7C	45	2.5	13	13	11396011	1402016
7C	50	2.5	13	13	11396011	1166146
7C	55	2.5	13	13	11396011	640845
7C	60	2.5	13	13	11396011	404346
7C	65	2.5	13	13	11396011	364955
7C	70	2.5	13	13	11396011	101556
7C	75	2.5	13	13	11396011	75293
7C	80	2.5	13	13	11396011	71904
7C	85	2.5	13	13	11396011	52090
7C	90	2.5	13	13	11396011	43326
7C	95	2.5	13	13	11396011	30673
7C	100	2.5	13	13	11396011	28626
7C	105	2.5	13	13	11396011	18913
7C	110	2.5	13	13	11396011	14681
7C	115	2.5	13	13	11396011	13389
7C	120	2.5	13	13	11396011	8448
7D	5	2.5	13	13	8645389	3773849
7D	10	2.5	13	13	8645389	3363447
7D	15	2.5	13	13	8645389	2797593
7D	20	2.5	13	13	8645389	1810442
7D	25	2.5	13	13	8645389	1647345

Table C.7–continued from previous page

Code	t(min)	E(V/cm)	BS(g/L)	AN(g/L)	N_0(CFU/g TS)	$N_{Observed}$(CFU/g TS)
7D	30	2.5	13	13	8645389	1502397
7D	35	2.5	13	13	8645389	1308533
7D	40	2.5	13	13	8645389	1113742
7D	45	2.5	13	13	8645389	905283
7D	50	2.5	13	13	8645389	626303
7D	55	2.5	13	13	8645389	423433
7D	60	2.5	13	13	8645389	267168
7D	65	2.5	13	13	8645389	88468
7D	70	2.5	13	13	8645389	55820
7D	75	2.8	13	13	8645389	50908
7D	80	2.5	13	13	8645389	39517
7D	85	2.5	13	13	8645389	32869
7D	90	2.5	13	13	8645389	22222
7D	95	2.5	13	13	8645389	19806
7D	100	2.5	13	13	8645389	17652
7D	105	2.5	13	13	8645389	13702
7D	110	2.5	13	13	8645389	10884
7D	115	2.5	13	13	8645389	9264
7D	120	2.5	13	13	8645389	5331

C.2   Experimental data–pH and temperature

Table C.8: pH and temperature data of the 1st experimental series

Code	E(V/cm)	BS(g/L)	AN(g/L)	t(min)	pH			T(°C)		
					C	A	Overall	C	A	Overall
1A	2.8	13	26	0	8.17	8.17	7.45	23	23	23.0
1A	2.8	13	26	5	8.72	8.10	7.45	37	32	29.8
1A	2.8	13	26	10	8.98	7.85	7.45	45	43	42.6
1A	2.8	13	26	15	8.99	7.32	7.45	49	48	48.2
1A	2.8	13	26	20	9.12	5.01	7.45	64	64	59.2
1A	2.8	13	26	25	9.32	4.42	7.45	72	72	69.0
1A	2.8	13	26	30	9.64	3.21	7.45	80	81	74.0
1A	2.8	13	26	35	10.39	1.54	7.45	84	85	74.5
1A	2.8	13	26	40	12.40	2.21	7.45	87	88	85.6
1A	2.8	13	26	45	12.87	2.43	7.45	92	93	91.0
1A	2.8	13	26	50	13.20	1.89	7.45	95	95	94.0
1A	2.8	13	26	55	13.48	2.76	7.45	96	97	95.0
1A	2.8	13	26	60	12.20	2.98	7.45	96	97	94.0
1A	2.8	13	26	65	12.21	2.73	7.45	96	98	96.0
1A	2.8	13	26	70	12.67	3.10	7.45	97	98	97.6
1A	2.8	13	26	75	12.23	2.63	7.45	97	98	97.6
1A	2.8	13	26	80	12.72	2.34	7.45	97	98	97.6
1A	2.8	13	26	85	12.24	2.40	7.45	97	98	97.6
1A	2.8	13	26	90	12.30	2.80	7.45	97	98	97.6
1A	2.8	13	26	95	12.76	2.89	7.45	97	98	97.6
1B	2.8	13	26	0	8.29	8.29	7.81	23	23	23.0
1B	2.8	13	26	5	8.75	7.98	7.81	37	32	29.8
1B	2.8	13	26	10	8.79	7.62	7.81	45	43	42.6

Continued on next page

207

Table C.8–continued from previous page

Code	E(V/cm)	BS(g/L)	AN(g/L)	t(min)	pH			T(°C)		
					C	A	Overall	C	A	Overall
1B	2.8	13	26	15	8.89	6.52	7.81	49	48	48.2
1B	2.8	13	26	20	9.16	6.12	7.81	64	64	59.2
1B	2.8	13	26	25	8.98	4.23	7.81	72	72	69.0
1B	2.8	13	26	30	9.87	3.16	7.81	80	81	74.0
1B	2.8	13	26	35	10.45	2.18	7.81	84	85	74.5
1B	2.8	13	26	40	12.23	1.97	7.81	87	88	85.6
1B	2.8	13	26	45	12.34	2.25	7.81	92	93	91.0
1B	2.8	13	26	50	13.45	1.65	7.81	95	95	94.0
1B	2.8	13	26	55	13.76	2.76	7.81	96	97	95.0
1B	2.8	13	26	60	13.25	2.55	7.81	96	97	94.0
1B	2.8	13	26	65	13.32	2.65	7.81	96	98	96.0
1B	2.8	13	26	70	12.87	2.98	7.81	97	98	97.6
1B	2.8	13	26	75	12.98	2.86	7.81	97	98	97.6
1B	2.8	13	26	80	12.76	2.67	7.81	97	98	97.6
1B	2.8	13	26	85	12.26	2.98	7.81	97	98	97.6
1B	2.8	13	26	90	12.87	2.17	7.81	97	98	97.6
1B	2.8	13	26	95	12.98	2.15	7.81	97	98	97.6
1C	2.8	13	26	0	8.11	8.11	7.82	23	23	23.0
1C	2.8	13	26	5	8.17	7.50	7.82	37	32	29.8
1C	2.8	13	26	10	8.65	7.21	7.82	45	43	42.6
1C	2.8	13	26	15	8.97	6.09	7.82	49	48	48.2
1C	2.8	13	26	20	9.01	5.36	7.82	64	64	59.2
1C	2.8	13	26	25	9.31	3.80	7.82	72	72	69.0
1C	2.8	13	26	30	9.65	3.79	7.82	80	81	74.0
1C	2.8	13	26	35	10.98	3.63	7.82	84	85	74.5

Table C.8–continued from previous page

Code	E(V/cm)	BS(g/L)	AN(g/L)	t(min)	pH			T(°C)		
					C	A	Overall	C	A	Overall
1C	2.8	13	26	40	13.24	2.65	7.82	87	88	85.6
1C	2.8	13	26	45	13.17	2.23	7.82	92	93	91.0
1C	2.8	13	26	50	13.15	1.98	7.82	95	95	94.0
1C	2.8	13	26	55	12.65	2.76	7.82	96	97	95.0
1C	2.8	13	26	60	12.07	2.56	7.82	96	97	94.0
1C	2.8	13	26	65	13.12	2.18	7.82	96	98	96.0
1C	2.8	13	26	70	13.65	2.11	7.82	97	98	97.6
1C	2.8	13	26	75	12.32	2.65	7.82	97	98	97.6
1C	2.8	13	26	80	13.00	2.15	7.82	97	98	96.4
1C	2.8	13	26	85	12.43	1.98	7.82	97	98	97.6
1C	2.8	13	26	90	13.13	2.87	7.82	97	98	97.6
1C	2.8	13	26	95	12.34	2.87	7.82	97	98	97.6
1D	2.8	13	26	0	8.15	8.15	8.15	23	23	23.0
1D	2.8	13	26	5	8.76	7.23	8.15	37	32	29.8
1D	2.8	13	26	10	8.56	7.10	8.15	45	43	42.6
1D	2.8	13	26	15	8.43	6.32	8.15	49	48	48.2
1D	2.8	13	26	20	8.96	6.13	8.15	64	64	59.2
1D	2.8	13	26	25	9.54	5.40	8.15	72	72	69.0
1D	2.8	13	26	30	9.34	4.34	8.15	80	81	74.0
1D	2.8	13	26	35	9.87	3.73	8.15	84	85	74.5
1D	2.8	13	26	40	10.65	3.34	8.15	87	88	85.6
1D	2.8	13	26	45	13.76	2.87	8.15	92	93	91.0
1D	2.8	13	26	50	13.73	2.23	8.15	95	95	94.0
1D	2.8	13	26	55	13.72	2.12	8.15	96	97	95.0
1D	2.8	13	26	60	12.98	1.98	8.15	96	97	94.0

Table C.8–continued from previous page

Code	E(V/cm)	BS(g/L)	AN(g/L)	t(min)	pH			T(°C)		
					C	A	Overall	C	A	Overall
1D	2.8	13	26	65	13.45	2.54	8.15	96	98	96.0
1D	2.8	13	26	70	13.87	3.27	8.15	97	98	97.6
1D	2.8	13	26	75	13.76	3.67	8.15	97	98	97.6
1D	2.8	13	26	80	13.34	2.75	8.15	97	98	97.6
1D	2.8	13	26	85	13.87	2.45	8.15	97	98	97.6
1D	2.8	13	26	90	12.76	2.78	8.15	97	98	97.6
1D	2.8	13	26	95	12.69	2.65	8.15	97	98	97.6

Table C.9: pH and temperature data of the 2nd experimental series

Code	E(V/cm)	BS(g/L)	AN(g/L)	t(min)	pH			T(°C)		
					C	A	Overall	C	A	Overall
2A	2.8	25	13	0	8.16	8.16	8.29	20	20	20.0
2A	2.8	25	13	5	8.45	7.97	8.29	33	32	26.3
2A	2.8	25	13	10	8.54	7.56	8.29	43	41	37.3
2A	2.8	25	13	15	8.67	6.32	8.29	46	45	44.0
2A	2.8	25	13	20	8.89	6.23	8.29	55	55	53.0
2A	2.8	25	13	25	9.23	6.08	8.29	66	66	64.1
2A	2.8	25	13	30	9.54	5.55	8.29	74	73	72.0
2A	2.8	25	13	35	9.78	5.23	8.29	83	83	81.3
2A	2.8	25	13	40	10.43	5.12	8.29	87	87	87.5
2A	2.8	25	13	45	10.43	4.87	8.29	94	94	93.1
2A	2.8	25	13	50	12.67	4.23	8.29	95	95	95.0
2A	2.8	25	13	55	12.65	4.12	8.29	96	96	95.3
2A	2.8	25	13	60	12.44	4.09	8.29	96	97	95.9
2A	2.8	25	13	65	12.98	3.78	8.29	96	97	96.0
2A	2.8	25	13	70	13.23	3.34	8.29	96	97	96.0
2A	2.8	25	13	75	13.76	3.45	8.29	96	97	96.0
2A	2.8	25	13	80	13.65	3.57	8.29	96	97	96.0
2A	2.8	25	13	85	13.43	3.32	8.29	96	97	96.0
2A	2.8	25	13	90	12.98	3.32	8.29	96	97	96.0
2A	2.8	25	13	95	13.65	3.14	8.29	96	97	96.0
2B	2.8	25	13	0	8.17	8.17	8.28	20	20	20.0
2B	2.8	25	13	5	8.56	8.08	8.28	33	32	26.3
2B	2.8	25	13	10	8.76	7.88	8.28	43	41	37.3
2B	2.8	25	13	15	8.87	7.23	8.28	46	45	44.0

Table C.9–continued from previous page

Code	E(V/cm)	BS(g/L)	AN(g/L)	t(min)	pH			T(°C)		
					C	A	Overall	C	A	Overall
2B	2.8	25	13	20	8.97	7.07	8.28	55	55	53.0
2B	2.8	25	13	25	8.98	6.43	8.28	66	66	64.1
2B	2.8	25	13	30	9.54	6.23	8.28	74	73	72.0
2B	2.8	25	13	35	9.86	6.12	8.28	83	83	81.3
2B	2.8	25	13	40	10.54	5.56	8.28	87	87	87.5
2B	2.8	25	13	45	10.87	5.43	8.28	94	94	93.1
2B	2.8	25	13	50	11.34	4.56	8.28	95	95	95.0
2B	2.8	25	13	55	11.87	4.32	8.28	96	96	95.3
2B	2.8	25	13	60	12.76	4.12	8.28	96	97	95.9
2B	2.8	25	13	65	12.45	3.54	8.28	96	97	96.0
2B	2.8	25	13	70	12.98	3.45	8.28	96	97	96.0
2B	2.8	25	13	75	12.57	3.57	8.28	96	97	96.0
2B	2.8	25	13	80	13.45	3.48	8.28	96	97	96.0
2B	2.8	25	13	85	13.30	3.22	8.28	96	97	96.0
2B	2.8	25	13	90	12.65	3.09	8.28	96	97	96.0
2B	2.8	25	13	95	12.54	3.12	8.28	96	97	96.0
2C	2.8	25	13	0	8.12	8.12	8.29	20	20	20.0
2C	2.8	25	13	5	8.45	7.88	8.29	33	32	26.3
2C	2.8	25	13	10	8.98	7.67	8.29	43	41	37.3
2C	2.8	25	13	15	8.93	7.12	8.29	46	45	44.0
2C	2.8	25	13	20	9.12	6.88	8.29	55	55	53.0
2C	2.8	25	13	25	9.23	6.56	8.29	66	66	64.1
2C	2.8	25	13	30	9.56	6.12	8.29	74	73	72.0
2C	2.8	25	13	35	9.87	5.53	8.29	83	83	81.3
2C	2.8	25	13	40	10.34	5.12	8.29	87	87	87.5

Table C.9–continued from previous page

Code	E(V/cm)	BS(g/L)	AN(g/L)	t(min)	pH			T(°C)		
					C	A	Overall	C	A	Overall
2C	2.8	25	13	45	10.78	4.87	8.29	94	94	93.1
2C	2.8	25	13	50	12.30	4.64	8.29	95	95	95.0
2C	2.8	25	13	55	12.47	3.65	8.29	96	96	95.3
2C	2.8	25	13	60	12.43	3.12	8.29	96	97	95.9
2C	2.8	25	13	65	12.24	3.23	8.29	96	97	96.0
2C	2.8	25	13	70	12.34	3.25	8.29	96	97	96.0
2C	2.8	25	13	75	12.23	3.34	8.29	96	97	96.0
2C	2.8	25	13	80	13.32	3.12	8.29	96	97	96.0
2C	2.8	25	13	85	11.65	3.32	8.29	96	97	96.0
2C	2.8	25	13	90	11.87	3.21	8.29	96	97	96.0
2C	2.8	25	13	95	11.43	3.23	8.29	96	97	96.0
2D	2.8	25	13	0	8.16	8.16	8.29	20	20	20.0
2D	2.8	25	13	5	8.76	7.86	8.29	33	32	26.3
2D	2.8	25	13	10	8.89	7.43	8.29	43	41	37.3
2D	2.8	25	13	15	9.31	7.10	8.29	46	45	44.0
2D	2.8	25	13	20	9.44	6.45	8.29	55	55	53.0
2D	2.8	25	13	25	9.54	6.24	8.29	66	66	64.1
2D	2.8	25	13	30	9.87	6.04	8.29	74	73	72.0
2D	2.8	25	13	35	10.23	5.45	8.29	83	83	81.3
2D	2.8	25	13	40	11.33	5.14	8.29	87	87	87.5
2D	2.8	25	13	45	11.76	4.89	8.29	94	94	93.1
2D	2.8	25	13	50	12.54	4.70	8.29	95	95	95.0
2D	2.8	25	13	55	12.45	4.26	8.29	96	96	95.3
2D	2.8	25	13	60	12.87	4.08	8.29	96	97	95.9
2D	2.8	25	13	65	12.23	3.34	8.29	96	97	96.0

Table C.9–continued from previous page

Code	E(V/cm)	BS(g/L)	AN(g/L)	t(min)	pH			T(°C)		
					C	A	Overall	C	A	Overall
2D	2.8	25	13	70	12.65	3.22	8.29	96	97	96.0
2D	2.8	25	13	75	13.32	3.78	8.29	96	97	96.0
2D	2.8	25	13	80	13.42	3.23	8.29	96	97	96.0
2D	2.8	25	13	85	13.12	3.56	8.29	96	97	96.0
2D	2.8	25	13	90	12.87	3.34	8.29	96	97	96.0
2D	2.8	25	13	95	12.56	3.76	8.29	96	97	96.0

Table C.10: pH and temperature data of the 3rd experimental series

Code	E(V/cm)	BS(g/L)	AN(g/L)	t(min)	pH			T(°C)		
					C	A	Overall	C	A	Overall
3A	2.8	13	13	0	8.14	8.14	8.15	18	18	18.0
3A	2.8	13	13	5	8.52	8.09	8.15	35	36	21.1
3A	2.8	13	13	10	8.76	7.87	8.15	45	43	23.3
3A	2.8	13	13	15	9.23	7.54	8.15	52	51	26.6
3A	2.8	13	13	20	9.43	6.54	8.15	63	62	30.8
3A	2.8	13	13	25	9.65	6.12	8.15	66	67	35.5
3A	2.8	13	13	30	9.98	5.67	8.15	71	72	42.1
3A	2.8	13	13	35	10.67	5.21	8.15	78	76	56.5
3A	2.8	13	13	40	11.45	4.89	8.15	83	80	64.6
3A	2.8	13	13	45	11.55	4.67	8.15	86	84	72.4
3A	2.8	13	13	50	12.23	4.22	8.15	89	85	73.5
3A	2.8	13	13	55	12.54	3.76	8.15	96	87	76.5
3A	2.8	13	13	60	12.87	3.12	8.15	96	92	82.3
3A	2.8	13	13	65	12.76	3.45	8.15	96	93	84.3
3A	2.8	13	13	70	13.56	3.68	8.15	96	95	85.6
3A	2.8	13	13	75	13.16	3.56	8.15	96	97	85.6
3A	2.8	13	13	80	13.35	3.45	8.15	96	97	85.6
3A	2.8	13	13	85	13.42	3.58	8.15	96	97	85.6
3A	2.8	13	13	90	13.32	3.12	8.15	96	97	85.6
3A	2.8	13	13	95	13.54	3.53	8.15	96	97	85.6
3B	2.8	13	13	0	8.21	8.21	8.15	18	18	18.0
3B	2.8	13	13	5	8.32	8.12	8.15	35	36	21.1
3B	2.8	13	13	10	8.54	7.89	8.15	45	43	23.3
3B	2.8	13	13	15	8.87	7.78	8.15	52	51	26.6

Table C.10–continued from previous page

Code	E(V/cm)	BS(g/L)	AN(g/L)	t(min)	pH			T(°C)		
					C	A	Overall	C	A	Overall
3B	2.8	13	13	20	9.21	7.57	8.15	63	62	30.8
3B	2.8	13	13	25	9.43	6.45	8.15	66	67	35.5
3B	2.8	13	13	30	9.56	6.11	8.15	71	72	42.1
3B	2.8	13	13	35	9.78	5.34	8.15	78	76	56.5
3B	2.8	13	13	40	11.20	4.78	8.15	83	80	64.6
3B	2.8	13	13	45	12.65	4.12	8.15	86	84	72.4
3B	2.8	13	13	50	12.89	3.56	8.15	89	85	73.5
3B	2.8	13	13	55	13.32	3.27	8.15	96	87	76.5
3B	2.8	13	13	60	13.34	3.16	8.15	96	92	82.3
3B	2.8	13	13	65	13.65	3.34	8.15	96	93	84.3
3B	2.8	13	13	70	13.45	3.56	8.15	96	95	85.6
3B	2.8	13	13	75	13.67	3.02	8.15	96	97	85.6
3B	2.8	13	13	80	13.54	3.67	8.15	96	97	85.6
3B	2.8	13	13	85	12.43	3.09	8.15	96	97	85.6
3B	2.8	13	13	90	11.34	3.66	8.15	96	97	85.6
3B	2.8	13	13	95	12.56	3.23	8.15	96	97	85.6
3C	2.8	13	13	0	8.13	8.13	8.14	18	18	18.0
3C	2.8	13	13	5	8.45	7.89	8.14	35	36	21.1
3C	2.8	13	13	10	8.65	7.34	8.14	45	43	23.3
3C	2.8	13	13	15	9.87	6.89	8.14	52	51	26.6
3C	2.8	13	13	20	9.12	5.66	8.14	63	62	30.8
3C	2.8	13	13	25	9.56	5.12	8.14	66	67	35.5
3C	2.8	13	13	30	9.65	5.10	8.14	71	72	42.1
3C	2.8	13	13	35	10.56	5.08	8.14	78	76	56.5
3C	2.8	13	13	40	12.13	4.88	8.14	83	80	64.6

Table C.10–continued from previous page

Code	E(V/cm)	BS(g/L)	AN(g/L)	t(min)	pH			T(°C)		
					C	A	Overall	C	A	Overall
3C	2.8	13	13	45	12.31	4.72	8.14	86	84	72.4
3C	2.8	13	13	50	12.14	4.34	8.14	89	85	73.5
3C	2.8	13	13	55	12.23	4.13	8.14	96	87	76.5
3C	2.8	13	13	60	11.98	3.66	8.14	96	92	82.3
3C	2.8	13	13	65	11.32	3.56	8.14	96	93	84.3
3C	2.8	13	13	70	12.32	3.32	8.14	96	95	85.6
3C	2.8	13	13	75	12.34	3.78	8.14	96	97	85.6
3C	2.8	13	13	80	11.52	3.34	8.14	96	97	85.6
3C	2.8	13	13	85	12.62	3.12	8.14	96	97	85.6
3C	2.8	13	13	90	11.45	3.09	8.14	96	97	85.6
3C	2.8	13	13	95	11.42	3.33	8.14	96	97	85.6
3D	2.8	13	13	0	8.14	8.14	8.15	18	18	18.0
3D	2.8	13	13	5	8.45	7.78	8.15	35	36	21.1
3D	2.8	13	13	10	8.56	7.43	8.15	45	43	23.3
3D	2.8	13	13	15	8.78	7.12	8.15	52	51	26.6
3D	2.8	13	13	20	8.96	6.47	8.15	63	62	30.8
3D	2.8	13	13	25	9.54	6.21	8.15	66	67	35.5
3D	2.8	13	13	30	9.34	6.34	8.15	71	72	42.1
3D	2.8	13	13	35	9.87	6.21	8.15	78	76	56.5
3D	2.8	13	13	40	10.56	5.78	8.15	83	80	64.6
3D	2.8	13	13	45	11.78	4.32	8.15	86	84	72.4
3D	2.8	13	13	50	12.87	4.21	8.15	89	85	73.5
3D	2.8	13	13	55	12.89	3.45	8.15	96	87	76.5
3D	2.8	13	13	60	12.23	3.21	8.15	96	92	82.3
3D	2.8	13	13	65	12.34	3.08	8.15	96	93	84.3

Table C.10–continued from previous page

Code	E(V/cm)	BS(g/L)	AN(g/L)	t(min)	pH			T(°C)		
					C	A	Overall	C	A	Overall
3D	2.8	13	13	70	12.21	3.27	8.15	96	95	85.6
3D	2.8	13	13	75	12.12	3.12	8.15	96	97	85.6
3D	2.8	13	13	80	12.32	3.14	8.15	96	97	85.6
3D	2.8	13	13	85	13.45	3.23	8.15	96	97	85.6
3D	2.8	13	13	90	13.56	3.21	8.15	96	97	85.6
3D	2.8	13	13	95	13.34	3.34	8.15	96	97	85.6

Table C.11: pH and temperature data of the 4th experimental series

Code	E(V/cm)	BS(g/L)	AN(g/L)	t(min)	pH			T(°C)		
					C	A	Overall	C	A	Overall
4A	2.5	25	13	0	8.21	8.21	8.15	17.1	17.1	17.1
4A	2.5	25	13	5	8.38	7.83	8.15	25.0	25.0	18.9
4A	2.5	25	13	10	8.78	7.76	8.15	30.0	30.0	26.4
4A	2.5	25	13	15	8.98	7.45	8.15	35.0	34.0	31.7
4A	2.5	25	13	20	9.14	7.12	8.15	38.0	39.0	37.4
4A	2.5	25	13	25	9.00	6.45	8.15	45.0	45.0	43.3
4A	2.5	25	13	30	9.43	6.12	8.15	52.0	52.0	50.5
4A	2.5	25	13	35	9.56	5.54	8.15	58.0	58.0	57.4
4A	2.5	25	13	40	10.54	5.23	8.15	63.0	63.0	62.1
4A	2.5	25	13	45	10.65	4.76	8.15	73.0	73.0	71.4
4A	2.5	25	13	50	11.54	4.34	8.15	79.0	80.0	78.3
4A	2.5	25	13	55	11.87	4.23	8.15	86.0	86.0	85.5
4A	2.5	25	13	60	12.10	3.89	8.15	90.0	91.0	90.3
4A	2.5	25	13	65	12.23	3.76	8.15	94.0	95.0	93.9
4A	2.5	25	13	70	12.09	3.65	8.15	95.0	96.0	94.7
4A	2.5	25	13	75	12.67	3.67	8.15	95.5	96.0	95.1
4A	2.5	25	13	80	12.87	3.56	8.15	95.5	96.0	95.5
4A	2.5	25	13	85	11.78	4.76	8.15	95.5	96.0	95.1
4A	2.5	25	13	90	12.76	4.87	8.15	95.5	96.0	94.9
4A	2.5	25	13	95	11.67	4.23	8.15	95.5	96.0	95.0
4B	2.5	25	13	0	8.12	8.12	8.14	17.1	17.1	17.1
4B	2.5	25	13	5	8.25	7.76	8.14	25.0	25.0	18.9
4B	2.5	25	13	10	8.56	7.34	8.14	30.0	30.0	26.4
4B	2.5	25	13	15	8.76	7.27	8.14	35.0	34.0	31.7

Table C.11–continued from previous page

Code	E(V/cm)	BS(g/L)	AN(g/L)	t(min)	pH			T(°C)		
					C	A	Overall	C	A	Overall
4B	2.5	25	13	20	8.89	7.05	8.14	38.0	39.0	37.4
4B	2.5	25	13	25	9.23	6.76	8.14	45.0	45.0	43.3
4B	2.5	25	13	30	9.76	6.45	8.14	52.0	52.0	50.5
4B	2.5	25	13	35	9.89	5.54	8.14	58.0	58.0	57.4
4B	2.5	25	13	40	10.13	5.34	8.14	63.0	63.0	62.1
4B	2.5	25	13	45	10.45	4.34	8.14	73.0	73.0	71.4
4B	2.5	25	13	50	12.45	4.23	8.14	79.0	80.0	78.3
4B	2.5	25	13	55	11.78	4.13	8.14	86.0	86.0	85.5
4B	2.5	25	13	60	11.45	3.98	8.14	90.0	91.0	90.3
4B	2.5	25	13	65	11.34	3.76	8.14	94.0	95.0	93.9
4B	2.5	25	13	70	11.78	3.87	8.14	95.0	96.0	94.7
4B	2.5	25	13	75	11.98	3.65	8.14	95.5	96.0	95.1
4B	2.5	25	13	80	11.87	3.23	8.14	95.5	96.0	95.5
4B	2.5	25	13	85	12.32	3.32	8.14	95.5	96.0	95.1
4B	2.5	25	13	90	12.45	3.23	8.14	95.5	96.0	94.9
4B	2.5	25	13	95	12.32	3.3	8.14	95.5	96.0	95.0
4C	2.5	25	13	0	8.17	8.17	8.15	17.1	17.1	17.1
4C	2.5	25	13	5	8.34	7.56	8.15	25.0	25.0	18.9
4C	2.5	25	13	10	8.45	7.54	8.15	30.0	30.0	26.4
4C	2.5	25	13	15	8.65	7.1	8.15	35.0	34.0	31.7
4C	2.5	25	13	20	9.15	6.45	8.15	38.0	39.0	37.4
4C	2.5	25	13	25	9.34	6.21	8.15	45.0	45.0	43.3
4C	2.5	25	13	30	9.56	5.87	8.15	52.0	52.0	50.5
4C	2.5	25	13	35	9.78	5.45	8.15	58.0	58.0	57.4
4C	2.5	25	13	40	9.43	5.32	8.15	63.0	63.0	62.1

Table C.11–continued from previous page

Code	E(V/cm)	BS(g/L)	AN(g/L)	t(min)	pH			T(°C)		
					C	A	Overall	C	A	Overall
4C	2.5	25	13	45	10.67	5.12	8.15	73.0	73.0	71.4
4C	2.5	25	13	50	11.47	4.56	8.15	79.0	80.0	78.3
4C	2.5	25	13	55	12.43	4.12	8.15	86.0	86.0	85.5
4C	2.5	25	13	60	12.67	3.87	8.15	90.0	91.0	90.3
4C	2.5	25	13	65	12.56	3.56	8.15	94.0	95.0	93.9
4C	2.5	25	13	70	12.78	3.65	8.15	95.0	96.0	94.7
4C	2.5	25	13	75	12.76	3.12	8.15	95.5	96.0	95.1
4C	2.5	25	13	80	12.53	3.1	8.15	95.5	96.0	95.5
4C	2.5	25	13	85	12.87	3.32	8.15	95.5	96.0	95.1
4C	2.5	25	13	90	12.54	3.12	8.15	95.5	96.0	94.9
4C	2.5	25	13	95	12.65	3.07	8.15	95.5	96.0	95.0
4D	2.5	25	13	0	8.16	8.16	8.15	17.1	17.1	17.1
4D	2.5	25	13	5	8.43	7.98	8.15	25.0	25.0	18.9
4D	2.5	25	13	10	8.76	7.73	8.15	30.0	30.0	26.4
4D	2.5	25	13	15	8.89	7.34	8.15	35.0	34.0	31.7
4D	2.5	25	13	20	9.16	7.23	8.15	38.0	39.0	37.4
4D	2.5	25	13	25	9.54	6.76	8.15	45.0	45.0	43.3
4D	2.5	25	13	30	9.65	6.45	8.15	52.0	52.0	50.5
4D	2.5	25	13	35	9.89	6.67	8.15	58.0	58.0	57.4
4D	2.5	25	13	40	10.23	6.56	8.15	63.0	63.0	62.1
4D	2.5	25	13	45	10.45	5.67	8.15	73.0	73.0	71.4
4D	2.5	25	13	50	11.34	5.34	8.15	79.0	80.0	78.3
4D	2.5	25	13	55	11.78	5.12	8.15	86.0	86.0	85.5
4D	2.5	25	13	60	11.89	4.34	8.15	90.0	91.0	90.3
4D	2.5	25	13	65	12.65	3.43	8.15	94.0	95.0	93.9

Table C.11–continued from previous page

Code	E(V/cm)	BS(g/L)	AN(g/L)	t(min)	pH			T(°C)		
					C	A	Overall	C	A	Overall
4D	2.5	25	13	70	12.54	3.23	8.15	95.0	96.0	94.7
4D	2.5	25	13	75	12.67	3.24	8.15	95.5	96.0	95.1
4D	2.5	25	13	80	12.45	3.12	8.15	95.5	96.0	95.5
4D	2.5	25	13	85	12.56	3.43	8.15	95.5	96.0	95.1
4D	2.5	25	13	90	12.67	3.2	8.15	95.5	96.0	94.9
4D	2.5	25	13	95	12.56	3.1	8.15	95.5	96.0	95.0

Table C.12: pH and temperature data of the 5th experimental series

Code	E(V/cm)	BS(g/L)	AN(g/L)	t(min)	pH			T(°C)		
					C	A	Overall	C	A	Overall
5A	2.5	13	26	0	8.18	8.18	8.15	19.7	19.7	19.7
5A	2.5	13	26	5	8.45	8.02	8.15	37.0	27.0	23.0
5A	2.5	13	26	10	8.89	7.12	8.15	41.0	40.0	32.7
5A	2.5	13	26	15	9.13	6.32	8.15	41.0	40.0	32.7
5A	2.5	13	26	20	9.32	6.13	8.15	50.0	49.0	39.5
5A	2.5	13	26	25	9.65	5.52	8.15	53.0	60.0	47.8
5A	2.5	13	26	30	9.87	5.16	8.15	57.0	64.0	54.7
5A	2.5	13	26	35	9.98	4.45	8.15	69.0	74.0	65.5
5A	2.5	13	26	40	10.76	4.34	8.15	73.0	80.0	73.9
5A	2.5	13	26	45	11.65	4.32	8.15	80.0	86.5	78.0
5A	2.5	13	26	50	11.89	3.89	8.15	86.0	88.0	83.0
5A	2.5	13	26	55	11.97	3.78	8.15	88.0	90.0	86.0
5A	2.5	13	26	60	12.34	3.65	8.15	90.0	92.0	90.0
5A	2.5	13	26	65	12.54	3.76	8.15	91.0	94.0	91.2
5A	2.5	13	26	70	12.43	4.87	8.15	91.0	94.0	91.2
5A	2.5	13	26	75	12.43	4.87	8.15	92.0	95.0	93.7
5A	2.5	13	26	80	11.32	4.78	8.15	92.0	95.0	93.3
5A	2.5	13	26	85	12.12	4.98	8.15	93.0	96.0	94.3
5A	2.5	13	26	90	11.98	3.98	8.15	95.0	96.0	94.6
5A	2.5	13	26	95	11.65	3.87	8.15	95.0	96.0	94.6
5B	2.5	13	26	0	8.14	8.14	8.17	19.7	19.7	19.7
5B	2.5	13	26	5	8.67	8.00	8.17	37.0	27.0	23.0
5B	2.5	13	26	10	8.98	7.45	8.17	41.0	40.0	32.7
5B	2.5	13	26	15	9.23	7.11	8.17	41.0	40.0	32.7

Table C.12–continued from previous page

Code	E(V/cm)	BS(g/L)	AN(g/L)	t(min)	pH			T(°C)		
					C	A	Overall	C	A	Overall
5B	2.5	13	26	20	9.43	6.34	8.17	50.0	49.0	39.5
5B	2.5	13	26	25	9.97	5.53	8.17	53.0	60.0	47.8
5B	2.5	13	26	30	10.24	5.13	8.17	57.0	64.0	54.7
5B	2.5	13	26	35	10.64	4.43	8.17	69.0	74.0	65.5
5B	2.5	13	26	40	10.9	4.34	8.17	73.0	80.0	73.9
5B	2.5	13	26	45	11.34	4.27	8.17	80.0	86.5	78.0
5B	2.5	13	26	50	11.87	3.98	8.17	86.0	88.0	83.0
5B	2.5	13	26	55	11.98	3.78	8.17	88.0	90.0	86.0
5B	2.5	13	26	60	12.13	4.07	8.17	90.0	92.0	90.0
5B	2.5	13	26	65	12.43	3.9	8.17	91.0	94.0	91.2
5B	2.5	13	26	70	12.32	3.78	8.17	91.0	94.0	91.2
5B	2.5	13	26	75	12.23	3.76	8.17	92.0	95.0	93.7
5B	2.5	13	26	80	12.27	3.87	8.17	92.0	95.0	93.3
5B	2.5	13	26	85	11.97	3.98	8.17	93.0	96.0	94.3
5B	2.5	13	26	90	12.54	4.09	8.17	95.0	96.0	94.6
5B	2.5	13	26	95	11.87	4.13	8.17	95.0	96.0	94.6
5C	2.5	13	26	0	8.15	8.15	8.0	19.7	19.7	19.7
5C	2.5	13	26	5	8.56	7.34	8.0	37.0	27.0	23.0
5C	2.5	13	26	10	8.89	7.12	8.0	41.0	40.0	32.7
5C	2.5	13	26	15	9.15	7.02	8.0	41.0	40.0	32.7
5C	2.5	13	26	20	9.56	6.45	8.0	50.0	49.0	39.5
5C	2.5	13	26	25	9.45	5.54	8.0	53.0	60.0	47.8
5C	2.5	13	26	30	9.67	5.17	8.0	57.0	64.0	54.7
5C	2.5	13	26	35	10.45	4.45	8.0	69.0	74.0	65.5
5C	2.5	13	26	40	10.65	4.23	8.0	73.0	80.0	73.9

Table C.12–continued from previous page

Code	E(V/cm)	BS(g/L)	AN(g/L)	t(min)	pH			T(°C)		
					C	A	Overall	C	A	Overall
5C	2.5	13	26	45	11.54	3.78	8.0	80.0	86.5	78.0
5C	2.5	13	26	50	11.56	3.89	8.0	86.0	88.0	83.0
5C	2.5	13	26	55	11.98	3.76	8.0	88.0	90.0	86.0
5C	2.5	13	26	60	12.54	3.67	8.0	90.0	92.0	90.0
5C	2.5	13	26	65	12.12	4.65	8.0	91.0	94.0	91.2
5C	2.5	13	26	70	12.65	3.54	8.0	91.0	94.0	91.2
5C	2.5	13	26	75	11.8	3.78	8.0	92.0	95.0	93.7
5C	2.5	13	26	80	11.59	3.56	8.0	92.0	95.0	93.3
5C	2.5	13	26	85	12.34	3.76	8.0	93.0	96.0	94.3
5C	2.5	13	26	90	12.12	4.23	8.0	95.0	96.0	94.6
5C	2.5	13	26	95	11.87	3.67	8.0	95.0	96.0	94.6
5D	2.5	13	26	0	8.13	8.14	8.14	19.7	19.7	19.7
5D	2.5	13	26	5	8.43	7.98	8.14	37.0	27.0	23.0
5D	2.5	13	26	10	8.55	7.65	8.14	41.0	40.0	32.7
5D	2.5	13	26	15	9.23	6.65	8.14	41.0	40.0	32.7
5D	2.5	13	26	20	9.43	6.12	8.14	50.0	49.0	39.5
5D	2.5	13	26	25	9.67	6.23	8.14	53.0	60.0	47.8
5D	2.5	13	26	30	9.45	5.56	8.14	57.0	64.0	54.7
5D	2.5	13	26	35	10.13	5.32	8.14	69.0	74.0	65.5
5D	2.5	13	26	40	10.34	4.54	8.14	73.0	80.0	73.9
5D	2.5	13	26	45	11.23	4.32	8.14	80.0	86.5	78.0
5D	2.5	13	26	50	11.67	4.15	8.14	86.0	88.0	83.0
5D	2.5	13	26	55	11.78	3.98	8.14	88.0	90.0	86.0
5D	2.5	13	26	60	12.54	3.32	8.14	90.0	92.0	90.0
5D	2.5	13	26	65	12.76	3.43	8.14	91.0	94.0	91.2

Table C.12–continued from previous page

Code	E(V/cm)	BS(g/L)	AN(g/L)	t(min)	pH			T(°C)		
					C	A	Overall	C	A	Overall
5D	2.5	13	26	70	12.45	3.32	8.14	91.0	94.0	91.2
5D	2.5	13	26	75	11.89	4.11	8.14	92.0	95.0	93.7
5D	2.5	13	26	80	11.87	3.87	8.14	92.0	95.0	93.3
5D	2.5	13	26	85	11.76	3.67	8.14	93.0	96.0	94.3
5D	2.5	13	26	90	11.65	3.56	8.14	95.0	96.0	94.6
5D	2.5	13	26	95	12.34	3.89	8.14	95.0	96.0	94.6

Table C.13: pH and temperature data of the 6th experimental series

Code	E(V/cm)	BS(g/L)	AN(g/L)	t(min)	pH			T(°C)		
					C	A	Overall	C	A	Overall
6A	2.5	13	26	0	8.15	8.15	8.18	18.0	18.0	18.0
6A	2.5	13	26	5	8.65	7.78	8.18	27.0	24.0	21.4
6A	2.5	13	26	10	8.45	7.45	8.18	37.0	35.0	33.0
6A	2.5	13	26	15	9.23	7.12	8.18	44.0	42.0	43.0
6A	2.5	13	26	20	9.65	6.34	8.18	53.0	53.0	51.6
6A	2.5	13	26	25	9.87	6.23	8.18	60.0	59.0	58.9
6A	2.5	13	26	30	9.98	5.56	8.18	67.0	67.0	63.1
6A	2.5	13	26	35	10.17	5.34	8.18	73.0	73.0	72.5
6A	2.5	13	26	40	10.45	5.12	8.18	76.0	76.0	75.5
6A	2.5	13	26	45	10.56	4.78	8.18	81.0	79.0	78.8
6A	2.5	13	26	50	11.65	4.32	8.18	84.0	82.0	81.5
6A	2.5	13	26	55	11.89	4.23	8.18	85.0	85.0	84.5
6A	2.5	13	26	60	12.65	3.46	8.18	86.6	86.0	86.5
6A	2.5	13	26	65	12.43	3.63	8.18	88.0	86.6	86.6
6A	2.5	13	26	70	12.54	3.75	8.18	90.0	89.0	89.5
6A	2.5	13	26	75	12.12	3.34	8.18	90.0	90.0	90.0
6A	2.5	13	26	80	12.45	3.56	8.18	90.0	90.0	90.0
6A	2.5	13	26	85	12.65	3.67	8.18	91.0	91.5	90.5
6A	2.5	13	26	90	12.43	4.32	8.18	91.0	91.0	90.4
6A	2.5	13	26	95	12.34	4.23	8.18	92.0	91.0	90.5
6B	2.5	13	26	0	8.17	8.17	8.16	18.0	18.0	18.0
6B	2.5	13	26	5	8.34	7.87	8.16	27.0	24.0	21.4
6B	2.5	13	26	10	8.43	7.23	8.16	37.0	35.0	33.0
6B	2.5	13	26	15	8.45	7.12	8.16	44.0	42.0	43.0

Table C.13–continued from previous page

Code	E(V/cm)	BS(g/L)	AN(g/L)	t(min)	pH			T(°C)		
					C	A	Overall	C	A	Overall
6B	2.5	13	26	20	8.98	6.78	8.16	53.0	53.0	51.6
6B	2.5	13	26	25	9.13	6.10	8.16	60.0	59.0	58.9
6B	2.5	13	26	30	9.34	5.43	8.16	67.0	67.0	63.1
6B	2.5	13	26	35	9.67	5.13	8.16	73.0	73.0	72.5
6B	2.5	13	26	40	10.32	5.08	8.16	76.0	76.0	75.5
6B	2.5	13	26	45	10.56	4.45	8.16	81.0	79.0	78.8
6B	2.5	13	26	50	10.78	4.34	8.16	84.0	82.0	81.5
6B	2.5	13	26	55	11.67	3.89	8.16	85.0	85.0	84.5
6B	2.5	13	26	60	11.89	3.67	8.16	86.6	86.0	86.5
6B	2.5	13	26	65	12.34	3.45	8.16	88.0	86.6	86.6
6B	2.5	13	26	70	12.56	3.12	8.16	90.0	89.0	89.5
6B	2.5	13	26	75	12.34	3.24	8.16	90.0	90.0	90.0
6B	2.5	13	26	80	11.67	4.03	8.16	90.0	90.0	90.0
6B	2.5	13	26	85	11.78	3.54	8.16	91.0	91.5	90.5
6B	2.5	13	26	90	11.56	3.54	8.16	91.0	91.0	90.4
6B	2.5	13	26	95	12.78	3.89	8.16	92.0	91.0	90.5
6C	2.5	13	26	0	8.16	8.16	8.13	18.0	18.0	18.0
6C	2.5	13	26	5	8.76	7.78	8.13	27.0	24.0	21.4
6C	2.5	13	26	10	8.89	7.23	8.13	37.0	35.0	33.0
6C	2.5	13	26	15	9.45	6.88	8.13	44.0	42.0	43.0
6C	2.5	13	26	20	9.76	6.34	8.13	53.0	53.0	51.6
6C	2.5	13	26	25	9.98	6.08	8.13	60.0	59.0	58.9
6C	2.5	13	26	30	10.14	5.56	8.13	67.0	67.0	63.1
6C	2.5	13	26	35	10.43	5.23	8.13	73.0	73.0	72.5
6C	2.5	13	26	40	10.45	5.12	8.13	76.0	76.0	75.5

Table C.13–continued from previous page

Code	E(V/cm)	BS(g/L)	AN(g/L)	t(min)	pH			T(°C)		
					C	A	Overall	C	A	Overall
6C	2.5	13	26	45	10.67	4.34	8.13	81.0	79.0	78.8
6C	2.5	13	26	50	10.87	4.23	8.13	84.0	82.0	81.5
6C	2.5	13	26	55	10.56	4.14	8.13	85.0	85.0	84.5
6C	2.5	13	26	60	11.54	3.76	8.13	86.6	86.0	86.5
6C	2.5	13	26	65	11.87	3.23	8.13	88.0	86.6	86.6
6C	2.5	13	26	70	12.34	3.45	8.13	90.0	89.0	89.5
6C	2.5	13	26	75	12.56	3.78	8.13	90.0	90.0	90.0
6C	2.5	13	26	80	11.98	3.76	8.13	90.0	90.0	90.0
6C	2.5	13	26	85	11.56	3.83	8.13	91.0	91.5	90.5
6C	2.5	13	26	90	11.67	3.94	8.13	91.0	91.0	90.4
6C	2.5	13	26	95	12.02	3.10	8.13	92.0	91.0	90.5
6D	2.5	13	26	0	8.17	8.17	8.16	18.0	18.0	18.0
6D	2.5	13	26	5	8.32	7.78	8.16	27.0	24.0	21.4
6D	2.5	13	26	10	8.78	7.45	8.16	37.0	35.0	33.0
6D	2.5	13	26	15	8.98	7.10	8.16	44.0	42.0	43.0
6D	2.5	13	26	20	9.13	6.54	8.16	53.0	53.0	51.6
6D	2.5	13	26	25	9.67	6.04	8.16	60.0	59.0	58.9
6D	2.5	13	26	30	9.56	5.89	8.16	67.0	67.0	63.1
6D	2.5	13	26	35	9.89	5.56	8.16	73.0	73.0	72.5
6D	2.5	13	26	40	10.56	5.23	8.16	76.0	76.0	75.5
6D	2.5	13	26	45	10.67	5.12	8.16	81.0	79.0	78.8
6D	2.5	13	26	50	10.78	4.45	8.16	84.0	82.0	81.5
6D	2.5	13	26	55	11.67	4.13	8.16	85.0	85.0	84.5
6D	2.5	13	26	60	11.87	4.07	8.16	86.6	86.0	86.5
6D	2.5	13	26	65	12.76	3.76	8.16	88.0	86.6	86.6

Table C.13–continued from previous page

Code	E(V/cm)	BS(g/L)	AN(g/L)	t(min)	pH			T(°C)		
					C	A	Overall	C	A	Overall
6D	2.5	13	26	70	12.45	3.56	8.16	90.0	89.0	89.5
6D	2.5	13	26	75	12.76	3.78	8.16	90.0	90.0	90.0
6D	2.5	13	26	80	12.65	3.45	8.16	90.0	90.0	90.0
6D	2.5	13	26	85	12.43	3.78	8.16	91.0	91.5	90.5
6D	2.5	13	26	90	12.13	3.56	8.16	91.0	91.0	90.4
6D	2.5	13	26	95	12.05	3.45	8.16	92.0	91.0	90.5

Table C.14: pH and temperature data of the 7th experimental series

Code	E(V/cm)	BS(g/L)	AN(g/L)	t(min)	pH			T(°C)		
					C	A	Overall	C	A	Overall
7A	2.5	13	13	0	8.14	8.14	8.29	20.0	20	20.0
7A	2.5	13	13	5	8.34	7.98	8.29	29.0	29	23.4
7A	2.5	13	13	10	8.67	7.65	8.29	34.0	32	29.7
7A	2.5	13	13	15	9.23	7.34	8.29	34.0	37	34.2
7A	2.5	13	13	20	9.45	7.12	8.29	42.0	42	39.4
7A	2.5	13	13	25	9.78	6.45	8.29	47.0	47	45.5
7A	2.5	13	13	30	9.90	6.23	8.29	53.0	53	51.4
7A	2.5	13	13	35	10.16	5.34	8.29	58.0	58	56.6
7A	2.5	13	13	40	10.34	5.28	8.29	63.0	63	61.6
7A	2.5	13	13	45	10.65	5.17	8.29	68.0	68	67.3
7A	2.5	13	13	50	10.67	4.56	8.29	73.0	73	71.2
7A	2.5	13	13	55	11.57	4.36	8.29	78.0	79	78.4
7A	2.5	13	13	60	11.67	4.02	8.29	83.0	85	84.3
7A	2.5	13	13	65	11.78	3.89	8.29	89.0	91	90.1
7A	2.5	13	13	70	11.98	3.45	8.29	92.5	93	93.3
7A	2.5	13	13	75	11.76	3.65	8.29	93.0	95	94.3
7A	2.5	13	13	80	12.10	3.45	8.29	96.0	96	95.0
7A	2.5	13	13	85	12.45	3.48	8.29	95.0	96	95.1
7A	2.5	13	13	90	12.13	3.23	8.29	95.0	96	95.2
7A	2.5	13	13	95	12.24	3.76	8.29	96.0	97	96.3
7B	2.5	13	13	0	8.17	8.17	8.29	20.0	20	20.0
7B	2.5	13	13	5	8.35	8.12	8.29	29.0	29	23.4
7B	2.5	13	13	10	8.56	7.68	8.29	34.0	32	29.7
7B	2.5	13	13	15	9.13	7.34	8.29	34.0	37	34.2

Table C.14–continued from previous page

Code	E(V/cm)	BS(g/L)	AN(g/L)	t(min)	pH			T(°C)		
					C	A	Overall	C	A	Overall
7B	2.5	13	13	20	9.32	7.23	8.29	42.0	42	39.4
7B	2.5	13	13	25	9.73	6.65	8.29	47.0	47	45.5
7B	2.5	13	13	30	9.87	6.28	8.29	53.0	53	51.4
7B	2.5	13	13	35	10.24	6.06	8.29	58.0	58	56.6
7B	2.5	13	13	40	10.24	5.67	8.29	63.0	63	61.6
7B	2.5	13	13	45	11.42	5.21	8.29	68.0	68	67.3
7B	2.5	13	13	50	11.65	5.10	8.29	73.0	73	71.2
7B	2.5	13	13	55	11.34	4.32	8.29	78.0	79	78.4
7B	2.5	13	13	60	11.89	4.34	8.29	83.0	85	84.3
7B	2.5	13	13	65	12.21	4.12	8.29	89.0	91	90.1
7B	2.5	13	13	70	12.12	3.37	8.29	92.5	93	93.3
7B	2.5	13	13	75	12.34	3.28	8.29	93.0	95	94.3
7B	2.5	13	13	80	12.27	3.32	8.29	96.0	96	95.0
7B	2.5	13	13	85	12.37	3.54	8.29	95.0	96	95.1
7B	2.5	13	13	90	12.38	3.23	8.29	95.0	96	95.2
7B	2.5	13	13	95	12.23	3.45	8.29	96.0	97	96.3
7C	2.5	13	13	0	8.16	8.16	8.29	20.0	20	20.0
7C	2.5	13	13	5	8.28	8.06	8.29	29.0	29	23.4
7C	2.5	13	13	10	8.46	7.76	8.29	34.0	32	29.7
7C	2.5	13	13	15	8.78	7.32	8.29	34.0	37	34.2
7C	2.5	13	13	20	9.08	7.34	8.29	42.0	42	39.4
7C	2.5	13	13	25	9.25	6.61	8.29	47.0	47	45.5
7C	2.5	13	13	30	9.24	6.67	8.29	53.0	53	51.4
7C	2.5	13	13	35	9.87	6.63	8.29	58.0	58	56.6
7C	2.5	13	13	40	10.43	5.34	8.29	63.0	63	61.6

Table C.14–continued from previous page

Code	E(V/cm)	BS(g/L)	AN(g/L)	t(min)	pH			T(°C)		
					C	A	Overall	C	A	Overall
7C	2.5	13	13	45	10.87	5.12	8.29	68.0	68	67.3
7C	2.5	13	13	50	11.56	5.07	8.29	73.0	73	71.2
7C	2.5	13	13	55	11.67	4.23	8.29	78.0	79	78.4
7C	2.5	13	13	60	11.87	4.36	8.29	83.0	85	84.3
7C	2.5	13	13	65	11.75	4.15	8.29	89.0	91	90.1
7C	2.5	13	13	70	12.21	3.36	8.29	92.5	93	93.3
7C	2.5	13	13	75	12.23	3.45	8.29	93.0	95	94.3
7C	2.5	13	13	80	12.37	3.65	8.29	96.0	96	95.0
7C	2.5	13	13	85	12.32	3.67	8.29	95.0	96	95.1
7C	2.5	13	13	90	12.36	3.45	8.29	95.0	96	95.2
7C	2.5	13	13	95	12.32	3.47	8.29	96.0	97	96.3
7D	2.5	13	13	0	8.17	8.17	8.29	20.0	20	20.0
7D	2.5	13	13	5	8.21	8.05	8.29	29.0	29	23.4
7D	2.5	13	13	10	8.43	7.78	8.29	34.0	32	29.7
7D	2.5	13	13	15	8.57	6.82	8.29	34.0	37	34.2
7D	2.5	13	13	20	9.09	6.42	8.29	42.0	42	39.4
7D	2.5	13	13	25	9.23	6.21	8.29	47.0	47	45.5
7D	2.5	13	13	30	9.45	6.10	8.29	53.0	53	51.4
7D	2.5	13	13	35	9.86	5.68	8.29	58.0	58	56.6
7D	2.5	13	13	40	10.23	5.30	8.29	63.0	63	61.6
7D	2.5	13	13	45	10.87	5.12	8.29	68.0	68	67.3
7D	2.5	13	13	50	11.34	5.10	8.29	73.0	73	71.2
7D	2.5	13	13	55	11.76	4.76	8.29	78.0	79	78.4
7D	2.5	13	13	60	11.54	4.43	8.29	83.0	85	84.3
7D	2.5	13	13	65	11.50	4.16	8.29	89.0	91	90.1

Table C.14–continued from previous page

Code	E(V/cm)	BS(g/L)	AN(g/L)	t(min)	pH			T(°C)		
					C	A	Overall	C	A	Overall
7D	2.5	13	13	70	12.23	3.76	8.29	92.5	93	93.3
7D	2.5	13	13	75	12.26	3.45	8.29	93.0	95	94.3
7D	2.5	13	13	80	12.32	3.87	8.29	96.0	96	95.0
7D	2.5	13	13	85	12.08	3.67	8.29	95.0	96	95.1
7D	2.5	13	13	90	12.22	3.23	8.29	95.0	96	95.2
7D	2.5	13	13	95	12.13	3.34	8.29	96.0	97	96.3

Appendix D

Experimental data–PAA decay

Table D.1: PAA decay data of the 1st experimental series

Code	E(g/L)	BS(g/L)	AN(g/L)	t–interval(min)	PAA	
					C_0	C_t
1A	2.8	13	26	0	13	7.6500
1A	2.8	13	26	1	13	5.8000
1A	2.8	13	26	2	13	4.3200
1A	2.8	13	26	3	13	3.3400
1A	2.8	13	26	4	13	2.4300
1A	2.8	13	26	5	13	1.9300
1A	2.8	13	26	6	13	1.3900
1A	2.8	13	26	7	13	1.0300
1A	2.8	13	26	8	13	0.7800
1A	2.8	13	26	9	13	0.5500
1A	2.8	13	26	10	13	0.4100
1A	2.8	13	26	11	13	0.3600
1A	2.8	13	26	12	13	0.2700
1A	2.8	13	26	13	13	0.1600

Code	E(g/L)	BS(g/L)	AN(g/L)	t–interval(min)	PAA	
					C_0	C_t
1A	2.8	13	26	14	13	0.1200
1A	2.8	13	26	15	13	0.0990
1A	2.8	13	26	16	13	0.0720
1A	2.8	13	26	17	13	0.0600
1A	2.8	13	26	18	13	0.0420
1A	2.8	13	26	19	13	0.0310
1A	2.8	13	26	20	13	0.0230
1A	2.8	13	26	21	13	0.0190
1A	2.8	13	26	22	13	0.0130
1A	2.8	13	26	23	13	0.0096
1B	2.8	13	26	0	13	8.3000
1B	2.8	13	26	1	13	6.2100
1B	2.8	13	26	2	13	4.9800
1B	2.8	13	26	3	13	3.1200
1B	2.8	13	26	4	13	2.5100
1B	2.8	13	26	5	13	1.7300
1B	2.8	13	26	6	13	1.3500
1B	2.8	13	26	7	13	1.0200
1B	2.8	13	26	8	13	0.7500
1B	2.8	13	26	9	13	0.5600
1B	2.8	13	26	10	13	0.4500
1B	2.8	13	26	11	13	0.2900
1B	2.8	13	26	12	13	0.2100
1B	2.8	13	26	13	13	0.1800
1B	2.8	13	26	14	13	0.1600

Code	E(g/L)	BS(g/L)	AN(g/L)	t–interval(min)	PAA	
					C_0	C_t
1B	2.8	13	26	15	13	0.1000
1B	2.8	13	26	16	13	0.0750
1B	2.8	13	26	17	13	0.0560
1B	2.8	13	26	18	13	0.0400
1B	2.8	13	26	19	13	0.0290
1B	2.8	13	26	20	13	0.0270
1B	2.8	13	26	21	13	0.0150
1B	2.8	13	26	22	13	0.0140
1B	2.8	13	26	23	13	0.0093
1C	2.8	13	26	0	13	8.2000
1C	2.8	13	26	1	13	5.7600
1C	2.8	13	26	2	13	3.9000
1C	2.8	13	26	3	13	3.4100
1C	2.8	13	26	4	13	2.4100
1C	2.8	13	26	5	13	1.8500
1C	2.8	13	26	6	13	1.3700
1C	2.8	13	26	7	13	1.0400
1C	2.8	13	26	8	13	0.7900
1C	2.8	13	26	9	13	0.5900
1C	2.8	13	26	10	13	0.4100
1C	2.8	13	26	11	13	0.3100
1C	2.8	13	26	12	13	0.2500
1C	2.8	13	26	13	13	0.1900
1C	2.8	13	26	14	13	0.1300
1C	2.8	13	26	15	13	0.0970

Code	E(g/L)	BS(g/L)	AN(g/L)	t–interval(min)	PAA	
					C_0	C_t
1C	2.8	13	26	16	13	0.0700
1C	2.8	13	26	17	13	0.0530
1C	2.8	13	26	18	13	0.0390
1C	2.8	13	26	19	13	0.0320
1C	2.8	13	26	20	13	0.0210
1C	2.8	13	26	21	13	0.0160
1C	2.8	13	26	22	13	0.0120
1C	2.8	13	26	23	13	0.0094
1D	2.8	13	26	0	13	7.9100
1D	2.8	13	26	1	13	6.1000
1D	2.8	13	26	2	13	4.6000
1D	2.8	13	26	3	13	3.4500
1D	2.8	13	26	4	13	2.5300
1D	2.8	13	26	5	13	1.8800
1D	2.8	13	26	6	13	1.3800
1D	2.8	13	26	7	13	1.0300
1D	2.8	13	26	8	13	0.7200
1D	2.8	13	26	9	13	0.5700
1D	2.8	13	26	10	13	0.4400
1D	2.8	13	26	11	13	0.3300
1D	2.8	13	26	12	13	0.2300
1D	2.8	13	26	13	13	0.1700
1D	2.8	13	26	14	13	0.1100
1D	2.8	13	26	15	13	0.0980
1D	2.8	13	26	16	13	0.0800

Code	E(g/L)	BS(g/L)	AN(g/L)	t–interval(min)	PAA	
					C_0	C_t
1D	2.8	13	26	17	13	0.0520
1D	2.8	13	26	18	13	0.0410
1D	2.8	13	26	19	13	0.0300
1D	2.8	13	26	20	13	0.0210
1D	2.8	13	26	21	13	0.0180
1D	2.8	13	26	22	13	0.0130
1D	2.8	13	26	23	13	0.0092

Table D.2: PAA decay data of the 2nd experimental series

Code	E(g/L)	BS(g/L)	AN(g/L)	t–interval(min)	PAA	
					C_0	C_t
2A	2.8	25	13	0	25	20.2000
2A	2.8	25	13	1	25	15.4000
2A	2.8	25	13	2	25	11.1900
2A	2.8	25	13	3	25	8.3200
2A	2.8	25	13	4	25	6.2000
2A	2.8	25	13	5	25	4.3000
2A	2.8	25	13	6	25	3.7300
2A	2.8	25	13	7	25	2.5300
2A	2.8	25	13	8	25	1.9500
2A	2.8	25	13	9	25	1.4400
2A	2.8	25	13	10	25	1.0900
2A	2.8	25	13	11	25	0.7200
2A	2.8	25	13	12	25	0.5600
2A	2.8	25	13	13	25	0.4500
2A	2.8	25	13	14	25	0.3400
2A	2.8	25	13	15	25	0.2500
2A	2.8	25	13	16	25	0.1900
2A	2.8	25	13	17	25	0.1410
2A	2.8	25	13	18	25	0.0980
2A	2.8	25	13	19	25	0.0800
2A	2.8	25	13	20	25	0.0600
2A	2.8	25	13	21	25	0.0500
2A	2.8	25	13	22	25	0.0320
2A	2.8	25	13	23	25	0.0280

Code	E(g/L)	BS(g/L)	AN(g/L)	t–interval(min)	PAA	
					C_0	C_t
2A	2.8	25	13	24	25	0.0180
2A	2.8	25	13	25	25	0.0140
2A	2.8	25	13	26	25	0.0100
2B	2.8	25	13	0	25	17.9400
2B	2.8	25	13	1	25	14.5000
2B	2.8	25	13	2	25	14.0000
2B	2.8	25	13	3	25	8.7000
2B	2.8	25	13	4	25	6.1700
2B	2.8	25	13	5	25	5.1000
2B	2.8	25	13	6	25	3.4500
2B	2.8	25	13	7	25	2.4300
2B	2.8	25	13	8	25	1.9400
2B	2.8	25	13	9	25	1.4500
2B	2.8	25	13	10	25	1.2300
2B	2.8	25	13	11	25	0.8200
2B	2.8	25	13	12	25	0.6100
2B	2.8	25	13	13	25	0.4700
2B	2.8	25	13	14	25	0.3500
2B	2.8	25	13	15	25	0.2700
2B	2.8	25	13	16	25	0.1700
2B	2.8	25	13	17	25	0.1230
2B	2.8	25	13	18	25	0.1000
2B	2.8	25	13	19	25	0.0700
2B	2.8	25	13	20	25	0.0590
2B	2.8	25	13	21	25	0.0430

Code	E(g/L)	BS(g/L)	AN(g/L)	t–interval(min)	PAA	
					C_0	C_t
2B	2.8	25	13	22	25	0.0320
2B	2.8	25	13	23	25	0.0220
2B	2.8	25	13	24	25	0.0150
2B	2.8	25	13	25	25	0.0120
2B	2.8	25	13	26	25	0.0095
2C	2.8	25	13	0	25	22.3000
2C	2.8	25	13	1	25	16.3000
2C	2.8	25	13	2	25	11.9800
2C	2.8	25	13	3	25	7.9000
2C	2.8	25	13	4	25	6.2200
2C	2.8	25	13	5	25	4.5300
2C	2.8	25	13	6	25	3.4200
2C	2.8	25	13	7	25	2.7200
2C	2.8	25	13	8	25	1.8900
2C	2.8	25	13	9	25	1.3900
2C	2.8	25	13	10	25	1.0200
2C	2.8	25	13	11	25	0.8100
2C	2.8	25	13	12	25	0.5700
2C	2.8	25	13	13	25	0.3900
2C	2.8	25	13	14	25	0.3100
2C	2.8	25	13	15	25	0.2400
2C	2.8	25	13	16	25	0.1820
2C	2.8	25	13	17	25	0.1500
2C	2.8	25	13	18	25	0.1030
2C	2.8	25	13	19	25	0.0810

Code	E(g/L)	BS(g/L)	AN(g/L)	t–interval(min)	PAA	
					C_0	C_t
2C	2.8	25	13	20	25	0.0540
2C	2.8	25	13	21	25	0.0400
2C	2.8	25	13	22	25	0.0290
2C	2.8	25	25	23	25	0.0220
2C	2.8	25	13	24	25	0.0183
2C	2.8	25	13	25	25	0.0130
2C	2.8	25	13	26	25	0.0097
2D	2.8	25	13	0	25	23.0000
2D	2.8	25	13	1	25	17.0000
2D	2.8	25	13	2	25	10.3200
2D	2.8	25	13	3	25	8.2900
2D	2.8	25	13	4	25	6.1900
2D	2.8	25	13	5	25	4.6000
2D	2.8	25	13	6	25	3.1000
2D	2.8	25	13	7	25	2.5800
2D	2.8	25	13	8	25	1.9000
2D	2.8	25	13	9	25	1.4500
2D	2.8	25	13	10	25	1.0100
2D	2.8	25	13	11	25	0.7900
2D	2.8	25	13	12	25	0.6900
2D	2.8	25	13	13	25	0.4500
2D	2.8	25	13	14	25	0.3200
2D	2.8	25	13	15	25	0.2300
2D	2.8	25	13	16	25	0.2000
2D	2.8	25	13	17	25	0.1300

Code	E(g/L)	BS(g/L)	AN(g/L)	t–interval(min)	PAA	
					C_0	C_t
2D	2.8	25	13	18	25	0.1040
2D	2.8	25	13	19	25	0.0690
2D	2.8	25	13	20	25	0.0530
2D	2.8	25	13	21	25	0.0390
2D	2.8	25	13	22	25	0.0310
2D	2.8	25	13	23	25	0.0230
2D	2.8	25	13	24	25	0.0185
2D	2.8	25	13	25	25	0.0150
2D	2.8	25	13	26	25	0.0098

Table D.3: PAA decay data of the 3$^{\text{rd}}$ experimental series

Code	E(g/L)	BS(g/L)	AN(g/L)	t–interval(min)	PAA	
					C_0	C_t
3A	2.8	13	13	0	13	8.3000
3A	2.8	13	13	1	13	6.2000
3A	2.8	13	13	2	13	4.5600
3A	2.8	13	13	3	13	3.4500
3A	2.8	13	13	4	13	2.8400
3A	2.8	13	13	5	13	1.9800
3A	2.8	13	13	6	13	1.4100
3A	2.8	13	13	7	13	1.0700
3A	2.8	13	13	8	13	0.7800
3A	2.8	13	13	9	13	0.6500
3A	2.8	13	13	10	13	0.5300
3A	2.8	13	13	11	13	0.3400
3A	2.8	13	13	12	13	0.2700
3A	2.8	13	13	13	13	0.1600
3A	2.8	13	13	14	13	0.1500
3A	2.8	13	13	15	13	0.0800
3A	2.8	13	13	16	13	0.0700
3A	2.8	13	13	17	13	0.0400
3A	2.8	13	13	18	13	0.0510
3A	2.8	13	13	19	13	0.0300
3A	2.8	13	13	20	13	0.0210
3A	2.8	13	13	21	13	0.0180
3A	2.8	13	13	22	13	0.0130
3A	2.8	13	13	23	13	0.0087

Code	E(g/L)	BS(g/L)	AN(g/L)	t–interval(min)	PAA	
					C_0	C_t
3B	2.8	13	13	0	13	8.2500
3B	2.8	13	13	1	13	6.1000
3B	2.8	13	13	2	13	4.2000
3B	2.8	13	13	3	13	3.6300
3B	2.8	13	13	4	13	1.9600
3B	2.8	13	13	5	13	1.6800
3B	2.8	13	13	6	13	1.3200
3B	2.8	13	13	7	13	0.9200
3B	2.8	13	13	8	13	0.8200
3B	2.8	13	13	9	13	0.4600
3B	2.8	13	13	10	13	0.4200
3B	2.8	13	13	11	13	0.2800
3B	2.8	13	13	12	13	0.2100
3B	2.8	13	13	13	13	0.1800
3B	2.8	13	13	14	13	0.1100
3B	2.8	13	13	15	13	0.1400
3B	2.8	13	13	16	13	0.0600
3B	2.8	13	13	17	13	0.0600
3B	2.8	13	13	18	13	0.0340
3B	2.8	13	13	19	13	0.0310
3B	2.8	13	13	20	13	0.0220
3B	2.8	13	13	21	13	0.0190
3B	2.8	13	13	22	13	0.0110
3B	2.8	13	13	23	13	0.0095
3C	2.8	13	13	0	13	8.0000

Code	E(g/L)	BS(g/L)	AN(g/L)	t–interval(min)	PAA	
					C_0	C_t
3C	2.8	13	13	1	13	5.2300
3C	2.8	13	13	2	13	3.6000
3C	2.8	13	13	3	13	2.7800
3C	2.8	13	13	4	13	2.4800
3C	2.8	13	13	5	13	2.1400
3C	2.8	13	13	6	13	1.5300
3C	2.8	13	13	7	13	1.1400
3C	2.8	13	13	8	13	0.6800
3C	2.8	13	13	9	13	0.5600
3C	2.8	13	13	10	13	0.4300
3C	2.8	13	13	11	13	0.3300
3C	2.8	13	13	12	13	0.2800
3C	2.8	13	13	13	13	0.1900
3C	2.8	13	13	14	13	0.1300
3C	2.8	13	13	15	13	0.0800
3C	2.8	13	13	16	13	0.0900
3C	2.8	13	13	17	13	0.0700
3C	2.8	13	13	18	13	0.0420
3C	2.8	13	13	19	13	0.0270
3C	2.8	13	13	20	13	0.0230
3C	2.8	13	13	21	13	0.0160
3C	2.8	13	13	22	13	0.0120
3C	2.8	13	25	23	13	0.0096
3D	2.8	13	13	0	13	7.7500
3D	2.8	13	13	1	13	6.2000

Code	E(g/L)	BS(g/L)	AN(g/L)	t–interval(min)	PAA	
					C_0	C_t
3D	2.8	13	13	2	13	5.4500
3D	2.8	13	13	3	13	3.4300
3D	2.8	13	13	4	13	2.6300
3D	2.8	13	13	5	13	1.5900
3D	2.8	13	13	6	13	1.2600
3D	2.8	13	13	7	13	0.9800
3D	2.8	13	13	8	13	0.7800
3D	2.8	13	13	9	13	0.6100
3D	2.8	13	13	10	13	0.3300
3D	2.8	13	13	11	13	0.2900
3D	2.8	13	13	12	13	0.1900
3D	2.8	13	13	13	13	0.1800
3D	2.8	13	13	14	13	0.1400
3D	2.8	13	13	15	13	0.0900
3D	2.8	13	13	16	13	0.0800
3D	2.8	13	13	17	13	0.0500
3D	2.8	13	13	18	13	0.0350
3D	2.8	13	13	19	13	0.0350
3D	2.8	13	13	20	13	0.0240
3D	2.8	13	13	21	13	0.0150
3D	2.8	13	13	22	13	0.0140
3D	2.8	13	13	23	13	0.0098

Table D.4: PAA decay data of the 4th experimental series

Code	E(g/L)	BS(g/L)	AN(g/L)	t–interval(min)	PAA	
					C$_0$	C$_t$
4A	2.5	25	13	0	25	20.4000
4A	2.5	25	13	1	25	15.7000
4A	2.5	25	13	2	25	12.1400
4A	2.5	25	13	3	25	8.6500
4A	2.5	25	13	4	25	5.6500
4A	2.5	25	13	5	25	4.9800
4A	2.5	25	13	6	25	3.7400
4A	2.5	25	13	7	25	2.7800
4A	2.5	25	13	8	25	1.9900
4A	2.5	25	13	9	25	1.4900
4A	2.5	25	13	10	25	1.0900
4A	2.5	25	13	11	25	0.9300
4A	2.5	25	13	12	25	0.6900
4A	2.5	25	13	13	25	0.4800
4A	2.5	25	13	14	25	0.3600
4A	2.5	25	13	15	25	0.2800
4A	2.5	25	13	16	25	0.1900
4A	2.5	25	13	17	25	0.1470
4A	2.5	25	13	18	25	0.1100
4A	2.5	25	13	19	25	0.0850
4A	2.5	25	13	20	25	0.0650
4A	2.5	25	13	21	25	0.0460
4A	2.5	25	13	22	25	0.0370
4A	2.5	25	13	23	25	0.0270

Continued on next page

Code	E(g/L)	BS(g/L)	AN(g/L)	t–interval(min)	PAA	
					C_0	C_t
4A	2.5	25	13	24	25	0.0190
4A	2.5	25	13	25	25	0.0140
4A	2.5	25	13	26	25	0.0100
4B	2.5	25	13	0	25	19.2000
4B	2.5	25	13	1	25	13.3000
4B	2.5	25	13	2	25	10.4300
4B	2.5	25	13	3	25	8.1200
4B	2.5	25	13	4	25	5.9800
4B	2.5	25	13	5	25	4.3400
4B	2.5	25	13	6	25	3.2300
4B	2.5	25	13	7	25	2.2300
4B	2.5	25	13	8	25	1.8700
4B	2.5	25	13	9	25	1.3800
4B	2.5	25	13	10	25	1.0400
4B	2.5	25	13	11	25	0.6500
4B	2.5	25	13	12	25	0.5400
4B	2.5	25	13	13	25	0.4100
4B	2.5	25	13	14	25	0.3100
4B	2.5	25	13	15	25	0.2100
4B	2.5	25	13	16	25	0.1760
4B	2.5	25	13	17	25	0.1240
4B	2.5	25	13	18	25	0.0980
4B	2.5	25	13	19	25	0.0680
4B	2.5	25	13	20	25	0.0540
4B	2.5	25	13	21	25	0.0410

Code	E(g/L)	BS(g/L)	AN(g/L)	t–interval(min)	PAA	
					C_0	C_t
4B	2.5	25	13	22	25	0.0280
4B	2.5	25	13	23	25	0.0210
4B	2.5	25	13	24	25	0.0165
4B	2.5	25	13	25	25	0.0120
4B	2.5	25	13	26	25	0.0097
4C	2.5	25	13	0	25	25.0000
4C	2.5	25	13	1	25	14.9000
4C	2.5	25	13	2	25	11.1400
4C	2.5	25	13	3	25	8.3000
4C	2.5	25	13	4	25	6.1900
4C	2.5	25	13	5	25	4.6200
4C	2.5	25	13	6	25	3.4400
4C	2.5	25	13	7	25	2.5700
4C	2.5	25	13	8	25	1.9200
4C	2.5	25	13	9	25	1.4300
4C	2.5	25	13	10	25	1.0700
4C	2.5	25	13	11	25	0.7900
4C	2.5	25	13	12	25	0.5900
4C	2.5	25	13	13	25	0.4400
4C	2.5	25	13	14	25	0.3300
4C	2.5	25	13	15	25	0.2500
4C	2.5	25	13	16	25	0.1840
4C	2.5	25	13	17	25	0.1400
4C	2.5	25	13	18	25	0.1020
4C	2.5	25	13	19	25	0.0760

Code	E(g/L)	BS(g/L)	AN(g/L)	t–interval(min)	PAA	
					C_0	C_t
4C	2.5	25	13	20	25	0.0570
4C	2.5	25	13	21	25	0.0430
4C	2.5	25	13	22	25	0.0310
4C	2.5	25	25	23	25	0.0230
4C	2.5	25	13	24	25	0.0177
4C	2.5	25	13	25	25	0.0130
4C	2.5	25	13	26	25	0.0098
4D	2.5	25	13	0	25	19.8000
4D	2.5	25	13	1	25	15.3000
4D	2.5	25	13	2	25	11.0600
4D	2.5	25	13	3	25	8.0000
4D	2.5	25	13	4	25	6.1100
4D	2.5	25	13	5	25	4.6700
4D	2.5	25	13	6	25	3.3400
4D	2.5	25	13	7	25	2.4800
4D	2.5	25	13	8	25	1.9400
4D	2.5	25	13	9	25	1.4200
4D	2.5	25	13	10	25	1.0780
4D	2.5	25	13	11	25	0.8000
4D	2.5	25	13	12	25	0.5200
4D	2.5	25	13	13	25	0.4300
4D	2.5	25	13	14	25	0.3400
4D	2.5	25	13	15	25	0.2300
4D	2.5	25	13	16	25	0.1600
4D	2.5	25	13	17	25	0.1510

Code	E(g/L)	BS(g/L)	AN(g/L)	t–interval(min)	PAA	
					C_0	C_t
4D	2.5	25	13	18	25	0.1000
4D	2.5	25	13	19	25	0.0690
4D	2.5	25	13	20	25	0.0560
4D	2.5	25	13	21	25	0.0390
4D	2.5	25	13	22	25	0.0350
4D	2.5	25	13	23	25	0.0240
4D	2.5	25	13	24	25	0.0157
4D	2.5	25	13	25	25	0.0110
4D	2.5	25	13	26	25	0.0095

Table D.5: PAA decay data of the 5th experimental series

Code	E(g/L)	BS(g/L)	AN(g/L)	t–interval(min)	PAA	
					C_0	C_t
5A	2.5	13	26	0	13	8.2000
5A	2.5	13	26	1	13	5.8700
5A	2.5	13	26	2	13	4.6300
5A	2.5	13	26	3	13	3.4200
5A	2.5	13	26	4	13	2.5300
5A	2.5	13	26	5	13	1.8300
5A	2.5	13	26	6	13	1.3700
5A	2.5	13	26	7	13	1.0260
5A	2.5	13	26	8	13	0.7600
5A	2.5	13	26	9	13	0.5300
5A	2.5	13	26	10	13	0.4300
5A	2.5	13	26	11	13	0.3400
5A	2.5	13	26	12	13	0.2500
5A	2.5	13	26	13	13	0.1790
5A	2.5	13	26	14	13	0.1270
5A	2.5	13	26	15	13	0.0970
5A	2.5	13	26	16	13	0.0740
5A	2.5	13	26	17	13	0.0600
5A	2.5	13	26	18	13	0.0410
5A	2.5	13	26	19	13	0.0310
5A	2.5	13	26	20	13	0.0250
5A	2.5	13	26	21	13	0.0180
5A	2.5	13	26	22	13	0.0130
5A	2.5	13	26	23	13	0.0093

Code	E(g/L)	BS(g/L)	AN(g/L)	t–interval(min)	PAA	
					C_0	C_t
5B	2.5	13	26	0	13	7.9000
5B	2.5	13	26	1	13	5.9800
5B	2.5	13	26	2	13	4.5300
5B	2.5	13	26	3	13	3.3100
5B	2.5	13	26	4	13	2.3200
5B	2.5	13	26	5	13	1.8600
5B	2.5	13	26	6	13	1.3800
5B	2.5	13	26	7	13	1.0280
5B	2.5	13	26	8	13	0.7800
5B	2.5	13	26	9	13	0.5800
5B	2.5	13	26	10	13	0.4200
5B	2.5	13	26	11	13	0.3100
5B	2.5	13	26	12	13	0.2100
5B	2.5	13	26	13	13	0.1700
5B	2.5	13	26	14	13	0.1330
5B	2.5	13	26	15	13	0.0990
5B	2.5	13	26	16	13	0.0720
5B	2.5	13	26	17	13	0.0530
5B	2.5	13	26	18	13	0.0390
5B	2.5	13	26	19	13	0.0280
5B	2.5	13	26	20	13	0.0220
5B	2.5	13	26	21	13	0.0160
5B	2.5	13	26	22	13	0.0110
5B	2.5	13	26	23	13	0.0096
5C	2.5	13	26	0	13	8.1000

Code	E(g/L)	BS(g/L)	AN(g/L)	t–interval(min)	PAA	
					C_0	C_t
5C	2.5	13	26	1	13	6.0000
5C	2.5	13	26	2	13	4.4300
5C	2.5	13	26	3	13	3.1400
5C	2.5	13	26	4	13	2.4700
5C	2.5	13	26	5	13	1.8400
5C	2.5	13	26	6	13	1.3900
5C	2.5	13	26	7	13	1.0310
5C	2.5	13	26	8	13	0.7900
5C	2.5	13	26	9	13	0.5900
5C	2.5	13	26	10	13	0.4400
5C	2.5	13	26	11	13	0.3200
5C	2.5	13	26	12	13	0.2700
5C	2.5	13	26	13	13	0.1720
5C	2.5	13	26	14	13	0.1400
5C	2.5	13	26	15	13	0.1000
5C	2.5	13	26	16	13	0.0750
5C	2.5	13	26	17	13	0.0550
5C	2.5	13	26	18	13	0.0420
5C	2.5	13	26	19	13	0.0320
5C	2.5	13	26	20	13	0.0210
5C	2.5	13	26	21	13	0.0190
5C	2.5	13	26	22	13	0.0120
5C	2.5	13	26	23	13	0.0093
5D	2.5	13	26	0	13	7.9800
5D	2.5	13	26	1	13	5.9700

Code	E(g/L)	BS(g/L)	AN(g/L)	t–interval(min)	PAA	
					C_0	C_t
5D	2.5	13	26	2	13	4.3400
5D	2.5	13	26	3	13	3.4100
5D	2.5	13	26	4	13	2.5200
5D	2.5	13	26	5	13	1.8500
5D	2.5	13	26	6	13	1.3500
5D	2.5	13	26	7	13	1.0270
5D	2.5	13	26	8	13	0.7500
5D	2.5	13	26	9	13	0.5600
5D	2.5	13	26	10	13	0.4100
5D	2.5	13	26	11	13	0.3000
5D	2.5	13	26	12	13	0.2100
5D	2.5	13	26	13	13	0.1770
5D	2.5	13	26	14	13	0.1280
5D	2.5	13	26	15	13	0.0980
5D	2.5	13	26	16	13	0.0730
5D	2.5	13	26	17	13	0.0540
5D	2.5	13	26	18	13	0.0400
5D	2.5	13	26	19	13	0.0300
5D	2.5	13	26	20	13	0.0230
5D	2.5	13	26	21	13	0.0170
5D	2.5	13	26	22	13	0.0140
5D	2.5	13	26	23	13	0.0095

Table D.6: PAA decay data of the 6$^{\text{th}}$ experimental series

Code	E(g/L)	BS(g/L)	AN(g/L)	t–interval(min)	PAA	
					C$_0$	C$_t$
6A	2.5	25	26	0	25	22.0000
6A	2.5	25	26	1	25	16.2000
6A	2.5	25	26	2	25	11.9800
6A	2.5	25	26	3	25	8.7500
6A	2.5	25	26	4	25	6.3600
6A	2.5	25	26	5	25	4.8000
6A	2.5	25	26	6	25	3.5600
6A	2.5	25	26	7	25	2.6200
6A	2.5	25	26	8	25	1.9400
6A	2.5	25	26	9	25	1.4900
6A	2.5	25	26	10	25	1.0900
6A	2.5	25	26	11	25	0.8200
6A	2.5	25	26	12	25	0.6200
6A	2.5	25	26	13	25	0.4700
6A	2.5	25	26	14	25	0.3600
6A	2.5	25	26	15	25	0.2700
6A	2.5	25	26	16	25	0.1900
6A	2.5	25	26	17	25	0.1500
6A	2.5	25	26	18	25	0.1200
6A	2.5	25	26	19	25	0.0800
6A	2.5	25	26	20	25	0.0620
6A	2.5	25	26	21	25	0.0450
6A	2.5	25	26	22	25	0.0330
6A	2.5	25	26	23	25	0.0250

Code	E(g/L)	BS(g/L)	AN(g/L)	t–interval(min)	PAA	
					C_0	C_t
6A	2.5	25	26	24	25	0.0190
6A	2.5	25	26	25	25	0.0145
6A	2.5	25	26	26	25	0.0110
6B	2.5	25	26	0	25	19.8500
6B	2.5	25	26	1	25	13.7000
6B	2.5	25	26	2	25	10.8700
6B	2.5	25	26	3	25	7.9800
6B	2.5	25	26	4	25	6.1200
6B	2.5	25	26	5	25	4.4000
6B	2.5	25	26	6	25	3.3400
6B	2.5	25	26	7	25	2.4900
6B	2.5	25	26	8	25	1.8900
6B	2.5	25	26	9	25	1.3800
6B	2.5	25	26	10	25	1.0200
6B	2.5	25	26	11	25	0.7700
6B	2.5	25	26	12	25	0.5600
6B	2.5	25	26	13	25	0.4100
6B	2.5	25	26	14	25	0.3100
6B	2.5	25	26	15	25	0.2200
6B	2.5	25	26	16	25	0.1700
6B	2.5	25	26	17	25	0.1200
6B	2.5	25	26	18	25	0.1000
6B	2.5	25	26	19	25	0.0650
6B	2.5	25	26	20	25	0.0530
6B	2.5	25	26	21	25	0.0410

Code	E(g/L)	BS(g/L)	AN(g/L)	t–interval(min)	PAA	
					C_0	C_t
6B	2.5	25	26	22	25	0.0290
6B	2.5	25	26	23	25	0.0210
6B	2.5	25	26	24	25	0.0170
6B	2.5	25	26	25	25	0.0126
6B	2.5	25	26	26	25	0.0089
6C	2.5	25	26	0	25	23.0000
6C	2.5	25	26	1	25	14.8000
6C	2.5	25	26	2	25	11.1300
6C	2.5	25	26	3	25	8.3000
6C	2.5	25	26	4	25	6.1900
6C	2.5	25	26	5	25	4.6200
6C	2.5	25	26	6	25	3.4400
6C	2.5	25	26	7	25	2.5700
6C	2.5	25	26	8	25	1.9200
6C	2.5	25	26	9	25	1.4300
6C	2.5	25	26	10	25	1.0700
6C	2.5	25	26	11	25	0.7900
6C	2.5	25	26	12	25	0.5900
6C	2.5	25	26	13	25	0.4400
6C	2.5	25	26	14	25	0.3300
6C	2.5	25	26	15	25	0.2500
6C	2.5	25	26	16	25	0.1800
6C	2.5	25	26	17	25	0.1400
6C	2.5	25	26	18	25	0.1100
6C	2.5	25	26	19	25	0.0760

Code	E(g/L)	BS(g/L)	AN(g/L)	t–interval(min)	PAA	
					C_0	C_t
6C	2.5	25	26	20	25	0.0570
6C	2.5	25	26	21	25	0.0420
6C	2.5	25	26	22	25	0.0310
6C	2.5	25	26	23	25	0.0230
6C	2.5	25	26	24	25	0.0180
6C	2.5	25	26	25	25	0.0130
6C	2.5	25	26	26	25	0.0098
6D	2.5	25	26	0	25	19.5000
6D	2.5	25	26	1	25	14.9000
6D	2.5	25	26	2	25	11.1000
6D	2.5	25	26	3	25	8.4200
6D	2.5	25	26	4	25	6.0200
6D	2.5	25	26	5	25	4.6500
6D	2.5	25	26	6	25	3.3900
6D	2.5	25	26	7	25	2.5800
6D	2.5	25	26	8	25	1.9100
6D	2.5	25	26	9	25	1.4500
6D	2.5	25	26	10	25	1.0800
6D	2.5	25	26	11	25	0.8000
6D	2.5	25	26	12	25	0.6000
6D	2.5	25	26	13	25	0.4500
6D	2.5	25	26	14	25	0.3200
6D	2.5	25	26	15	25	0.2600
6D	2.5	25	26	16	25	0.2000
6D	2.5	25	26	17	25	0.1320

Code	E(g/L)	BS(g/L)	AN(g/L)	t–interval(min)	PAA	
					C_0	C_t
6D	2.5	25	26	18	25	0.1080
6D	2.5	25	26	19	25	0.0680
6D	2.5	25	26	20	25	0.0560
6D	2.5	25	26	21	25	0.0440
6D	2.5	25	26	22	25	0.0320
6D	2.5	25	26	23	25	0.0240
6D	2.5	25	26	24	25	0.0160
6D	2.5	25	26	25	25	0.0140
6D	2.5	25	26	26	25	0.0097

Table D.7: PAA decay data of the 7$^{\text{th}}$ experimental series

Code	E(g/L)	BS(g/L)	AN(g/L)	t–interval(min)	PAA C_0	C_t
7A	2.5	13	13	0	13	8.1000
7A	2.5	13	13	1	13	5.8000
7A	2.5	13	13	2	13	4.4300
7A	2.5	13	13	3	13	3.3400
7A	2.5	13	13	4	13	2.5200
7A	2.5	13	13	5	13	1.9300
7A	2.5	13	13	6	13	1.3600
7A	2.5	13	13	7	13	1.0300
7A	2.5	13	13	8	13	0.8300
7A	2.5	13	13	9	13	0.6100
7A	2.5	13	13	10	13	0.4900
7A	2.5	13	13	11	13	0.3200
7A	2.5	13	13	12	13	0.2900
7A	2.5	13	13	13	13	0.1900
7A	2.5	13	13	14	13	0.1380
7A	2.5	13	13	15	13	0.1100
7A	2.5	13	13	16	13	0.0760
7A	2.5	13	13	17	13	0.0570
7A	2.5	13	13	18	13	0.0430
7A	2.5	13	13	19	13	0.0310
7A	2.5	13	13	20	13	0.0240
7A	2.5	13	13	21	13	0.0190
7A	2.5	13	13	22	13	0.0140
7A	2.5	13	13	23	13	0.0099

Continued on next page

Code	E(g/L)	BS(g/L)	AN(g/L)	t–interval(min)	PAA	
					C_0	C_t
7B	2.5	13	13	0	13	8.3000
7B	2.5	13	13	1	13	6.1000
7B	2.5	13	13	2	13	4.5300
7B	2.5	13	13	3	13	3.3000
7B	2.5	13	13	4	13	2.4300
7B	2.5	13	13	5	13	1.7500
7B	2.5	13	13	6	13	1.4600
7B	2.5	13	13	7	13	1.0160
7B	2.5	13	13	8	13	0.6900
7B	2.5	13	13	9	13	0.4800
7B	2.5	13	13	10	13	0.3900
7B	2.5	13	13	11	13	0.2900
7B	2.5	13	13	12	13	0.1900
7B	2.5	13	13	13	13	0.1600
7B	2.5	13	13	14	13	0.1290
7B	2.5	13	13	15	13	0.0980
7B	2.5	13	13	16	13	0.0700
7B	2.5	13	13	17	13	0.0600
7B	2.5	13	13	18	13	0.0390
7B	2.5	13	13	19	13	0.0290
7B	2.5	13	13	20	13	0.0230
7B	2.5	13	13	21	13	0.0172
7B	2.5	13	13	22	13	0.0120
7B	2.5	13	13	23	13	0.0089
7C	2.5	13	13	0	13	7.9700

Code	E(g/L)	BS(g/L)	AN(g/L)	t–interval(min)	PAA	
					C_0	C_t
7C	2.5	13	13	1	13	5.8200
7C	2.5	13	13	2	13	4.5200
7C	2.5	13	13	3	13	3.4100
7C	2.5	13	13	4	13	2.4700
7C	2.5	13	13	5	13	1.8500
7C	2.5	13	13	6	13	1.3200
7C	2.5	13	13	7	13	1.0230
7C	2.5	13	13	8	13	0.7600
7C	2.5	13	13	9	13	0.5700
7C	2.5	13	13	10	13	0.4200
7C	2.5	13	13	11	13	0.3100
7C	2.5	13	13	12	13	0.2300
7C	2.5	13	13	13	13	0.1700
7C	2.5	13	13	14	13	0.1330
7C	2.5	13	13	15	13	0.0890
7C	2.5	13	13	16	13	0.0730
7C	2.5	13	13	17	13	0.0500
7C	2.5	13	13	18	13	0.0410
7C	2.5	13	13	19	13	0.0300
7C	2.5	13	13	20	13	0.0220
7C	2.5	13	13	21	13	0.0175
7C	2.5	13	13	22	13	0.0130
7C	2.5	13	13	23	13	0.0095
7D	2.5	13	13	0	13	7.8200
7D	2.5	13	13	1	13	5.9800

Code	E(g/L)	BS(g/L)	AN(g/L)	t–interval(min)	PAA	
					C_0	C_t
7D	2.5	13	13	2	13	4.3200
7D	2.5	13	13	3	13	3.2300
7D	2.5	13	13	4	13	2.4900
7D	2.5	13	13	5	13	1.9000
7D	2.5	13	13	6	13	1.3800
7D	2.5	13	13	7	13	1.0280
7D	2.5	13	13	8	13	0.7800
7D	2.5	13	13	9	13	0.5800
7D	2.5	13	13	10	13	0.4100
7D	2.5	13	13	11	13	0.3300
7D	2.5	13	13	12	13	0.2400
7D	2.5	13	13	13	13	0.1500
7D	2.5	13	13	14	13	0.1310
7D	2.5	13	13	15	13	0.0980
7D	2.5	13	13	16	13	0.0740
7D	2.5	13	13	17	13	0.0430
7D	2.5	13	13	18	13	0.0420
7D	2.5	13	13	19	13	0.0320
7D	2.5	13	13	20	13	0.0210
7D	2.5	13	13	21	13	0.0150
7D	2.5	13	13	22	13	0.0110
7D	2.5	13	13	23	13	0.0094

Appendix E

STATATISCTIA 10 output of stepwise regression
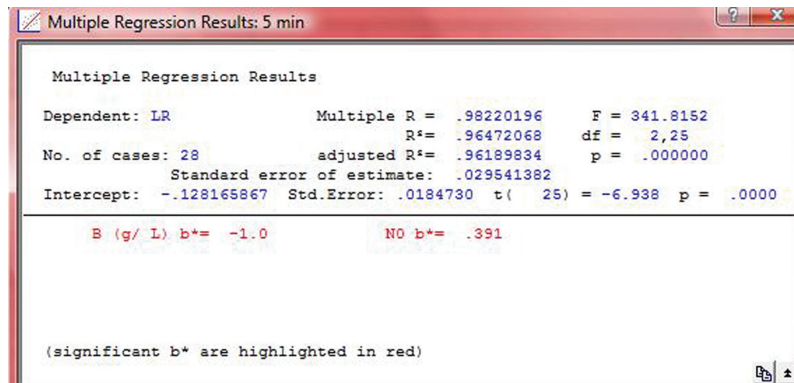
Figure E.1: Statistica output of stepwise regression of t–interval of 5 min
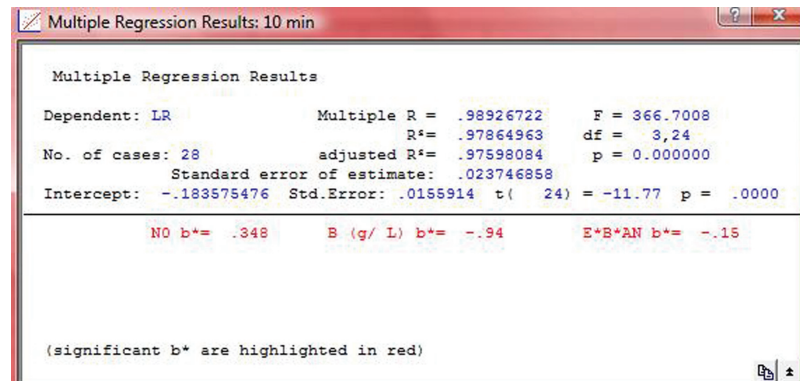
Figure E.2: Statistica output of stepwise regression of t–interval of 10 min
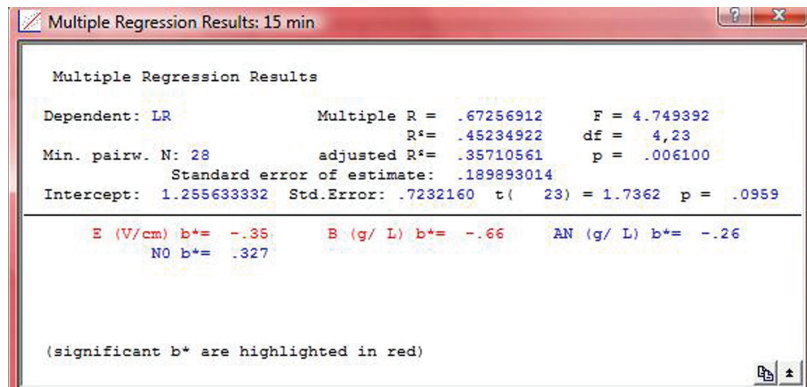
Figure E.3: Statistica output of stepwise regression of t–interval of 15 min
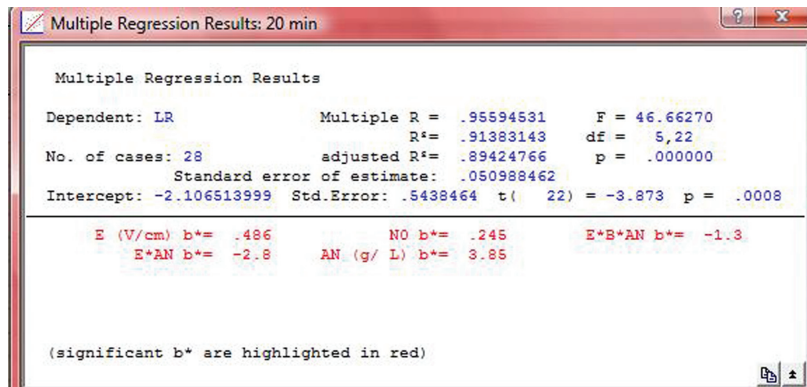
Figure E.4: Statistica output of stepwise regression of t–interval of 20 min
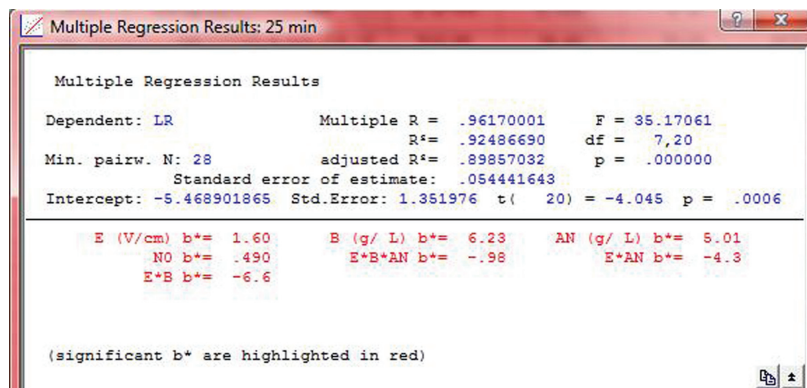
Figure E.5: Statistica output of stepwise regression of t–interval of 25 min

Figure E.6: Statistica output of stepwise regression of t–interval of 30 min

Figure E.7: Statistica output of stepwise regression of t–interval of 35 min

Figure E.8: Statistica output of stepwise regression of t–interval of 40 min

Figure E.9: Statistica output of stepwise regression of t–interval of 45 min

Figure E.10: Statistica output of stepwise regression of t–interval of 50 min

Figure E.11: Statistica output of stepwise regression of t–interval of 55 min

Figure E.12: Statistica output of stepwise regression of t–interval of 60 min

Figure E.13: Statistica output of stepwise regression of t–interval of 65 min

Figure E.14: Statistica output of stepwise regression of t–interval of 70 min

271

Figure E.15: Statistica output of stepwise regression of t–interval of 75 min

Figure E.16: Statistica output of stepwise regression of t–interval of 80 min

Figure E.17: Statistica output of stepwise regression of t–interval of 85 min

Figure E.18: Statistica output of stepwise regression of t–interval of 90 min

Appendix F

Survival curve fitting and MATLAB® script

F.1 Survival curve fitting
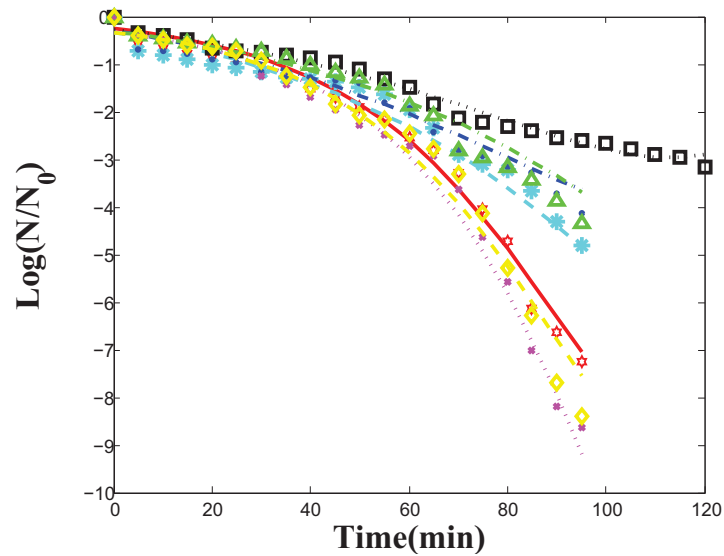
Figure F.1: *C. perfringens* spore survival curve fitting with BE1 model
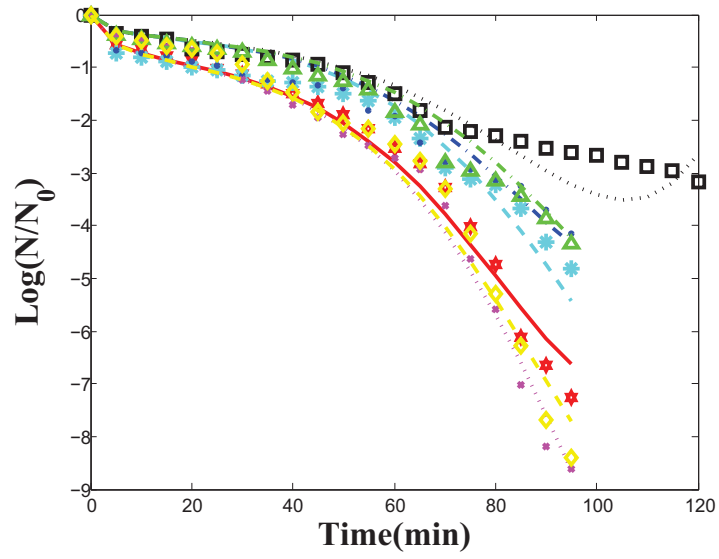
Figure F.2: *C. perfringens* spore survival curve fitting with BE2 model
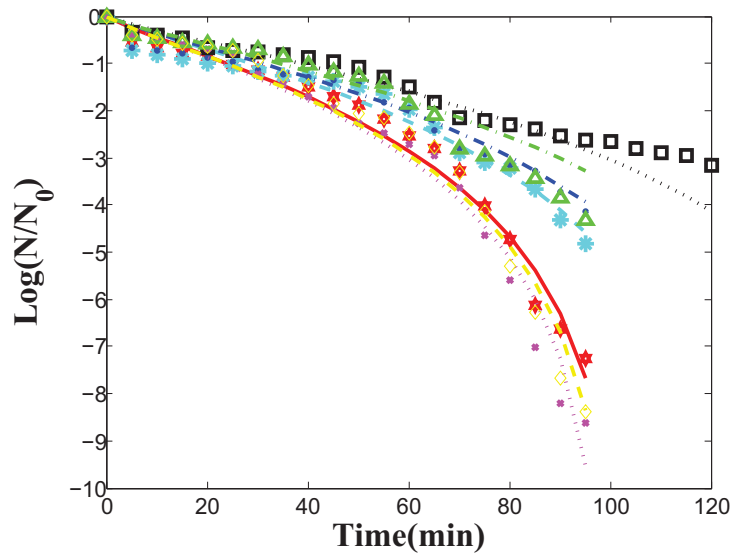
Figure F.3: *C. perfringens* spore survival curve fitting with BE3 model
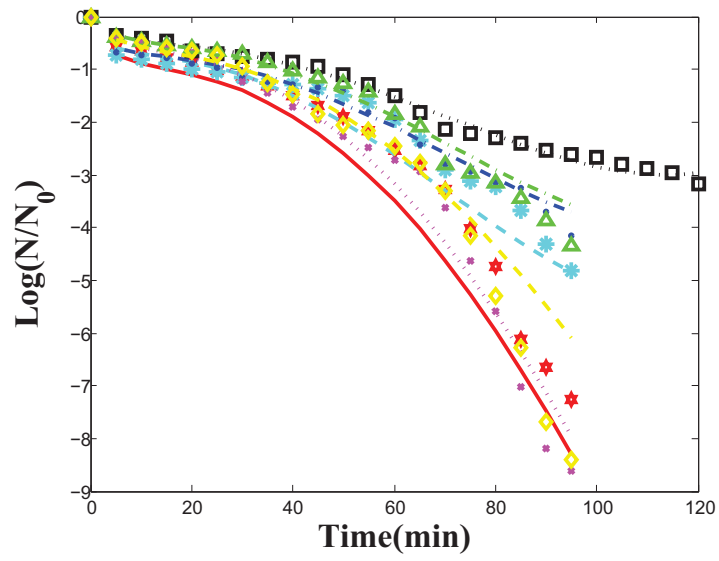
Figure F.4: *C. perfringens* spore survival curve fitting with BE4 model
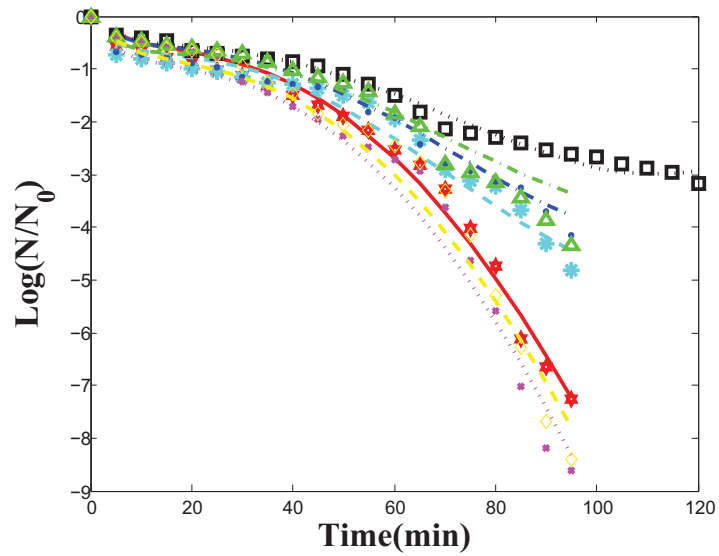
Figure F.5: *C. perfringens* spore survival curve fitting with BE5 model
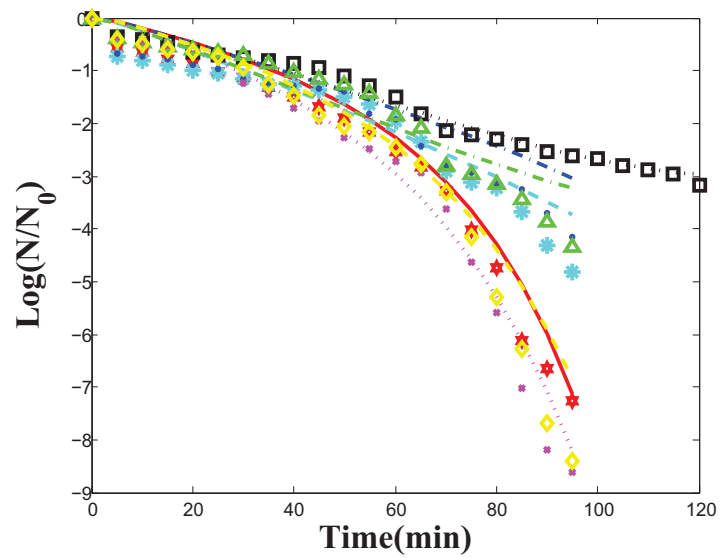
Figure F.6: *C. perfringens* spore survival curve fitting with BE6 model

F.2 MATLAB® script

```
clc
global Y_1A Y_1B Y_1C Y_1D Y_1E Y_1F Y_1G Y_real_P2;
global y0;
global t1;
Y_real=xlsread('new_data2.xlsx',1,'A1:G145')
j=1;
Y_1A=Y_real(1:20,:);
Y_1B=Y_real(21:40,:);
Y_1C=Y_real(41:60,:);
Y_1D=Y_real(61:85,:);
Y_1E=Y_real(86:105,:);
Y_1F=Y_real(106:125,:);
Y_1G=Y_real(126:145,:);


x0= [
 0.018400314759502
 0.382772730216103
 0.197510543119892
 0.000294970203578
-0.000008177949453
-3.674033958536992
 7.151428748409225
-67.898252397217959
 5.941662845784197
];
Kmax=-[-100;-100;-100;-100;-100;-100;-100;-100;-100;-100;-100;-100];
Kmin=[-100;-100;-100;-100;-100;-100;-100;-100;-100;-100;-100;-100];
```

```matlab
    options = optimset('TolFun',1e-12,'TolCon',1e-12,'MaxFunEvals',10^100,
    'MaxIter',5*10^100,'TolX',0.00001);
    [x,fval] = fminsearch(@Mainpredict2,x0,options)


%Main program
    clc
    clear all
    close all
    global teta ;
    global t;
    global y_experiment;
    global y0;


%Import Experimental Data

    global y0;
    global t1;
    Y_real=xlsread('new_data2.xlsx',1,'A1:G145');
    j=1;
    Y_1A=Y_real(1:20,:);
    Y_1B=Y_real(21:40,:);
    Y_1C=Y_real(41:60,:);
    Y_1D=Y_real(61:85,:);
    Y_1E=Y_real(86:105,:);
    Y_1F=Y_real(106:125,:);
    Y_1G=Y_real(126:145,:);

    teta=[
    0.040291072393973
    0.846315206761136
```

```
0.217586782360042

0.991865076321868

0.841293948411824

0.032783153706994

2.834320813107218

];

a1=teta(1);

b1=teta(2);

n1=teta(3);

d1=teta(4);

e1=teta(5);

n2=teta(6);

n3=teta(7);

BS1=Y_1A(1,3);AN1=Y_1A(1,4);E1=Y_1A(1,2);

BS2=Y_1B(1,3);AN2=Y_1B(1,4);E2=Y_1B(1,2);

BS3=Y_1C(1,3);AN3=Y_1C(1,4);E3=Y_1C(1,2);

BS4=Y_1D(1,3);AN4=Y_1D(1,4);E4=Y_1D(1,2);

BS5=Y_1E(1,3);AN5=Y_1E(1,4);E5=Y_1E(1,2);

BS6=Y_1F(1,3);AN6=Y_1F(1,4);E6=Y_1F(1,2);

BS7=Y_1G(1,3);AN7=Y_1G(1,4);E7=Y_1G(1,2);

y_experiment1=log10(Y_1A(:,7)./Y_1A(:,6));

y_experiment2=log10(Y_1B(:,7)./Y_1B(:,6));

y_experiment3=log10(Y_1C(:,7)./Y_1C(:,6));

y_experiment4=log10(Y_1D(:,7)./Y_1D(:,6));

y_experiment5=log10(Y_1E(:,7)./Y_1E(:,6));

y_experiment6=log10(Y_1F(:,7)./Y_1F(:,6));

y_experiment7=log10(Y_1G(:,7)./Y_1G(:,6));

t1=Y_1A(:,1);

t4=Y_1D(:,1);

N01=Y_1A(1,6);N02=Y_1B(1,6);N03=Y_1C(1,6);N04=Y_1D(1,6);
```

280

```
N05=Y_1E(1,6);N06=Y_1F(1,6);N07=Y_1G(1,6);

N01=Y_1A(1,6);N02=Y_1B(1,6);N03=Y_1C(1,6);

N04=Y_1D(1,6);N05=Y_1E(1,6);N06=Y_1F(1,6);N07=Y_1G(1,6);


Y1=-1/(b1-1).*(log10(d1+(b1-1)*a1*BS1^n1*AN1^n2*E1^n3*t1.^e1*N01^(b1-1)));

Y2=-1/(b1-1).*(log10(d1+(b1-1)*a1*BS2^n1*AN2^n2*E2^n3*t1.^e1*N02^(b1-1)));

Y3=-1/(b1-1).*(log10(d1+(b1-1)*a1*BS3^n1*AN3^n2*E3^n3*t1.^e1*N03^(b1-1)));

Y4=-1/(b1-1).*(log10(d1+(b1-1)*a1*BS4^n1*AN4^n2*E4^n3*t4.^e1*N04^(b1-1)));

Y5=-1/(b1-1).*(log10(d1+(b1-1)*a1*BS5^n1*AN5^n2*E5^n3*t1.^e1*N05^(b1-1)));

Y6=-1/(b1-1).*(log10(d1+(b1-1)*a1*BS6^n1*AN6^n2*E6^n3*t1.^e1*N06^(b1-1)));

Y7=-1/(b1-1).*(log10(d1+(b1-1)*a1*BS7^n1*AN7^n2*E7^n3*t1.^e1*N07^(b1-1)));


%------------------------------------------------
 Y=[Y1;Y2;Y3;Y4;Y5;Y6;Y7];
 z1=abs(Y1-y_experiment1);
 z2=abs(Y2-y_experiment2);
 z3=abs(Y3-y_experiment3);
 z4=abs(Y4-y_experiment4);
 z5=abs(Y5-y_experiment5);
 z6=abs(Y6-y_experiment6);
 z7=abs(Y7-y_experiment7);
 yobs=[y_experiment1;y_experiment2;y_experiment3;y_experiment4;
 y_experiment5;y_experiment6;y_experiment7;];
 ymean=mean(yobs);
 z=sum(z1.^2)+sum(z2.^2)+sum(z3.^2)+sum(z4.^2)+sum(z5.^2)+sum(z6.^2)+sum(z7.^2)
 ts=(yobs-ymean).^2;
 Tss=sum(ts)
 Rs=(Y-yobs).^2;
 Rss=sum(Rs)
 n=length(yobs);
```

```
  p=length(teta)
  r=1-(Rss/(n-p))/(Tss/(n-1))
%PLOT
  figure(1);
  plot(t1,y_experiment1,'rh','MarkerSize',7); % up to 70
  hold on;
  plot(t1,Y1,'Color','r');
  plot(t1,y_experiment2,'c*','MarkerSize',10); % up to 70
  plot(t1,Y2,'c--');
  plot(t1,y_experiment3,'bo','MarkerSize',2); % up to 70
  plot(t1,Y3,'b-.');
  plot(t4,y_experiment4,'ks'); % up to 70
  plot(t4,Y4,'black:');
  plot(t1,y_experiment5,'mx'); % up to 70
  plot(t1,Y5,'m:');
  plot(t1,y_experiment6,'g^'); % up to 70
  plot(t1,Y6,'g-.');
  plot(t1,y_experiment7,'yd'); % up to 70
  plot(t1,Y7,'y--');
 set(gca, 'fontsize', 12)
 xlabel('Time(min)', 'Fontsize', 18, 'FontWeight', 'bold', 'FontName',
 'Times New Roman');ylabel( 'Log(N/N_0)', 'Fontsize', 18,    'FontWeight', 'bold',
 'FontName', 'Times New Roman');

  x=[0;-8];
  y=[0;-8];
  figure(2)
  hold
  plot([0;round(min(Y1)-1)],[0;round(min(Y1)-1)],'r')
  plot(y_experiment1,Y1,'bo')
```

```matlab
grid on

set(gca, 'fontsize', 12, 'GridLineStyle','-')

xlabel('LR-Predicated', 'Fontsize', 18, 'FontWeight', 'bold', 'FontName',
'Times New Roman');ylabel( 'LR-Observed', 'Fontsize', 18, 'FontWeight',
'bold', 'FontName', 'Times New Roman');

figure(3)

hold

plot([0;round(min(Y2)-1)],[0;round(min(Y2)-1)],'r')

plot(y_experiment2,Y2,'bo')

grid on

set(gca, 'fontsize', 12, 'GridLineStyle','-')

xlabel('LR-Predicated', 'Fontsize', 18, 'FontWeight', 'bold', 'FontName',
'Times New Roman');ylabel( 'LR-Observed', 'Fontsize', 18, 'FontWeight',
'bold', 'FontName', 'Times New Roman');

figure(4)

hold

plot([0;round(min(Y3)-1)],[0;round(min(Y3)-1)],'r')

plot(y_experiment3,Y3,'bo')

grid on

set(gca, 'fontsize', 12, 'GridLineStyle','-')

xlabel('LR-Predicated', 'Fontsize', 18, 'FontWeight', 'bold', 'FontName',
'Times New Roman');ylabel( 'LR-Observed', 'Fontsize', 18, 'FontWeight',
'bold', 'FontName', 'Times New Roman');

figure(5)

hold

plot([0;round(min(Y4)-1)],[0;round(min(Y4)-1)],'r')

plot(y_experiment4,Y4,'bo')

grid on

set(gca, 'fontsize', 12,'GridLineStyle','-')

xlabel('LR-Predicated', 'Fontsize', 18, 'FontWeight', 'bold', 'FontName',
```

```
'Times New Roman');ylabel( 'LR-Observed', 'Fontsize', 18, 'FontWeight',

'bold', 'FontName', 'Times New Roman');

figure(6)

hold

plot([0;round(min(Y5)-1)],[0;round(min(Y5)-1)],'r')

plot(y_experiment5,Y5,'bo')

grid on

set(gca, 'fontsize', 12, 'GridLineStyle','-')

xlabel('LR-Predicated', 'Fontsize', 18, 'FontWeight', 'bold', 'FontName',

'Times New Roman');ylabel( 'LR-Observed', 'Fontsize', 18, 'FontWeight',

'bold', 'FontName', 'Times New Roman');

figure(7)

hold

plot([0;round(min(Y6)-1)],[0;round(min(Y6)-1)],'r')

plot(y_experiment6,Y6,'bo')

grid on

set(gca, 'fontsize', 12, 'linewidth', 1.5, 'GridLineStyle','-')

xlabel('LR-Predicated', 'Fontsize', 18, 'FontWeight', 'bold', 'FontName',

'Times New Roman');ylabel( 'LR-Observed', 'Fontsize',   18, 'FontWeight',

'bold', 'FontName', 'Times New Roman');

figure(8)

hold

plot([0;round(min(Y7)-1)],[0;round(min(Y7)-1)],'r')

plot(y_experiment7,Y7,'bo')

grid on

set(gca, 'fontsize', 12, 'GridLineStyle','-')

xlabel('LR-Predicated', 'Fontsize', 18, 'FontWeight', 'bold', 'FontName',

'Times New Roman');ylabel( 'LR-Observed', 'Fontsize', 18, 'FontWeight',

'bold', 'FontName', 'Times New Roman')
```

Appendix G

Experimental data–OD readings and spores count

Table G.1: OD reading and spore count data for the LIEF trigged germination

Code	E(V/cm)	t–interval (min)	OD$_{600}$	N$_0$(CFU/g TS)	N$_{60}$(CFU/g TS)	
					No heat	**Heat**
1a	2.5	0	1.500	12918660	12660287	5950335
1a	2.5	25	1.500	12918660	12660287	5950335
1a	2.5	30	1.340	12918660	12660287	5950335
1a	2.5	35	1.030	12918660	12660287	5950335
1a	2.5	40	0.878	12918660	12660287	5950335
1a	2.5	45	0.742	12918660	12660287	5950335
1a	2.5	50	0.692	12918660	12660287	5950335
1a	2.5	55	0.692	12918660	12660287	5950335
1a	2.5	60	0.692	12918660	12660287	5950335
1b	2.5	0	1.500	12918660	12686124	5886362
1b	2.5	25	1.500	12918660	12686124	5886362
1b	2.5	30	1.370	12918660	12686124	5886362

Code	E(V/cm)	t–interval(min)	OD$_{600}$	N$_0$(CFU/g TS)	N$_{120}$(CFU/g TS)	
					No heat	Heat
1b	2.5	35	1.060	12918660	12686124	5886362
1b	2.5	40	0.881	12918660	12686124	5886362
1b	2.5	45	0.741	12918660	12686124	5886362
1b	2.5	50	0.696	12918660	12686124	5886362
1b	2.5	55	0.696	12918660	12686124	5886362
1b	2.5	60	0.696	12918660	12686124	5886362
1c	2.5	0	1.500	12918660	12647368	5817790
1c	2.5	25	1.500	12918660	12647368	5817790
1c	2.5	30	1.350	12918660	12647368	5817790
1c	2.5	35	1.040	12918660	12647368	5817790
1c	2.5	40	0.863	12918660	12647368	5817790
1c	2.5	45	0.738	12918660	12647368	5817790
1c	2.5	50	0.689	12918660	12647368	5817790
1c	2.5	55	0.689	12918660	12647368	5817790
1c	2.5	60	0.689	12918660	12647368	5817790
1d	2.5	0	1.500	12918660	12634450	5837116
1d	2.5	25	1.500	12918660	12634450	5837116
1d	2.5	30	1.360	12918660	12634450	5837116
1d	2.5	35	1.070	12918660	12634450	5837116
1d	2.5	40	0.873	12918660	12634450	5837116
1d	2.5	45	0.744	12918660	12634450	5837116
1d	2.5	50	0.693	12918660	12634450	5837116
1d	2.5	55	0.693	12918660	12634450	5837116
1d	2.5	60	0.693	12918660	12634450	5837116
2a	2.8	0	1.500	12918660	12556938	5458501

Code	E(V/cm)	t–interval(min)	OD$_{600}$	N$_0$(CFU/g TS)	N$_{120}$(CFU/g TS)	
					No heat	**Heat**
2a	2.8	20	1.500	12918660	12556938	5458501
2a	2.8	25	1.216	12918660	12556938	5458501
2a	2.8	30	0.878	12918660	12556938	5458501
2a	2.8	35	0.686	12918660	12556938	5458501
2a	2.8	40	0.652	12918660	12556938	5458501
2a	2.8	45	0.652	12918660	12556938	5458501
2a	2.8	50	0.652	12918660	12556938	5458501
2b	2.8	0	1.500	12918660	12544019	5519368
2b	2.8	20	1.500	12918660	12544019	5519368
2b	2.8	25	1.220	12918660	12544019	5519368
2b	2.8	30	0.901	12918660	12544019	5519368
2b	2.8	35	0.698	12918660	12544019	5519368
2b	2.8	40	0.660	12918660	12544019	5519368
2b	2.8	45	0.660	12918660	12544019	5519368
2b	2.8	50	0.660	12918660	12544019	5519368
2c	2.8	0	1.500	12918660	12518181	5450416
2c	2.8	20	1.500	12918660	12518181	5450416
2c	2.8	25	1.200	12918660	12518181	5450416
2c	2.8	30	0.887	12918660	12518181	5450416
2c	2.8	35	0.689	12918660	12518181	5450416
2c	2.8	40	0.653	12918660	12518181	5450416
2c	2.8	45	0.653	12918660	12518181	5450416
2c	2.8	50	0.653	12918660	12518181	5450416
2d	2.8	0	1.500	12918660	12492344	5514121
2c	2.8	20	1.500	12918660	12492344	5514121

Code	E(V/cm)	t–interval(min)	OD$_{600}$	N$_0$(CFU/g TS)	N$_{120}$(CFU/g TS)	
					No heat	**Heat**
2d	2.8	25	1.180	12918660	12492344	5514121
2d	2.8	30	0.891	12918660	12492344	5514121
2d	2.8	35	0.681	12918660	12492344	5514121
2d	2.8	40	0.662	12918660	12492344	5514121
2d	2.8	45	0.662	12918660	12492344	5514121
2d	2.8	50	0.662	12918660	12492344	5514121